AD-A092 545 AIR FORCE INST OF TECH WRIGHT-PATTERSON AFB OH F/G 4/1
RELATIVISTIC ELECTRON PRECIPITATION: AN OBSERVATIONAL STUDY.(U)
1980 L J ANDREOLI
UNCLASSIFIED AFIT-CI-80-26D NL

1 OF 4
AD
A092545

14 UNCLASS

SECURITY CLASSIFICATION OF THIS PAGE (When Data Entered)

AFIT-CI- **REPORT DOCUMENTATION PAGE**

READ INSTRUCTIONS BEFORE COMPLETING FORM

1. REPORT NUMBER 80-26D	2. GOVT ACCESSION NO. AD-A092545	3. RECIPIENT'S CATALOG NUMBER
4. TITLE (and Subtitle) Relativistic Electron Precipitation: An Observational Study.		5. TYPE OF REPORT & PERIOD COVERED THESIS/DISSERTATION
		6. PERFORMING ORG. REPORT NUMBER
7. AUTHOR(s) Leopold Joseph Andreoli		8. CONTRACT OR GRANT NUMBER(s) Doctoral thesis
9. PERFORMING ORGANIZATION NAME AND ADDRESS AFIT STUDENT AT: University of California, L.A.		10. PROGRAM ELEMENT, PROJECT, TASK AREA & WORK UNIT NUMBERS
11. CONTROLLING OFFICE NAME AND ADDRESS AFIT/NR WPAFB OH 45433		12. REPORT DATE 1980
		13. NUMBER OF PAGES 279
14. MONITORING AGENCY NAME & ADDRESS (if different from Controlling Office) 322		15. SECURITY CLASS. (of this report) UNCLASS
		15a. DECLASSIFICATION/DOWNGRADING SCHEDULE

16. DISTRIBUTION STATEMENT (of this Report)

APPROVED FOR PUBLIC RELEASE; DISTRIBUTION UNLIMITED

DTIC ELECTE DEC 0 8 1980 E

17. DISTRIBUTION STATEMENT (of the abstract entered in Block 20, if different from Report)

18. SUPPLEMENTARY NOTES

APPROVED FOR PUBLIC RELEASE: IAW AFR 190-17

FREDRIC C. LYNCH, Major, USAF
Director of Public Affairs

Air Force Institute of Technology (ATC)
Wright-Patterson AFB, OH 45433

19. KEY WORDS (Continue on reverse side if necessary and identify by block number)

20. ABSTRACT (Continue on reverse side if necessary and identify by block number)

ATTACHED

DD FORM 1 JAN 73 1473 EDITION OF 1 NOV 65 IS OBSOLETE

UNCLASS

SECURITY CLASSIFICATION OF THIS PAGE (When Data Entered)

UNIVERSITY OF CALIFORNIA

Los Angeles

Relativistic Electron Precipitation:
An Observational Study

A dissertation submitted in partial satisfaction
of the requirements for the degree Doctor of Philosophy
in Atmospheric Sciences

by

Leopold Joseph Andreoli

1980

The dissertation of Leopold Joseph Andreoli is approved.

Charles F. Kennel

Margaret G. Kivelson

George L. Siscoe

S. V. Venkateswaran

Richard M. Thorne, Committee Chairman

UNIVERSITY OF CALIFORNIA, LOS ANGELES

1980

Dedicated to Kathleen, David, Michael and Donna.

TABLE OF CONTENTS

LIST OF TABLES

LIST OF FIGURES

ACKNOWLEDGEMENTS

I am grateful for having had the rare opportunity to work under the supervision of someone with the insight of Dr. Richard M. Thorne. I thank Dr. S. V. Venkateswaran for three and one-half years of guidance, inspiration, and friendship. Dr. George L. Siscoe has added significant breadth to my knowledge of the space sciences. Conversations with Drs. Charles F. Kennel and Margaret Kivelson were helpful and inspiring. I owe special thanks to Drs. Thorne and Kivelson for editing the manuscript and suggesting style changes.

Finally I thank Miss Sherry Lovell for typing this dissertation and Mrs. Dorothy Deutsch, Mr. Ted Doty, Mrs. Kathryn Drake and Mr. Wes Radlein for support and friendship. While a graduate student, I have been supported by the U. S. Air Force Institute of Technology.

The S3-2 and S3-3 data bases were provided by the prime investigator, Dr. A.L. Vampola, The Aerospace Corporation, ElSegundo, Ca. I am most grateful for many helpful conversations with him and Dr. J. Fennell and for their hospitality while I analyzed the data sets.

VITA

November 11, 1945--Born, Philadelphia, Pennsylvania

1967--B.S., Saint Joseph's College, Philadelphia

1967--Commissioned USAF

1970-1971--M.S., University of Michigan

1979--Major, USAF

ABSTRACT OF THE DISSERTATION

Relativistic Electron Precipitation:

An Observational Study

by

Leopold Joseph Andreoli

Doctor of Philosophy in Atmospheric Sciences

University of California, Los Angeles, 1980

Professor Richard M. Thorne, Chair

The object of this dissertation is to analyze satellite data to investigate the morphology of strong diffusion relativistic electron precipitation (REP) events with the ultimate purpose of gaining insights into the precipitation mechanism and determining atmospheric consequences. Analysis of fourteen (14) months of magnetic electron spectrometer and proton telescope data from the Air Force S3-3 satellite from July 1976 to September 1977 is presented. Analysis techniques and data catalogues are presented in detail. Three distinct classes of REPs were discovered: an overwhelming majority (96.5%) exhibited precipitation in a large range of energies below 1 MeV for electrons with concurrent proton precipitation; the smallest class (1.3%) also exhibited concurrent electron and proton precipitation but the electron

and proton precipitation but the electron precipitation occurred only at energies above 1 MeV; a third class (2.2%) had no associated proton precipitation and electrons precipitated only at energies below a few hundred keV. In addition, all REPs have a 10-20% frequency of occurrence that linearly increases with magnetic activity, show seasonal variation with equinoxial maxima and solstice minima, have mostly small latitudinal (~0.5L) and large longitudinal (1000-10,000km) extents, and occur most frequency (9 out of 10) in the local night-time sector.

A theoretical approach to the REP mechanism is presented. Interaction of the radiation belt electron and ring current protong populations with electrostatic and electromagnetic ion cyclotron and whistler mode chorus waves can account for the three classes of precipitation, respectively. Examples of each class are presented in detail.

Finally, an investigation of the energy deposition rates from these events and their ultimate effect on the ionized and neutral atmosphere with emphasis on ozone modification is presented. The local hydroxyl concentration can be increased up to a factor of 10 and the local ozone concentration can be decreased by 10-30% by REP events.

Introduction

HF radio waves can propagate from transmitter to receiver via refractive interaction with the ionosphere (see Fig. 1). This propagation is known as forward scatter or skywave propagation. The received signal can be diminished (in power) if the electron density below the scattering altitude is enhanced in any way. Signal absorption occurs during the day due to the natural increase of free electrons below the scattering altitude by solar ionizing radiation (1000-1100^{o}A). Absorption can also be increased by precipitating energetic particles (e.g., solar protons) that reach altitudes below the scattering altitude. One well known class of absorption event is the Polar Cap Absorption (PCA) events which occur over the polar region following the outburst of energetic protons during flare activity on the sun. A lesser known but more frequent class of events involves the precipitation of relativistic electrons and these will be the subject of this dissertation.

Relativistic Electron Precipitation (REP) events were first observed as anomalous daytime absorption of forward scatter (more correctly - ionospheric refraction) HF signals by Bailey and Pomerantz (1965). The detection system used by Bailey and Pomerantz consisted of three paths each in Alaska and Antarctica operating near 23 MHZ with skywave scattering points over the invariant latitude (Λ) range 58-77^{o} (L = 3.6-20.0). The scattering altitude was estimated to be ~70 km. Peak signal absorption typically occurred between Λ= 62-66^{o} (L = 4.5-6.0); namely, within the region of long term trapping for

FIG 1. Illustration of one-hop skywave propagation via the Ionosphere.

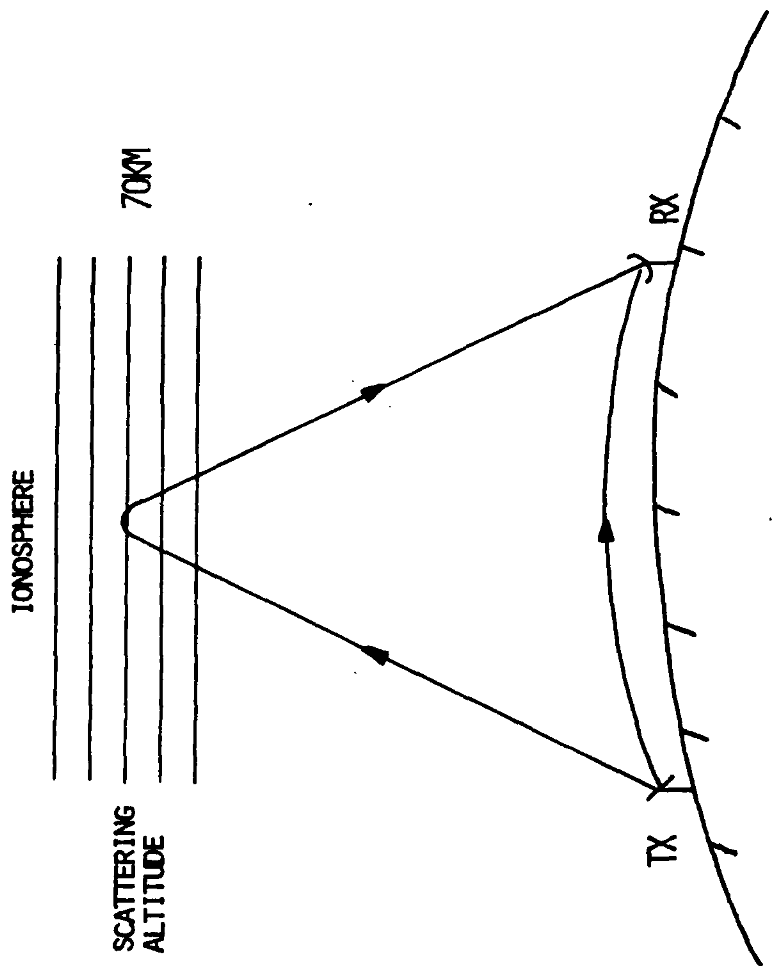
IONOSPHERE
70KM
SCATTERING ALTITUDE
RX
TX

radiation belt particles.

Since solar protons could be ruled out due to the absence of absorption over the higher latitude polar cap region ($\Lambda > 72^o$; L > 10), absorption was attributed to a locally precipitated source of particles. These particles dissipate most of their energy at altitudes determined by their range in the atmosphere and thus by their energy (Aikin and Bauer, 1965). As shown in Fig. 2, protons require at least several MeV while electrons require only a few hundred keV of energy to penetrate below 70 km. This, however, immediately excludes the main bulk of auroral electrons (~1-10 keV) as the precipitating particles causing absorption and indeed visible auroral activity (monitored by all sky cameras) was found to have no correlation with dayside HF absorption (Bailey et al., 1970). Since protons of several MeV energy are tenuous beyond (L ~ 3.5) and do not exhibit outer zone integral flux variations of the order estimated for strong ionospheric absorption (~40 cm^{-2} str^{-1} sec^{-1} for protons), Bailey and Pomerantz concluded that trapped electrons at energies greater than 400 keV were the cause. In situ satellite measurements have also demonstrated that relativistic electrons trapped from $\Lambda = 55\text{-}60^o$ (L= 3-4) can exhibit order of magnitude flux decreases during disturbed times (Frank, 1965). Furthermore, since the maximum observed absorption intensities occur at higher L values than the normally expected peak intensity of trapped electrons, Bailey and Pomerantz (1965) concluded the mechanism operates more efficiently near the trapping boundary.

Since Bailey and Pomerantz only observed the events during the daytime, they assumed, inconclusively, that the precipitating mechanism is more intense on the dayside. It must be noted that this type of measurement is highly frequency dependent. This is supported by the fact that as the forward scatter observing frequency changed from 50 MHz in the early 1950's to 35 MHz pre-IQSY (Int'l Quiet Sun Year) and finally to 23 MHz post IQSY, ability to detect less intense events improved. The day/night occurrence probability of REPs will be further discussed as we review subsequent measurements.

Other types of observations were soon employed to verify inferences based on the forward scatter results. Riometers which integrate the effect of precipitating particles (and radiation) of all energies were used to confirm signal absorption (Bailey et al., 1970). All sky cameras (observing auroral activity), ionosondes (for Es, sporadic E layer, detection), magnetometers (Bailey et al., 1966) and balloon X-ray measurements (for energy spectrum information) (Barcus and Rosenberg, 1966) basically confirmed signal absorption differences between daytime REPs and nighttime Es (absorption by precipitating 5-20 keV electrons). In addition, estimates of precipitating electron spectra for REP and Es conditions for quiet to severely disturbed magnetic conditions were constructed from X-ray and forward scatter measurements (Bailey et al., 1966; Bailey et al., 1970). Comparison of X-ray and forward-scatter-deduced spectra for the same event revealed the marked inability of the forward scatter system alone to detect the presence of relativistic electrons due

FIG 2. Atmospheric penetration depths for protons and electrons assuming vertical incidence (adopted from Aikin and Bauer, 1965).

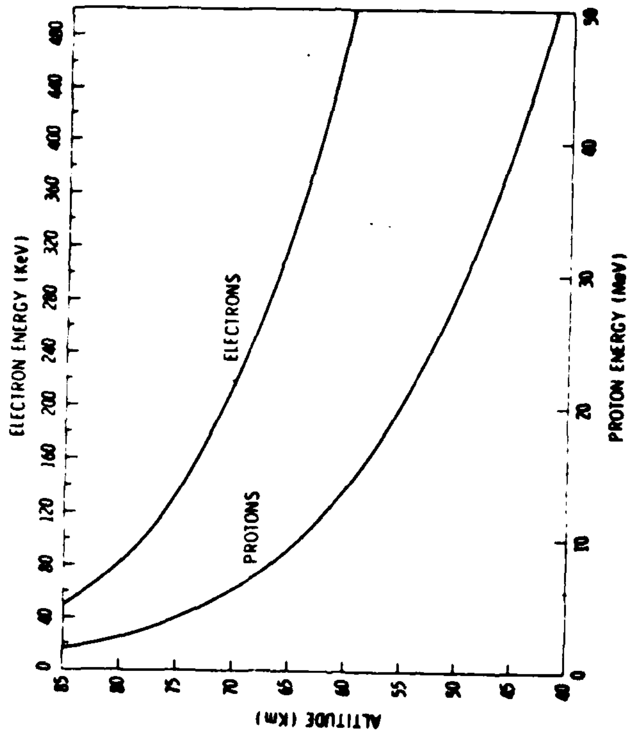
ELECTRON ENERGY (KeV)
ELECTRONS
PROTONS
PROTON ENERGY (MeV)
ALTITUDE (Km)

to the large uncertainty in scattering altitude (Rosenberg et al., 1972). Spectra derived from various sources will be compared later.

Another drawback to estimating REP spectra from forward scatter measurements alone is the uncertainty of absolute absorption. The signal power received is enhanced by increases in the electron density at the scattering altitude as well as diminished by increases in electron density along the signal path below the scattering altitude, thus an accurate measure of absorption is difficult.

REPs (and PCAs) appear as absorption on forward scatter records by day. At night, although the scattering altitude is higher (by 10-20 km), there are insufficient free electrons below the scattering altitude to produce signal absorption and even the strongest precipitation events appear as signal enhancements. Riometers, however, continue to show absorption during such nighttime events (Bailey, 1968).

Two Alaskan paths at $\Lambda = 65^{\circ}$ and 62° (L = 5.7 and 4.6) were chosen for long term statistical study (Bailey, 1968). For the period 1 March 1964 to 31 December 1966, REPs producing absorption $\geq$ 8 db occurred on 319 days with maxima at equinoxes and minima at solstices. The 93 medium and large REPs (absorption $\geq$ 14 db) for the same period are not associated with sudden commencement (SC) geomagnetic storms, but the events mostly occurred on magnetically disturbed days, lasted from 1-6 hours (with some seeming to last 24 hrs) and were mainly confined to the 12 hour period centered on local noon.

After 1967, the system detection capability became erratic due to the increasing solar activity. The system was terminated for various additional reasons early in 1973 (Sullivan, 1979). Attempts were made to obtain some 1969 forward scatter data for correlation and calibration with OV1-19 satellite spectrometer data (see Appendix A) but all of the forward scatter data except for the first five months of 1969 had been lost (Lincoln, 1978).

In 1968-1971, the Norwegian Defense Research Establishment (NDRE) undertook a program entitled "Omega Research in Norway" (Larsen, 1973). This program monitored the VLF (12.3 kHz) short hop (433 km) path between the transmitter at Aldra, $\Lambda = 63.7^{\circ}$ ($L \sim 5.1$), and the receiver at Tromsø, $\Lambda = 66.5^{\circ}$ ($L \sim 6.3$), both in Norway, for PCA, substorm, REP, and stratospheric warming research. Phase recordings of the VLF signal perpendicular (to propagation plane) and parallel magnetic components provide sensitive detection of ionization variations below the scattering altitude of about 60-65 km daytime and 80-90 km nighttime (Larsen, 1973). A diurnal effect is seen as an advance shift in baseline of 60-80 μsec from local night to day. REPs (and PCA/solar flare events) are readily observed both day and night as phase advances beyond the normal undisturbed levels.

Thorne and Larsen (1976) compared the Norwegian VLF and Alaskan HF observations of REPs and Auroral Electrojet (AE) Indices (for substorm identification) for the period January-May, 1969. They indicate "...a direct correlation between the onset of intense nighttime REP events with substorms while dayside REPs are far less frequent, are shorter in duration and are often delayed by as much as several hours from the onset of substorm activity" (Thorne and Larsen, 1976). Figure 3 shows for example, a simultaneous increase in AE and VLF phase advance in Norway at 2100 UT followed 1-1 1/2 hrs later by the HF absorption in Alaska. This sequence agrees with the observation of the 25-26 August 1967 substorm by Hones et al., (1971) but not their inference of gradient drifting electrons injected at substorm onset since the gradient drift lifetimes of relativistic electrons are on the order of minutes (Thorne and Larsen, 1976). In addition, only a select class of substorms can trigger dayside REPs (Rosenberg et al., 1972; Thorne and Larsen, 1976) and substorm intensity is only weakly correlated in the selection of which substorm will spawn a REP (Thorne and Larsen, 1976).

Many observers using riometers (Brown, 1964; Jelly and Brice, 1967) and chains of riometers (Ansari, 1965; Lukkari et al., 1975; Lukkari and Kangas, 1976; Lukkari et al., 1977) have observed similar relations between subauroral energetic electron precipitation and slowly varying absorption (SVA), substorm onsets, and magnetic pulsations. Riometers observe total absorption occurring both above and below the scattering altitudes of VLF and HF systems and alone cannot determine where (in altitude) the absorption occurs nor yield a precise precipitation spectrum (Bailey, 1968).

Balloon-borne measurements of X-rays during REP events (usually with uncollimated NaI detectors near 32 km altitude) have the advantage over riometer measurements in sensitivity, time resolution, and the fact that they provide an

FIG 3. Time sequence of (A) HF absorption (dark shaded area) in Alaska; (b) VLF phase advance (shaded) from normal nighttime trace (dashed line); (c) AE index for 13-14 March 1969 from Thorne and Larsen, 1976.

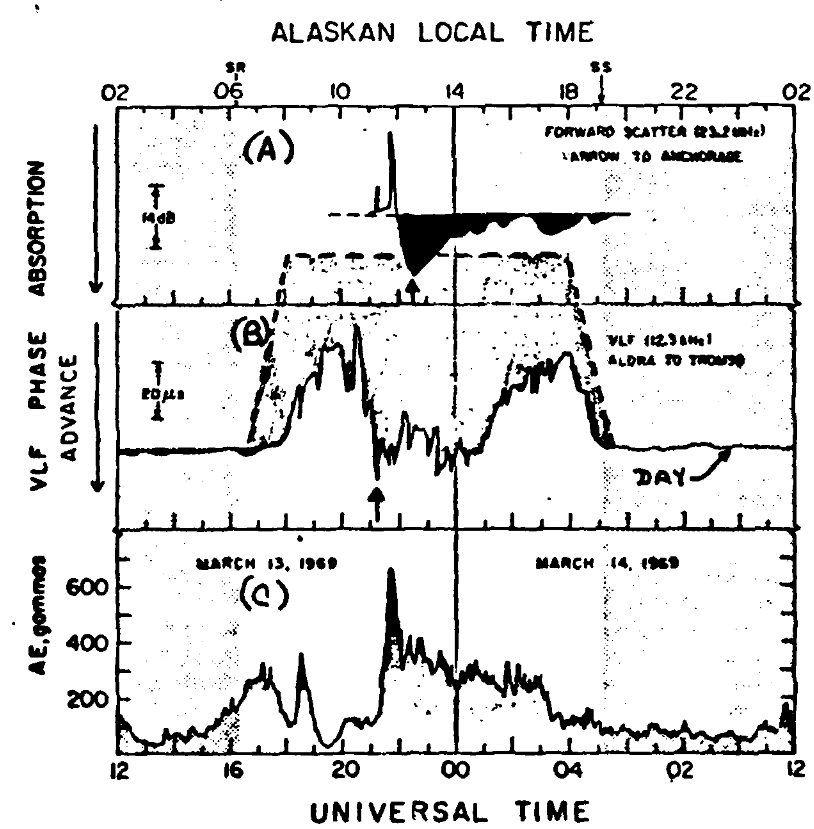
ALASKAN LOCAL TIME
SR
SS
02
06
10
14
18
22
02
(A)
FORWARD SCATTER (23.2 MHz)
ABSORPTION
14 dB
(B)
VLF PHASE ADVANCE
20 μs
DAY
MARCH 13, 1969
MARCH 14, 1969
(C)
AE, gammas
600
400
200
12
16
20
00
04
02
12
UNIVERSAL TIME

energy spectrum (Bewersdorff et al., 1968). In addition to the disadvantages of imprecise balloon location (~ 100 km horizontally) and proton contamination of X-ray scintillators, the theoretically predicted X-ray spectrum (the scintillator measures mostly secondaries) is very sensitive to the assumed incident electron spectrum, usually in exponential form (~ exp E/Eo), and atmospheric depth (Bailey et al., 1970). Only six or seven X-ray measurement deduced electron energy spectra during energetic electron precipitation events have published and range from spectra constructed by the addition of soft (Eo = 9 KEV) and hard (Eo = 40 KEV) components (Bailey et al., 1970) to very hard (Eo = 180-200 KEV) spectra (Rosenberg et al., 1972; Parks et al., 1979).

Rockets have carried spectral and integral electron spectrometers (Matthews and Simons, 1973; Vij et al., 1975; Matthews et al., 1976) as well as having boosted parachute-borne X-ray scintillators (Vij et al., 1975) during REP and auroral events. Simultaneous electron (rocket to 275 km apogee) and X-ray (rocket boost to 60 km) observations show fair agreement at least in the much "softer" auroral events (Vij et al., 1975). The spectrometers yield a more precise electron energy spectrum and, depending on instrument orientation and flight configuration, add pitch angle distribution information. An obvious drawback of this type of experiment for REP research is the lack of morphological statistics due to prohibitive logistics expense.

Satellite X-ray spectrometer experiments provide simultaneous measurements over a wide range of local times because of their extensive fields of view (Imhof et al., 1974) as well as opportunities for coordinated studies with particle spectrometers for improved spatial/temporal resolution (Imhof et al., 1975). Comparison of X-ray and particle measurements show agreement to only a few hundred keV and that impulsive (< 5 min duration) events near the energetic trapping boundary were substorm correlated (Imhof et al., 1978). Coordinated two satellites X-ray and particle measurements show significant variations in local time dependence of energetic electron precipitation though fluxes seemed greater in late morning than early morning.

The majority of satellite REP measurements have been made with integral (Brown and Stone, 1972; Larsen and Thomas, 1974; Morfill et al., 1975) and spectral (Vampola, 1969; Vampola, 1971 a band b; Imhof et al., 1973; Imhof et al., 1975) particle spectrometers. REP precipitation is observed to be a narrow ($\Delta L \sim .5\text{-}1.5$) phenomenon. Figure 4 shows an invariant latitude versus magnetic local time plot of electron precipitation spikes with E > 425 keV from the last five months of 1967 from the low polar orbit satellite OGO 4 (Brown and Stone, 1972). Notice a relative scarcity of events between 06-12 MLT. Also, the events extend from approximately the middle of the outer electron zone to the limit of closed field lines with the highest density clustered about the limit of stable trapping. A general shift to lower invariant latitudes is observed with increasing geomagnetic activity. Event time scales range from several minutes to several hours. Approximately five times as many events occur at 2200 MLT as at 1000 MLT. This study was extended by the use of the > 500 keV measurements on board another low polar orbit satellite ESRO 4 with similar results (Morfill et al., 1975).

Another investigation of magnetic electron spectrometer data of precipitating electrons in the energy range 225 keV < E < 2.47 MeV aboard polar orbit satellite OV3-3 for the period August 1966-September 1967 show common occurrences of precipitation at local evening and midnight in a narrow region ($\Delta L \sim 0.5$) at the local limit of trapping (Vampola, 1971). Rare events (3) at local evening just inside the plasmapause where higher energy electrons (> 1 MeV) are preferentially precipitating were also found.

Measurements of precipitating electrons from > 48 keV to > 434 keV on the polar orbit satellite ESRO 1A during the REP of 2 February 1969 at local morning at $\Lambda = 63^{o}$-70^{o} (L = 4.9-8.5) have been reported by Larsen and Thomas (1974). The energy spectrum for this event is a bit "harder" than those previously obtained by rocket measurements (Matthews and Simons, 1973) but much harder than those deduced from balloon X-ray measurements (Bailey et al., 1970).

Figure 5 compares REP energy spectra from various sources previously discussed with typical discrete and diffuse auroral spectra (Lui et al., 1977). Satellite-borne spectrometers, particularly spectral spectrometers, have measured the hardest spectra in comparison with non satellite spectra and represent the most direct means of examining REPs of all intensities.

FIG 4. Latitude-local time plot of all 425 keV electron spike observations from Brown and Stone, 1972.

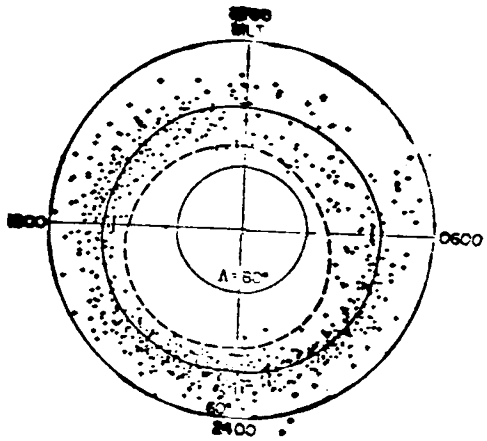
0600
2400
60°

FIG 5. Differential energy spectra of precipitating electrons of the following types: (A) Diffuse aurora (Lui et al., 1977); (B) Discrete aurora (Lui et al., 1977); (C) Balloon X-ray (Bailey et al., 1970); (D) Rocket (Matthews and Simons, 1973); (E) Satellite (Larsen and Thomas, 1974); (F) Satellite (Vampola, 1971).

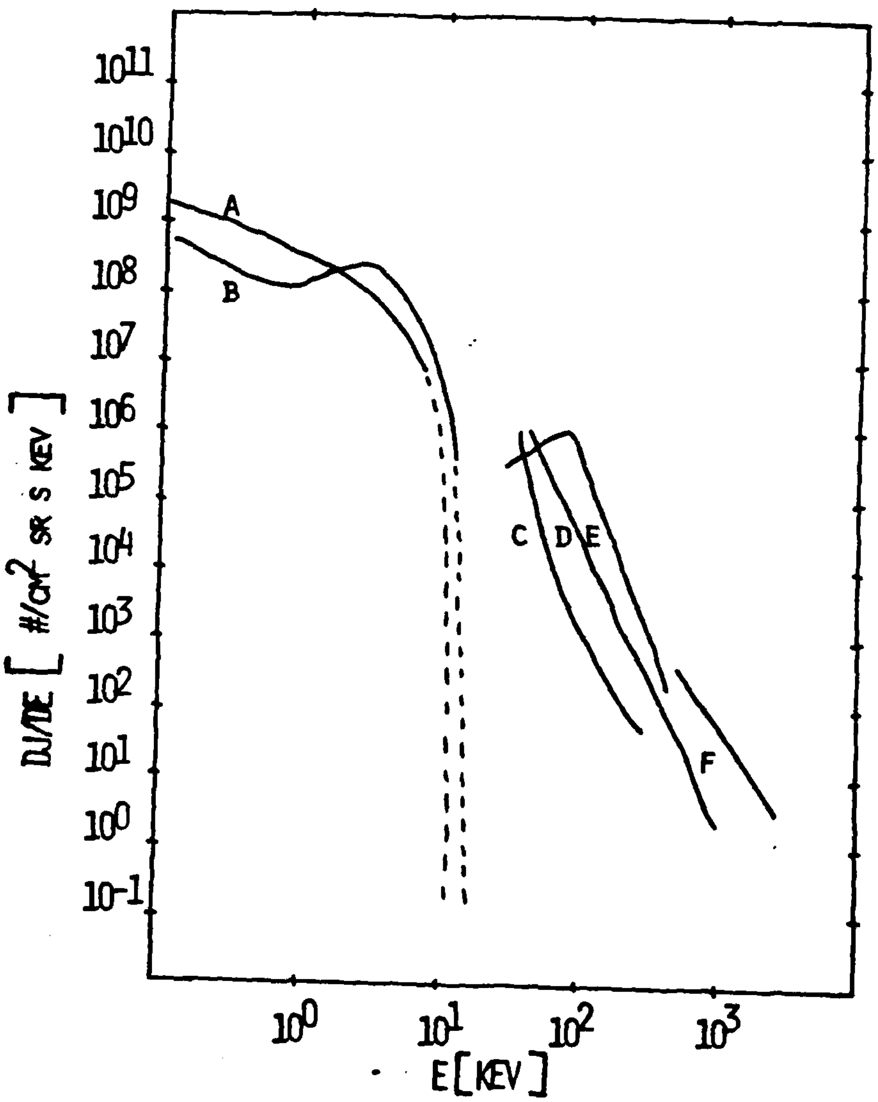

10^{11}
10^{10}
10^{9}
10^{8}
10^{7}
10^{6}
10^{5}
10^{4}
10^{3}
10^{2}
10^{1}
10^{0}
10^{-1}
DJ/DE [#/CM^2 SR S KEV]
A
B
C
D
E
F
10^{0}
10^{1}
10^{2}
10^{3}
E [KEV]

It was the purpose of this dissertation to determine the mechanisms responsible for REP events, their relative importance and atmospheric consequences through the study of satellite data. Magnetic electron spectrometer data on the low polar orbit satellites OV1-19 and S3-3 were graciously provided by the instrument builder and prime investigator, A. L. Vampola, Aerospace Corp., El Segundo, Ca. An exhaustive study of the OV1-19 data set was performed but for various reasons the data set yielded only marginally significant results. This study is described in detail with results in Appendix A. The S3-3 data set has few of the drawbacks of the OV1-19 data set and is the main source of study here. The S3-3 satellite orbit and orientation as well as particle and wave measurements are described in Appendix B.

This thesis is arranged with four main chapters. In Chapter 1, details of the S3-3 REP event morphology are presented. A description of the objective and subjective analysis of the data needed to identify events is contained in Appendix C.

Chapter 2 contains a general background of the types of mechanisms previously postulated and others newly discovered capable of explaining REPs. The mechanisms are compared with the classes of events found in Chapter 1. In addition, a case study of each type is presented with the view of advancing the knowledge of each mechanism.

Chapter 3 compares the atmospheric energy deposition profiles for REP and REP X-rays with profiles from other sources.

Profiles for REPs of various classes and intensities are presented as well as determinations of their importance and consequences in ionization production and ozone chemistry. The electron and X-ray deposition calculations are presented in Appendix D.

Chapter 4 summarizes the findings and discusses the conclusions and outlooks.

CHAPTER 1. EVENT MORPHOLOGY

1.1 Results

We present here the statistical data on REP occurrence measured on S3-3 during a 14 month period from 11 July 1976 to 29 September 1977. The S3-3 data collection specifications are described in Appendix B. The methodology of selecting REPs as well as the data base description is provided in Appendix C. Fig. 1.1, a-c, shows a summary of the S3-3 data set; the plot includes daily values of the highest energy channel (in keV) exhibiting strong diffusion precipitation (Panel A); the daily number of outer zone (L=4-8) passages (Panel B); the daily mean of the hourly equatorial DST in gamma units (Panel C); and the daily Ap, equivalent daily planetary magnetic amplitude in 2 gamma units (Panel D). Outer zone coverage (Panel B) was fairly uniform throughout the data set (although 29 days had no coverage) averaging a little over 5 outer zone passages per day. Coverage was a function of tape recorder capacity, power limitations, microfiche availability, etc. DST and Ap are presented to represent the relative magnetic condition of the magnetosphere since AE, the Auroral Electrojet Index, was not yet available for this time period. AE indices for five stations, AE (5), for seven 2 day periods in 1977, however, were available and are discussed in the next section. (Allen, private communication, 1979.)

1.2 Frequency of Occurrence and Magnetic Dependence

The monthly average frequency of occurrence of REP events observed during the satellite transit of the outer radiation zone (L=4-8)

FIGURE 1.1a,b,c. Daily values from 11 July 1976 to 29 September 1977. Plots are given of REPs with highest energy channel exhibiting strong diffusion (Panel A); the total number of outer zone passings, L=4-8 (Panel B); daily mean of the hourly Dst, γ (Panel C); Ap, equivalent daily planetary magnetic index, 2γ (Panel D).

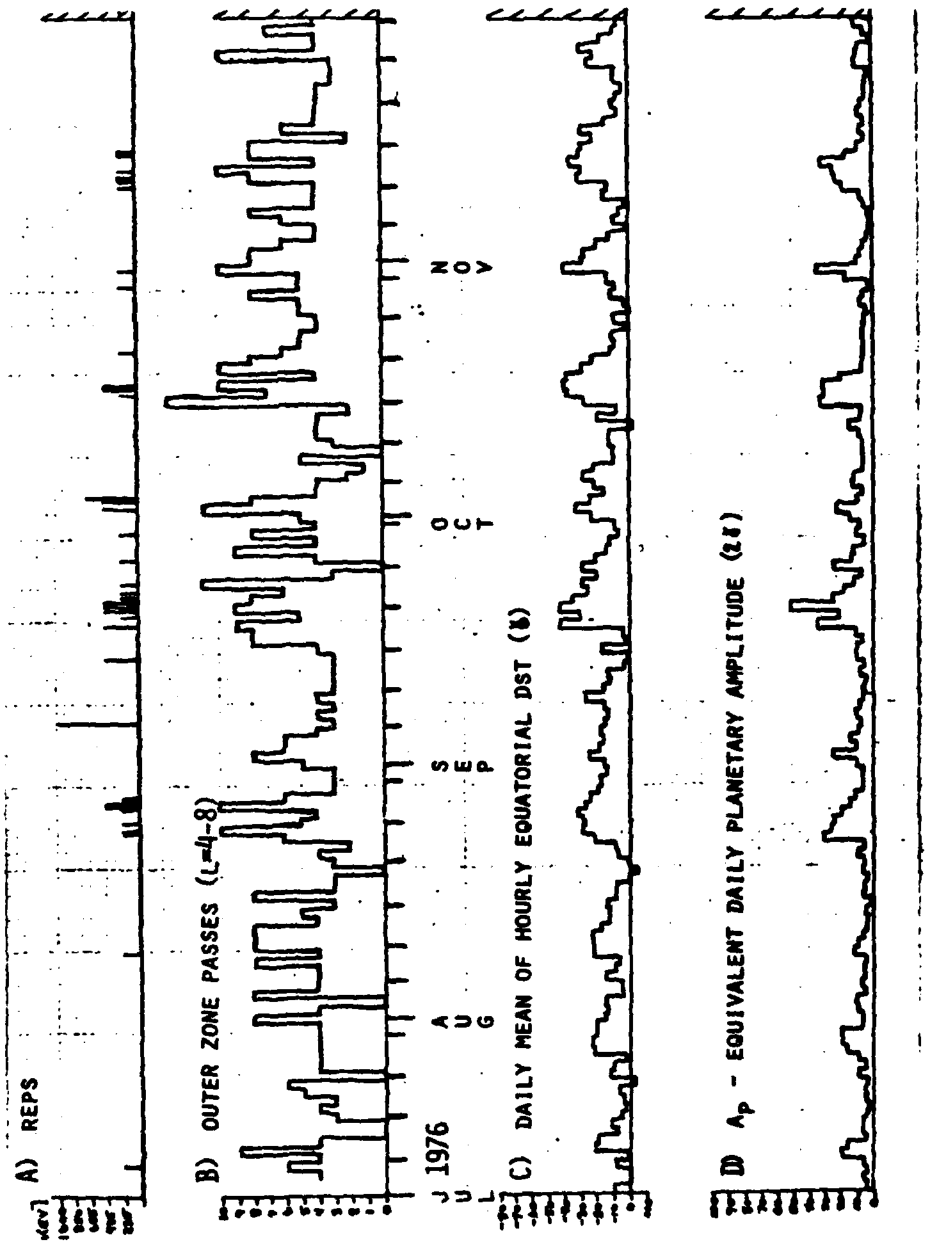
A) REPS
B) OUTER ZONE PASSES (L=4-8)
C) DAILY MEAN OF HOURLY EQUATORIAL DST (γ)
D) A_p - EQUIVALENT DAILY PLANETARY AMPLITUDE (2γ)
1976
JUL
AUG
SEP
OCT
NOV

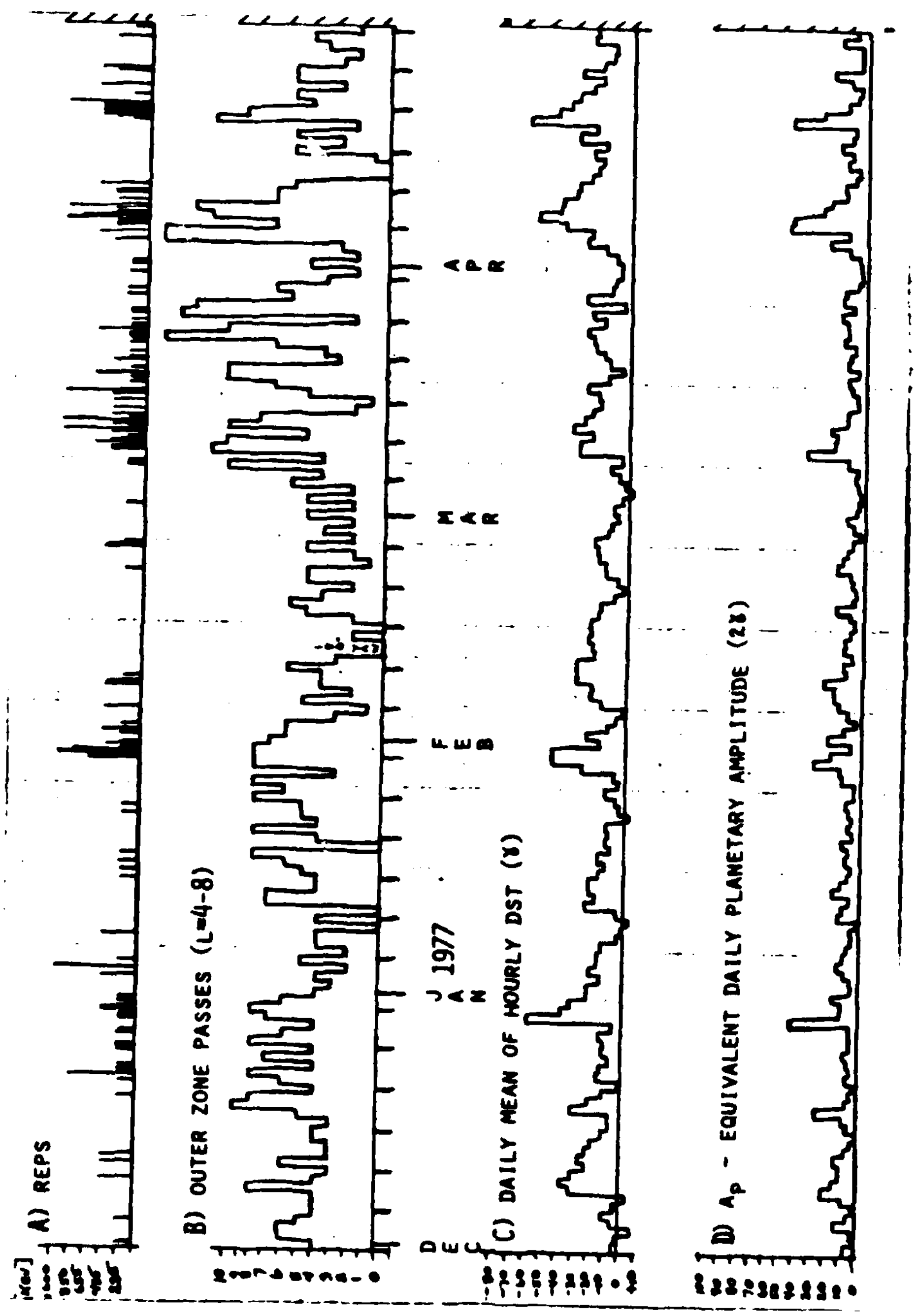
A) REPS
B) OUTER ZONE PASSES (L=4-8)
C) DAILY MEAN OF HOURLY DST (γ)
D) A_p - EQUIVALENT DAILY PLANETARY AMPLITUDE (2γ)
DEC
JAN 1977
FEB
MAR
APR

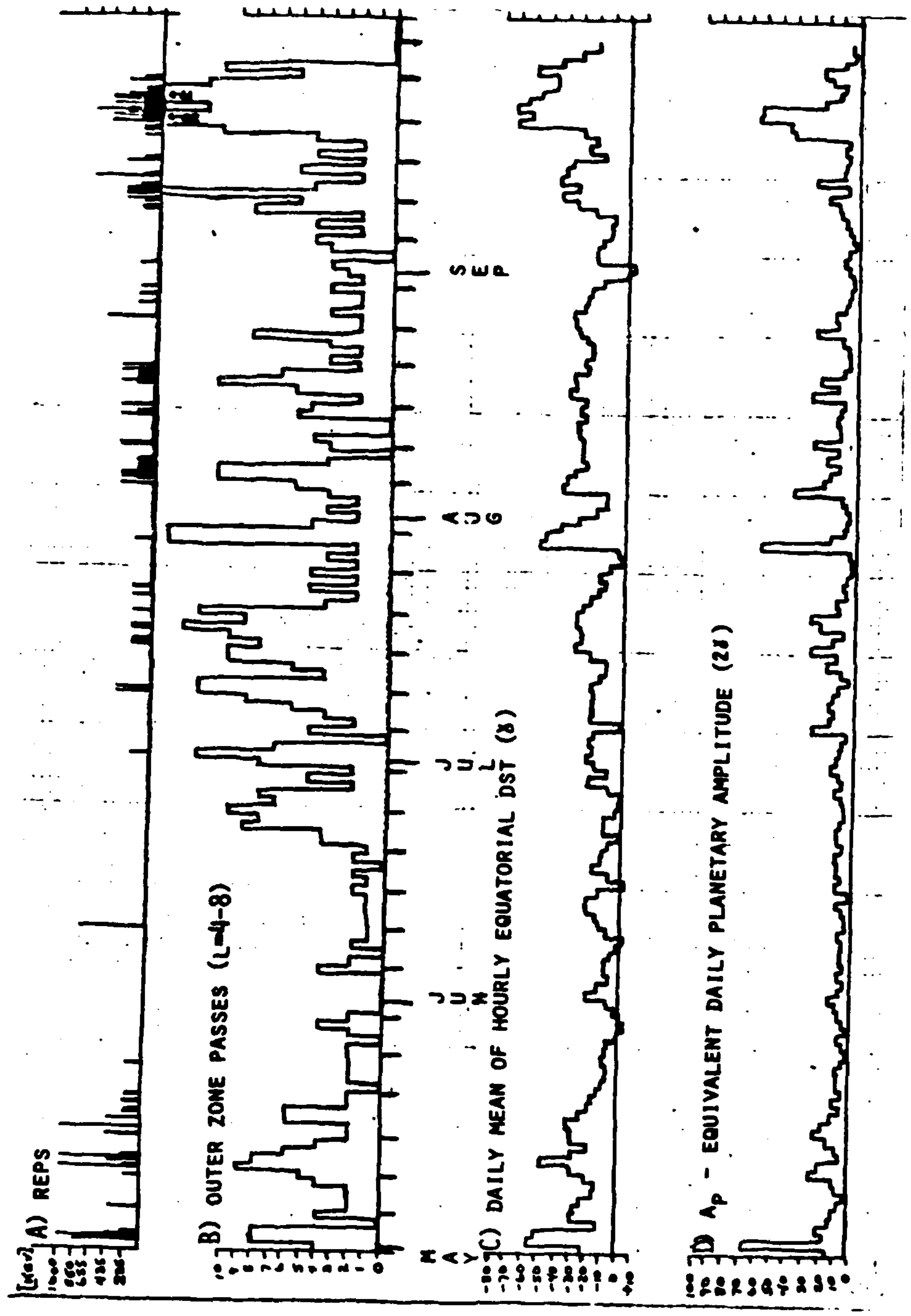
A) REPS
B) OUTER ZONE PASSES (L=4-8)
C) DAILY MEAN OF HOURLY EQUATORIAL DST (γ)
D) A_p - EQUIVALENT DAILY PLANETARY AMPLITUDE (2γ)
MAY
JUN
JUL
AUG
SEP

is represented in Fig. 1.2. Maximum occurrence is found near both (1976, 1977) autumnal equinoxes, at and slightly beyond vernal equinox, and near winter solstice while pronounced minima are evident near both (1976, 1977) summer solstices. This is generally consistent with the equinoxial maxima and solstice minima found by Bailey (1968). In this sense, the winter maxima is anomalous, but approximately five strong magnetically disturbed periods took place in Dec 1976-Jan 1977 (see Fig. 1.1b) probably accounting for the rise in activity. The magnetic dependence is apparent when the same monthly percentage of REPs normalized to outer zone coverage is plotted for days when $Ap > 30$ (Panel A), $20 \leq Ap < 30$ (Panel B), $10 \leq Ap < 20$ (Panel C), and $Ap < 10$ (Panel D) in Fig. 1.3 The anomalous winter maximum in Dec is apparent for $30 < Ap < 20$ while the Jan maximum is seen only for $20 < Ap < 30$. The remaining maxima and minima are fairly consistent with magnetic conditions.

Plotting the REP occurrence frequencies for all 14 months for different ranges of Ap (magnetospheric disturbance) (Fig. 1.4), one sees a nearly linear increase in REP occurrence with magnetic disturbances.

Fig. 1.5 shows S3-3 coverage of seven 2 day periods by AE index (Allen, private communication, 1979). This data is merely presented to support the fact that not all substorms trigger REPs (note particularly Panels A and E) in agreement with the findings of Rosenberg et al. 1972) and Thorne and Larsen (1976). The local times of collections for both Panels A (1 outer zone pass per rev) and E (2 outer zone passes

FIGURE 1.2 Monthly REP event percentage of occurrence normalized to outer zone coverage for July 1976-September 1977.

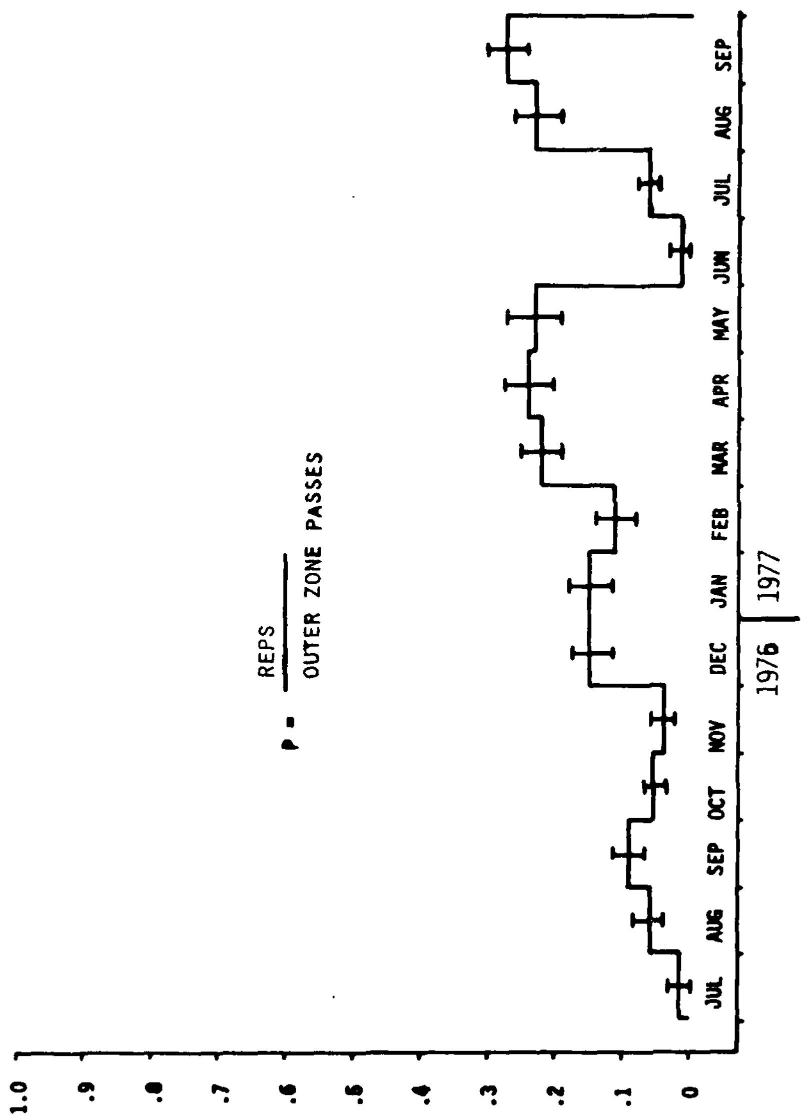
P = REPS / OUTER ZONE PASSES
1.0
.9
.8
.7
.6
.5
.4
.3
.2
.1
0
JUL
AUG
SEP
OCT
NOV
DEC
JAN
FEB
MAR
APR
MAY
JUN
JUL
AUG
SEP
1976
1977

FIGURE 1.3 Monthly percentage of REPs normalized to outer zone crossings (L=4-8) for magnetic conditions: $Ap > 30$ (Panel A); $20 \leq Ap < 30$ (Panel B); $10 \leq Ap < 20$ (Panel C); $Ap < 10$ (Panel D). Values for JAN and FEB in Panels A and B overlap. P=0 for both JAN and FEB in Panel A and P=0.86 and 0.39 for JAN and FEB respectively in Panel B.

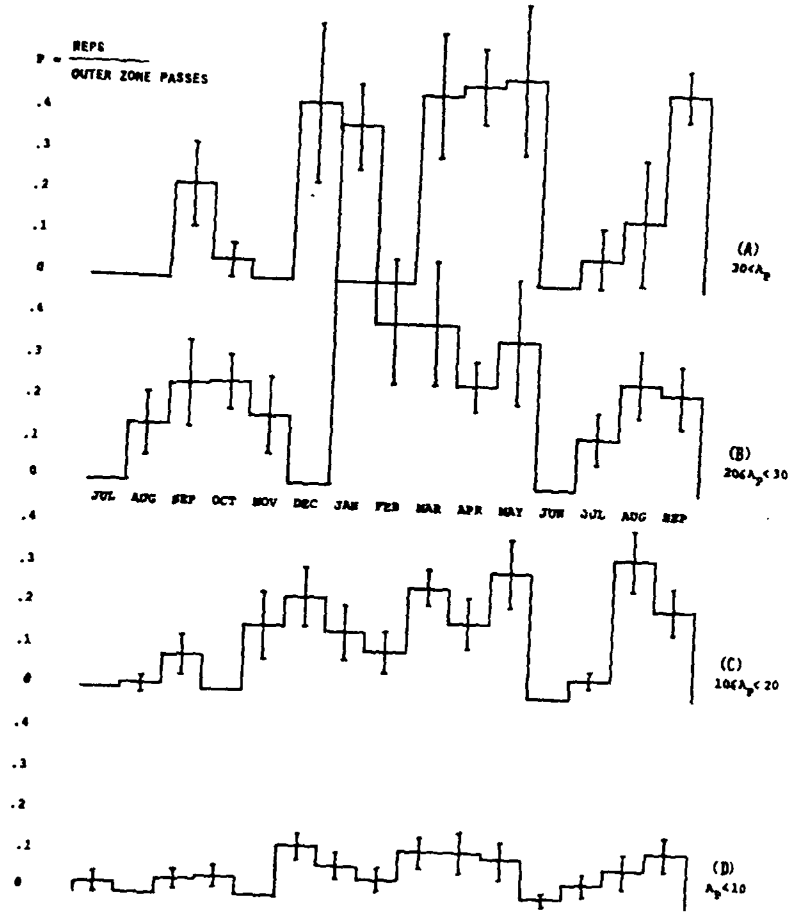
P = REPS / OUTER ZONE PASSES
(A)
30<A_p
(B)
20<A_p<30
JUL AUG SEP OCT NOV DEC JAN FEB MAR APR MAY JUN JUL AUG SEP
(C)
10<A_p<20
(D)
A_p<10

FIGURE 1.4 REP event percentage of occurrence normalized to outer zone coverage (L=4-8) versus magnetic conditions for all months JUL 1976-SEP 1977. Total number of outer zone passes for each category are in parentheses.

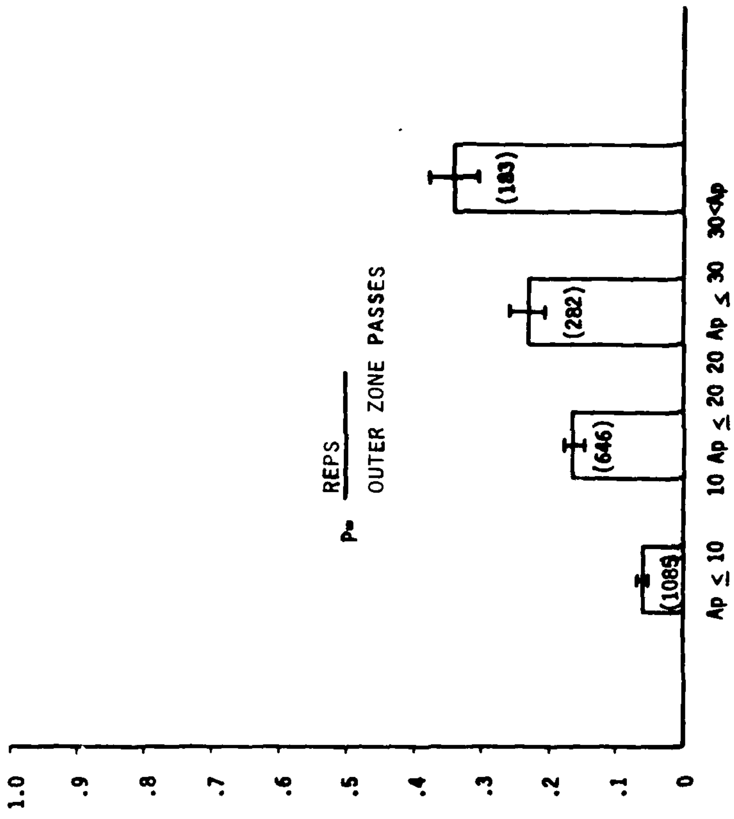
P=
REPS
OUTER ZONE PASSES
1.0
.9
.8
.7
.6
.5
.4
.3
.2
.1
0
Ap ≤ 10
10 Ap ≤ 20
20 Ap ≤ 30
30<Ap
(646)
(282)

FIGURE 1.5 Seven 2 day periods of AE index (γ) throughout 1977 with REPs indicated by arrows (↑) and hours of noncoverage by shaded horizontal bar (▬). AE = AU (Upper Trace) - AL (Lower Trace).

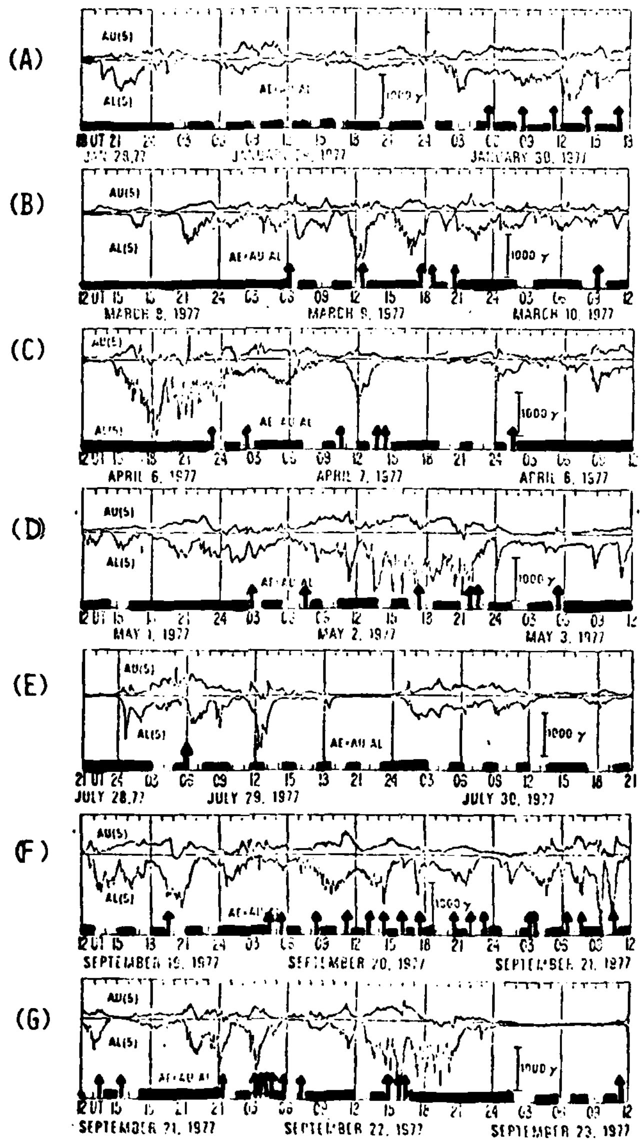
(A)
(B)
(C)
(D)
(E)
(F)
(G)
AU(5)
AL(5)
1000 γ
MARCH 8, 1977
MARCH 10, 1977
APRIL 6, 1977
MAY 1, 1977
MAY 3, 1977
JULY 28,77
JULY 29, 1977
JULY 30, 1977
SEPTEMBER 21, 1977
SEPTEMBER 22, 1977
SEPTEMBER 23, 1977

per rev) occurred near midnight where one would expect highest probability of detection (see Fig. 1.7 for example). Many of the outer zones, particularly the outer edge, in the passes of Panels A and E were very irregular showing trapped flux variations to nearly an order of magnitude though no precipitation was evident at the time of the pass. Also noticeable are times when substorms with large values ($\sim 900\gamma$) of AE do not spawn REPs (03-04L, 30 Jan 77, Panel A; 12-14L, 29 Jul 77, Panel E; 03-11L, 30 Jul 77, Panel E; 13-18L, 19 Sep 77, Panel F) while substorms corresponding to smaller AE may be associated with REPs (08-10L, 10 Mar 77, Panel B; 01-02L, 8 Apr 77, Panel C; 05-06L, 3 May 77, Panel D; 04-06L, 20 Sep 77, Panel F; 11-12L, 23 Sep 77, Panel G). This agrees again with Thorne and Larsen's (1976) finding of weak correlation between AE index and REP observations. An exception to this correlation is the REP activity at 03-04L, 22 Sep 77, Panel G, where a 1500 γ storm has associated REP activity for all four outer zone passes on the same revolution (see event catalogue, Appendix C, REV P 3569). This orbit was oriented in the 0200 and 1400 hrs MLT plane and could infer a longitudinal extent of nearly 10,000 km.

1.3 Local Time Dependence and Latitudinal Extent

To examine the local time morphology, REPs (Fig. 1.1, Panel A) were plotted for a given date versus magnetic local time (MLT) in Fig. 1.6. In order to test for any bias in the excursion of the orbit plane with time (skewed solid lines), we have sketched (hatched areas) the span of local times over which REPs could be observed in the range $4 \leq L \leq 8$ for a given local time orientation of this orbit plane. A

FIGURE 1.6 REPs by date versus MLT (hrs). Hatched area indicates regions of coverage ($4 \leq L \leq 8$) around the local time of the orbit plane (skewed solid line).

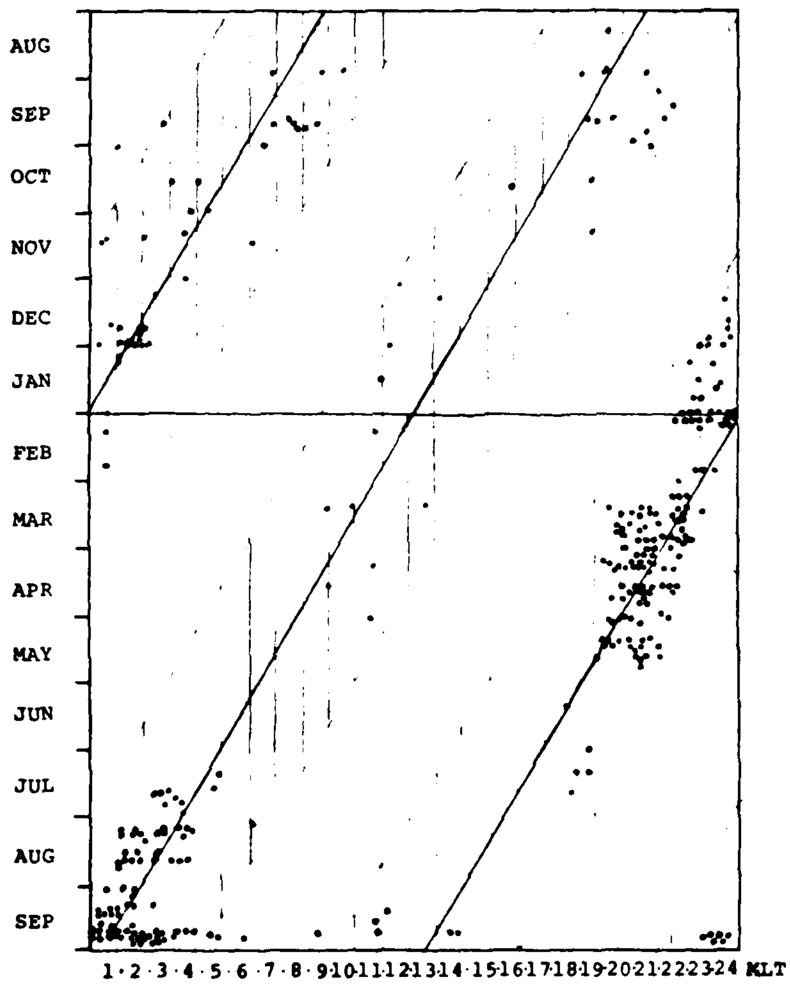
AUG
SEP
OCT
NOV
DEC
JAN
FEB
MAR
APR
MAY
JUN
JUL
AUG
SEP
1 2 3 4 5 6 7 8 9 10 11 12 13 14 15 16 17 18 19 20 21 22 23 24 MLT

possible apogee-perigee bias in the orbit plane was investigated but after careful analysis (see Appendix C) the bias was found to be insignificant. The most striking feature is the pronounced night-day asymmetry with the greatest number of REPs occurring in the night sector. A plot of the ratio of day to night REPs is presented in Fig. 1.7 as a function of magnetically disturbed conditions. Overall there is a 9:1 preference for nighttime REP events. This local time asymmetry is less for highly disturbed (Ap > 30) conditions.

The actual local time morphology of REP events is shown in Fig. 1.8 (dots indicate very narrow localized events and lines are drawn for extended events) where they are plotted against invariant latitude for varying magnetic conditions. Most events show narrow latitudinal extends ~0.5L (dots) while a few showed excursions up to 4-5L, mostly in the 235, 435 keV electron channels. Readily apparent is the relative lack of dayside REPs particularly during magnetically quiet days (Ap $\leq$ 10). Furthermore, the scarcity of REPs over the local time range 1300-1900 remains apparent for Ap $\geq$ 10. As can be seen from Fig 1.6 the orientation of the orbit plane for these MLTs covered roughly all months except the Mar-May maxima. Both autumnal equinoxes and the anomalous Dec-Jan maxima were covered so we believe that the statistics for the local afternoon hours are not biased by the orientation of the orbit plane: thus the tenuous afternoon statistics appear to be real. Also, for highly disturbed conditions (Ap $\geq$ 20) the event location moves towards lower invariant latitudes; this is most noticeable for Ap > 30.

FIGURE 1.7. Ratio of day (MLT 06-18) to night (MLT 18-06) for varying magnetic conditions.

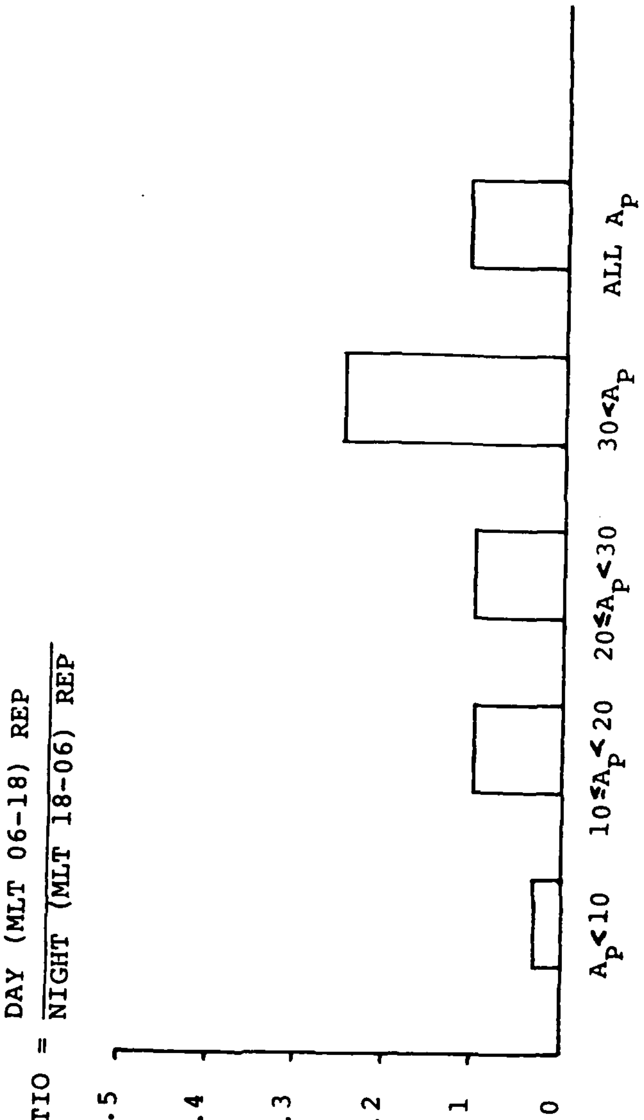
RATIO = DAY (MLT 06-18) REP / NIGHT (MLT 18-06) REP
.5
.4
.3
.2
.1
0
$A_P < 10$
$10 \leq A_P < 20$
$20 \leq A_P < 30$
$30 < A_P$
ALL A_P

FIGURE 1.8 REPs displayed by invariant latitude (degrees) versus MLT (hrs) for varying magnetic conditions. Lines indicate excursions of events in invariant latitude.

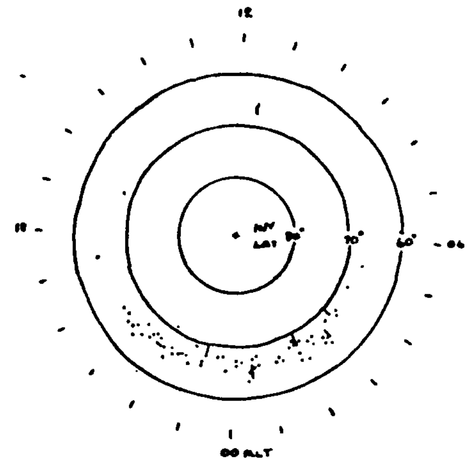

$A_p \leq 10$

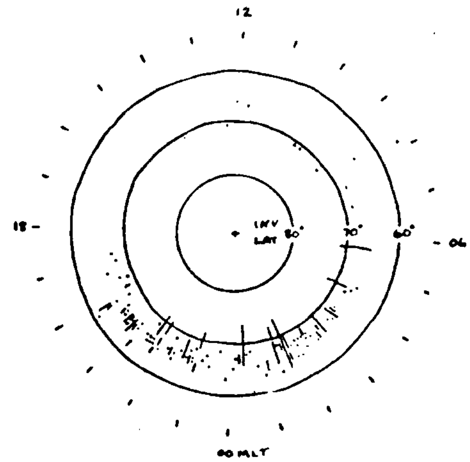

$10 < A_p \leq 20$

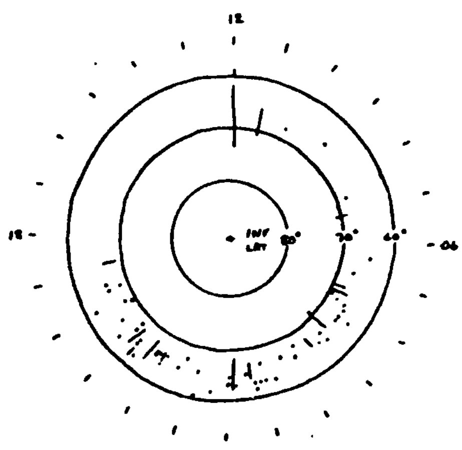

$20 < A_p \leq 30$

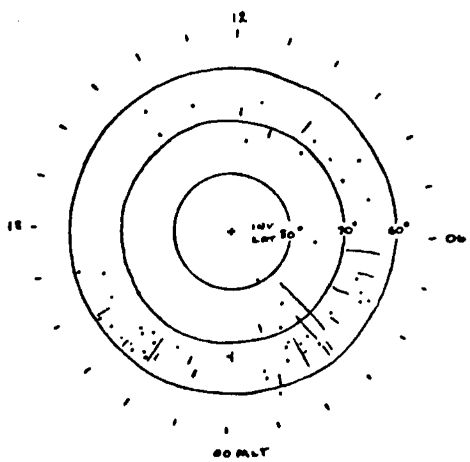

$A_p > 30$

1.4 Longitudinal Extent

The slow (1.5 hr/month) excursion of the orbit plane in local time (see Appendix B) does not allow direct analysis of longitudinal extent. Estimates, however, can be made from previously published ground based events (e.g. Bailey, 1968) though these would probably be a lower limit. In addition, general limits could be estimated on an individual case basis from the satellite revisit times (~3 hrs) where consecutive coverage exists.

Duration of ground based REP events was observed to be 1-6 hrs with some events lasting for 24 hrs (Bailey, 1968). Several S3-3 REPs seemed to last for 24 hrs but continuity of these events is uncertain since events can occur over a period of many substorms (e.g. Fig 1.5, Panel F). The maximum longitudinal extent at 60^{o} latitude is approximately 20,000 km. Bailey's 1 hr lower limit translates into 850 km which roughly agrees with Larsen's (1973) estimate of REPs extending greater than 1000 km. The 6 hour duration estimate translates to a 5,000 km longitudinal extent. For very disturbed times, all four outer zone crossings on the same 3 hour rev were on strong diffusion (see Fig 1.5, Panel (G), 22 Sep 1977, 0300-0500 UT) indicating longitudinal extents of 10000-15000 km.

1.5 REP - Proton Precipitation Correlation

In scanning through the data set it was immediately apparent that there was a high correlation between electron and proton precipitation (see catalogue remarks, Appendix C). Particularly noticeable was the similarity between precipitating fluxes in the 235 and 435 keV electron and the 80 keV proton channels. An example of this feature is presented in Fig 1.9 which shows the 12, 33, 235 keV electron channel and 80 keV proton channels for 30 Jan 1977. The 12 keV electrons are precipitating from 19590 UT to 20565 UT. Precipitation features for 33 and 235 keV electrons and >80 keV proton are evident at 19646-19700 UT, 19815 UT, and 20475 UT (proton precipitation began at 19580 UT). This suggests the precipitation mechanism for both electrons and protons may be either related or identical. Protons did, however, precipitate much more frequently than electrons and their zone of strong diffusion precipitation generally extended to lower latitude. This frequency difference can be readily seen in Fig 1.10 where the revs (1-4 outer zone passes per rev) with strong electron (E^-_{precip} > 235 keV) and proton (E^+_{precip} > 80 keV) precipitation normalized to the number of revs is plotted for increasingly disturbed magnetic conditions. Note that proton precipitation is seen on 65% of revs while electrons on 22% of revs for all magnetic conditions. The high occurrence of proton precipitation in the energy range (100-200 keV) has been previously observed (e.g. On ESRO 1A, Lindalen et al., 1971).

1.6 Classification of REP Events

Due to the strong correlation of REPs with proton (>80 keV) precipitation, the data set was analyzed for REPs without concurrent strong proton precipitation. Only 7 of 313 outer zone passes fell in this category. In addition, all 7 cases had concurrent 33 keV electrons precipitating on strong diffusion and were found at altitudes below 1500 km.

FIGURE 1.9 Flux versus UT plot of 12, 33, 235 keV electrons and 80 keV protons for rev 1656 30 Jan 1977

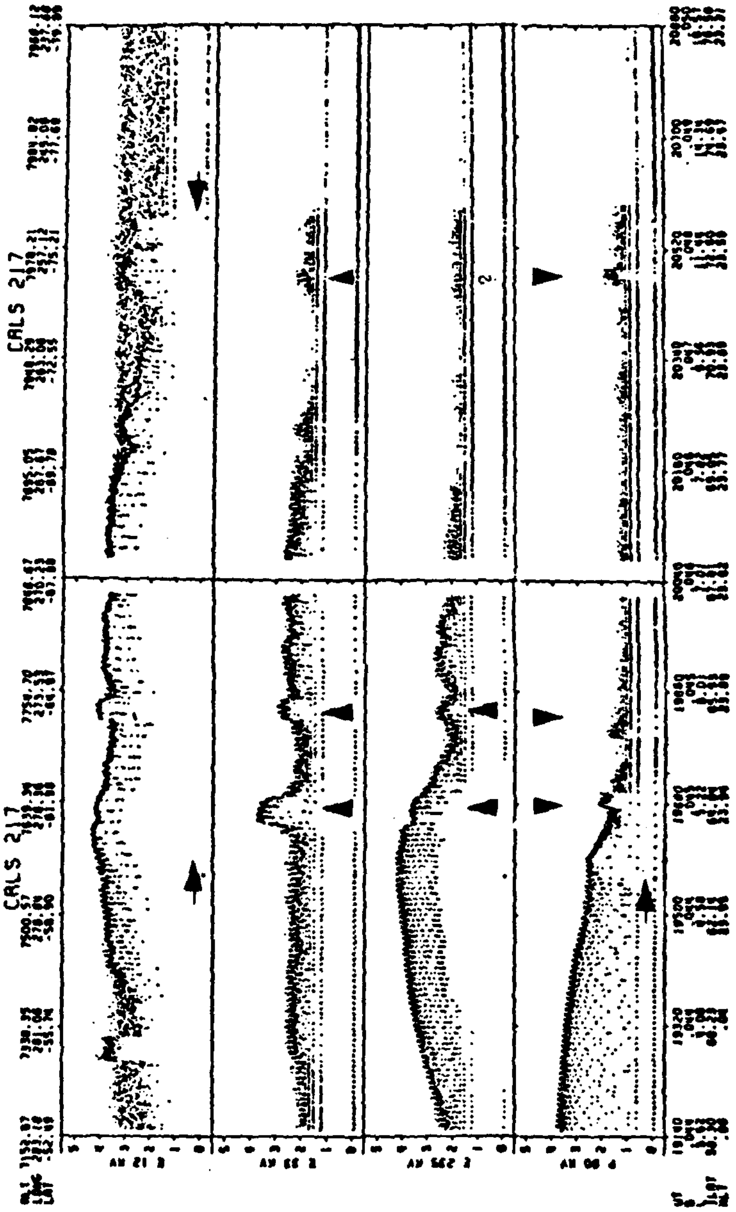
CALS 217
CALS 217

FIGURE 1.10 Percentage of revs (1-4 outer zone passes) with strong e^- or p^+ precipitation normalized to revs number by magnetic conditions.

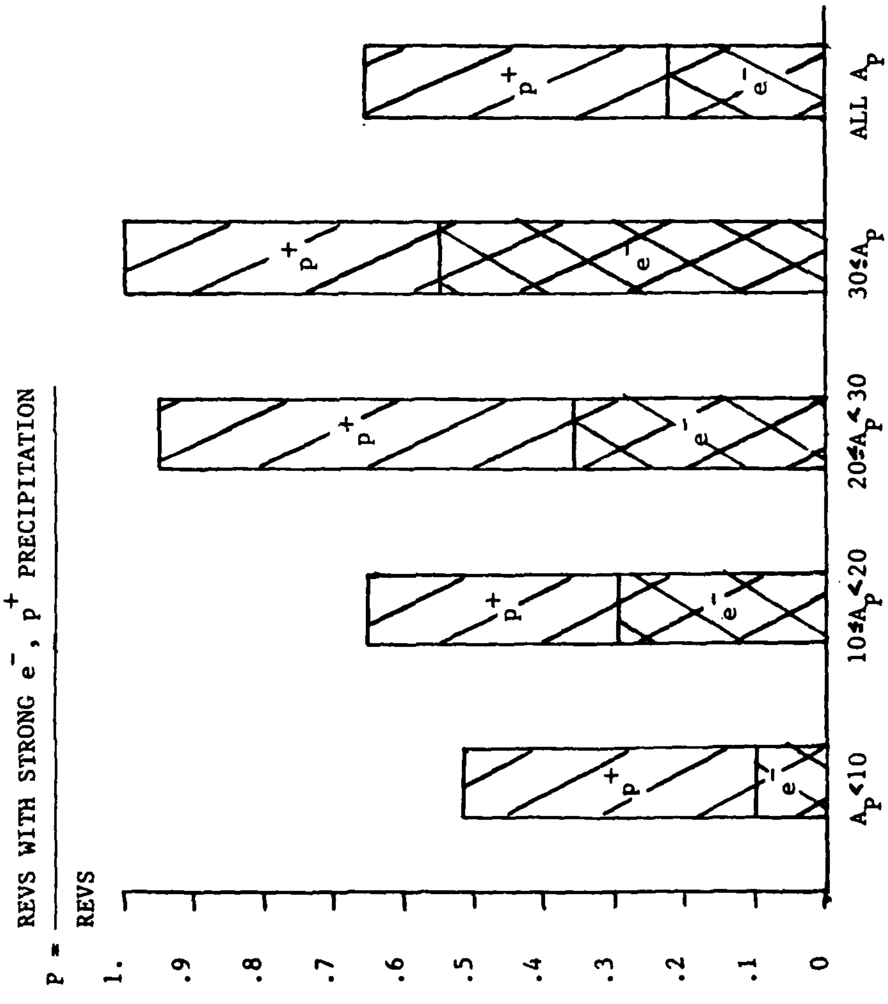

P = REVS WITH STRONG e⁻, p⁺ PRECIPITATION / REVS
1.
.9
.8
.7
.6
.5
.4
.3
.2
.1
0
p⁺
e⁻
A_p<10
10≤A_p<20
20≤A_p<30
30≤A_p
ALL A_p

Analysis of REP energy dependence revealed that the overwhelming majority of REPs had energies in the range 235-1000 keV on strong diffusion. Only 4 events had spectra such that only energies above 1 MeV were on strong diffusion. These same 4 cases were different in another way. They occurred equatorward of the outer edge of the outer zone; the remaining cases except for the seven above all occurred right at the outer edge or extended inward from the outer edge.

The four cases with strong precipitation only above 1 MeV were not among the seven cases which showed no concurrent proton precipitation. REPs could thus be divided into three distinct classes: those with strong diffusion precipitation below (302) and only above (4) 1 MeV with concurrent protons on strong diffusion and those with strong diffusion precipitation below 1 MeV but without strong proton precipitation (7). These classes are displayed in invariant latitude versus MLT in Fig 1.11 and will be discussed in detail in Chapter 2.

FIGURE 1.11 REP events displayed according to invariant latitude and MLT for the following classes: dots and lines (. |) for strong precipitation at energies $\leq$ 1 MeV with concurrent proton precipitation; squares (□) for strong precipitation at energies $\geq$ 1 MeV with concurrent proton precipitation; and circles (o) for strong precipitation at energies << 1 MeV without concurrent proton precipitation.

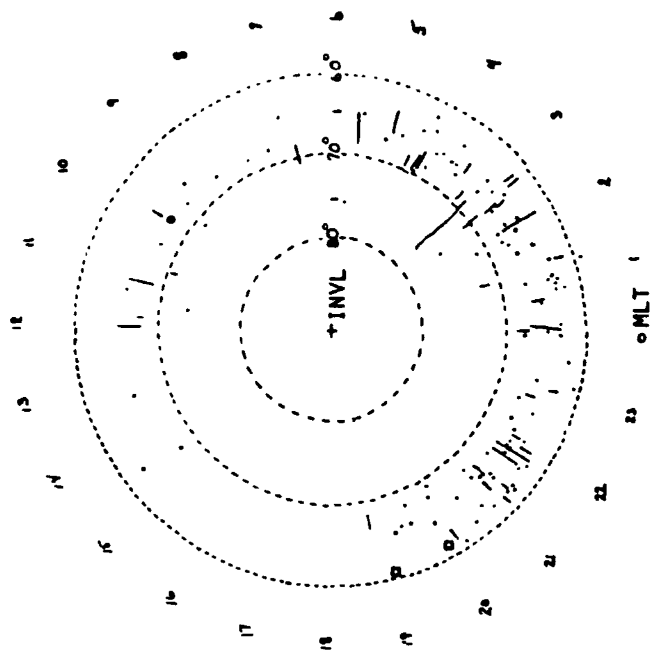

$A_p > 20$

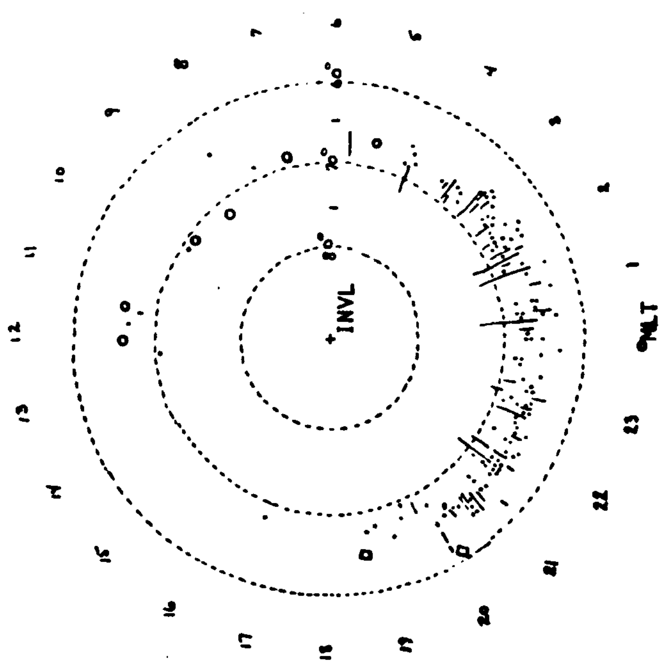

$A_p \leq 20$

CHAPTER 2. THEORY AND CASE STUDIES

2.1 Background

To account for the observed subauroral radio signal absorption, Bailey (1968) estimated that the precipitating electrons at energies exceeding several hundred keV required fluxes $J_p \gtrsim 10^3$ electrons/cm^{2}s str. Such intense subauroral (closed field lines) precipitation requires pitch angle scattering of trapped radiation belt electrons near the strong diffusion limit. This leads to an isotropic pitch angle distribution, i.e., precipitated flux $\simeq$ trapped flux (Kennel, 1969). The rapid scattering can occur during resonant interaction between plasma waves and particles in the magnetosphere. Either of the first two adiabatic invariants (μ and J) can be violated during the pitch angle diffusion and this can provide a major loss mechanism for geomagnetically trapped particles (Thorne, 1975).

The condition for first order resonant scattering with relativistic electrons is:

$$1 - \mu_{\parallel}\beta_{\parallel} = \frac{\Omega_-}{\omega\gamma} \qquad (1)$$

where $\mu_{\parallel} = \frac{K_{\parallel}c}{\omega}$, parallel (to ambient magnetic field) refractive index

$\beta_{\parallel} = \frac{V_{\parallel}}{c}$, normalized parallel electron velocity

ω = wave frequency

$\frac{\Omega_-}{\gamma}$ = relativistic electron gyrofrequency

$\gamma = (1-\beta^2)^{-1/2}$, relativistic mass enhancement factor

c = speed of light in vacuo

$K_{\parallel}$ = parallel propagation constant

(wave number)

Thorne (1977) has scaled the general morphology of velocity space surfaces for resonance with a wave of a given frequency and refractive index (Fig 2.1). Waves with $\mu_{\parallel} > 1$ generally require $\omega < \Omega_-$ to resonate with relativistic electrons because only this surface $(\frac{\omega}{\Omega_-} < 1)$ reaches the loss cone at relativistic energies. Waves with $\omega > \Omega_-$ even with $\mu_{\parallel} < 1$ as in the case of Auroral Kilometric Radiation (Kurth et al., 1975) do not usually resonate with relativistic electrons. A brief review of plasma waves follows.

Southwood (1978) has reviewed the plasma waves found in the magnetosphere. Four distinct classes of waves have been identified in the outer radiation zone $4 \lesssim L \lesssim 8$ where REP events are observed. The first class are electron electromagnetic waves at frequencies below the electron gyrofrequency; waves typically occur in the frequency band $.1 \lesssim \frac{\omega}{\Omega_-} \lesssim .5$. These so-called right hand polarized (Burton and Holzer, 1974) whistler mode "chorus" waves are generated at high altitudes (near the magnetic equator) outside the plasmasphere with typical wide band wave amplitudes ~ 10 m γ (Dunckel and Helliwell, 1969, Anderson and Maeda, 1977). The waves propagate down the field lines to low altitudes where they are the most frequently occurring emission outside the plasmapause (Kennel and Thorne, 1967; Thorne and Kennel, 1967; Gurnett et al., 1969; Dunckel and Helliwell, 1969; Tsurutani and Smith, 1974). Dunckel and Helliwell (1969) examined emission

FIGURE 2.1 Velocity space surfaces for resonance with a wave of frequency ω and parallel refractive index $\mu_{\parallel}$ for $\gamma_{\perp}$ versus $\gamma_{\parallel}$.

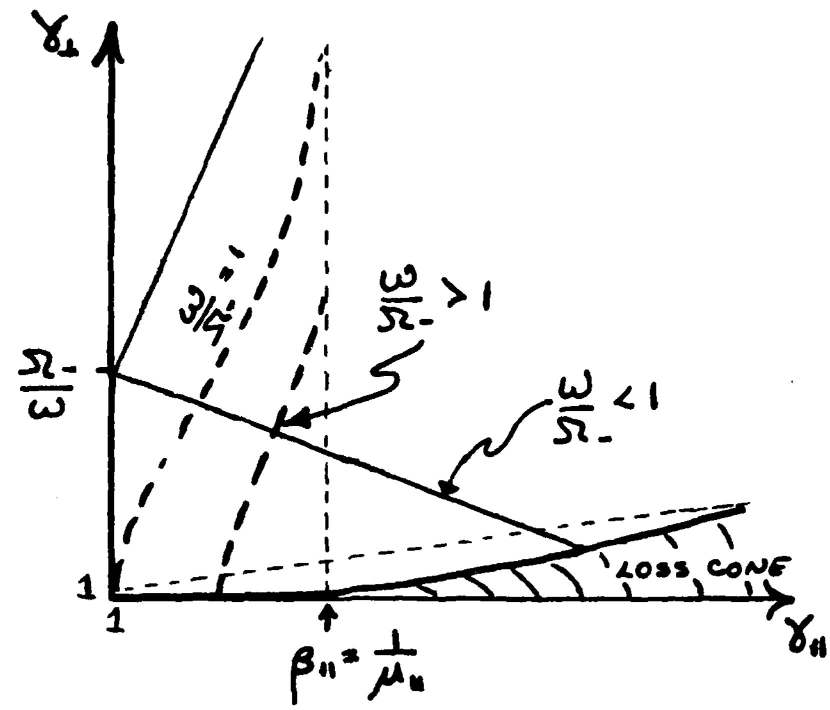
LOSS CONE

intensities for 300-500 Hz whistler mode chorus and found that they peak near 1000 MLT. Also, just outside the plasmapause, intensities increase abruptly at 0600 MLT and decrease gradually after 1400 MLT in agreement with OV3-3 1.3 kHz low altitude emissions (McPherson and Koons, 1970). A one year study of OGO-5 search coil magnetometer data show that equatorial chorus is strongly substorm correlated with two peaks: one at post midnight (L=5-8) and a second in the dawn to noon sector (L=7-11) (Tsurutani and Smith, 1977). The source of the waves is generation by loss cone instability associated with the pitch angle anisotropy of substorm injected electrons (Kennel and Petschek, 1966). Association of this wave phenomenon with precipitation of energetic electrons (10-100 keV) has been made by several authors (Dungey, 1963; Cornwall, 1964; Kennel and Petschek, 1966; Vampola et al, 1971; Thorne, 1974; Tsurutani and Smith, 1977).

The second class of waves are electron electrostatic waves found at frequencies above the electron gyrofrequency (Kennel et al., 1970). These so-called "n + 1/2" waves ($\frac{\omega}{\Omega_-} \simeq n + 1/2$) are found throughout the magnetosphere outside the plasmapause (Kennel et al., 1970; Shaw and Gurnett, 1975) and are thought to be generated by $\frac{\partial f}{\partial v} > 0$ electron distributions (Fredricks, 1971). The waves are localized about the geomagnetic equator from L=4-10 a majority of the time in the morning sector (Kennel et al., 1970; Fredericks and Scarf, 1973). Wave amplitudes range from 1-10 mV/m (Kennel et al., 1970) with excursions to 100 mV/m during substorms (Scarf et al., 1973). Theoretical parametric studies yielding realistic spatial growth rates for these waves have been accomplished (Young et al., 1973; Karpman et al., 1975; Ashour-Abdalla and Kennel, 1976) and computations of the resonant electron population show energies of 1-10 keV (possibly accounting for the diffuse aurora, Lyons, 1974) or higher (~ 100 keV) during substorms (Scarf et al., 1973). However, this class of waves does not resonate effectively with relativistic electrons in strong diffusion, requiring wave amplitudes in excess of 100 mV/m to cause strong diffusion of 100 keV electrons (see Fig. 2.2, Lyons, 1974). This class will not be considered further in this study.

Analagous to the right hand electron electromagnetic waves which cut off at Ω_-, there is a third class, the left hand ion electromagnetic waves below Ω_+ (e.g., Cornwall, 1965). In the micropulsation literature these are sometimes referred to as "PCl or IPDP micropulsations" or periodic emissions: PCl ("Pearls")are dispersive waves propagating along field lines thought to be generated by the loss cone distribution of ring current protons just inside the plasmapause (Cornwall, 1965; Cornwall et al., 1970; Williams and Lyons, 1974; Kaye et al., 1979); "IPDP," intervals of pulsations of diminishing period are non-dispersive waves propagating near dusk during substorm expansion (McPherson et al., 1968; Lukkari and Kangas, 1976; Bossen et al., 1976). In a statistical study by Bossen et al. (1976) EMIC occurred mostly about the dusk meridian with frequencies $\frac{\omega}{\Omega_+} \sim .1\text{-}.2$ and wave amplitudes 1-7γ during the main phase of geomagnetic storms. PCl turbulence has also been observed in detached plasma regions (Kivelson et al., 1972) prevalent in the late morning to dusk sector (Chappell,

FIGURE 2.2 Minimum wave amplitudes required for electron strong diffusion scattering at L=7 versus electron energy for electron thermal energies 0.1, 1 , 10 keV (Lyons, 1974)

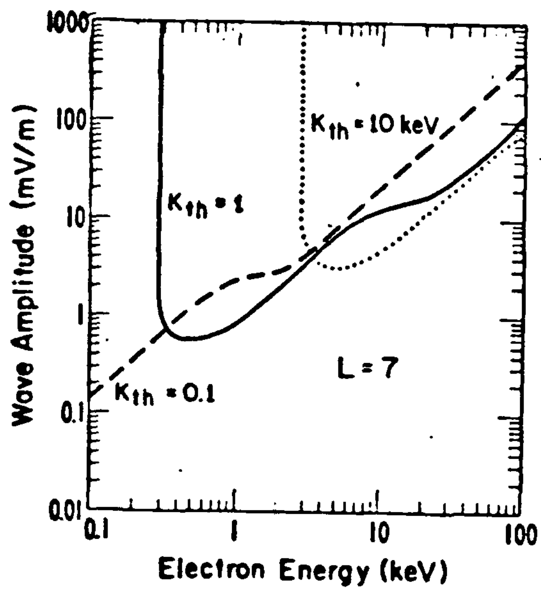
Wave Amplitude (mV/m)
1000
100
10
1
0.1
0.01
Kth = 1
Kth = 10 keV
Kth = 0.1
L = 7
0.1
1
10
100
Electron Energy (keV)

1974). Theoretical calculations show that these waves are candidates for hard REPs (precipitating electron energies $\gtrsim$1 MeV) in the evening plasmapause (Thorne and Kennel, 1971) and possibly during the day in detached plasmas (Thorne, 1974).

The last class of waves to be discussed here are the electrostatic ion cyclotron waves predicted by Kennel et al. (1970) after the analogous electrostatic electron wave discovery and measured by Gurnett and Frank (1977) and Kintner et al., (1978). These waves have frequencies $\Omega_+ < \omega < \Omega_{LHR}$, amplitudes on the order of a few 10's of mV/m, and are found at all local times at L > 6 (Gurnett and Frank, 1977; Kintner et al., 1978). Generation of the waves is thought to be by current driven instability low on the field line to yield resonant Landau growth (Kindel and Kennel, 1971; Ashour-Abdalla and Thorne, 1978) and/or equatorial anisotropic pitch angle instability due to distributions of hot protons (Coroniti et al., 1972; Ashour-Abdalla and Thorne, 1977; Ashour-Abdalla and Thorne, 1978). Observations have indeed correlated REPs with intense ELF electrostatic waves (Koons et al., 1972) and shown that some cases can be explained only as a low altitude phenomenon (Vampola, 1977).

2.2 Resonant Populations

Since the observational data covers the electron energy range 12 keV-1.6 MeV and proton range > 80 keV, > 150 keV etc., it is important to determine the electron and proton resonant populations for each wave phenomena if any success at discrimination (between wave mechanism) is to be accomplished. We proceed with calculations for each wave type.

2.2.1 Whistler Mode Chorus

The cold plasma dispersion relation for parallel whistler mode chorus propagation assuming $\Omega_+ << \omega << \Omega_-$ and $\mu_{\parallel} >> 1$ ($\omega_p >> \Omega_-$) is given by Kennel and Petschek (1966):

$$\mu_{\parallel}^2 \simeq \frac{\omega_p}{\omega \Omega_-} \left(1 - \omega/\Omega_-\right)^{-1} \tag{2}$$

where ω_p = plasma frequency.

Using this dispersion relation and the condition for first order cyclotron resonance with relativistic electrons (eq. 1) assuming $\beta_{\parallel} \simeq \beta$ (valid near the loss cone), Thorne (1974) has derived an expression for resonant electron energies:

$$\left(\gamma^2 - 1\right)_{res} \simeq \frac{2 E_m^- \Omega_-}{E_o^- \omega} \left(1 - \frac{\omega}{\Omega_-}\right)^3 \tag{3}$$

where $E_m^{\pm} = \frac{B^2}{8\pi N^{\pm}}$, magnetic energy per particle

B = local magnetic field value

$N^{\pm}$ = particle number density

$E_o^{\pm} = m^{\pm}c^2$, particle rest energy.

Thus the expression for the resonant electron population with whistler mode chorus waves of frequency ω is:

$$E_r^- = \left[\left(\frac{2 E_m^- \Omega_-}{E_o^- \omega} \left(1 - \frac{\omega}{\Omega_-}\right)^3 + 1 \right)^{1/2} - 1 \right] E_o^- \tag{4}$$

where E_r^- is the resonant electron energy.

Since $B \approx \frac{B_o}{L^3}$ at the equator where B_o = .311 Gauss and N varies from approximately $10^3/cm^3$ in the plasmasphere (L=4) to 1-10/cm^3 in the plasma trough region (L=5-8) for a K_p ~ 2-3 (Chappell et al., 1970), we have a range of E_m^- of .5 keV (L=4, N=10^3) to 150 keV (L=5, N=1) at the equator. Down on the field line (away from the equator) where B increases and N is less than ionospheric densities ($\lesssim 10^4$) the value of E_m^- can reach a few 100 keV. Values of N not greater than $10^4 cm^{-3}$ are used since whistler mode chorus propagating down the field line rapidly becomes perpendicular to the local magnetic field line and reflects at frequencies near the lower hybrid resonance (Thorne and Kennel, 1967). [For propagation at angles to the field line, the cumulative contribution from parallel velocity resonances is appropriate since higher order resonances become important (Stix, 1962; Kennel and Petschek, 1966) although this is not the case for electromagnetic waves with $k_\perp \simeq 0$.] So for $.1 \leq \frac{\omega}{\Omega_-} \leq .5$ (Tsurutani and Smith, 1977) and E_m^- = .5-150 keV (both typical equatorial values), we have E_r^- = 1-800 keV. Off the equator (down the field line where $\frac{\omega}{\Omega_-}$ is lower and E_m^- is higher) E_r^- is expected to reach values of nearly 10^3 keV.

For proton precipitation we use the resonance condition for first order (n=1) cyclotron resonance with protons

$$1 - \mu_{\parallel}\beta_{\parallel} = \frac{\Omega_+}{\omega} \qquad (5)$$

and the dispersion relation for whistlers to obtain

$$E_r^+ \simeq \left(\frac{m^+}{m^-}\right) E_m^+ \left(\frac{\omega}{\Omega_-}\right)\left(1 - \frac{\omega}{\Omega_-}\right) \tag{6}$$

where $\frac{m^+}{m^-} = 1.837 \times 10^3$, proton to electron mass ratio. We take $E_m^+ \simeq E_m^-$, since we assume the densities of electrons to be the same as protons (DeForest and McIlwain, 1971). Using the same range of values for $\frac{\omega}{\Omega_-}$ we can readily see that E_r^+ will typically be greater than an MeV (except in the dense plasmasphere) in agreement with Kennel and Petschek (1966).

Resonance energies for both electrons and protons are shown in Fig. 2.3. One readily sees that electrons can be resonant at energies up to several hundred keV while protons are resonant only at energies above 1 MeV.

2.2.2 Electromagnetic Ion Cyclotron (EMIC) Waves

The cold plasma dispersion relation for parallel propagating EMIC waves below Ω_+ is given by Kennel and Petschek (1966):

$$\mu_{\parallel}^2 = \frac{\omega_p^2}{\Omega_-\Omega_+}\left(1 - \frac{\omega}{\Omega_+}\right)^{-1} \tag{7}$$

Thorne and Kennel (1971) and Thorne (1974) have used equations (1) and (7) to derive the equation for resonant electrons with EMIC:

$$\left(\gamma^2 - 1\right)_{res} \simeq \frac{2E_m^-}{E_o^-}\left(\frac{m^+}{m^-}\right)\left(\frac{\Omega_+}{\omega}\right)^2\left(1 - \frac{\omega}{\Omega_+}\right) \tag{8}$$

FIGURE 2.3 Electron and proton resonant energies for the whistler mode chorus mechanism ($.1 \lesssim \frac{\omega}{\Omega_-} \lesssim .5$) [in keV] versus L for $N=10^4 cm^{-3}$ for L=4 and N=1, 10 cm^{-3} for $L \geq 5$.

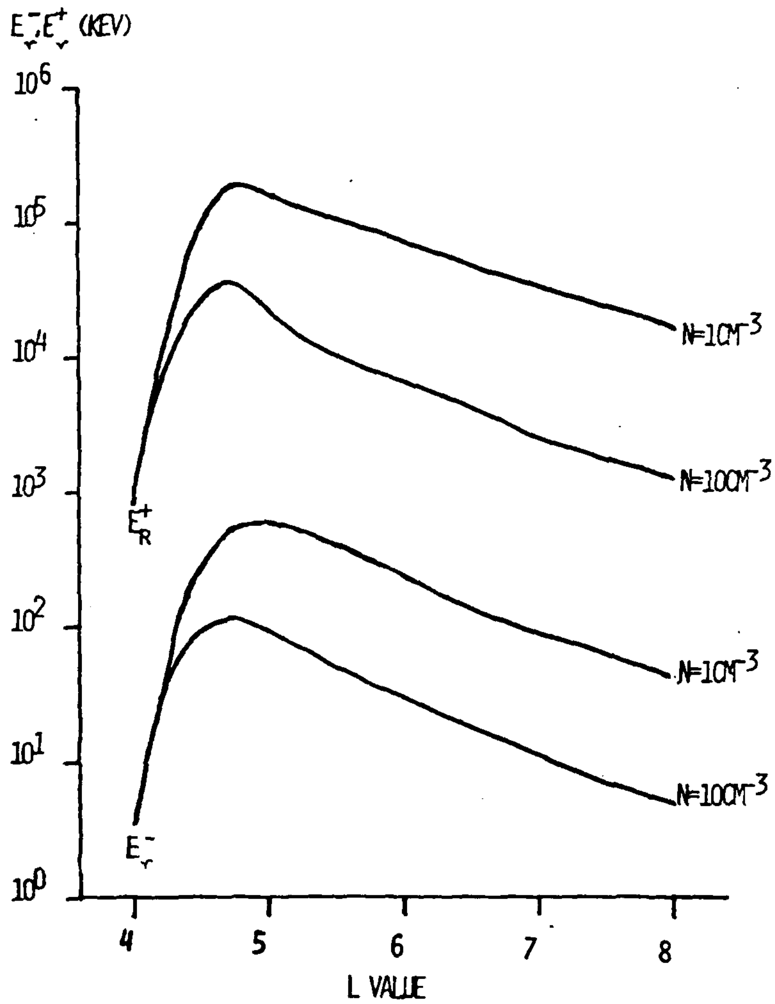

E_r^-, E_r^+ (KEV)
10^6
10^5
10^4
10^3
10^2
10^1
10^0
$N=1CM^{-3}$
$N=10CM^{-3}$
E_R^+
$N=1CM^{-3}$
$N=10CM^{-3}$
E_r^-
4
5
6
7
8
L VALUE

and we see that (8) becomes

$$E_r^- = \left\{ \left[\frac{2 E_m^- m^+ \Omega_+^2}{E_o^- m^- \omega^2} \left(1 - \frac{\omega}{\Omega_+}\right) + 1 \right]^{1/2} - 1 \right\} E_o^- \quad (9)$$

Using the previous value of $E_m^{\pm}$ at L=4, N=10^3cm^{-3}, and $\frac{\omega}{\Omega_+} \simeq .1-.5$ (Bossen et al., 1976) we see that $E_r^- \sim$ few MeV, see Fig 2.4. Even during intense injection events where EMIC waves may be generated outside the plasmasphere to L=8 due to enhanced ion fluxes and larger loss cone distributions (Coroniti et al., 1976), E_r^- for L=8, N=10, and $\frac{\omega}{\Omega_-} \sim .2$ is 5 MeV.

The equation for EMIC resonance with protons is given by Kennel and Petschek (1966):

$$E_r^+ = E_m^+ \left(\frac{\Omega_+}{\omega}\right)^2 \left(1 - \frac{\omega}{\Omega_+}\right)^3 \quad (10)$$

Using the same $E_m^{\pm}$ values and $\frac{\omega}{\Omega_+}$ = .1-.2 (Bossen et al., 1976) we see $E_r^+ \simeq$ 10s-100s keV near the outer edge of the plasmasphere.

In summary, EMIC waves resonate with electrons only at energies >> 1 MeV and only near 1 MeV in the relatively dense plasmasphere or detached plasma regions where N is relatively large and at the equator where B is lowest. The resonant proton population for the same wave mechanism is on the order of 10's and 100's keV.

2.2.3 Electrostatic Ion Cyclotron (ESIC) Waves

Since the frequency of ESIC waves is near the Ω_+, we can

FIGURE 2.4 Resonant electron energies versus L for the ion cyclotron ($\frac{\omega}{\Omega_+}$ = 0.5) wave mechanism for densities N=1, 10 cm^{-3} outside the plasmasphere and N=$10^3 cm^{-3}$ L=4 (Thorne and Kennel, 1971).

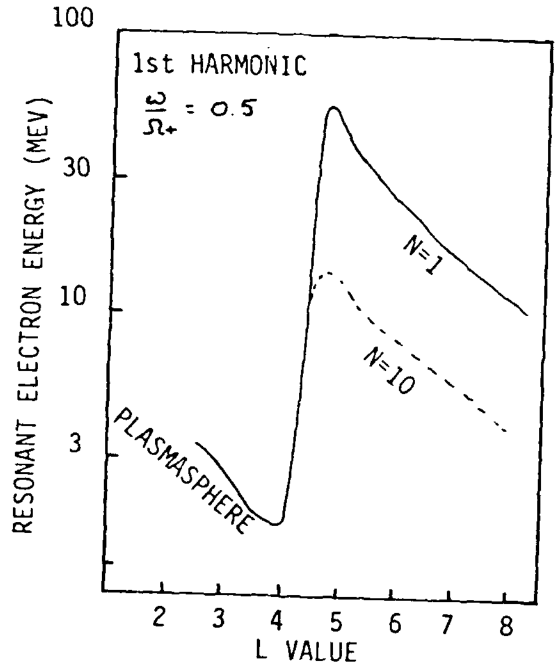
100
1st HARMONIC
ω/Ω+ = 0.5
30
10
3
RESONANT ELECTRON ENERGY (MEV)
N=1
N=10
PLASMASPHERE
2
3
4
5
6
7
8
L VALUE

eliminate the unity term in (1) to obtain:

$$\gamma^2 \mu_\parallel^2 \beta_\parallel^2 = \left(\frac{\Omega_-}{\omega}\right)^2 \tag{11}$$

Using $\gamma^2 \beta_\parallel^2 \simeq \gamma^2 - 1$ (valid for particles near the loss cone) in (11) we have:

$$\gamma^2 - 1 = \mu_\parallel^{-2} \left(\frac{\Omega_-}{\omega}\right)^2 \tag{12}$$

By writing the wave refractive index $\mu_\parallel^2 = \frac{c^2 K_\parallel^2}{\omega^2} \frac{f_+^2 \Omega_+^2}{V_{th}^{+2}}$, where Ω_+ is the ion gyroratio, V_{th} is the ion thermal speed, and $f_+ = V_{th}/\Omega_+$, eq. (12) becomes:

$$\left(\gamma^2 - 1\right)_{res} \simeq \left(\frac{\Omega_-}{\Omega_+}\right)^2 \left(\frac{V_{th}^+}{c}\right)^2 \left(\frac{1}{K_\parallel f_+}\right)^2 \tag{13}$$

Using $\left(\frac{V_{th}^+}{c}\right)^2 = 2 \frac{E_{th}^+}{E_o^+}$, where E_{th}^+ is the ion thermal energy, in (13) we have:

$$\left(\gamma^2 - 1\right)_{res} = \frac{2 E_{th}^+}{E_o^+} \left(\frac{m^+}{m^-}\right)^2 \left(\frac{1}{K_\parallel f_+}\right)^2 \tag{14}$$

The resonant electron energy for ESIC waves is thus:

$$E_r^- = \left\{ \left[\frac{2 E_{th}^+}{E_o^+} \left(\frac{m^+}{m^-}\right)^2 \left(\frac{1}{K_\parallel f_+}\right)^2 + 1 \right]^{1/2} - 1 \right\} E_o^- \tag{15}$$

Ashour-Abdalla and Thorne (1977 and 1978) have solved the electrostatic dispersion relation numerically and obtained k space contours of temporal and convective growth rates normalized to f_+ for typical equatorial and ionospheric conditions. If waves are excited by the current driven instability in the topside ionosphere with electron drifts just above the Kindel and Kennel (1971) marginal stability limit, 1 Re above the earth for $L \simeq 10$, $E_{th} \simeq 2$ev, the first three harmonics (typical of wave observations, Kintner et al., 1978) have typical values for $k_{\parallel} f_+ \simeq .26-.1$ (Ashour-Abdalla and Thorne, 1978). This yields values of $E_r^- \simeq 50-300$ keV. For excitation in the equatorial plasmasheet by the loss cone instability, typical equatorial parameters are $E_{th} \simeq 1$ keV, and $k_{\parallel} f_+ \simeq .4-.5$ for the first five harmonics. This gives $E_r^- \simeq 100$ keV - 2 MeV. Again using the first order cyclotron relation for resonance with protons (eq. 5) we have:

$$1 - \mu_{\parallel}\beta_{\parallel} = \frac{\Omega_+}{\omega}$$

Rewriting, we have

$$\beta_{\parallel}^2 = \frac{1}{\mu_{\parallel}^2}\left(1 - \frac{\Omega_+}{\omega}\right)^2$$

or

$$\beta_{\parallel}^2 = \left(\frac{\Omega_+}{\omega}\right)^2\left(1 - \frac{\omega}{\Omega_+}\right)^2 \frac{1}{\mu_{\parallel}^2}$$

Substituting for $\mu_{\parallel}^2$, we have:

$$\beta_{\parallel}^2 = \frac{v_{\parallel}^2}{c^2} = \frac{\Omega_+^2}{c^2 K_{\parallel}^2}\left(1 - \frac{\omega}{\Omega_+}\right)^2 \qquad (16)$$

and

$$\frac{1}{2} m^+ v_\parallel^2 = E_r^+ = \frac{V_{th}^2 \; m^+ \; c^2}{2 \, k_\parallel^2 \, \rho_+^2 \, c^2} \left(1 - \frac{\omega}{\Omega_+}\right)^2 \quad (17)$$

thus

$$E_r^+ = E_{th}^+ \left(\frac{1}{k_\parallel \rho_+}\right)^2 \left(1 - \frac{\omega}{\Omega_+}\right)^2 \quad (18)$$

Since $(\frac{1}{k_\parallel \rho_+})^2 \; (1 - \frac{\omega}{\Omega_+})^2$ is of the order one (1), $E_r^+ \simeq E_{th}^+$, i.e., 2 ev - 1 keV. It must be noted, however, that higher order resonances must be taken into account since these electrostatic ion cyclotron waves have polarizations $\frac{k_\perp}{k_\parallel} \simeq 10$ (Kintner et al., 1978). It will be shown in the next section that, unlike electromagnetic waves, resonant electrostatic wave amplitudes required for strong diffusion scattering decrease with increase in energy of the resonant population ($\gamma \to \infty$). Thus resonant energies for ions can easily reach a few 100 keV (Ashour-Abdalla and Thorne, 1978). So in summary, electrons with E_r^- $\simeq$ 50 keV-2MeV and ions with $E_r^+ \simeq 1 \simeq$ 100's keV can resonate with electrostatic ion cyclotron waves.

2.3 Wave Amplitudes

Now that the resonant electron and proton populatio[illegible] known for each wave mechanism, it is useful to determine [illegible] resonant wave amplitudes required for strong diffus[illegible] it relate the ability of observed wave amplitude[illegible]

AD-A092 545 AIR FORCE INST OF TECH WRIGHT-PATTERSON AFB OH F/G 4/1
RELATIVISTIC ELECTRON PRECIPITATION: AN OBSERVATIONAL STUDY.(U)
1980 L J ANDREOLI
UNCLASSIFIED AFIT-CI-80-26D NL

2 OF 4
AD
A092545

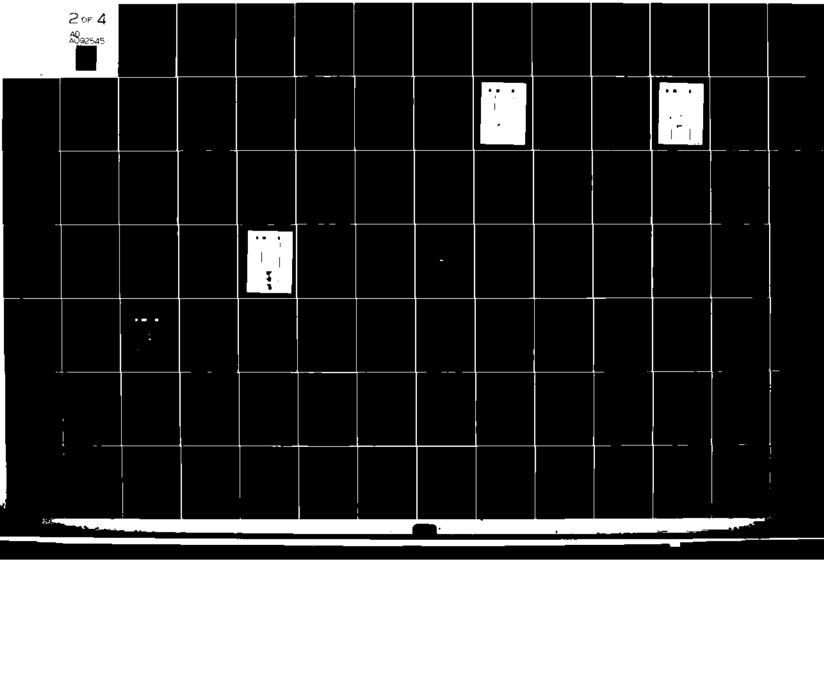

populations on strong diffusion but the equations will help later when examining real cases.

The condition for strong diffusion, i.e., very rapid scattering, is

$$\tau_D << \tau_{1/4B} \tag{19}$$

where τ_D = diffusion loss time

$\tau_{1/4B}$ = 1/4 bounce time

This permits the particle distribution to become isotropic even over the loss cone (= > $J_p \simeq J_t$). The loss time approaches a minimum value under strong diffusion and the diffusion coefficient, D, is larger than $1/\tau_{min}$, where τ_{min} is the minimum rate of diffusion loss. $\tau_{min} \simeq \frac{2\tau_{1/4B}}{\alpha_L^2}$ where α_L is the pitch angle of the loss cone.

2.3.1 Electromagnetic Waves

The action of electromagnetic waves on particles is mainly via pitch angle scattering. The pitch angle scattering coefficient, $D_{\alpha\alpha}$, is given by Kennel and Petschek (1966):

$$D_{\alpha\alpha} = \frac{(\Delta\alpha)^2}{2\Delta t} \simeq \pi \Omega_- \left(\frac{b}{B_o}\right)^2 \tag{20}$$

where b = wave amplitude

B_o = ambient magnetic field value

and for strong diffusion scattering one requires

$$D_{\alpha\alpha} \gtrsim D_{SD} \simeq \frac{\alpha_L^2}{2\tau_{1/4B}} \tag{21}$$

where α_L = loss cone pitch angle

D_{SD} = coefficient for strong diffusion.

Equation (20) can be rewritten including the relativistic mass correction and bounce averaging to obtain:

$$D_{\alpha\alpha} \simeq \frac{\pi \Omega_-}{\gamma} \left(\frac{b}{B_0}\right)^2 f \tag{22}$$

where f = is the fraction of the electron bounce orbit spent in resonance with waves.

For equatorial loss cones, $\alpha_L^2 \simeq \frac{1}{2L^3}$. For electrons, $\tau_{1/4B} \simeq \frac{LR_0}{v^-} \sim \frac{LR_0}{c}$ where R_0 = 1 earth radius. Equating (22) and (20) with substitutions yields a fluctuating field wave amplitude for strong electron diffusion:

$$b_{SD}^- = \left(\frac{B_0^2 \, c \, \gamma}{4\pi L^4 R_0 \Omega_- f}\right)^{1/2} \tag{23}$$

and

$$b_{SD}^- = \frac{100 \, \gamma^{1/2}}{L^{7/2}} \text{ (gammas) for } f = \frac{1}{5} \tag{24}$$

For ions, $\tau_{1/4B} = \frac{LR_0}{v^+} = \frac{LR_0}{(2E^+/E_0^+)^{1/2} c}$, $\Omega_- = \frac{m^+}{m^-}\Omega_+$, and $\gamma \sim 1$ where E^+ and E_0^+ are the ion energy and ion rest energy respectively. Likewise, the fluctuating field wave amplitude for strong ion diffusion is

$$b^{+}_{SD} = \left[\frac{m^{+}}{m^{-}} \left(\frac{2E^{+}}{E^{+}_{o}} \right)^{1/2} \frac{B_o^2 \, c}{4\pi L^4 R_o \Omega^{-} f} \right]^{1/2}$$

and (25)

$$b^{+}_{SD} = \frac{165 \, E^{+1/4}(KeV)}{L^{7/2}} \quad (\text{gammas})$$

Strong electron diffusion ($E^{-}_{\gamma} \sim 1/2 \rightarrow 1$ MeV; $\gamma \simeq 2$-3) thus requires amplitudes of 1 gamma at L=4 and 100 mγ at L=8. For ion strong diffusion ($E^{+}_{\gamma} \sim 50$ keV), amplitudes of 3.5 gammas at L=4 and 300 mγ at L=8 are required. These values are within the range of amplitudes for both electrons and ions for EMIC waves (1-7γ) found by Bossen et al. (1976) but only the most intense chorus events with amplitudes approximately 100 mγ (Tsurutani and Smith, 1977) meet the criteria for electrons at L=8.

2.3.2 Electrostatic Amplitudes

Electrostatic waves scatter electrons primarily by energy diffusion. Scattering by energy in the perpendicular (to the magnetic field line) direction at the edge of the loss cone requires a diffusion coefficient as follows:

$$D_{\perp\perp} = \frac{\langle \Delta v_{\perp} \rangle^2}{\Delta t} \tag{26}$$

For strong diffusion which can maintain isotropy over the loss cone one requires

$$D_{\perp\perp} \geq D_{SD} \simeq \frac{V_{res}^2 \alpha_L^2}{\tau_{1/4B}} \simeq \frac{V_{res}^2}{\tau_{1/4B}} \left(\frac{B_o}{B_A}\right) \quad (27)$$

where B_A = B(100 km).

An approximate expression for $D_{\perp\perp}$ as a function of electrostatic wave amplitude can be derived (e.g. Ashour-Abdalla and Thorne, 1978):

$$D_{\perp\perp}^{\pm} = \frac{\Omega_{\pm}}{\gamma^{\pm}} \frac{c^2 \hat{\mathcal{E}}_w^2}{B_o^2} \quad (28)$$

where $\mathcal{E}_w$ is the electric field amplitude of the electrostatic wave. Equating eqs. (27) and (28) and using $\tau_{1/4B} = \frac{LR_o}{v} \sim \frac{LR_o}{c}$, we have for the fluctuating wave amplitude for electron strong diffusion

$$\mathcal{E}_w^- = \left[\frac{c}{LR_o} \left(\frac{B_o}{B_A}\right) \frac{B_o^2 \gamma^-}{\Omega_-}\right]^{1/2} \quad (29)$$

At the equator $\frac{B_o}{B_A} \simeq \frac{1}{2L^3}$ and $\mathcal{E}_{w_{eq}}^- = [3.7 \times 10^8 \frac{\gamma^-}{L^7}]^{1/2} (\frac{mV}{m})$. For γ^- = 2-3, we have $\mathcal{E}_w^-$ = 20-250 $\frac{mV}{m}$ for L=8-4. In the topside ionosphere near 1 Re, $\frac{B_o}{B_A} \simeq \frac{1}{10}$, $B_o \simeq .05$, and $\mathcal{E}_{w,Re}^- = [1.4 \times 10^7 \frac{\gamma}{L}]^{1/2} (\frac{mV}{m})$. For γ^- = 2-3, we have $\mathcal{E}_w^- \simeq$ 1-3 $\frac{V}{m}$ for L=8-4.

For the concomitant ion strong diffusion using eq. (27) and

$$D_{SD}^{+} = \Omega_{+} c^2 \frac{\mathcal{E}_w^{+2}}{B_o^2} \quad (30)$$

we have

$$\mathcal{E}_w^+ = \left[\frac{c}{L R_o} \left(\frac{B_o}{B_A} \right) \left(\frac{B_o^2 \gamma^+ m^+}{\Omega_- m^-} \right) \left(\frac{2 E^+}{E_o^+} \right) \right]^{1/2} \quad (31)$$

and

$$\mathcal{E}_w^+ = \left[9.4 \times 10^6 \left(\frac{B_o}{B_A} \right) \frac{B_o \; E^+(keV)}{L} \right]^{1/2} \left(\frac{mV}{m} \right) \quad (32)$$

Again for the equator $\frac{B_o}{B_A} \simeq \frac{1}{2L^3}$ and $\gamma^+ = 1$ we have $\mathcal{E}_w^+ = 6 \frac{mV}{m}$ - 66 $\frac{V}{m}$ at L=8-4 for a 50 keV ring current proton. At the 1 Re, $\frac{B}{B_A} \simeq \frac{1}{10}$ B $\simeq$ .05 and $\gamma^+ = 1$, we have $\mathcal{E}_w^+ = 550 \frac{mV}{m} - 750 \frac{mV}{m}$ for a 50 keV ring current proton.

Electrostatic ion cyclotron waves have electric field amplitudes typically on the order of 10-100's $\frac{mV}{m}$ (Gurnett and Frank, 1977 and Kintner et al., 1978). Required wave amplitudes for both ions and electrons are easily met by these waves in the equatorial regime but not in the topside ionosphere.

Table 2.1 lists the range of parameters for strong ion and electron diffusion.

2.4 Case Studies

An example of each of the classes described in Section 1.6 is presented. Each example was selected as being most representative with amount of peripheral data available as an added factor.

2.4.1 Case 1, ESIC (rev 479, day 250, 6 SEP 1976).

The flux versus time plots for electron channels 12-1600 keV

TABLE 2.1 Theoretical REP mechanisms and characteristics.

THEORETICAL REP MECHANISMS

WAVE	FREQ	E^-_{RES}	E^+_{RES}	MIN AMP S.D. ELECTRONS	MIN AMP S.D. PROTONS
WHISTLER MODE CHORUS	$.1<\omega/\Omega\leq 1$	10-100s KEV	1-10 MEV	100mγ-γ	300mγ-3γ
EM ION CYCL	$\omega<\Omega_+$	1-10 MEV ($N=10^3$)	10 KEV-1 MEV	100mγ-γ	300mγ-3γ
ES ION CYCL	$\Omega_+<\omega<\omega_{LHR}$	10 KEV-2 MEV	100 EV-100s KEV	10s-1000mV/M	5-750mV/M

and protons 80-770 keV for three outer zone passes are shown in Fig 2.5 a,b,c, respectively. The low altitude outer zone pass at local evening (Fig 2.5a) shows an extended region of 12 keV precipitation (isotropic) at L $\simeq$ 5-10. This is actually an inverted V event which is bounded by 235 keV precipitation. At L=5 the precipitation extends to nearly 1 MeV electrons and 80 and 150 keV protons. This agrees well with the criteria of ESIC (Table 2.1). Fig 2.5b shows the outer zone pass at high altitude (~ 8000 km) near local dusk. Twelve (12) keV electrons are precipitating from L $\simeq$ 7-9 with two large spikes near L $\simeq$ 8.4. The two spikes are associated with two electrostatic shocks (Kintner, private communication) with perpendicular electric field $\mathcal{E}_{\perp} \simeq$ 500 mV/m. In addition > 80 and > 150 keV protons are precipitating from L $\cong$ 6. Although there is significant trapped 235 keV electron flux from L $\simeq$ 6.8-7.8, there is no precipitation. The next pass (Fig 2.5c) is a medium altitude (~ 5000 km) pass near local morning. Twelve (12) keV electron precipitation is evident from L $\simeq$ 6-13. Extensive 33 keV is coincident although not on strong diffusion from L $\simeq$ 9-12. The 235 keV channel shows "moderate" precipitation at L $\simeq$ 6-8. Significant fluxes of > 80 keV protons are present to roughly L $\simeq$ 12 without any precipitation. This fits the criteria of whistler mode chorus in Table 2.1.

Pitch angle plots of the low altitude local evening outer zone pass of rev 479 are shown in Fig 2.6. Panel (A) at 5962 UT shows a normal pitch angle distribution both down (0^{o}) and up (180^{o}) the local magnetic field line. Panel (B) shows the next distribution towards

FIGURE 2.5a Flux (counts/sec, every fourth data point) versus L value of low altitude (700 km) outer zone pass near local evening. Vertical arrows (↑) indicate singular precipitation and horizontal arrows (→ ←) indicate limits of extended precipitation.

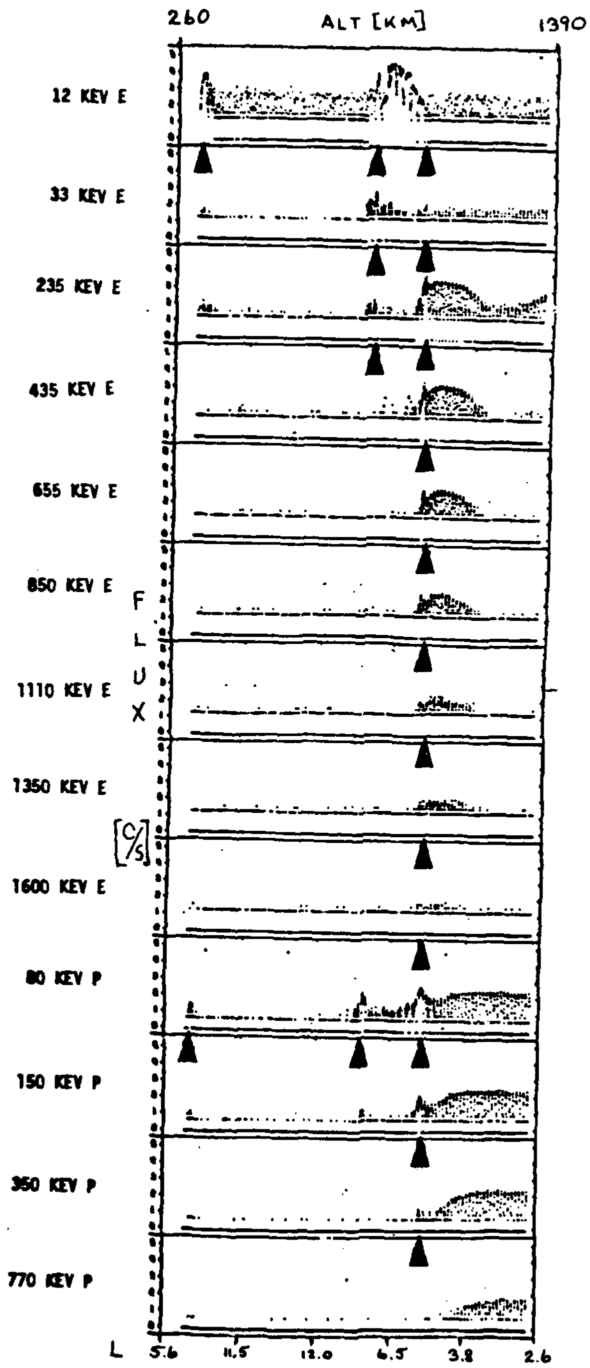
260
ALT [KM]
1390
12 KEV E
33 KEV E
235 KEV E
435 KEV E
655 KEV E
850 KEV E
1110 KEV E
1350 KEV E
1600 KEV E
80 KEV P
150 KEV P
350 KEV P
770 KEV P
FLUX
[C/S]
L
5.6
11.5
12.0
6.5
3.8
2.6

FIGURE 2.5b Same plots for high altitude (8000 km) passes at local dusk.

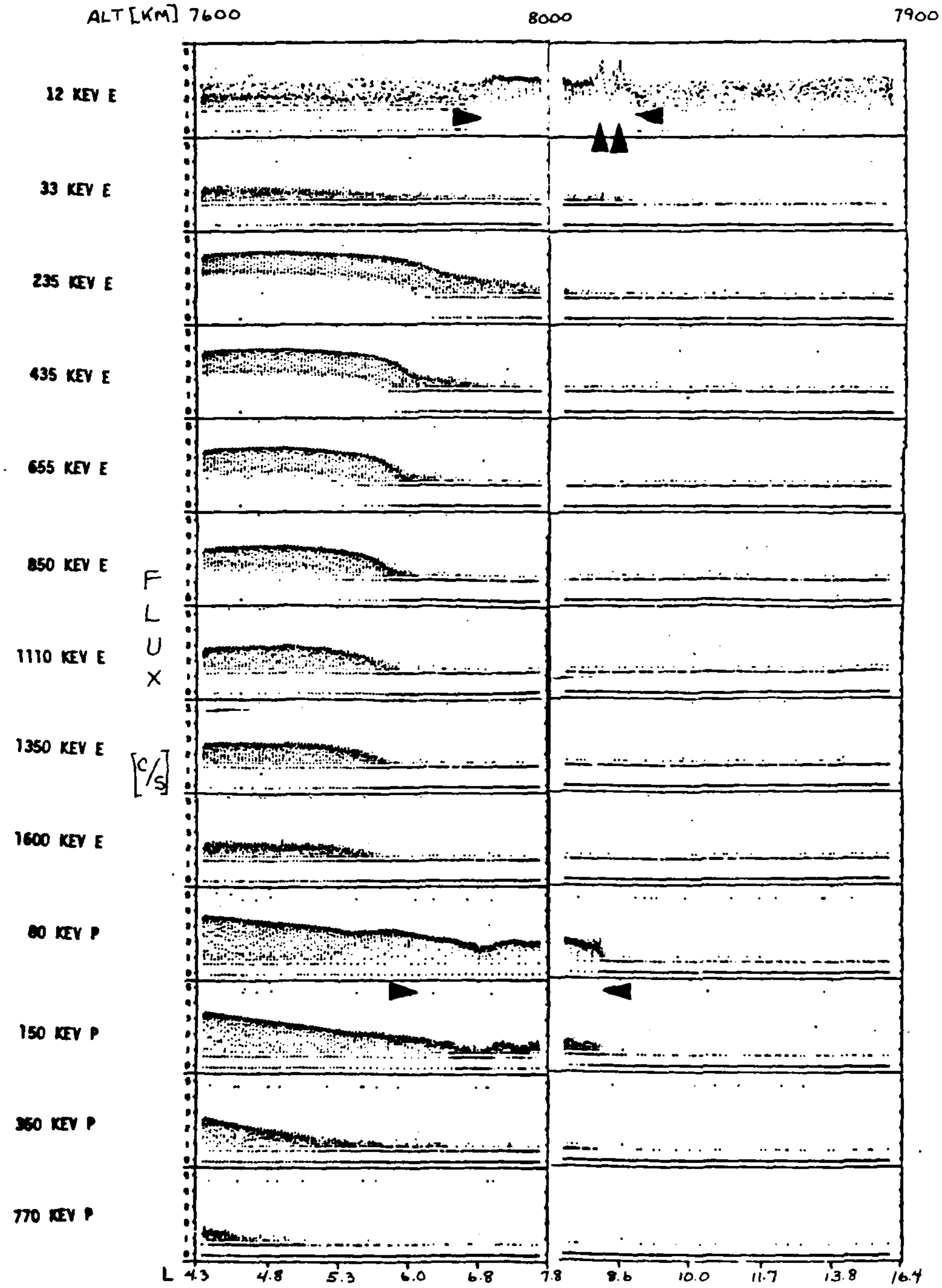

ALT [KM] 7600
8000
7900
12 KEV E
33 KEV E
235 KEV E
435 KEV E
655 KEV E
850 KEV E
1110 KEV E
1350 KEV E
1600 KEV E
80 KEV P
150 KEV P
360 KEV P
770 KEV P
FLUX
[c/s]
L
4.3
4.8
5.3
6.0
6.8
7.8
8.6
10.0
11.7
13.8
16.4

FIGURE 2.5c Same for medium altitude (5000 km) passes at local morning.

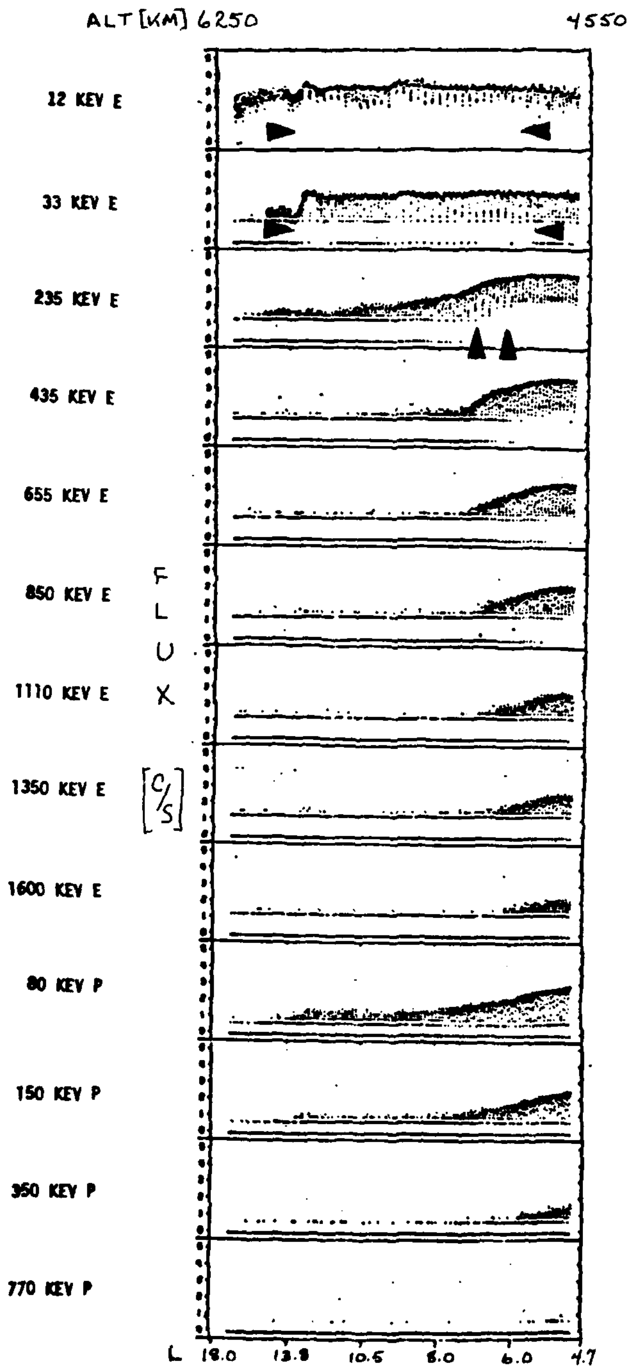

ALT [KM] 6250
4550
12 KEV E
33 KEV E
235 KEV E
435 KEV E
655 KEV E
850 KEV E
1110 KEV E
1350 KEV E
1600 KEV E
80 KEV P
150 KEV P
350 KEV P
770 KEV P
FLUX [C/S]
L 18.0 13.8 10.5 8.0 6.0 4.7

FIGURE 2.6 Pitch angle versus flux (counts/sec) for 235-1610 keV electron channels for 3 times in the local evening outer zone of rev 479. The upward loss cone (L.C. = 50^{0}) is indicated by the vertical line.

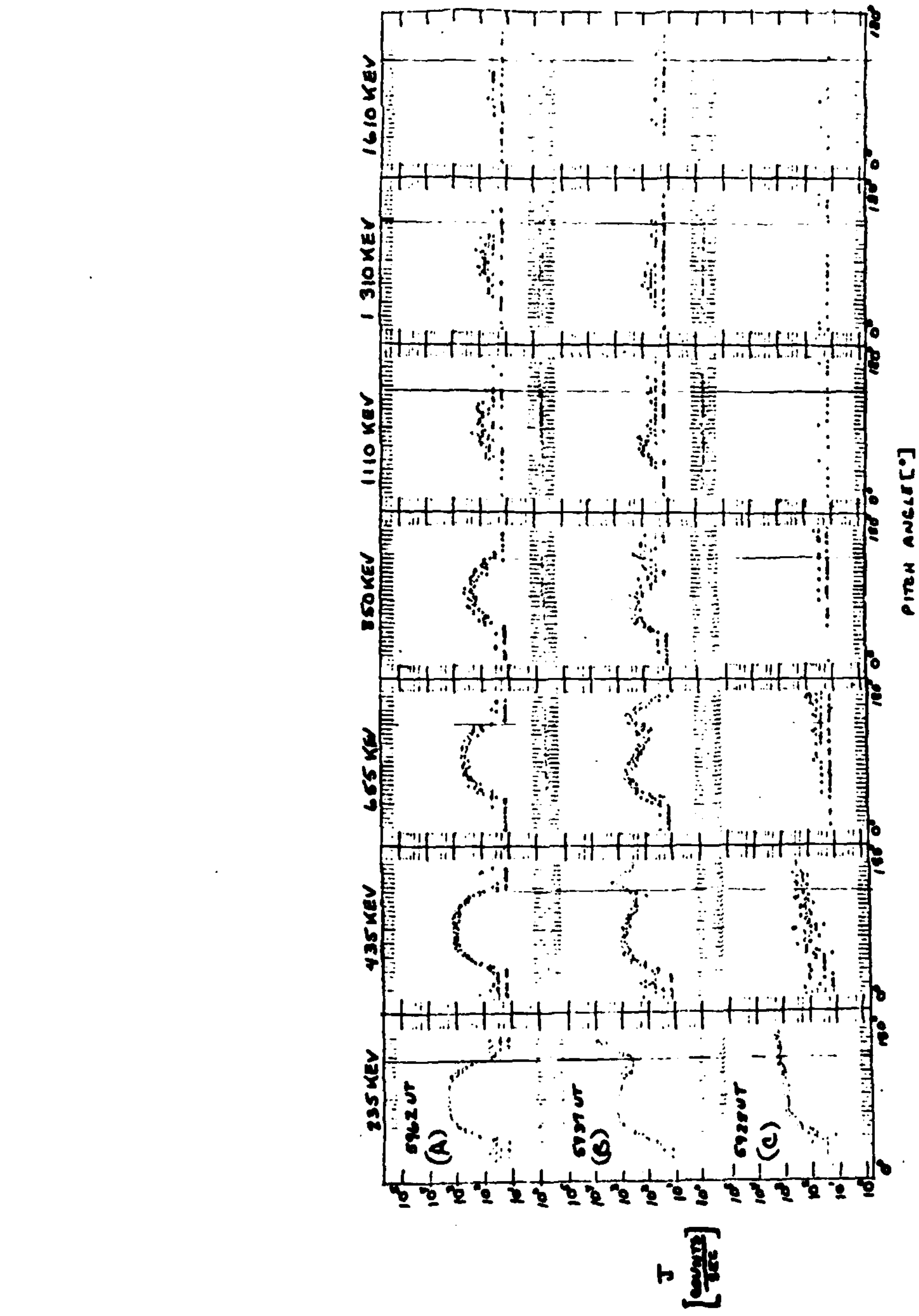

J
235 KEV
435 KEV
665 KEV
850 KEV
1110 KEV
1310 KEV
1610 KEV
(A)
(B)
(C)
PITCH ANGLE [°]

the outer edge of the outer zone with a large spike in the upward viewing loss cone. The very next distribution Panel (C) shows isotropic flux in the upward loss cone. Isotropic fluxes are evident to ~ 1 MeV.

Since the precipitating flux is higher than the locally trapped flux, one can estimate the altitude at which pitch angle scattering occurred (Vampola, 1977). This is accomplished by tracing the precipitation flux to the shape of the outer zone as illustrated in Fig 2.7. At L=4 the trapped flux would be roughly 2×10^4 counts/sec up the field line where the precipitation occurred. Fig 2.5b shows fluxes near L=4 of approximately 2×10^4 counts/sec. The altitude of this pass is ~ 7600 km. It must be noted that this "spikey" event is very rare with the overwhelming majority of precipitation cases showing flat isotropic fluxes.

Resonance with 1 MeV electrons at ~1 Re would require $\frac{1}{k_{\parallel} f_{+}}$ $\simeq$ .008, slightly smaller than values for first three harmonics calculated by Ashour-Abdalla and Thorne (1978). In addition, the wave amplitude is $\mathcal{E}_w \simeq 350 \frac{mV}{m}$. Both these calculations indicate that higher harmonics may play a very important role in the mechanism.

Fig 2.8a shows time spectrograms for the filtered plasma wave data (frequency .03-100 KHz) and low energy electron (.2-33 keV) and protons (.1-3.9 keV), 235 keV electrons and > 80 keV protons of the low altitude local evening pass. The 80 keV proton and 235 keV electrons are seen to precipitate (upward loss cone filled) at 5815 UT and 5950 UT (the spike occurred here). Between these times is the inverted V electron event. Plasma turbulence is also evident but not well

FIGURE 2.7 Enlargement of portions of Figure 2.5a.

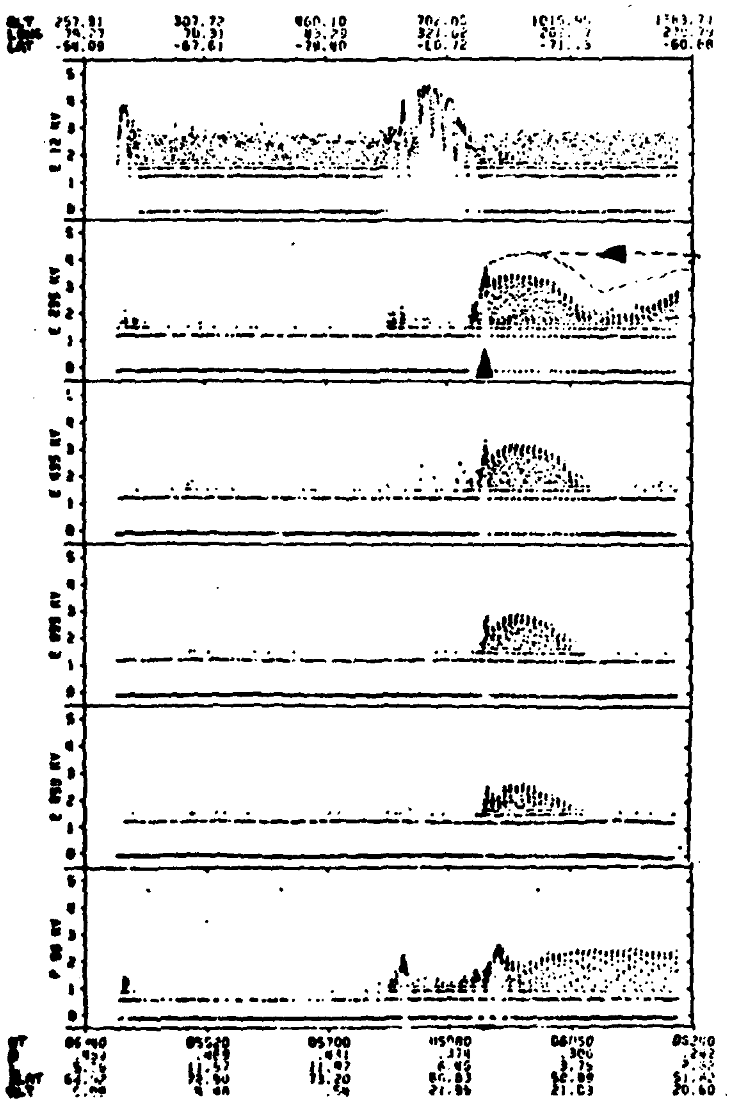

FIGURE 2.8a Spectrogram of plasma waves, 235 keV electrons, low energy electrons, low energy protons, 80 keV protons for the low altitude local evening pass.

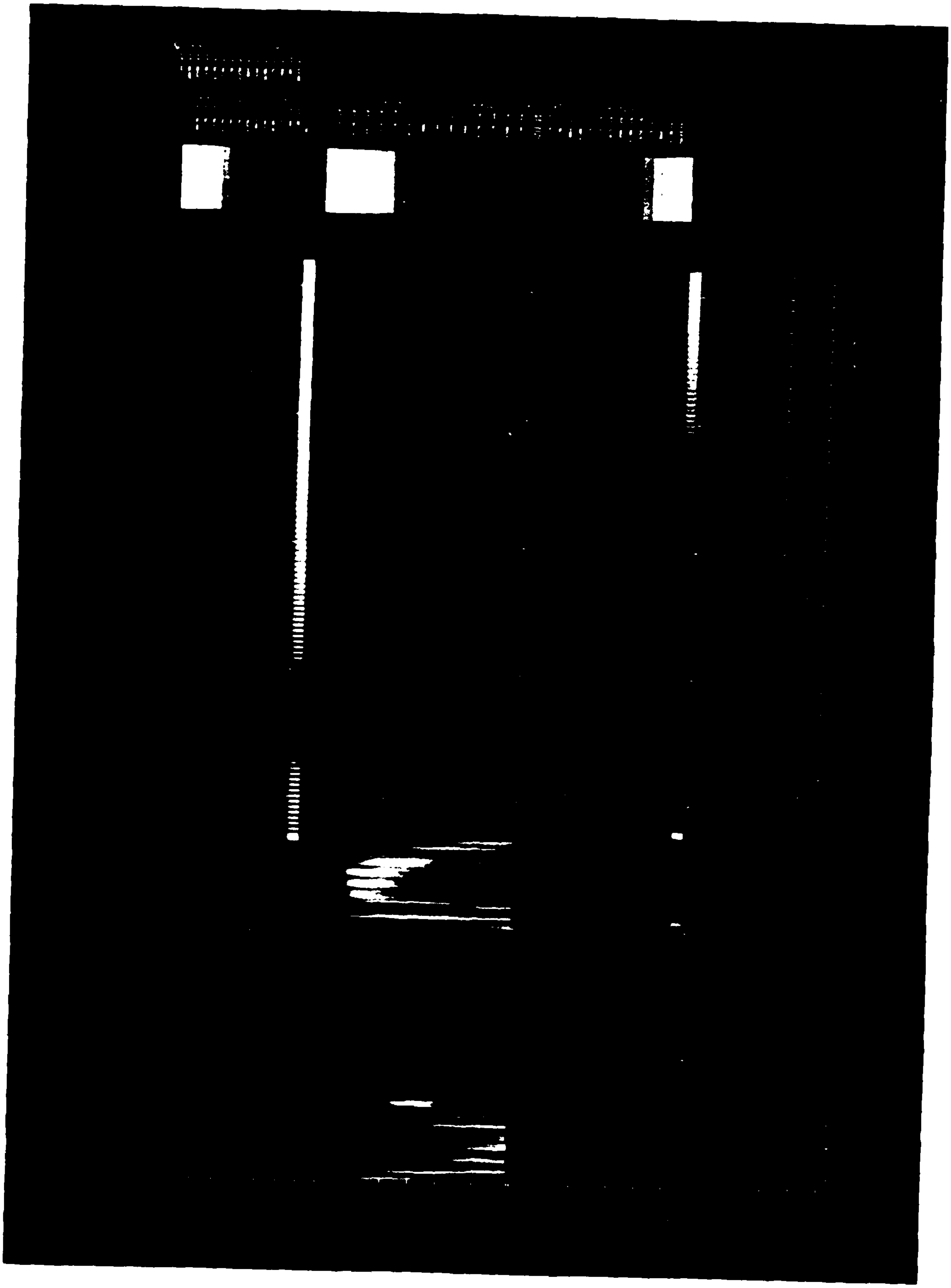

defined. Fig 2.8b shows the high altitude local dusk pass with the inverted V electrons evident from 10500 UT to 10700 UT with ion beams also evident between these times. Plasma turbulence is also evident between these times but the 235 keV electrons have been depleted.

Fig 2.9 shows the raw magnetogram for Kiruna (67^{o} 50'N, 20^{o} 25'E) for 4-6 September 1976. The period is relatively quiet from 0200 UT to 2200 UT 5 September 1976. A small substorm occurs shortly before midnight on 6 September and the estimate (to be shown later) of the extent of the precipitation in time is indicated by the arrows. In addition, the geosynchronous satellite, ATS-6, showed two small excursions in the 140-800 keV electron channel (see Fig 2.10).

The S3-2 satellite has a magnetic spectrometer similar to S3-3 (but only to electron energies of 400 keV). These satellites were coplanar at this time of year. The satellite tracks are shown in Fig 2.11. The X's indicate regions of precipitation for either satellite. The precipitation is first seen on S3-3 at 1.6 UT at 21.5 MLT (spike event). A similar spike event is then seen at 2.1 UT (both 200 and 400 keV channels) by S3-2 in the same location and altitude. Neither satellite observed precipitation electrons (protons were precipitating, Fig 2.5b) at local dusk. Both satellites observed precipitation near 200 keV at local morning at 3.05 UT (S3-2) and 3.8 UT (S3-3). The S3-2 satellite continues in orbit till precipitation at 200 keV is observed again at 3.65 UT at 3.0 MLT, 3.7 UT at 2.3 MLT, and 3.8 UT at 22.5 MLT. The extent of precipitation is thus $\simeq$2.2 hrs. The actual S3-2 flux versus times are shown in Fig 2.12a,b,c.

FIGURE 2.8b Same for the high altitude local dusk pass.

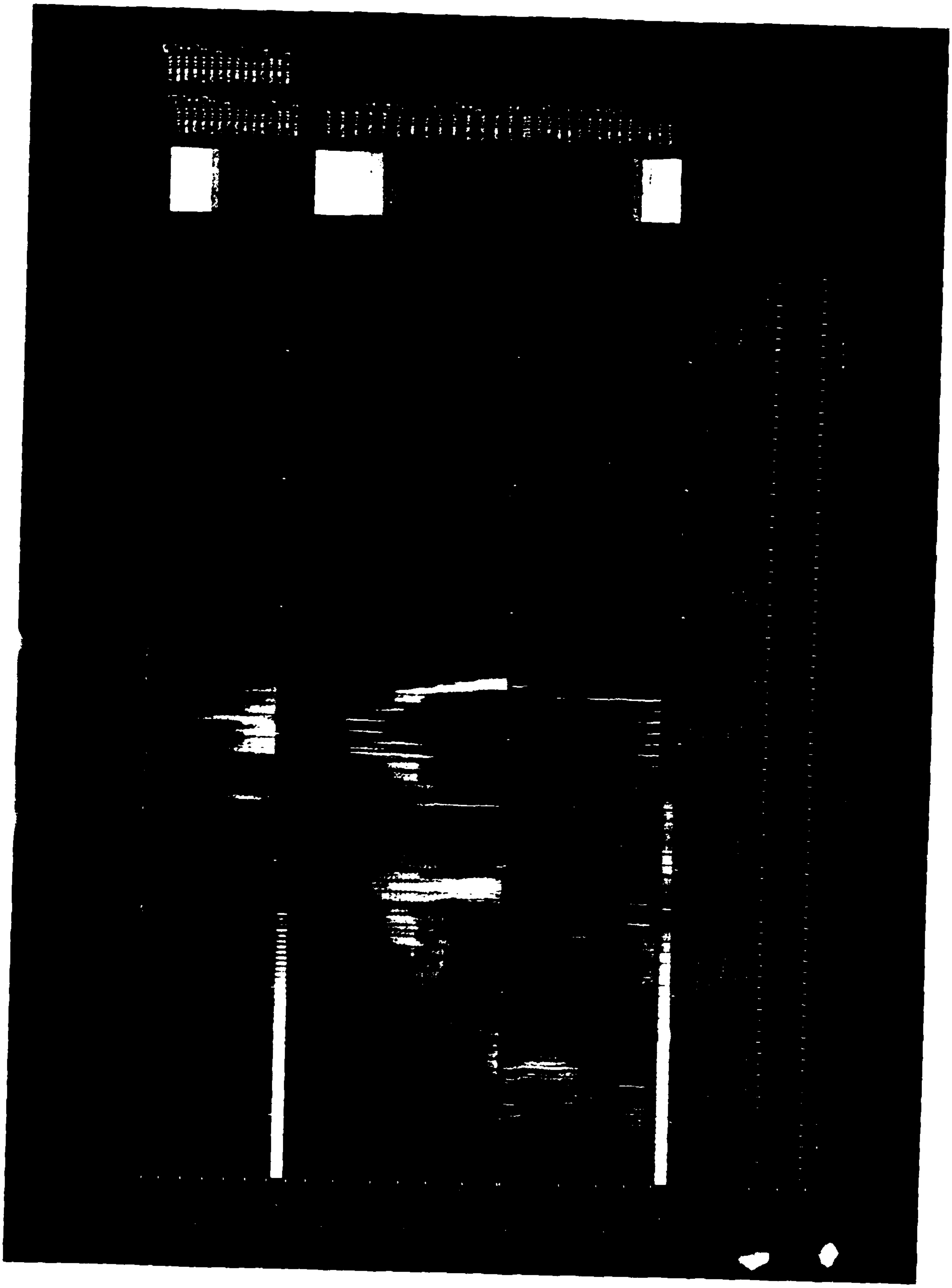

FIGURE 2.9 Kiruna raw magnetogram for 4-6 September 1976.

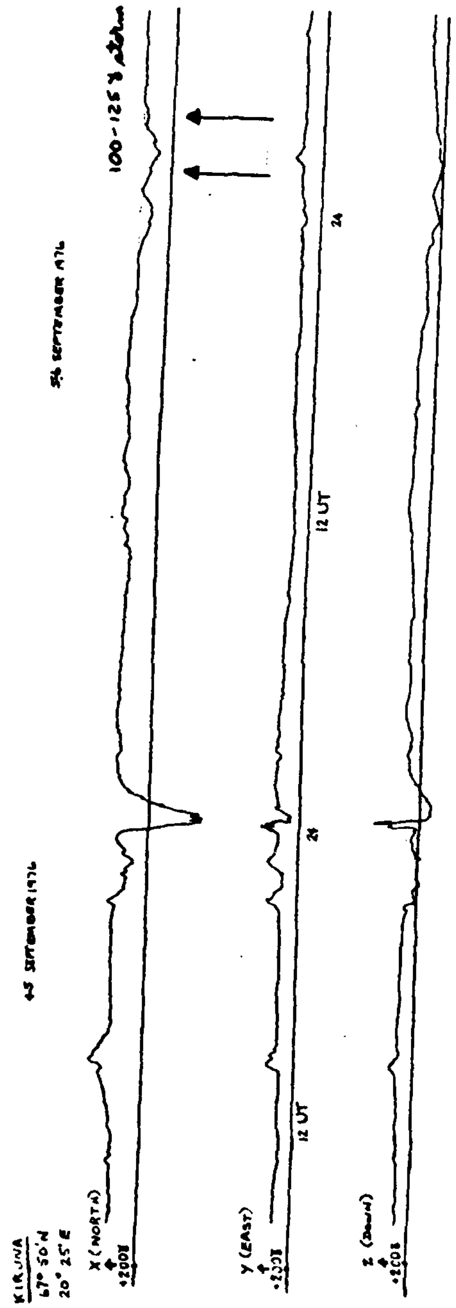
KIRUNA
X (NORTH)
Y (EAST)
12 UT
24
12 UT
24

FIGURE 2.10 ATS-6 for 6 September 1976. Arrows indicate beginning and ending of event.

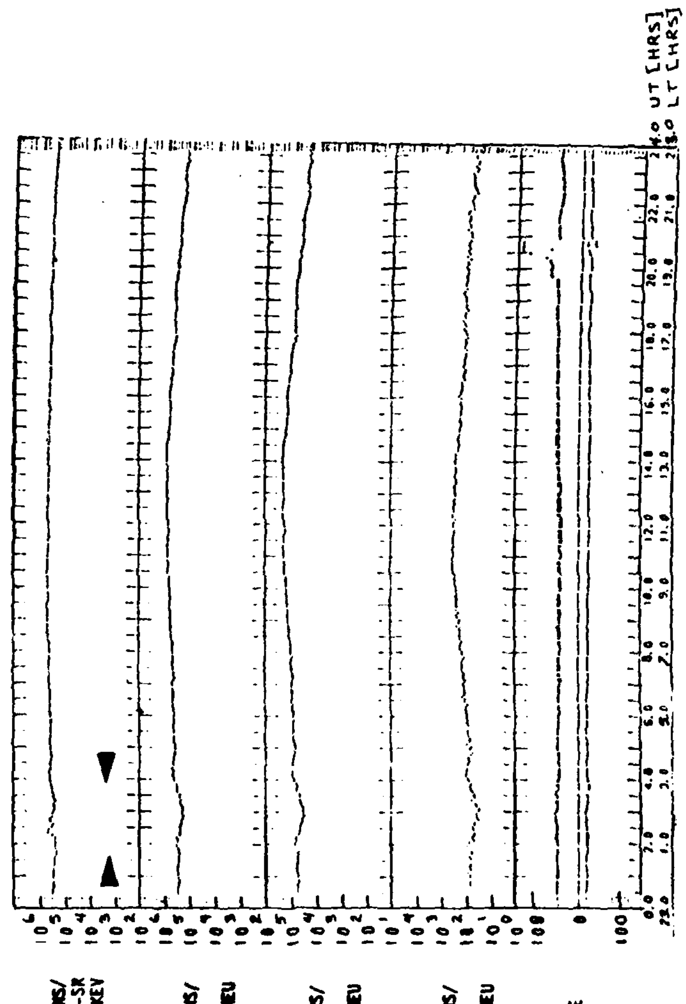
ELECTRONS/
CM2-SEC-SR
140-600KEV
ELECTRONS/
CM2-SEC
GT 0.7 MEV
ELECTRONS/
CM2-SEC
GT 1.6 MEV
ELECTRONS/
CM2-SEC
GT 3.9 MEV
B DIPOLE
GAMMAS
UT [HRS]
LT [HRS]

FIGURE 2.11 S3-2 (1, 2, 3) and S3-3 satellite (a, b, c) tracks for 6 September 1976 in invariant latitude versus MLT.

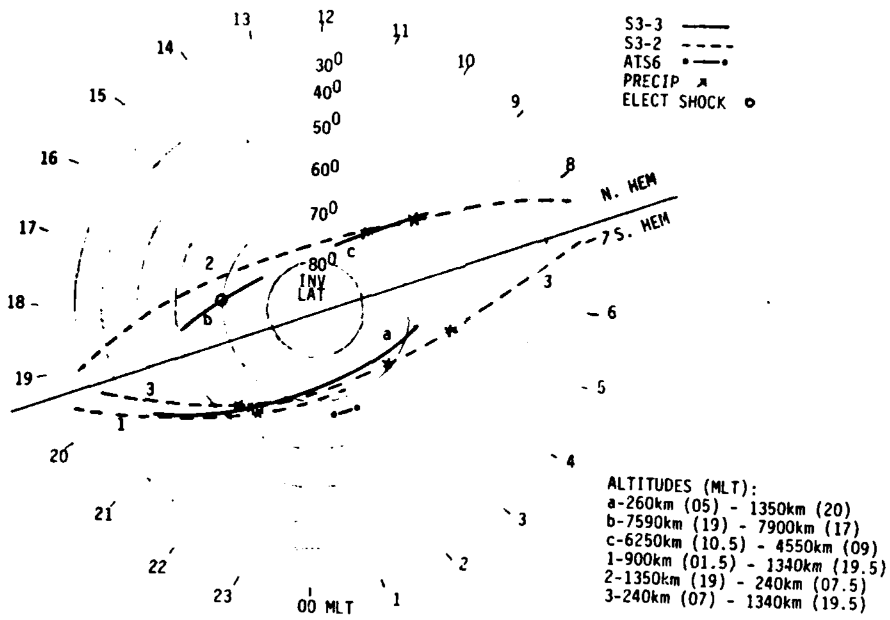

S3-3
S3-2
ATS6
PRECIP
ELECT SHOCK
N. HEM
S. HEM
INV LAT
30⁰
40⁰
50⁰
60⁰
70⁰
80⁰
00 MLT
ALTITUDES (MLT):
a-260km (05) - 1350km (20)
b-7590km (19) - 7900km (17)
c-6250km (10.5) - 4550km (09)
1-900km (01.5) - 1340km (19.5)
2-1350km (19) - 240km (07.5)
3-240km (07) - 1340km (19.5)

FIGURE 2.12a S3-2 flux versus time plots of pass 1, Figure 2.11. Arrows indicate precipitation.

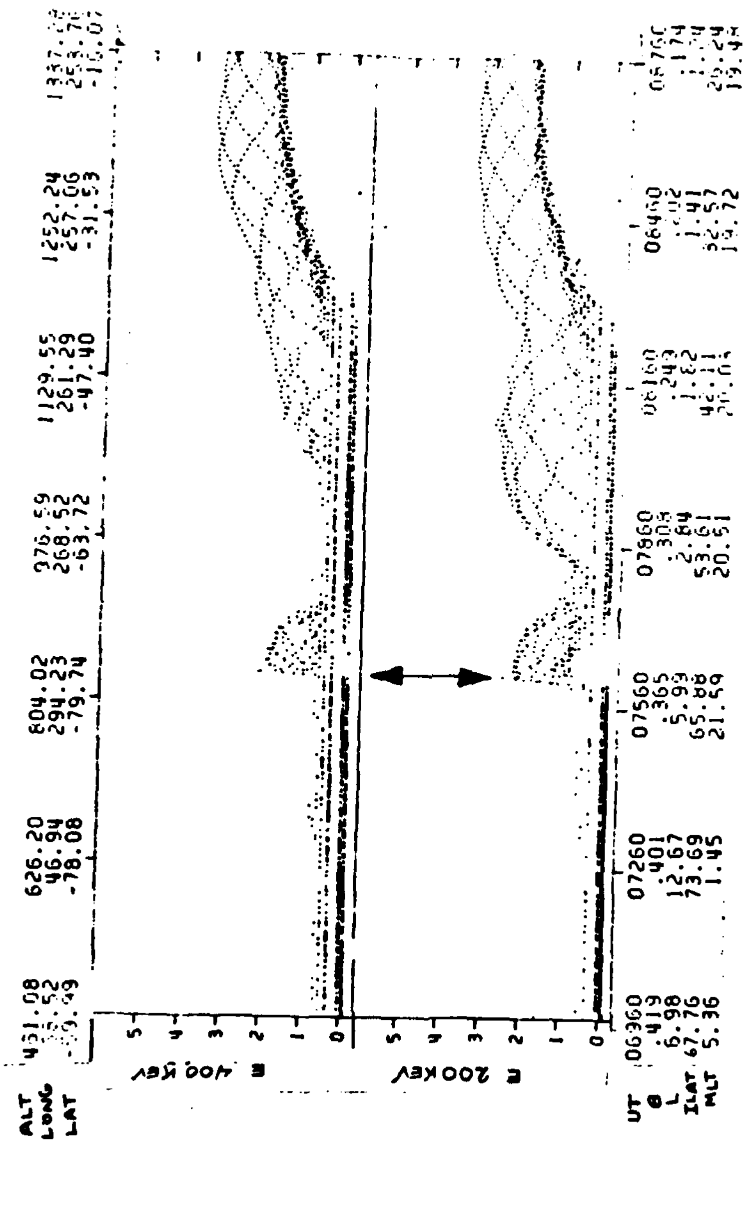

FIGURE 2.12b   Same for pass 2, Figure 2.11.

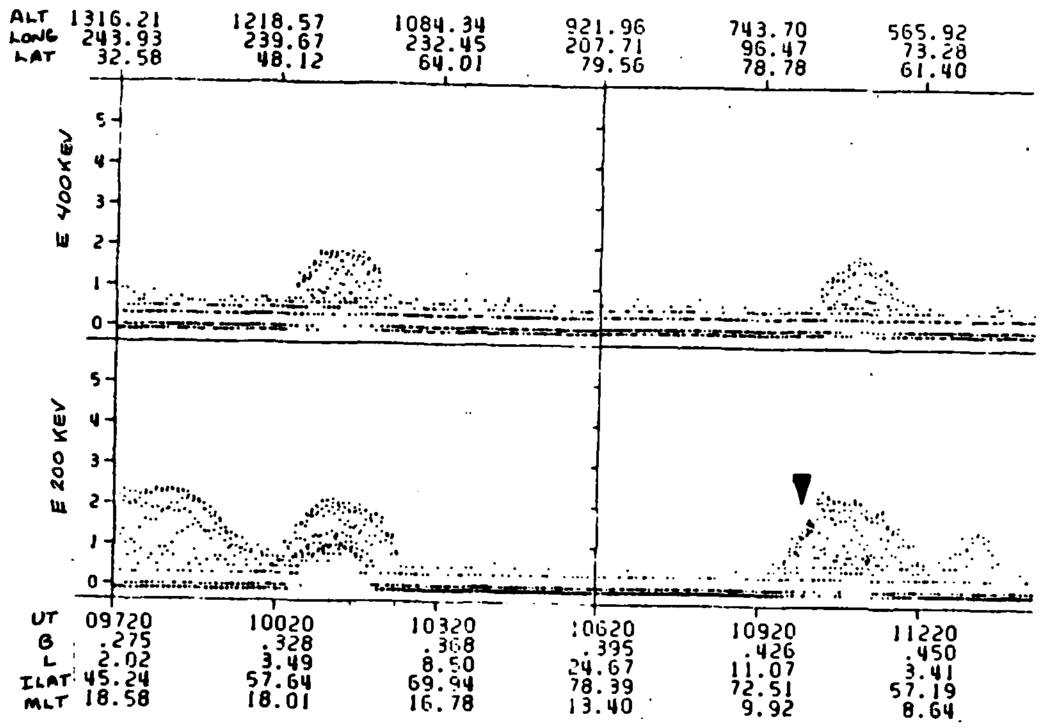

ALT 1316.21 1218.57 1084.34 921.96 743.70 565.92
LONG 243.93 239.67 232.45 207.71 96.47 73.28
LAT 32.58 48.12 64.01 79.56 78.78 61.40
E 400KEV
E 200 KEV
0 1 2 3 4 5
UT 09720 10020 10320 10620 10920 11220
B .275 .328 .368 .395 .426 .450
L 2.02 3.49 8.50 24.67 11.07 3.41
ILAT 45.24 57.64 69.94 78.39 72.51 57.19
MLT 18.58 18.01 16.78 13.40 9.92 8.64

FIGURE 2.12c   Same for pass 3, Figure 2.11.

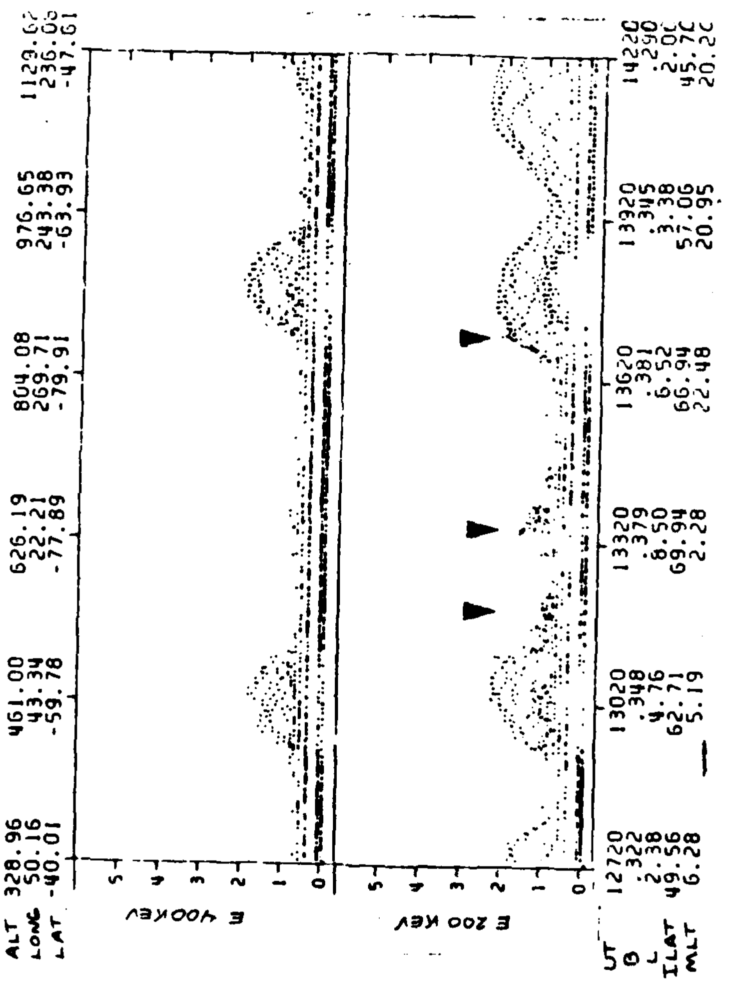
ALT
LONG
LAT
E 400KEV
E 200 KEV
UT
B
L
ILAT
MLT

In summary this event fits the criteria for ESIC mechanism at local evening with whistler mode chorus at local morning. This particular event seems to be a low altitude (~ 1.2 R_0) phenomenon correlated with a 120γ substorm and inverted V event.

2.4.2 Case 2, EMIC (rev 2484, day 132, 12 May 1977)

The flux versus time plot for the EMIC example is shown in Fig 2.13a,b. No precipitation is seen in the 12 or 33 keV electron channels for this local evening, high altitude (~7800 km) pass. In the 235 keV channel, however, the flux at L ≃ 4.3 falls an order of magnitude into the loss cone where normal loss cones are nearly 2 orders of magnitude deep. Proceeding up in energy, the loss cone at this same L value begins to fill until at 850 keV, the loss cones are nearly full (Fig 2.13b). Isotropic distributions are evident in the 1.1, 1.3, and 1.6 MeV channels. In addition, the > 80 keV protons are on strong diffusion from just equatorward of the electron precipitation and continuing poleward. The loss cone filling with increasing energy is evident in Fig 2.14 where pitch angle plots of flux for 160 keV to 1600 keV electron energies are shown. The upward observing loss cone is at 0^0 in these plots. This spectrum and concurrent proton precipitation is indicative of the EMIC mechanism.

The spectrogram for this pass is shown in Fig 2.15. Low energy electron and proton activity is evident poleward of the REP and only the > 80 keV is coincident. No plasma data was available for this pass.

No direct means of observing the plasmapause was available for

FIGURE 2.13a Flux versus time plots of electrons for local evening pass of 12 May 1977.

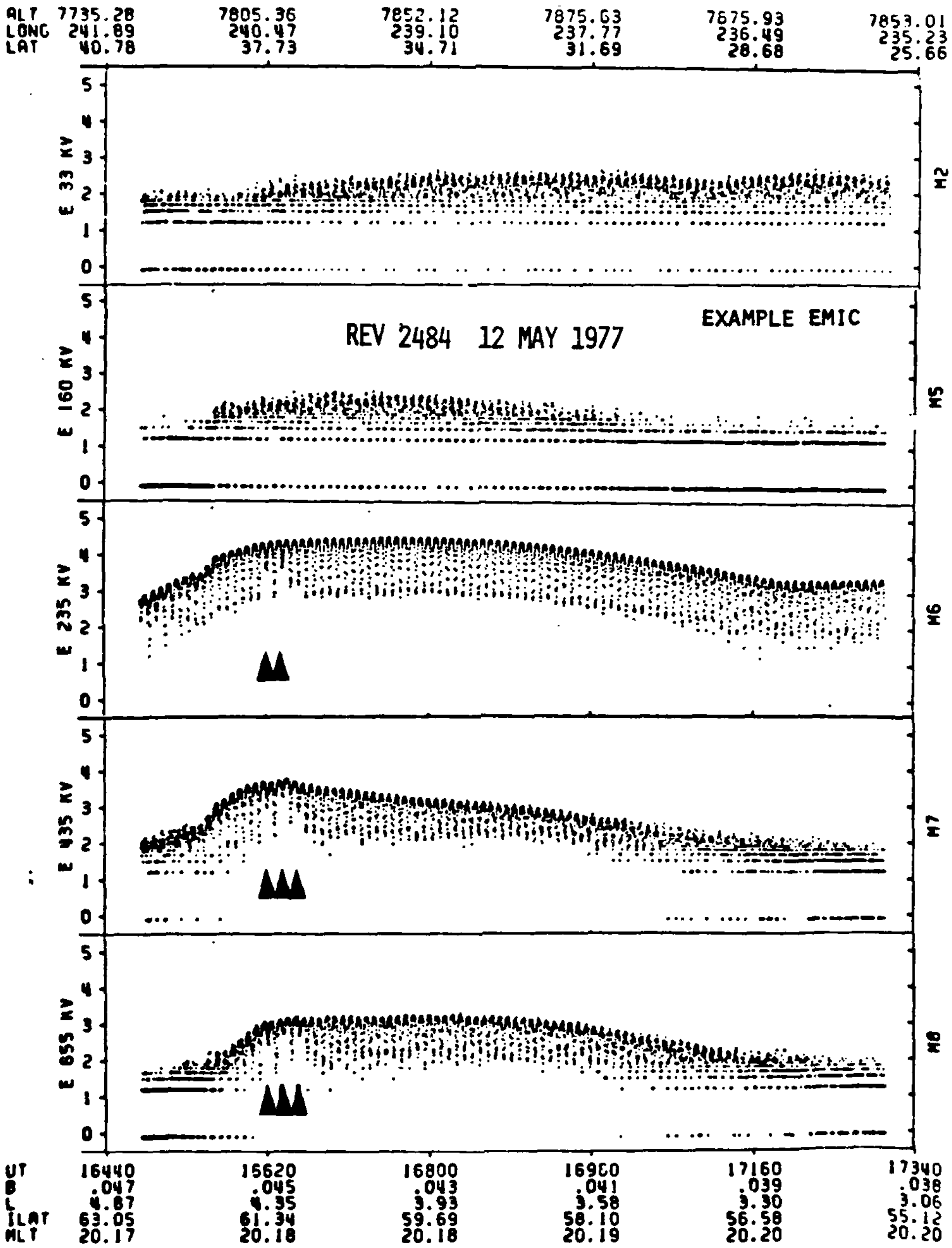
ALT 7735.28 7805.36 7852.12 7875.63 7875.93 7853.01
LONG 241.89 240.47 239.10 237.77 236.49 235.23
LAT 40.78 37.73 34.71 31.69 28.68 25.66
E 33 KV
M2
REV 2484 12 MAY 1977
EXAMPLE EMIC
E 160 KV
M5
E 235 KV
M6
E 435 KV
M7
E 655 KV
M8
UT 16440 16620 16800 16980 17160 17340
B .047 .045 .043 .041 .039 .038
L 4.87 4.35 3.93 3.58 3.30 3.06
ILAT 63.05 61.34 59.69 58.10 56.58 55.12
MLT 20.17 20.18 20.18 20.19 20.20 20.20

FIGURE 2.13b Same for higher energy electrons and protons.

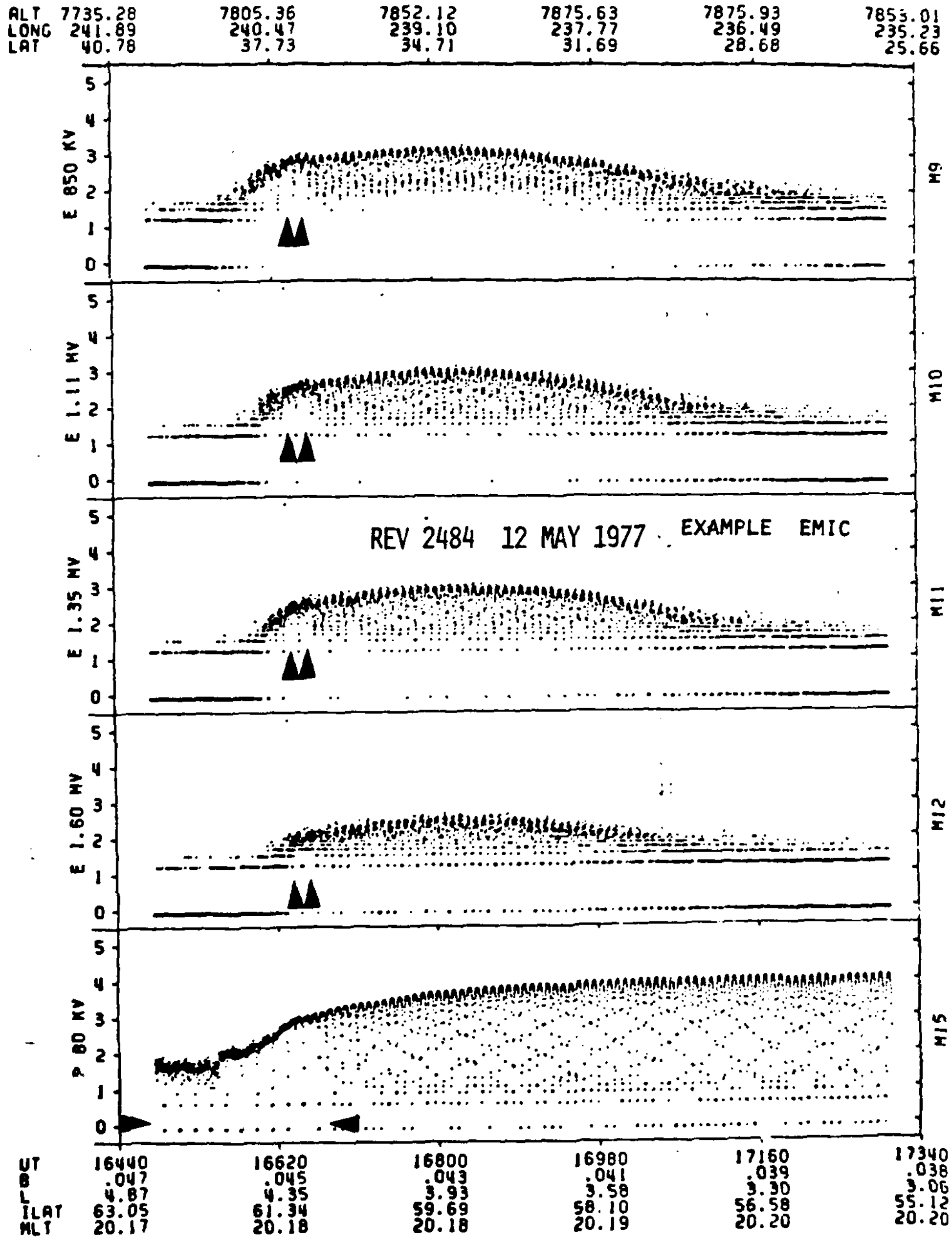
ALT 7735.28 7805.36 7852.12 7875.63 7875.93 7853.01
LONG 241.89 240.47 239.10 237.77 236.49 235.23
LAT 40.78 37.73 34.71 31.69 28.68 25.66
E 850 KV
M9
E 1.11 MV
M10
REV 2484 12 MAY 1977 EXAMPLE EMIC
E 1.35 MV
M11
E 1.60 MV
M12
P 80 KV
M15
UT 16440 16620 16800 16980 17160 17340
B .047 .045 .043 .041 .039 .038
L 4.87 4.35 3.93 3.58 3.30 3.06
ILAT 63.05 61.34 59.69 58.10 56.58 55.12
MLT 20.17 20.18 20.18 20.19 20.20 20.20

FIGURE 2.14 Pitch angle versus flux plots for electrons with energies 160-1600 keV for 12 May 1977.

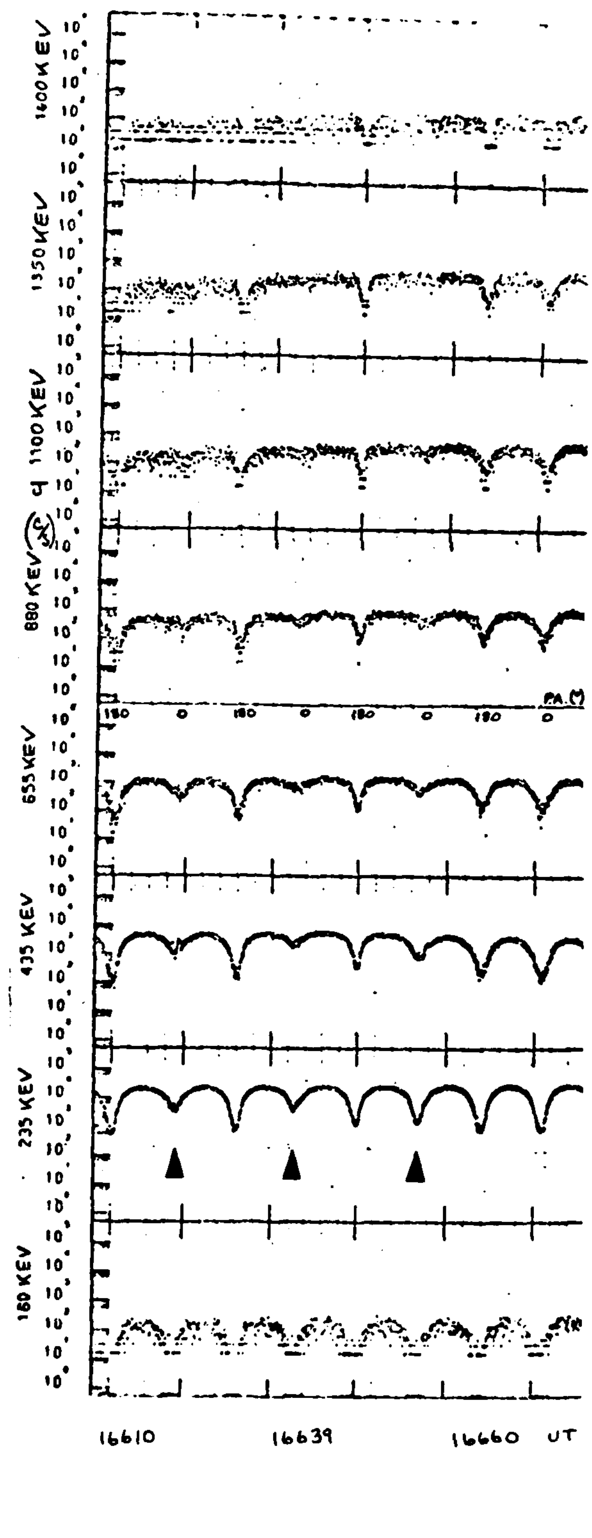
1600 KEV
1350 KEV
1100 KEV
880 KEV
655 KEV
435 KEV
235 KEV
160 KEV
P.A.
16610
16639
16660
UT

FIGURE 2.15 Spectrogram for 12 May 1977.

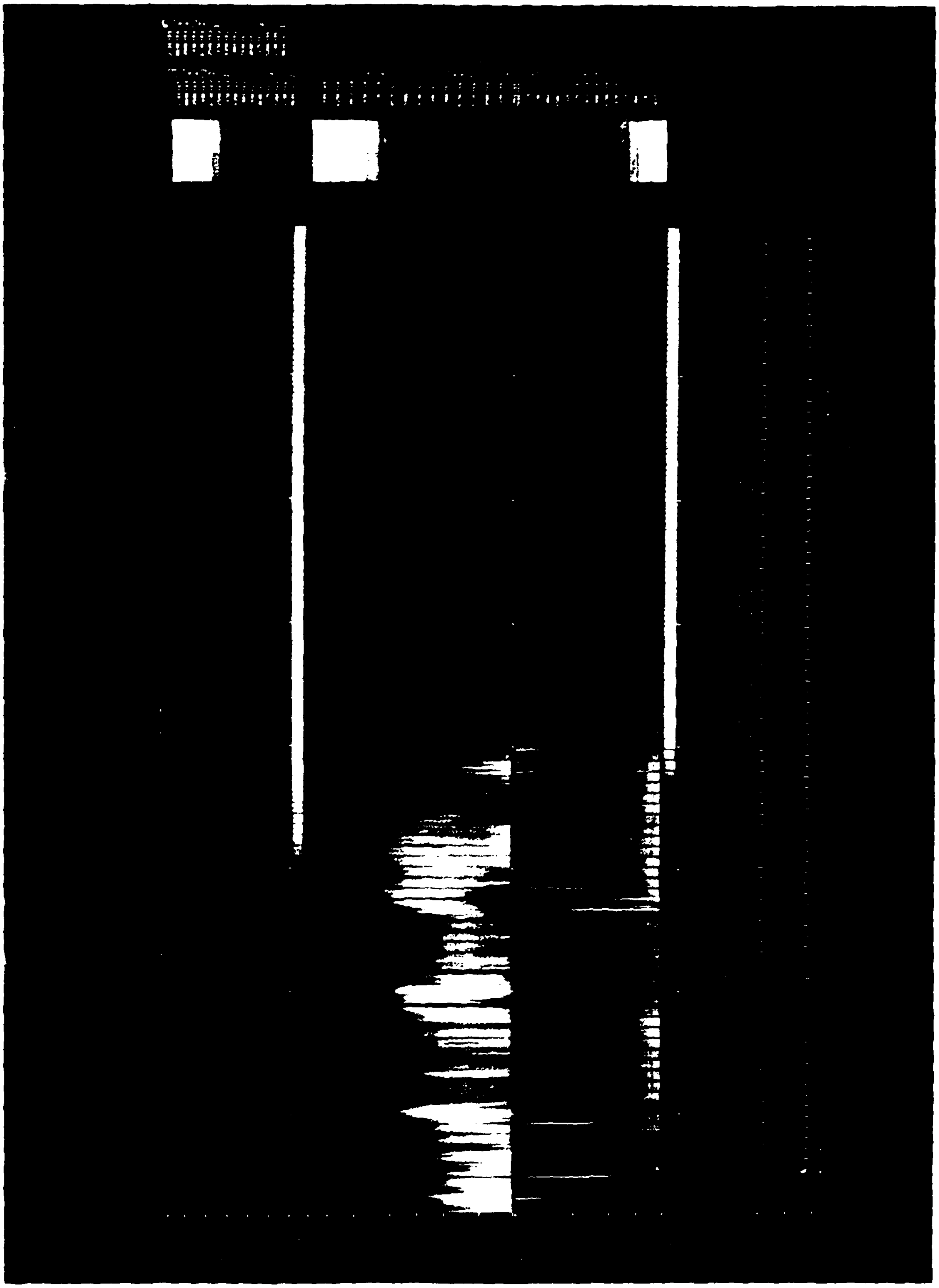

this pass. However Mizera (1974) has shown that the midnight plasmapause is ~.8 L equatorward of the energetic proton precipitation boundary. The electron and proton precipitation are nearly coincident at local evening. Since the plasmasphere bulges poleward from midnight to dusk, the REP may indeed be just within the plasmapause. Another rough approximation to the L value of the midnight-dawn plasmapause location is given empirically by Carpenter and Park (1973) from ATS-5 data:

$$L_{pp} = 5.7 - 0.47\ K_p \quad (29)$$

where Kp is the maximum geomagnetic planetary three-hour-range indices 12 hours previous to the event. The same formula may be used with Kp as the actual value at the time of the event. For UT of 4.6 hrs on 12 May 1977 the Kp at the time of event was ~ 4.5 and the max 12 hrs previous was 5.0. These two values yield Lpp = 3.3-3.9 as the midnight-dawn-noon plasmapause and approximately twice that value for the dusk plasmapause. These are sketched in Fig 2.16. For these rough approximations, the location of the precipitation of rev 2484 is clearly within the plasmasphere.

Finally, Fig 2.17 shows the ATS-6 electron data on 12 May 1977. The REP occurred during a highly disturbed period as indicated in the 140-600 keV electron channel. In addition, S3-3 showed precipitation (ESIC) at energies up to 435 keV on the preceding and following passes at the same local time. Only four of these events ($\bar{E}_p \geq$ 1 MeV) were observed for the entire data set.

FIGURE 2.16 Plasmapause relation to rev 2484, 12 May 1977 based on rough estimates.

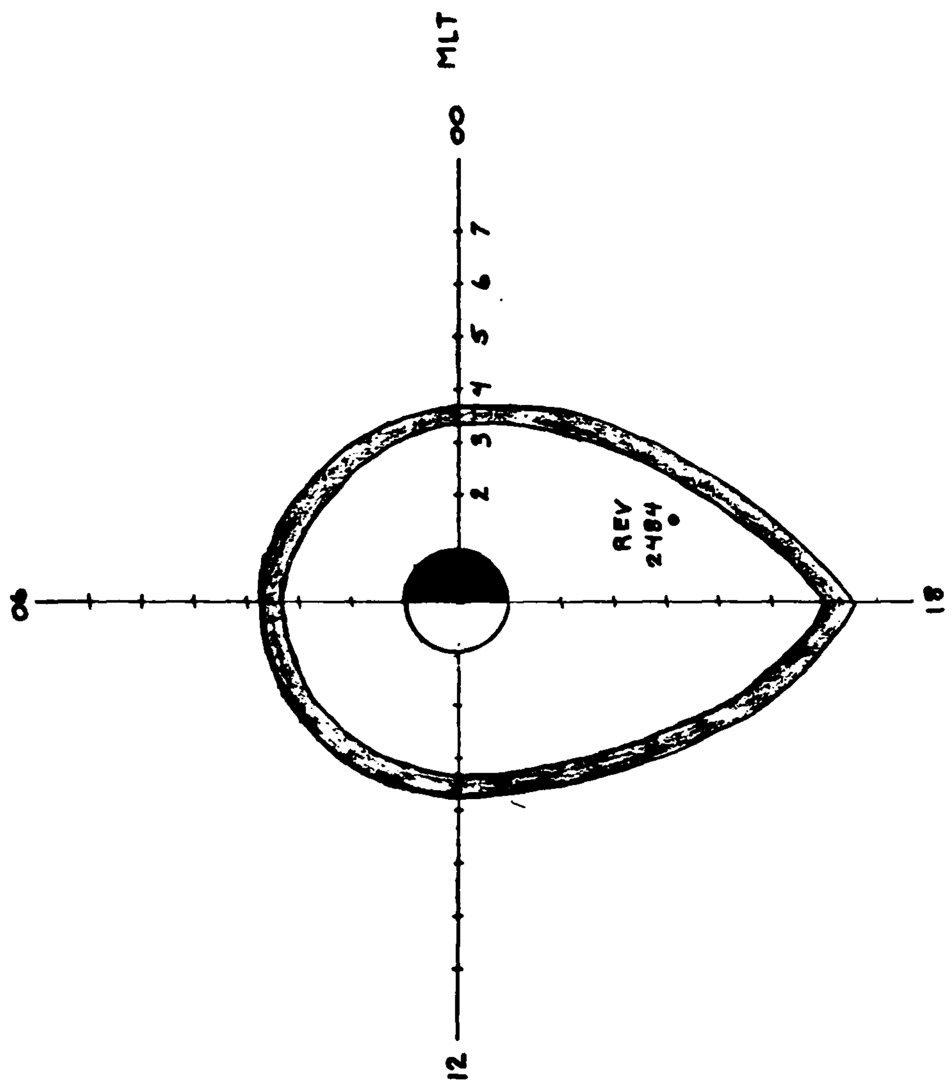
MLT
00
1 2 3 4 5 6 7
06
12
18
REV
2484

FIGURE 2.17 ATS-6 for 12 May 1977.

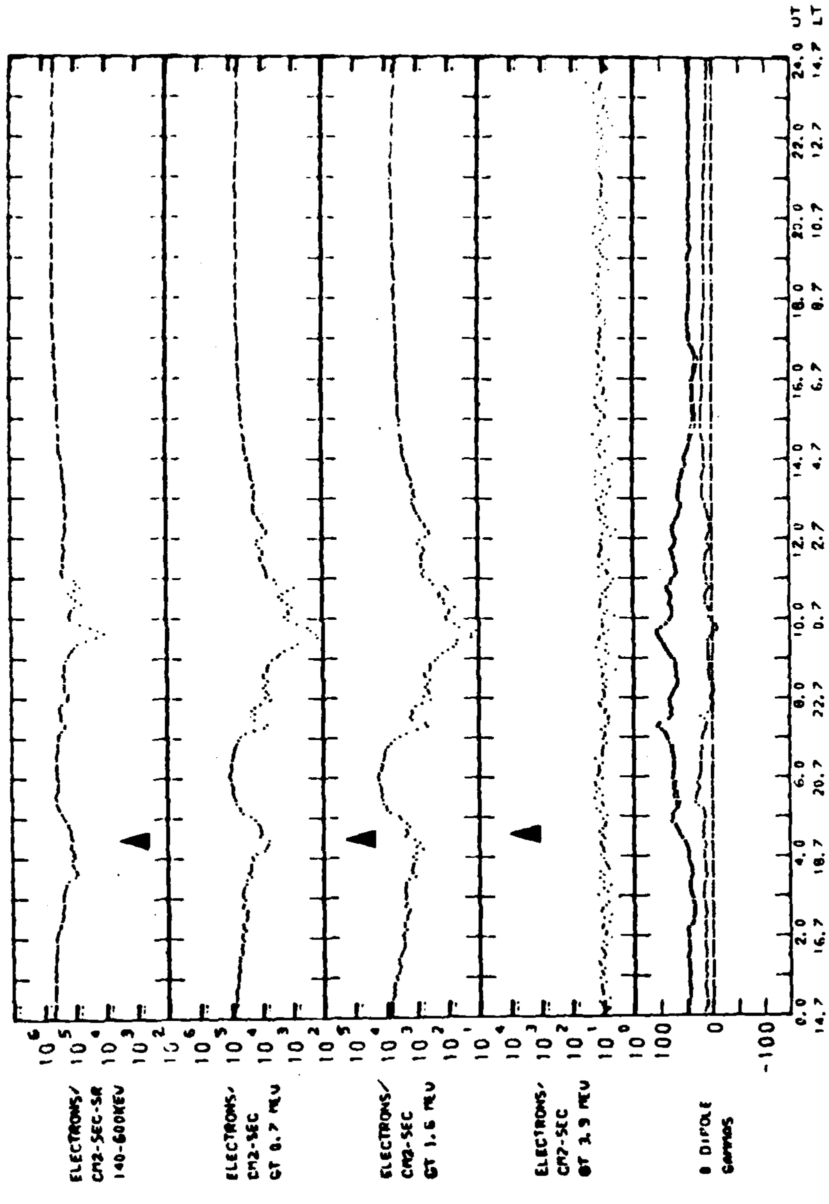
ELECTRONS/
CM2-SEC-SR
140-600KEV
ELECTRONS/
CM2-SEC
GT 0.7 MEV
ELECTRONS/
CM2-SEC
GT 1.6 MEV
ELECTRONS/
CM2-SEC
GT 3.9 MEV
B DIPOLE
GAMMAS
UT
LT

2.4.3 Case 3, Chorus (rev 1413, day 366, 31 December 1976)

The flux versus time plot for 31 December 1976 is shown in Fig 2.18. Only 33 and 235 keV electron precipitation is evident just prior to local noon at low altitude (550 km). No protons were precipitating on strong diffusion though they were present. The pitch angle plot for this event is shown in Fig 2.19 where the loss cone $\simeq 55^{0}$. Normal distributions are evident at 12812 UT but at the later times, 33 and 235 keV channels are isotropic in the upward viewing loss cone.

The spectrogram (Fig 2.20) shows evidence of plasma noise just above 30 Hz at and poleward of the REP (12820 UT). A faint band near 10 kHz is also evident.

FIGURE 2.18 Flux versus time plots for 31 December 1977. Arrows indicate strong diffusion precipitation

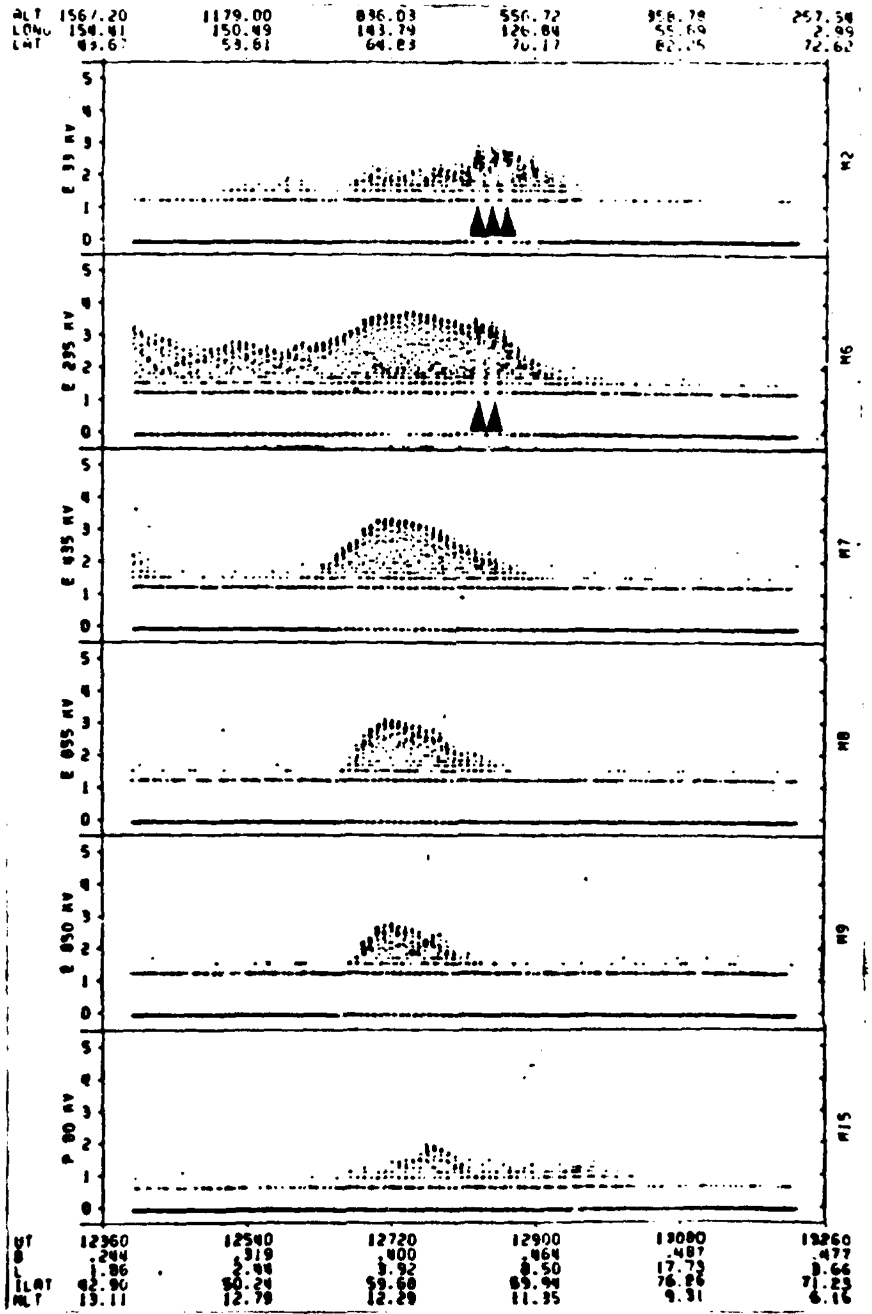

FIGURE 2.19 Pitch angle distributions for 33, 235, 435 keV electron channels for 31 December 1976.

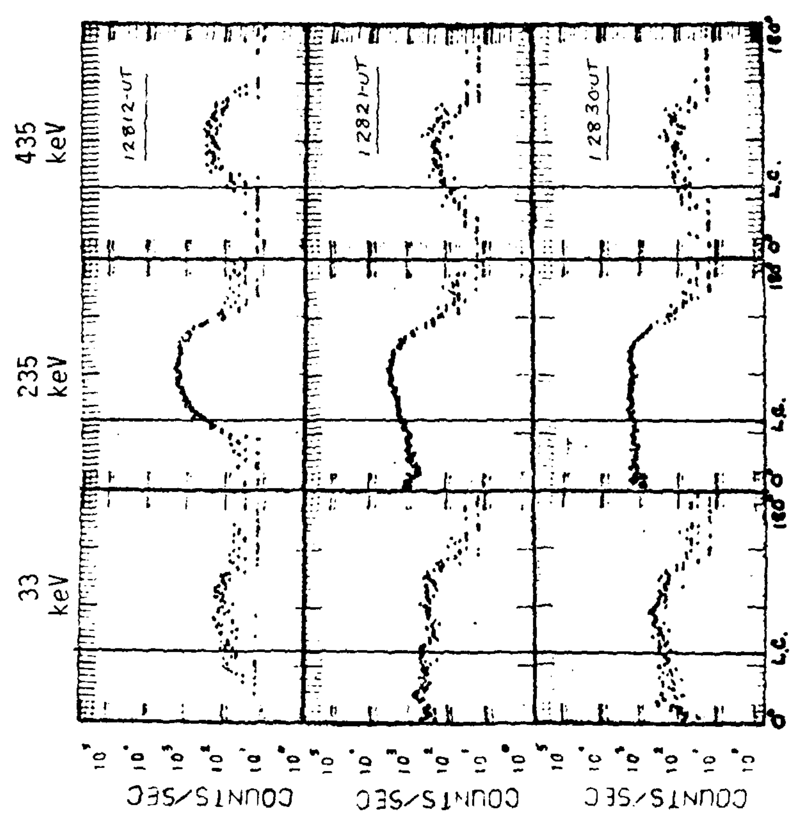
435 keV
235 keV
33 keV
12812-UT
12821-UT
12830UT
COUNTS/SEC
COUNTS/SEC
COUNTS/SEC
L.C.
L.C.
L.C.

FIGURE 2.20 Spectrogram for low altitude early morning pass on 31 December 1976.

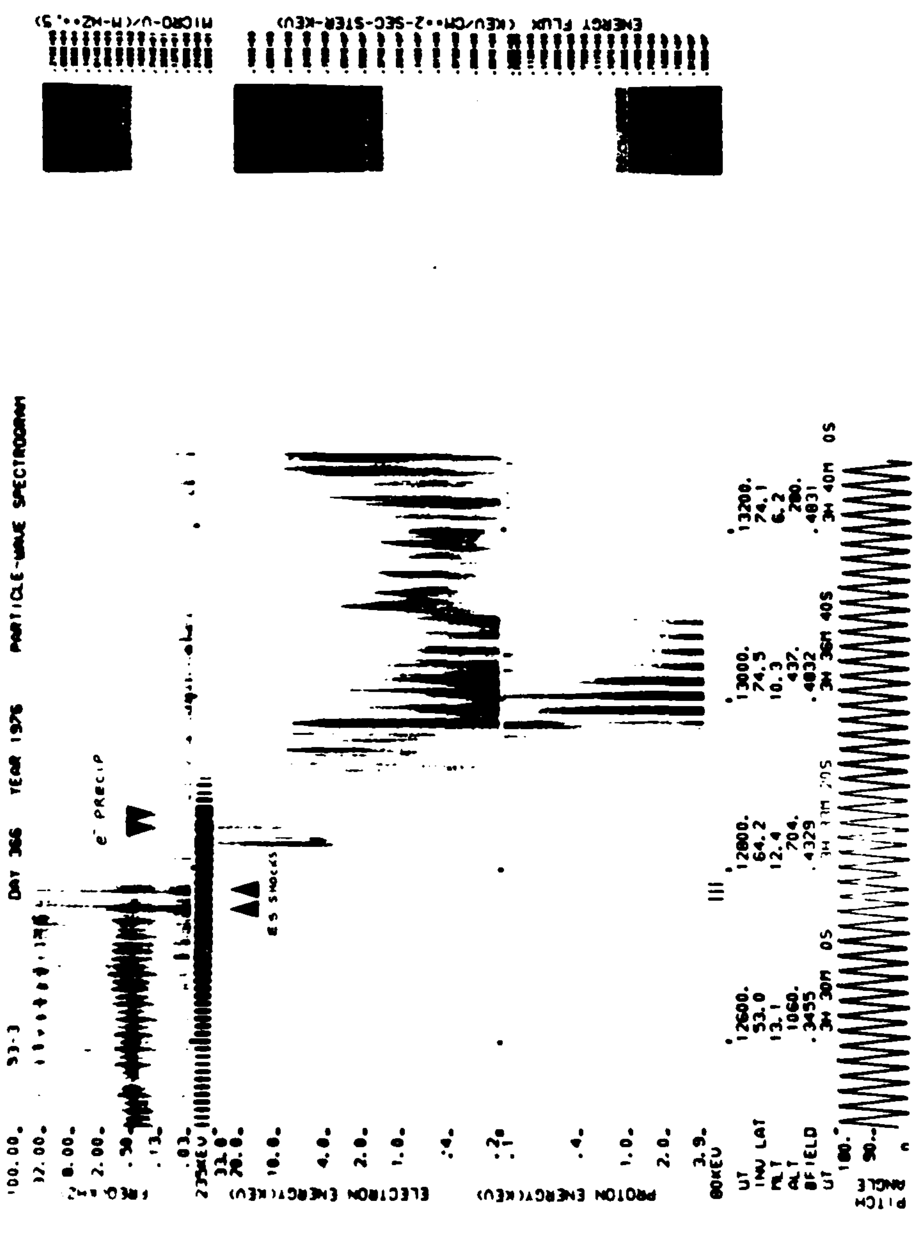

CHAPTER 3. ATMOSPHERIC CONSEQUENCES

3.1 Introduction and Background

The earth's atmosphere below 100 km has been the object of intense investigation over the past 10-15 years. It is well known that a variety of electromagnetic and particle radiation can deposit energy in this region and thus modify the local chemistry. The remainder of this section describes the ionization and neutral chemistry with special emphasis on ozone removal. In subsequent sections we examine the three examples in Chapter 2 and their effect on ozone.

The ionosphere below 100 km, known as the "D region," has been studied by several authors with respect to ionization by solar and galactic cosmic rays (Webber, 1962), primarily in the polar cap region ($\Lambda \gtrsim 75^o$): energetic electron precipitation in the auroral region, $\Lambda \simeq 70\text{-}75^o$ (Rees, 1963; Lerfold and Little, 1964; Bailey et al., 1970) and subauroral regions, $\Lambda \simeq 60\text{-}70^o$ (Bailey, 1968; Larsen, 1973; Reagan, 1977; Thorne, 1977b) and at mid latitudes, $\Lambda \lesssim 60^o$ (Potemra and Zmuda, 1970; Spjeldvik and Thorne, 1975a,b; Larsen et al., 1976). Solar UV, especially HLyα at 1216 A^o and HLyβ at 1025 A^o, produces the dominant primary ion in the quiet mesosphere through ionization of NO. Also, solar UV scattered from the sunlit hemisphere has long been thought to be an important ionizing radiation source at night. Solar UV (and X-ray) radiation is strongly absorbed below about 85 km where positive ion composition is dominated by multiply hydrated ion clusters of the type $H^+(H_2O)n$, $NO^+(H_2O)n$, and $H_3O^+(H_2O)n$ (Johannesen and

Krankow ski, 1972). O_2^-, the dominant negative ion below 80 km, is produced by electron attachment and interacts with CO, NO, HCO and $(H_2O)n$ to form heavy negative ion and large water clusters.

Although the precipitating particle energy is usually negligible compared to other ionizing sources below 100 km, it can be the dominant ionization source during disturbed conditions below 80 km (Thorne, 1977b). Particulate energy produces mostly primary ions O_2^+ and N_2^+, N^+, and O^+ of which ~94% are rapidly converted to O_2^+ through charge exchange with O_2 (Reagan et al., 1978) and ~6% to NO^+ by ion-atom interchange with N_2 and O_2 (Gunton et al., 1977). This disturbed increase in O_2^+ can thus modify the complex clustering reactions in the D-region.

A comparison of several ionizing sources is presented in Fig A.15 (Appendix A) where the overwhelming dominance of the largest solar proton event (SPE) of August 1972 is evident. Immense SPEs such as August 1972 are relatively rare and indeed REPs can frequently be the dominant ionization source below 100 km (Spjeldvik and Thorne, 1975a; Thorne, 1977b).

The production and removal of odd oxygen (O, O_3) is of paramount importance in neutral atmospheric chemistry below 100 km. Odd oxygen is produced primarily by photodissociation of molecular oxygen. The Chapman (1930) process, $O+O_3 \rightarrow 2O_2$, is now well known to account for only ~20% removal of odd oxygen. The major removal process includes catalytic loss cycles with chlorine compounds (e.g. Crutzen and Howard, 1978), and odd nitrogen and odd hydrogen species (Blake and Lindzen, 1973). The latter two are of particular interest here since they can be significantly modified by intense particle precipitation (Thorne, 1977a,b; 1979).

The bulk of odd oxygen depletion is through the following nitrogen chemistry important particularly below 50 km (Blake and Lindzen, 1973):

$$NO + O_3 \rightarrow NO_2 + O_2 \quad \text{(Davis et al., 1973)}$$

$$NO_2 + O \rightarrow NO + O_2 \quad \text{(Herron and Huie, 1972)}$$

REPs can be the dominant source of NO production by dissociation of N_2 in the mesosphere and a competing source with nitrous oxide upwelling from the Earth's surface in the upper stratosphere (Thorne, 1979).

Above 40 km the odd hydrogen chemistry begins to dominate in the removal of odd oxygen (Blake and Lindzen, 1973). Here the odd hydrogen is produced mainly by dissociation of water vapor by photons and O ('D) atoms and as a by-product of O_2^+ production by energetic particle precipitation (Rowe et al., 1974). In this way, the increase in O_2^+ during REPs may also affect the mesospheric removal of odd oxygen. Since energy deposition by REPs can dominate in the mesosphere, we shall subsequently examine the removal of odd oxygen by the enhanced odd hydrogen chemistry and its ozone consequences for the three REP examples of Chapter 2.

3.2 REP Energy Spectra and Atmospheric Energy Deposition

The precipitation spectra for the three cases presented in Chapter 2 are shown in Fig 3.1. The ESIC spectrum (Case 1) has the

FIGURE 3.1 Energy spectra for cases 1,2,3 of Chapter 2.

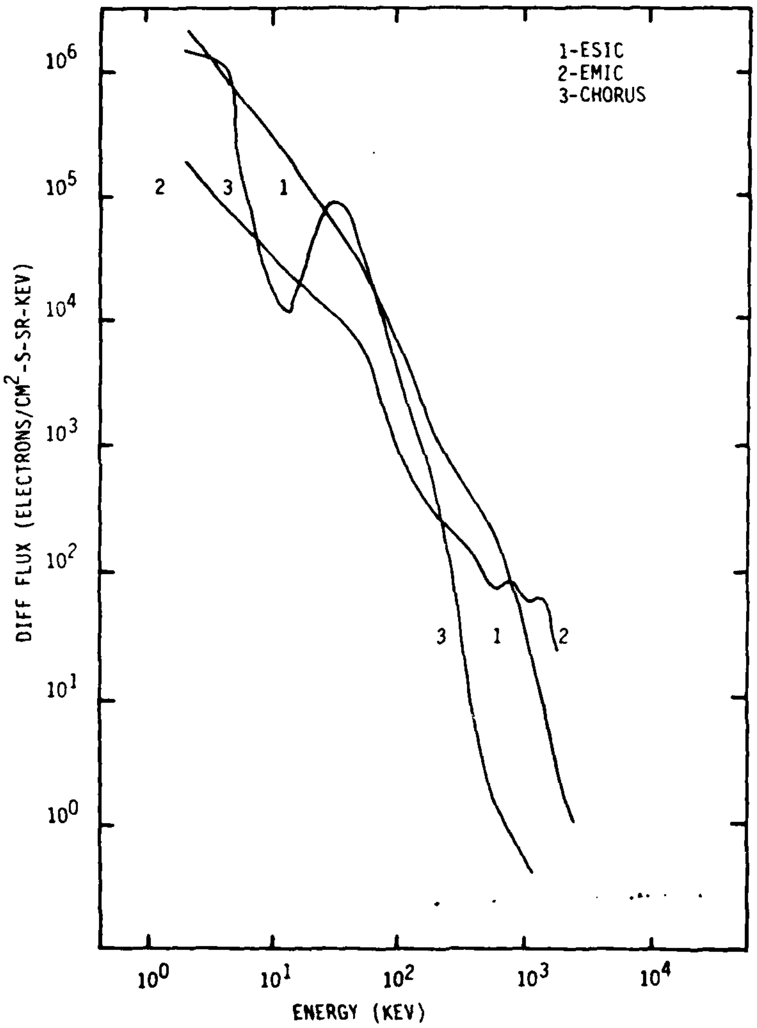
1-ESIC
2-EMIC
3-CHORUS
2
3
1
3
1
2
DIFF FLUX (ELECTRONS/CM2-S-SR-KEV)
10^6
10^5
10^4
10^3
10^2
10^1
10^0
10^0
10^1
10^2
10^3
10^4
ENERGY (KEV)

highest flux in the 100-800 keV range. The EMIC spectrum (Case 2) dominates at energies above 1 MeV and is comparable to the previously published spectrum of Vampola (1971). The chorus event is relatively weak dominating only near 3 and 30 keV. These REP spectra were input to the UCLA (Spjeldvik, 1974) electron precipitation model (see Appendix D). The ion pair production (assuming 35 keV per pair) versus altitude is shown in Fig 3.2. The Bremsstrahlung X-ray deposition profiles were also plotted in Fig 3.2. As expected, the ESIC curve dominates in the 70 km region, and EMIC in the 50-60 km region. Whistler events are relatively non-competitive with other REP spectra but may dominate local chemistry.

The ESIC case of Chapter 2 was used to model a typical REP to calculate the total energy deposition. The latitudinal extent was approximately 200-300 km based on the invariant latitude excursions of both S3-2 and S3-3. The longitudinal extent based on local time duration was 7,000-10,000 km. The event lasted approximately 2.2 hours. The peak ion production rate occured at ~73 km altitude with a value of $6.8 \times 10^{-}$ (cm^{-3} sec^{-1}). Assuming precipitation was nearly constant and uniform throughout the events (which is not likely), a peak value of ~1×10^{24} ion pairs cm^{-1} (column) or 3.5×10^{22} keV of energy was deposited during this event.

3.3 REP Induced Hydrogen and Ozone Modifications

The REP ion production rates versus altitude were processed to produce odd hydrogen (and thus hydroxyl) according to the chemical modelling of Heaps (1978). Fig 3.3 presents this model of odd hydrogen

FIGURE 3.2 Ion pair production rate versus altitude for ESIC, EMIC, and chorus events.

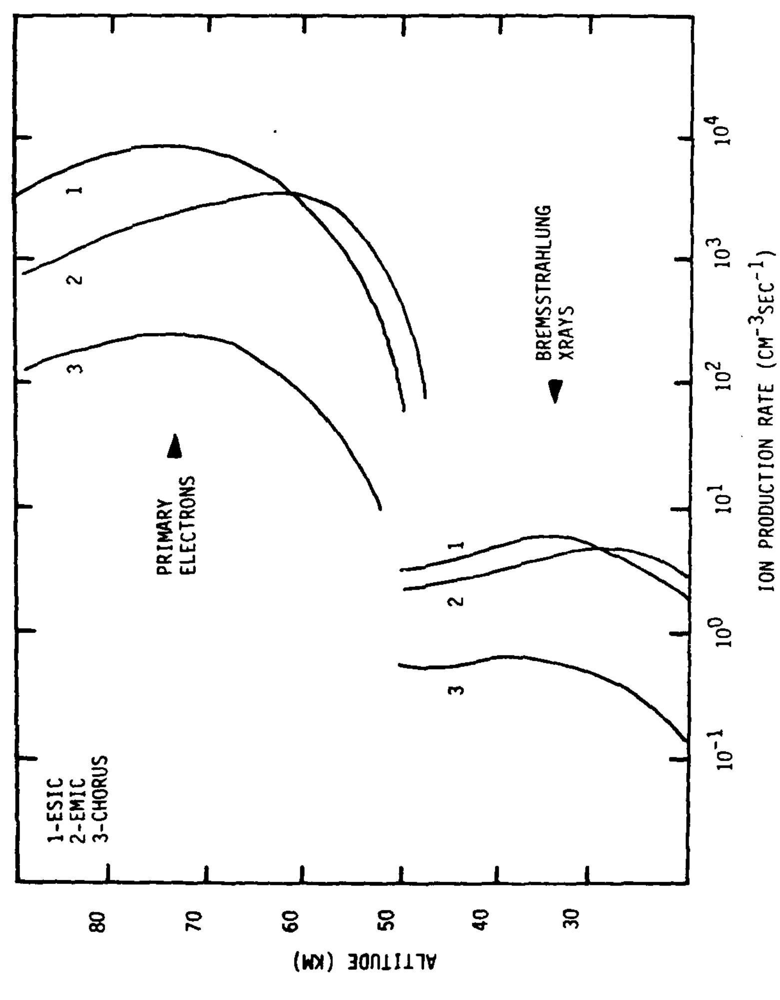

1-ESIC
2-EMIC
3-CHORUS
PRIMARY ELECTRONS
BREMSSTRAHLUNG XRAYS
1
2
3
1
2
3
ALTITUDE (KM)
80
70
60
50
40
30
ION PRODUCTION RATE (CM^{-3}SEC^{-1})
10^{-1}
10^{0}
10^{1}
10^{2}
10^{3}
10^{4}

FIGURE 3.3 Altitude profile of the odd hydrogen formation rate related to ion pair production.

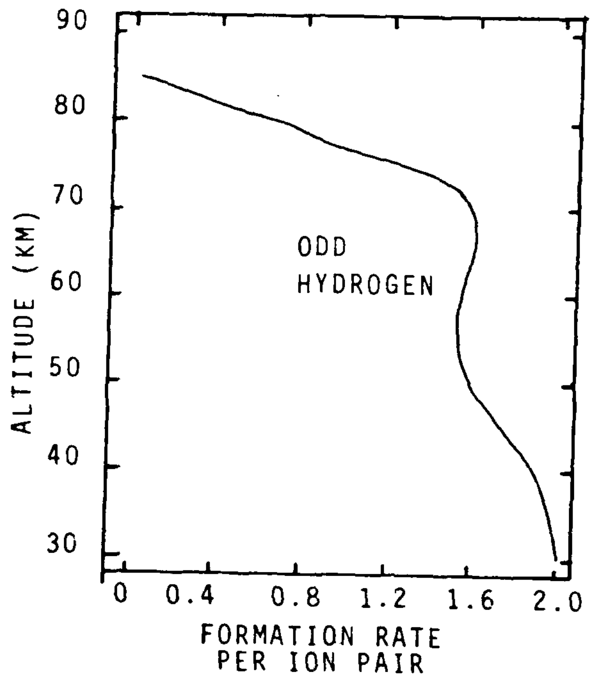
90
80
70
60
50
40
30
ALTITUDE (KM)
ODD
HYDROGEN
0
0.4
0.8
1.2
1.6
2.0
FORMATION RATE
PER ION PAIR

production as a function of ion pair production for disturbed conditions (higher ion production rate). The higher altitude limit for cluster ion formation is clearly indicated by the trailoff above 80 km. Since the nitrogen cycle dominates in the stratosphere, odd hydrogen is not expected to be important below 40 km.

After modelling the OH increases to the REP ionization rates, a numerical simulation fashioned after Blake and Lindzen (1973) was performed to calculate the relative change in ozone concentrations. The numerical simulation differs from Blake and Lindzen's model in that two reactions (OH nighttime source reaction and Chapman's (1930) original 3 body atomic oxygen collision equation to form O_2) are added, reaction rates are updated, and solar flux and ozone conentrations vary with time of day (DeVore, 1977).

The results for Case 1 and 2 (Fig 3.4a and b) are similar since they both occur during local evening. Factors of 10 and 4 increase in OH concentrations at 70 km immediately after precipitation commenced occurred for the ESIC and EMIC cases respectively. The enhancement continued throughout the night and several hours into the day. Ozone was not affected until sunrise due to the low nighttime O concentration but showed sunrise decreases of 10-15% for both cases. These diminished ozone concentrations lasted for several hours.

The chorus event (Case 3, Fig. 3.4c) occurred near local noon with a small enhancement in OH concentration and throughout the succeeding night. The ozone concentration showed an immediate response dropping by nearly 20%. The diminution of ozone ended at local sunset.

FIGURE 3.4a,b,c Ozone and hydroxyl concentrations [cm^{-3}] versus local time (hrs) for a. ESIC, b. EMIC, and c. chorus REP events.

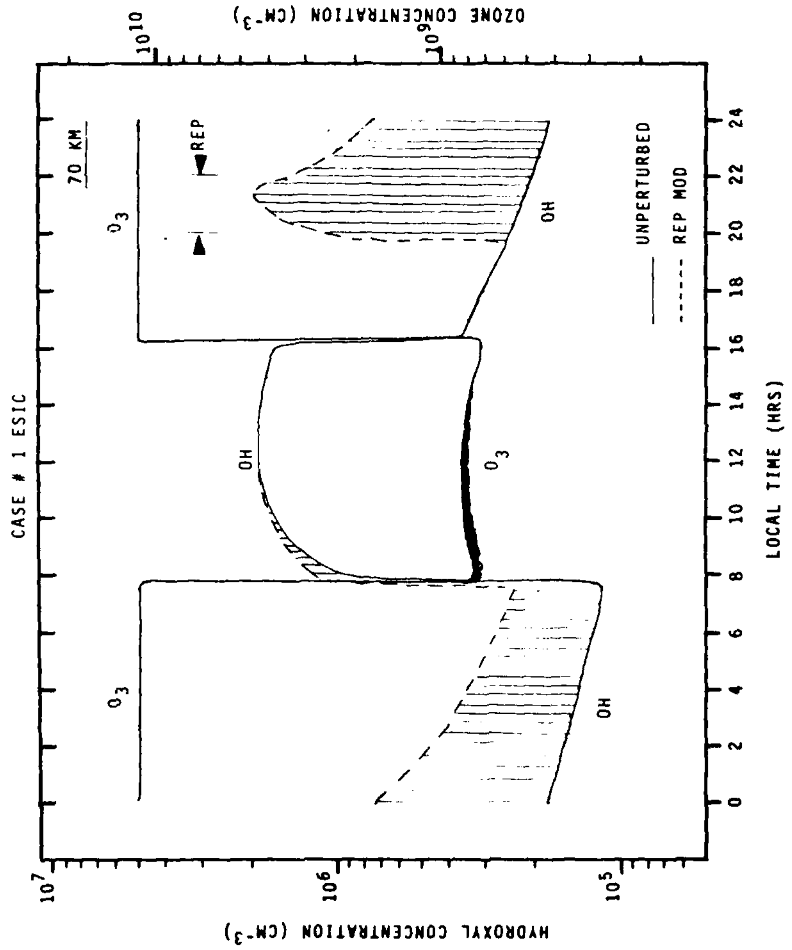
CASE # 1 ESIC
70 KM
O3
OH
REP
UNPERTURBED
REP MOD
LOCAL TIME (HRS)
HYDROXYL CONCENTRATION (CM-3)
OZONE CONCENTRATION (CM-3)

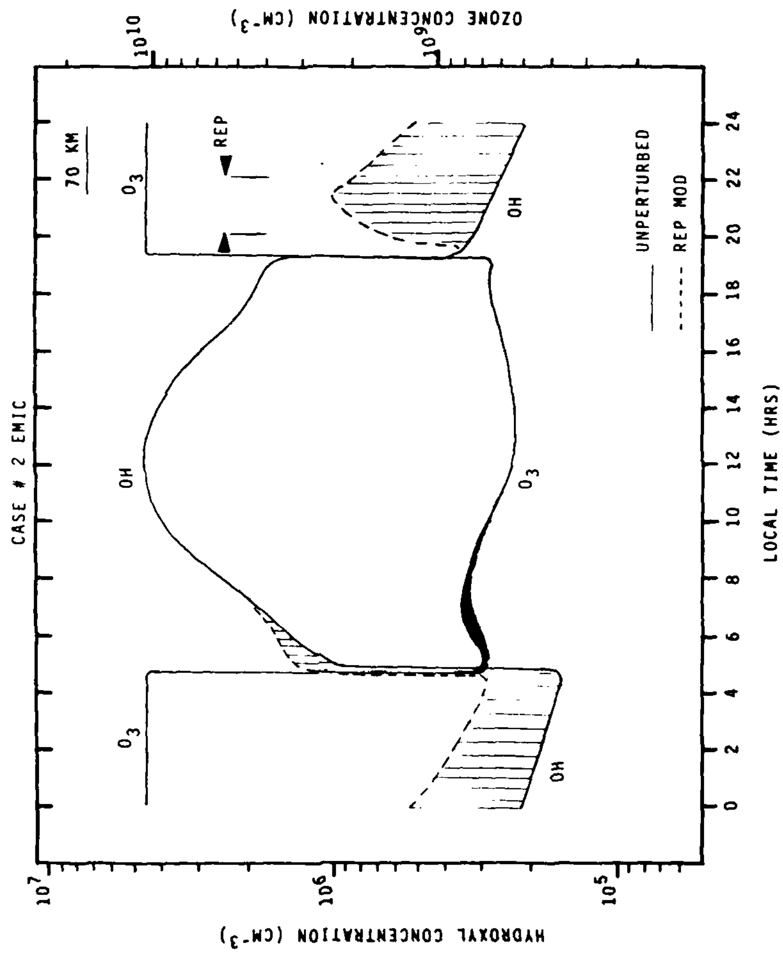

CASE # 2 EMIC
70 KM
REP
O3
OH
UNPERTURBED
REP MOD
LOCAL TIME (HRS)
HYDROXYL CONCENTRATION (CM-3)
OZONE CONCENTRATION (CM-3)

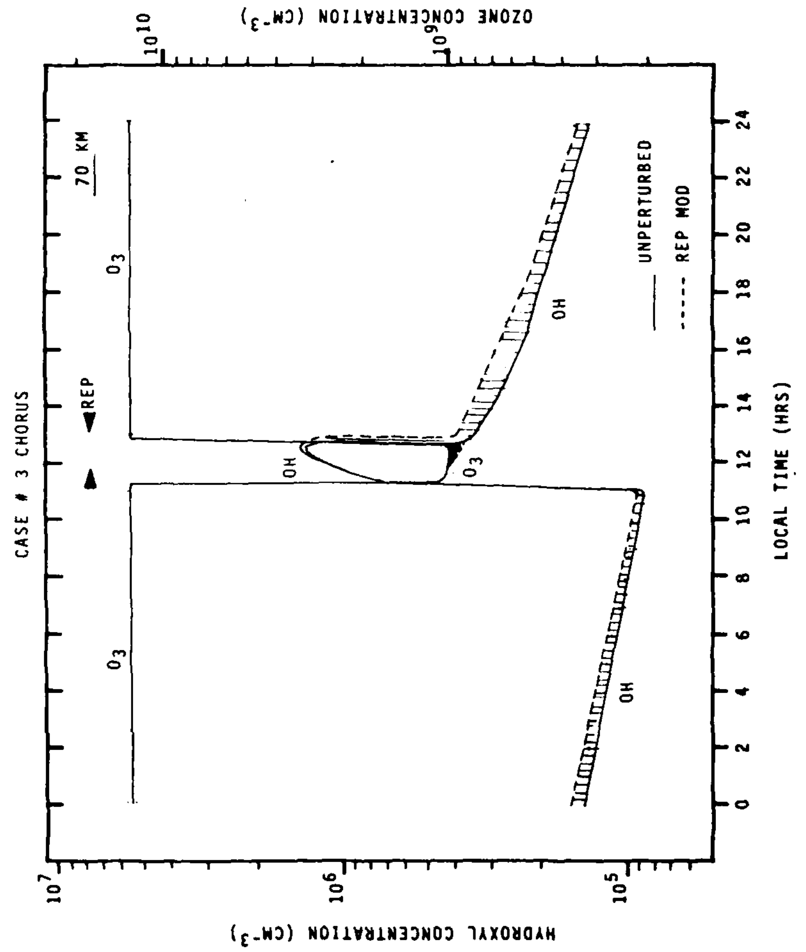
CASE # 3 CHORUS
70 KM
REP
O3
OH
UNPERTURBED
REP MOD
LOCAL TIME (HRS)
HYDROXYL CONCENTRATION (CM-3)
OZONE CONCENTRATION (CM-3)

A similar simulation with an intense REP modelled after the ESIC case, this time occurring at local noon, showed only a 17% increase in OH but more than a 30% decrease in ozone.

Altitude profiles of the ozone concentrations at the local time of maximum decrease, OH concentrations at the same time and at time of maximum OH enhancement for the three cases are presented in Figs 3.5a,b,c. Maximum ozone decreases occurred at 69 km for both the ESIC and EMIC cases and at 76 km for the chorus case. Only in the chorus case, where onset of OH enhancement and ozone diminution were simulatneous, did the deviations occur at the same altitude.

FIGURE 3.5a,b,c Altitude [km] profiles of ozone concentration at time of maximum decrease, hydroxyl concentration at the same time, and hydroxyl concentration at the time of maximum enhancement for a. ESIC, b. EMIC, c. chorus REP events.

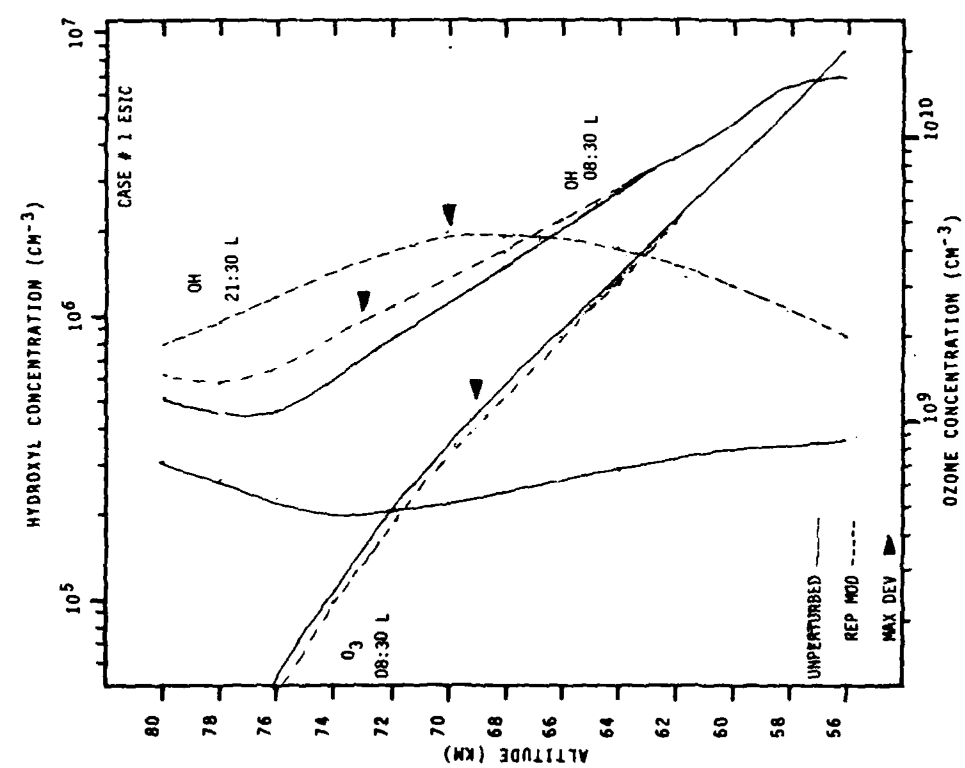

CASE # 1 ESIC
HYDROXYL CONCENTRATION (CM^{-3})
OZONE CONCENTRATION (CM^{-3})
ALTITUDE (KM)
OH
21:30 L
OH
08:30 L
O_3
08:30 L
UNPERTURBED
REP MOD
MAX DEV
10^5
10^6
10^7
10^9
10^{10}
80
78
76
74
72
70
68
66
64
62
60
58
56

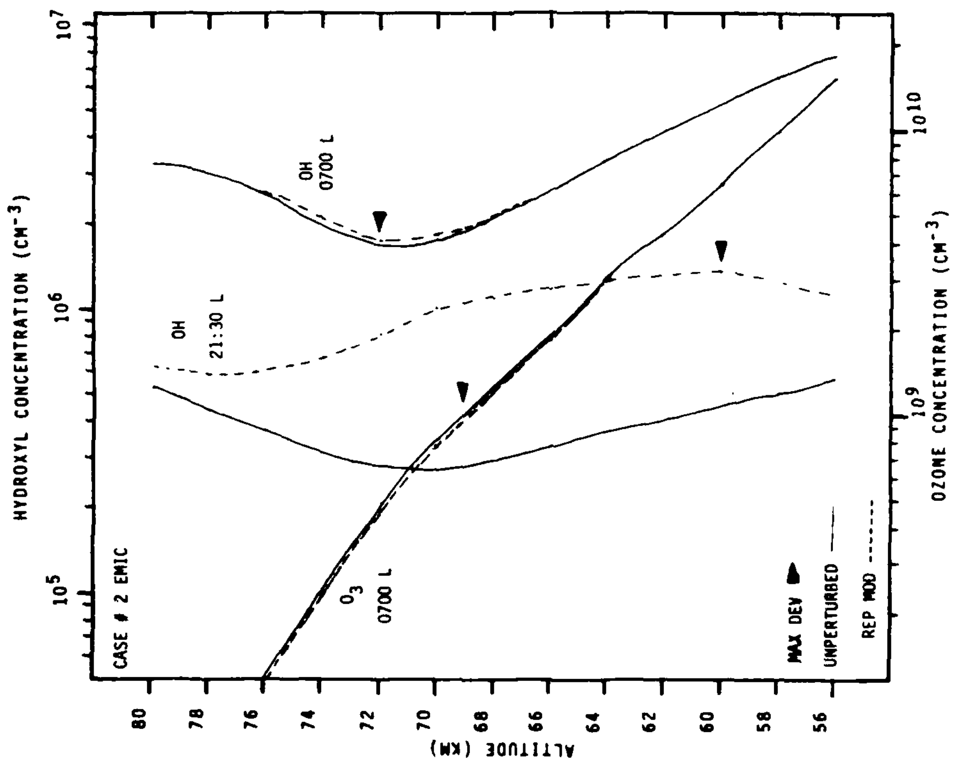
CASE # 2 EMIC
HYDROXYL CONCENTRATION (CM^{-3})
OZONE CONCENTRATION (CM^{-3})
ALTITUDE (KM)
10^5
10^6
10^7
10^9
10^{10}
80
78
76
74
72
70
68
66
64
62
60
58
56
OH
0700 L
OH
21:30 L
O_3
0700 L
MAX DEV
UNPERTURBED
REP MOD

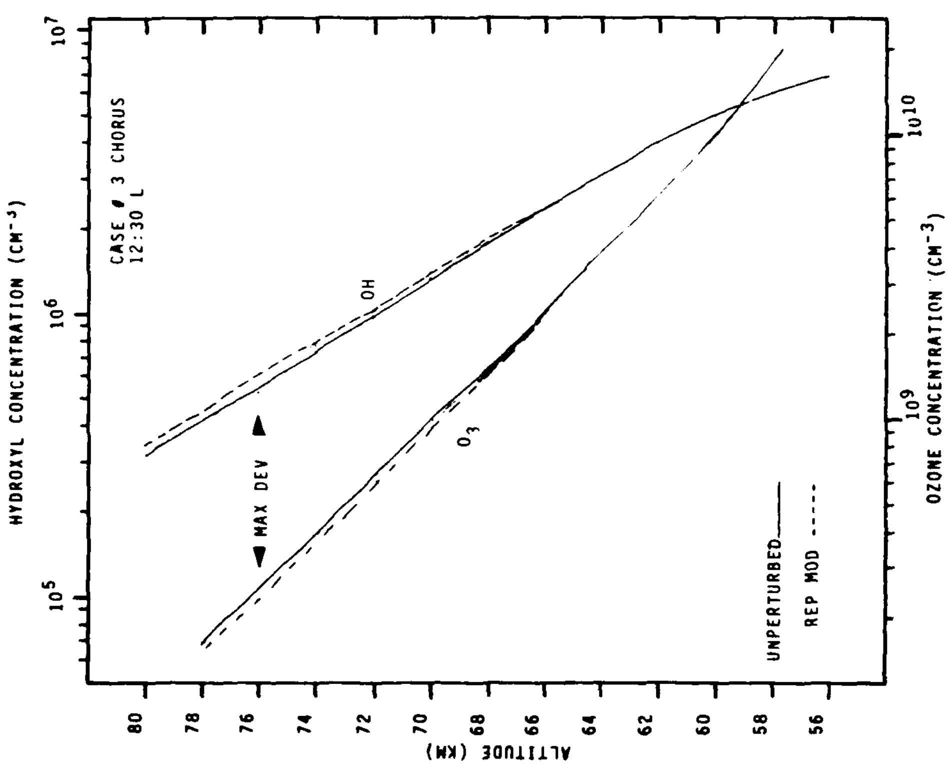
HYDROXYL CONCENTRATION (CM⁻³)
10^5
10^6
10^7
CASE # 3 CHORUS
12:30 L
OH
O3
MAX DEV
UNPERTURBED
REP MOD -----
10^9
10^10
OZONE CONCENTRATION (CM⁻³)
80
78
76
74
72
70
68
66
64
62
60
58
56
ALTITUDE (KM)

CHAPTER 4. SUMMARY, CONCLUSIONS AND OUTLOOK

I have presented here the results of two years of data analysis of fourteen months of satellite outer radiation zone coverage (Chapter 1). Theory and examples have been provided in an attempt to explain the types of REPs discovered in the analysis (Chapter 2). Finally, some atmospheric consequences were investigated (Chapter 3).

For the first time the properties of strong diffusion REPs have been studied using a relatively extensive, dense satellite data set and the following results have been obtained:

- REPs show a seasonal variation with equinoxial maxima and solstice minima in agreement with Bailey (1968).
- The occurrence frequency of REPs is nearly linear with general magnetic conditions again in agreement with Bailey (1968).
- Correlation of REP producing substorms and substorm indices (AE) are weak in the limited number of cases examined in agreement with Thorne and Larson (1976) and not all substorms produce REPs in agreement with Rosenberg et al. (1972) and Thorne and Larson (1976).
- Overall, only one out of ten REPs occur in daytime but as magnetic conditions become disturbed there is an increase in daytime REPs approaching three out of ten.
- REPs are estimated to extend in longitude from 1000 km to 10-15,000 km in general agreement with Larsen, 1973, and Bailey, 1966.

- 98% of all REPs occur concurrently with protons ($\geq$ 80 keV) precipitating on strong diffusion and many features of the precipitation are similar.
- Three distinct classes of REPs occurred: an overwhelming majority (96.5%) had strong diffusion precipitating spectra from hundreds to a thousand keV energy and all these events occurred near the outer bound of trapping simultaneously with proton precipitation; the smallest group (1.3%) had strong diffusion precipitating spectra only for electrons $\geq$1 MeV and again with concurrent proton precipitation but inward from the outer bound of trapping and probably within the plasmasphere; a slightly larger group (2.2%) had strong diffusion precipitation spectra only for electrons of a few hundred keV but with protons present with normal loss cone distributions (not precipitating on strong diffusion).

The theoretical investigation shows that REPs can be caused by radiation belt plasma interactions with plasma waves and that the electrostatic ion cyclotron (ESIC), electromagnetic ion cyclotron (EMIC) and whistler mode chorus waves can respectively account for the three distinct types of REPs discussed above.

Atmospheric consequences were investigated with the following results:

- ESIC and EMIC REPs deposit more energy into the atmosphere than chorus REPs.
- Immediate increases in the OH concentration up to a factor

of 10 are observed during REP occurrence and gradually return to normal within 24 hours.

- Ozone diminution only occurs simultaneously with daytime REPs, only after sunrise with nighttime REPs, and return to normal in several hours.

The following main conclusions may be drawn from these results:

- The ESIC wave interaction is by far the dominant cause of REPs.
- REPs are locally important in reducing ozone concentration (10-30%).

Based on all of the above, future considerations should include the following areas of endeavor:

- Although the concurrent proton precipitation seems to point to the anisotropic pitch angle instability at the equator rather than to a current driven instability low on the field line, results are inconclusive (Kintner et al. 1979). Resolution of the location of the instability would lead to better understanding of the trigger mechanism for REPs.
- Relativistic electron precipitation at rates less than strong diffusion were not analyzed here due to the difficulty with distinction of the pitch angle distribution and the instrument response limits for small loss cones. Weaker events (moderate diffusion) may be locally important to ozone chemistry particularly if they occur during the daytime.

- Though REPs locally increase the OH concentrations day or night, an investigation of long term effects on the atmosphere are important since it may be possible to dry out the mesosphere over a year's time and actually account for long term ozone buildups (Crutzen, private communication, 1980).

Appendix A - OVI-19 Data Set and Analysis

The data used for this study was collected by two magnetic spectrometers aboard Air Force Office of Aerospace Research satellite 1969-25C designated OV1-19 and provided by the instrument builder and prime investigator, A. L. Vampola, Aerospace Corp., El Segundo, Ca. The purpose of this study was to find the frequency of occurrence of REP events and determine the suitability of this type of data for future study.

The OV1-19 satellite was launched on 18 March 1969 into an elliptical orbit with apogee/perigee at 5790/467 km. Inclination was 104.8^{0} and the period 154 min. The satellite was spin stabilized at 8.4 rpm. A three-axis magnetometer tabulated aspect information. Four hours of continuous data was collected and transmitted each tape recorder dump. Over the life of the satellite, approximately 25% data coverage was achieved.

The two spectrometers were of the 180^{0} magnetic focusing type similar to those onboard AF/OAR satellite OV3-3 and schematically presented in Fig. A-1. (Vampola, 1969). One unit, the Low Energy Magnetic Spectrometer (LEMS), had eight electron channels from 53-444 keV with geometric factors as shown in Table A-1 and the other, the High Energy Magnetic Spectrometer (HEMS), had 16 electron detectors from 537 keV to 5.1 MeV as shown in Table A-2. The look direction of each instrument was perpendicular to the satellite spin axis (for pitch angle scanning) which was nominally perpendicular to the orbit plane. Flux counting rates were sampled once per second. As with

FIG A-1. OV3-3 180^{0} Magnetic Focussing Spectrometer (shown without baffling) from Vampola, 1969.

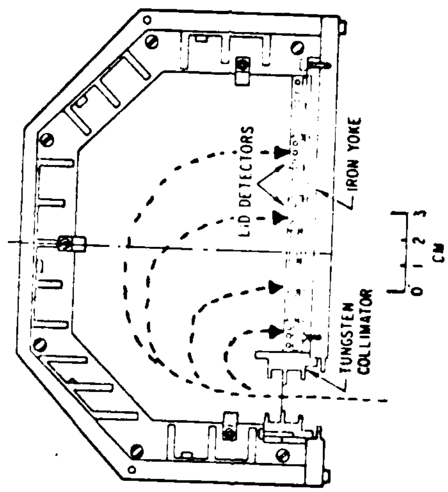
LiD DETECTORS
IRON YOKE
TUNGSTEN COLLIMATOR
0 1 2 3
CM

TABLE A-1. Low Energy Magnetic Spectrometer Channels, Energy, and Geometric Factors.

TABLE A-1. Low-Energy Magnetic Spectrometer

Detector	Electron Energy, kev	Geometric Energy Efficiency Factor, cm^2 ster kev
1	53_{-14}^{+16}	0.00205
2	92_{-16}^{+19}	0.0833
3	139_{-21}^{+22}	1.36
4	192 ± 24	2.53
5	250 ± 26	2.34
6	312 ± 27	2.16
7	376 ± 28	2.01
8	444 ± 29	1.86
9	Protons >55 Mev, bremsstrahlung background detection	

TABLE A-2. High Energy Magnetic Spectrometer Channels, Energy, and Geometric Factors.

TABLE A-2. High-Energy Magnetic Spectrometer

Detector	Energy, Mev	Geometric Energy Factor, cm² ster kev
1	$0.537_{-.114}^{+.119}$	45.7
2	$0.822_{-.114}^{+.126}$	36.5
3	$1.112_{-.124}^{+.129}$	30.1
4	$1.409_{-.126}^{+.138}$	25.5
5	$1.711_{-.126}^{+.133}$	22.1
6	$2.018_{-.130}^{+.134}$	19.4
7	$2.321_{-.129}^{+.130}$	17.3
8	$2.632_{-.134}^{+.134}$	15.7
9	$2.932_{-.129}^{+.139}$	14.3
10	$3.245_{-.134}^{+.138}$	13.1
11	$3.557_{-.134}^{+.133}$	12.1
12	$3.863_{-.138}^{+.136}$	11.3
13	$4.169_{-.136}^{+.141}$	10.5
14	$4.476_{-.137}^{+.147}$	9.87
15	$4.783_{-.140}^{+.147}$	9.29
16	$5.091_{-.136}^{+.152}$	8.67
17	Protons >130 Mev, background detection	bremsstrahlung

the OV3-3 units, the flux determinations were limited at low counting rates by statistical fluctuations and at high counting rates by telemetry quantization (Vampola, 1969). In addition, a rectangular energy versus geometric factor response is assigned for each actual channel response for data analysis as illustrated in Fig. A-2. Instrument response to an input spectrum zero everywhere in the loss cone and isotropic at some level outside the loss cone is shown for Channel 4 of the low energy unit in Fig. A-3. An order of magnitude drop in flux response roughly occurs 7^{o} into the loss cone.

A typical high to low altitude pass for Channel 7 of the low energy unit is shown in Fig. A-4. Inner zone (A), slot region (B), outer zone (C), and polar region (D) are distinctive features of the pass. The large variation in count rate is due to pitch angle sampling.

Fig. A-5 for an OV3-3 sample shows the outer zone at low altitude from L=3-6 with envelopes drawn for the top and bottom of the sampling scatter. The top envelope is representative of the locally trapped flux and the bottom is the flux furthest into the loss cone. When the two curves touch, as in Fig. A-5 at L=5.6, this indicates an isotropic pitch-angle distribution, as predicted for strong pitch angle diffusion. The analysis mode is then to view all of the available passes for this envelope closure. Final determination is made when flux vs pitch angle plots show isotropic fluxes filling the upward looking (downward flowing) loss cone.

In order to accomplish the task of analyzing the data set

FIG A-2. Geometric factor-energy response function assigned each channel for data analysis. Total area outside of the rectangle is about 15% but both functions contain equal areas. A slight bias towards higher energies for very steep spectra is produced (Vampola, 1969).

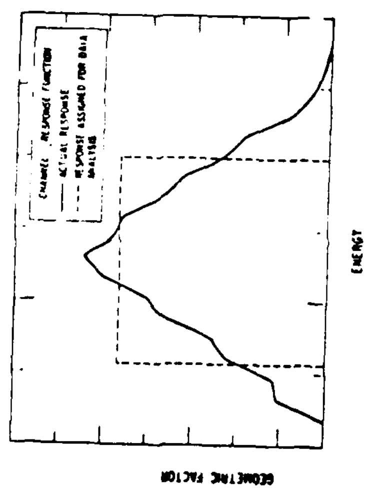
CHANNEL RESPONSE FUNCTION
ACTUAL RESPONSE
RESPONSE ASSIGNED FOR DATA ANALYSIS
ENERGY
GEOMETRIC FACTOR

FIG A-3. Instrument response-pitch angle output.

OV1-19 LEMS CHANNEL 4 (.192 MEV)   30 DEGREE LOSS-CONE

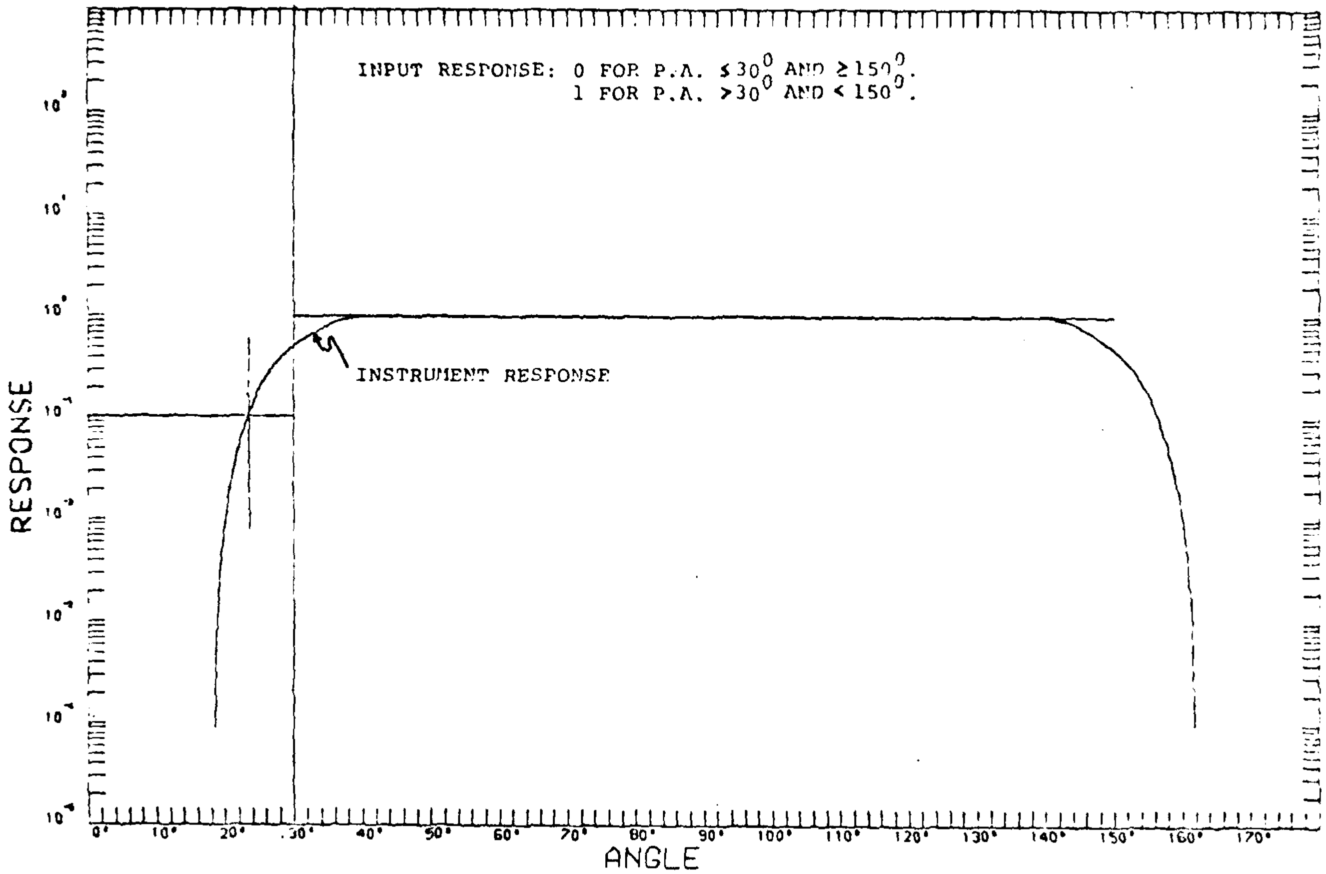

FIG A-4. Analog record of 376±28 keV electron data plotted as counting rate versus time on a pseudo-logarithmic scale. Universal time, magnetic field intensity, invariant latitude, L, altitude, and MLT are listed for 200-sec intervals. Pitch-angle distribution sampling produces the large variations in counting rate in several regions of the plot (Vampola, 1971).

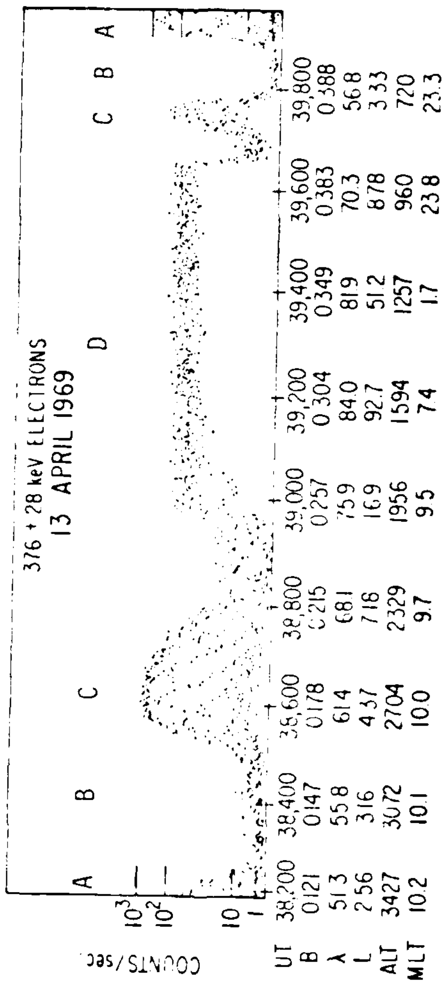
37.6 + 28 keV ELECTRONS
13 APRIL 1969
COUNTS/sec.
UT
B
λ
L
ALT
MLT

FIG A-5. Plots of instantaneous flux measurements versus L for the 712±137 keV electron channel from the OV3-3 magnetic spectrometer. The scatter in the data points is due to pitch-angle sampling. Envelope curves at the maximums and minimums are shown to emphasize the data that are isotropic in pitch angle (Koons et al, 1972).

AD-A092 545 AIR FORCE INST OF TECH WRIGHT-PATTERSON AFB OH F/G 4/1
RELATIVISTIC ELECTRON PRECIPITATION: AN OBSERVATIONAL STUDY.(U)
1980 L J ANDREOLI
UNCLASSIFIED AFIT-CI-80-26D NL

3 OF 4
AD
A092545

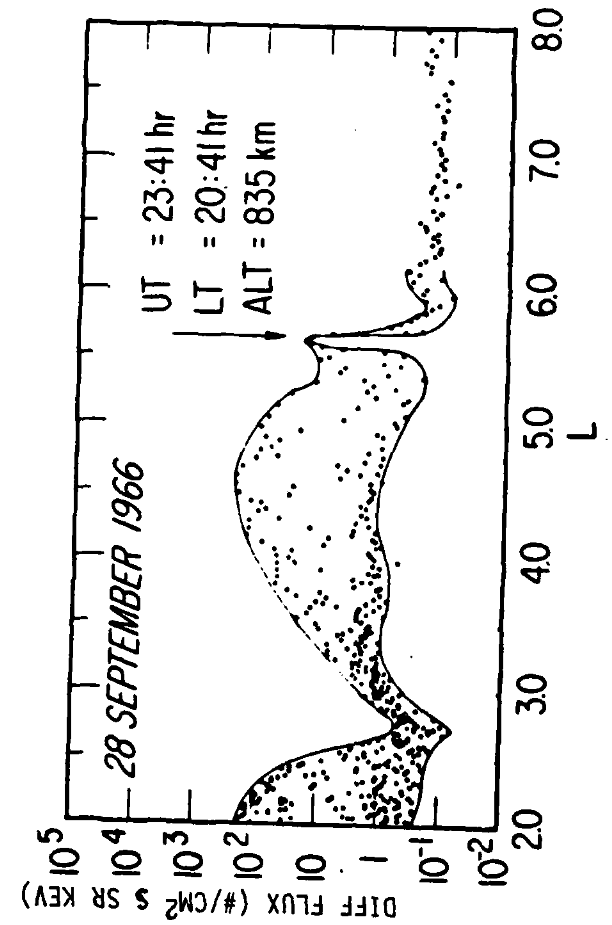
28 SEPTEMBER 1966
UT = 23:41 hr
LT = 20:41 hr
ALT = 835 km
DIFF FLUX (#/CM2 S SR KEV)
L

as objectively as possible, a set of criteria was developed for REP event identification. These are illustrated in flow chart form in Fig. A-6. The first criteria was that only data in the L range 4-7 would be studied. A total of 320 passes, clustered as high as 4 passes on a given day, was extracted from a data set spanning from day 77 of 1969 to day 13 of 1970 (301 days). Because of the finite width of the field-of-view ($\sim 10^0$) and the fact that the satellite orbit precluded pitch angle sampling to 0^0 (and 180^0) everywhere in the orbit, it was determined that data below 1000 km would yield loss cones large enough for a high frequency of complete loss cone sampling. This criteria eliminated 88 cases. The third criteria demanded that REP fluxes be high at higher energies (1 MeV ± 500 keV). Seventy-two cases failed on this criteria. Next we determined that if we had data at least 10^0 into the loss cone, we could identify real precipitation based on the channel response previously described. This eliminated 39 cases of which 17 were less than 10^0 into the loss cone and 22 did not sample the loss cone at all. In some cases (19), count rate sampling and pitch angle modulation were phased in such a way as to make event evaluation impossible. These cases were labeled "instrument problems" and eliminated. Finally, 103 cases remained in which an analysis could reasonably be made. These passes are shown as passes per day versus day of the year in Fig. A-7. Of these 103 "clean cases", only three exhibited isotropic fluxes into the loss cone at relativistic energies (identified by arrows on Fig. A-7).

The REP of 14 May 1969 (day 134) is of particular interest since it exhibited the "hardest" spectrum of the three REPs (spectra

FIG A-6. Flow chart illustrating process of elimination through the OV1-19 data set.

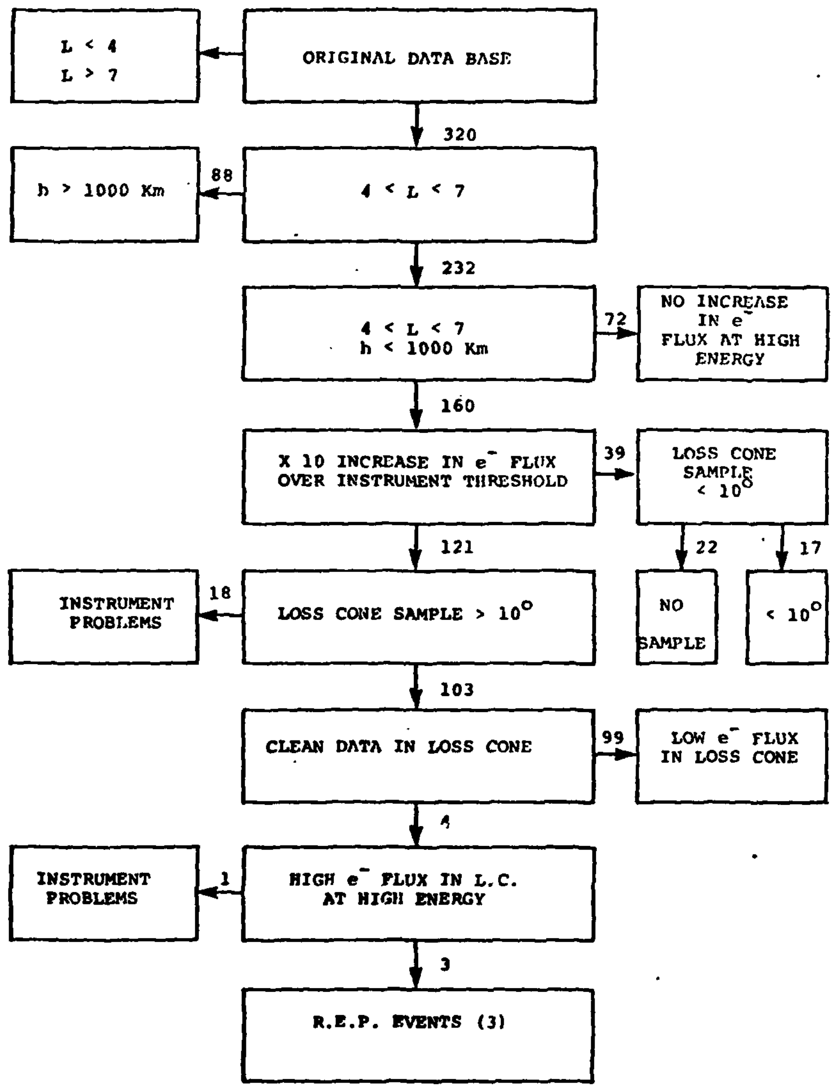
L < 4
L > 7
ORIGINAL DATA BASE
320
88
h > 1000 Km
4 < L < 7
232
4 < L < 7
h < 1000 Km
72
NO INCREASE IN e⁻ FLUX AT HIGH ENERGY
160
X 10 INCREASE IN e⁻ FLUX OVER INSTRUMENT THRESHOLD
39
LOSS CONE SAMPLE < 10°
121
22
17
INSTRUMENT PROBLEMS
18
LOSS CONE SAMPLE > 10°
NO SAMPLE
< 10°
103
CLEAN DATA IN LOSS CONE
99
LOW e⁻ FLUX IN LOSS CONE
4
INSTRUMENT PROBLEMS
1
HIGH e⁻ FLUX IN L.C. AT HIGH ENERGY
3
R.E.P. EVENTS (3)

FIG A-7. Outer zone passes per day versus day of the year for the OV1-19 data set. Arrows indicate the three event days.

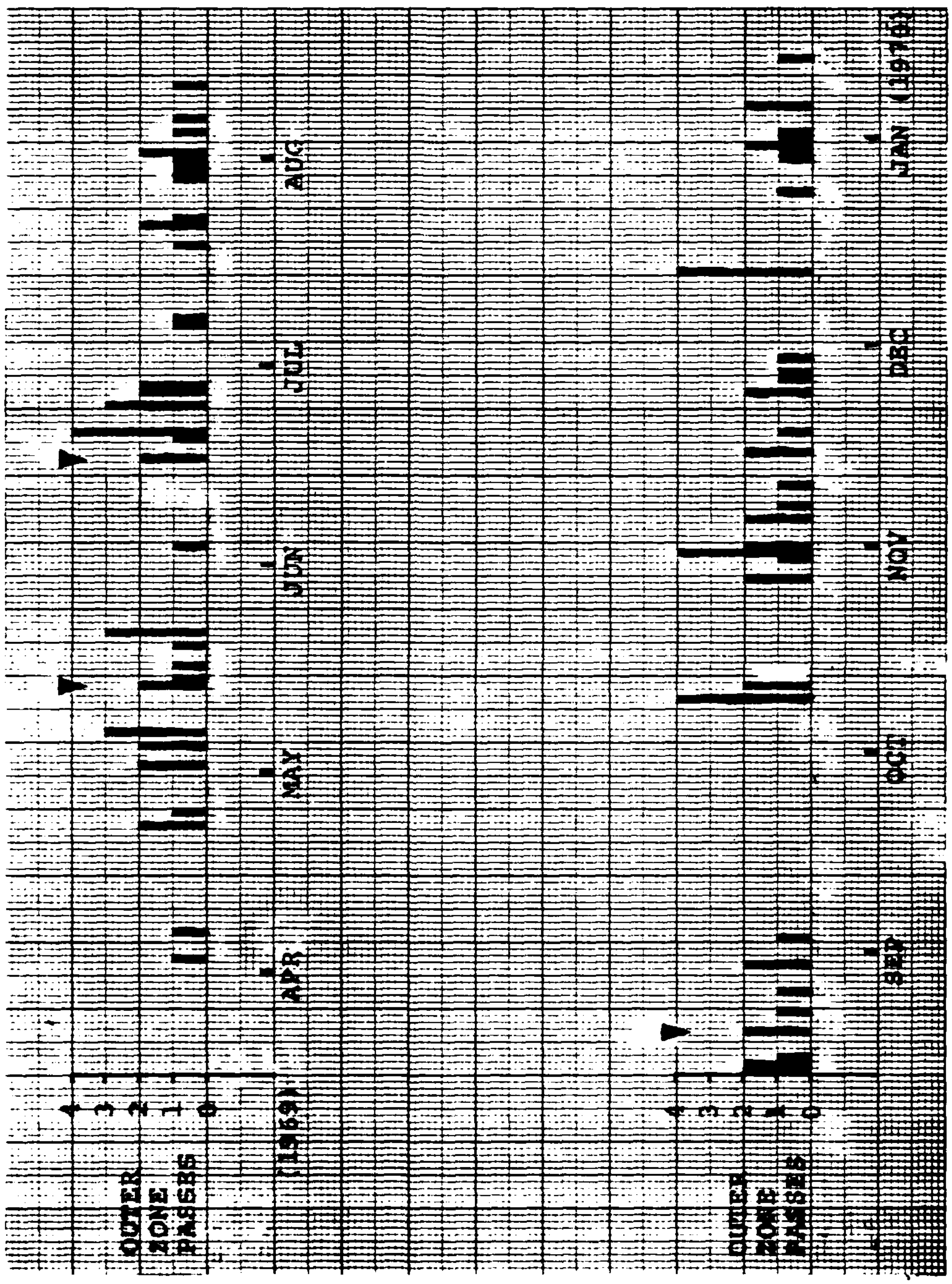
OUTER ZONE PASSES
4
3
2
1
0
(1969)
APR
MAY
JUN
JUL
AUG
OUTER ZONE PASSES
4
3
2
1
0
SEP
OCT
NOV
DEC
JAN (1970)

will be compared later) and falls in a period where Alaska forward scatter data exists. Figures A-8, a and b, show plots of differential electron fluxes versus U.T. (in seconds) for the various energy channels, LEMS Bremsstrahlung (background), and LEMS protons (>55 keV) for day 134. The higher energy electron channels exhibited low fluxes and are not shown. The outer edge of the outer zones at local morning (07:20 MLT: 79642-79659 U.T.) and local midnight (00:18 MLT; 80184-80225 U.T.) exhibit envelope closure. The local morning outer zone exhibited very high trapped fluxes (see Fig. A-9) at all energies but the loss cone (~55^{o}) was not sampled.

The pitch angle distribution for the local midnight (80196-80225 U.T.) outer zone transit are shown in Fig. A-10 for energy channels 192, 537, 822 keV. The nominal loss cone is ~66^{o} and the symbols "+/◇" represent instrument viewing positions up/down the local magnetic field line. The plots show high fluxes in the upward viewing loss cone at several instances in all energy channels while the downward viewing loss cone generally show normal trail-off to lower values. The large variation in precipitating fluxes is due either to the transition of the satellite through regions of strong and not so strong precipitation or spatial variations in trapped flux during the 30 seconds duration of the pitch and angle plot. The plots represent approximately seven complete (0-180^{o}) pitch angle distributions each and 537 keV channel has each data sample labeled with the last three digits of the U.T. in seconds. Deep in the loss cone two orders of magnitude variation occur between 210 and 218 whereas a half order of magnitude between 205 and 220 or 201 and 197 occur in the trapped distribution.

FIG A-8a. Differential electron fluxes versus UT (sec), B (Gauss), L, LAT (deg), ALT (km), for LEMS Proton, LEMS BREM, 822, 537, 444, 376 keV Electrons for DAY 134.

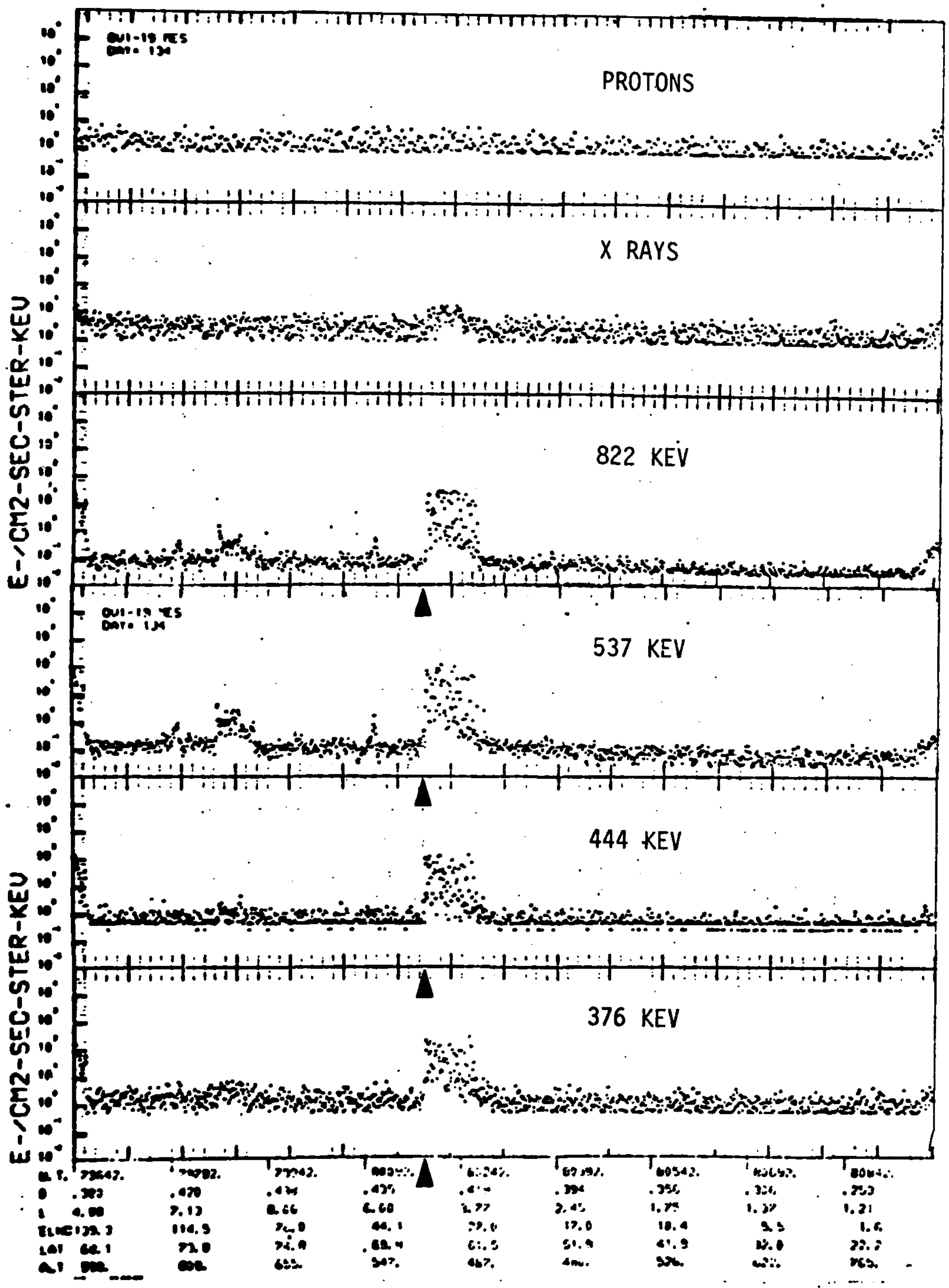
PROTONS
X RAYS
822 KEV
537 KEV
444 KEV
376 KEV
E-/CM2-SEC-STER-KEV
E-/CM2-SEC-STER-KEV

FIG A-8B. Differential electron fluxes versus UT (sec), B (Gauss), L, LAT (deg), ALT (km), for 312, 250, 192, 139, 92, 53 keV Electrons for DAY 134.

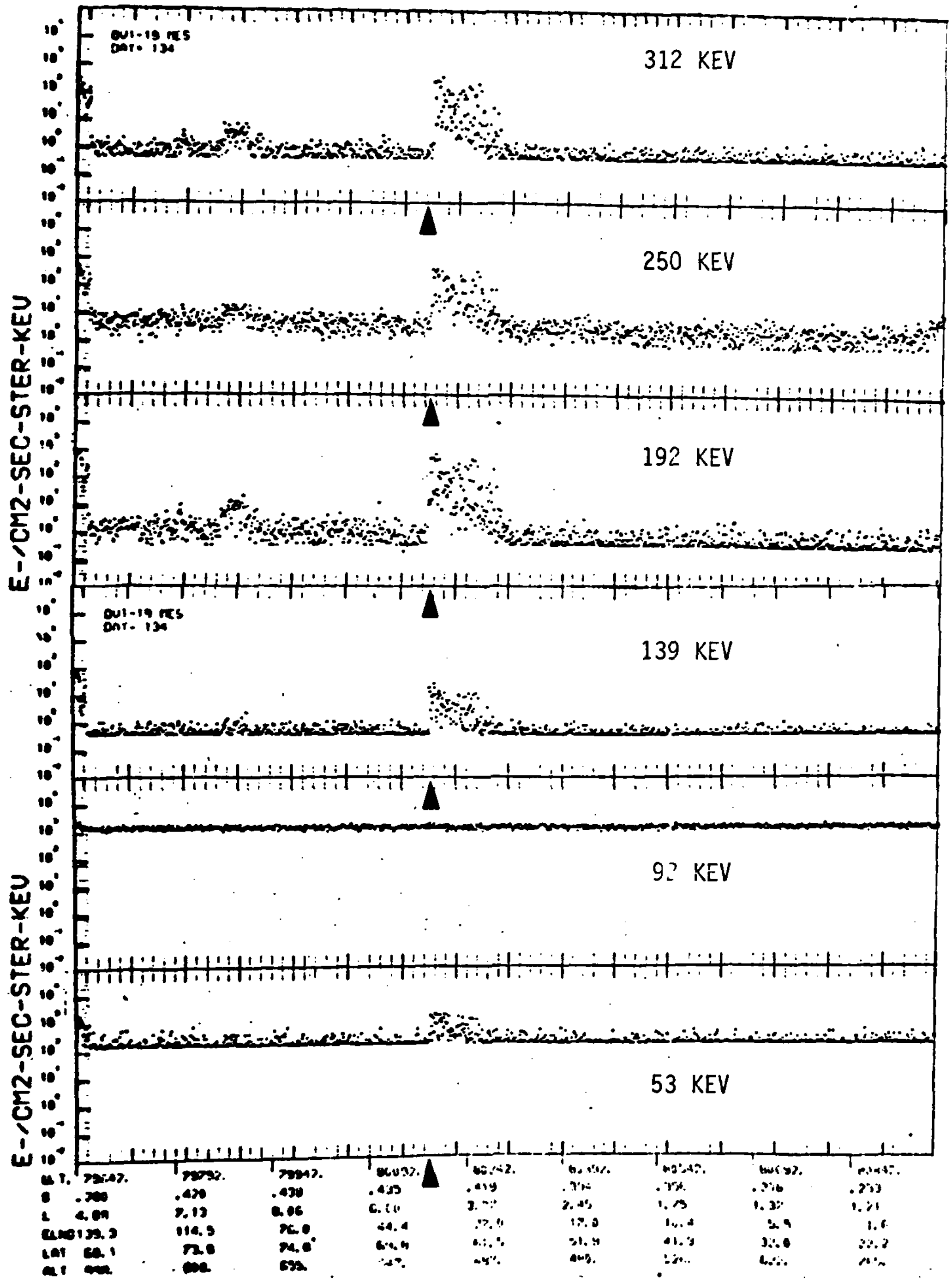
312 KEV
250 KEV
192 KEV
139 KEV
92 KEV
53 KEV
E-/CM2-SEC-STER-KEV
E-/CM2-SEC-STER-KEV

FIG A-9. Electron differential energy fluxes versus UT (hr), LT (hr), ALT (km), L, for 192, 537, 822 keV electrons for DAY 134 (14 MAY 1969).

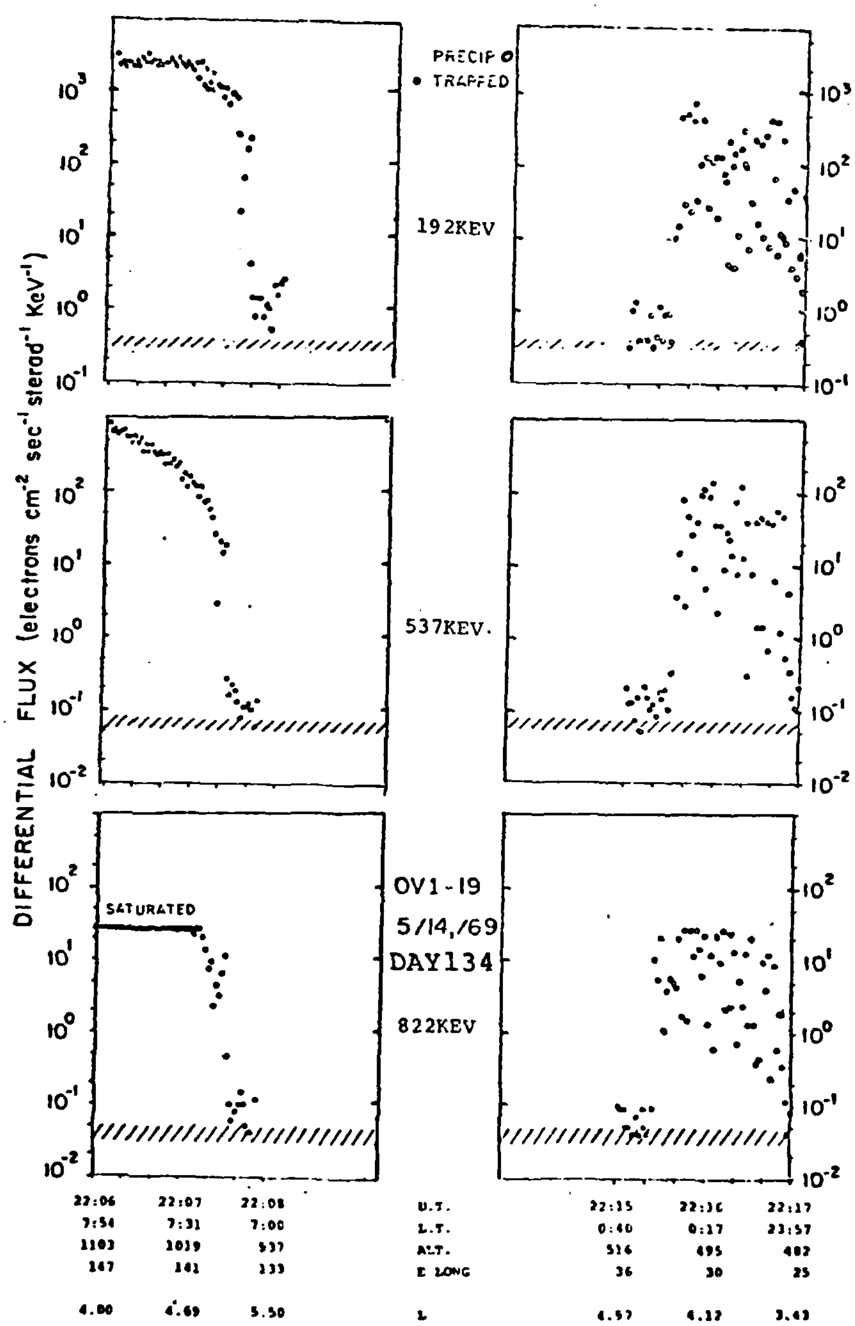
PRECIP o
• TRAPPED
192KEV
537KEV.
OV1-19
5/14/69
DAY134
822KEV
SATURATED
DIFFERENTIAL FLUX (electrons cm^{-2} sec^{-1} sterad^{-1} KeV^{-1})
U.T.
L.T.
ALT.
E LONG
L

FIG A-10. Flux versus Pitch Angle for electron channels 192, 537, and 822 keV for DAY 134. Flux upper limit in channel 822 keV is 2.696 x 10^1 since the high count rate meter coax cable from the HEMS to the satellite data system broke during launch.

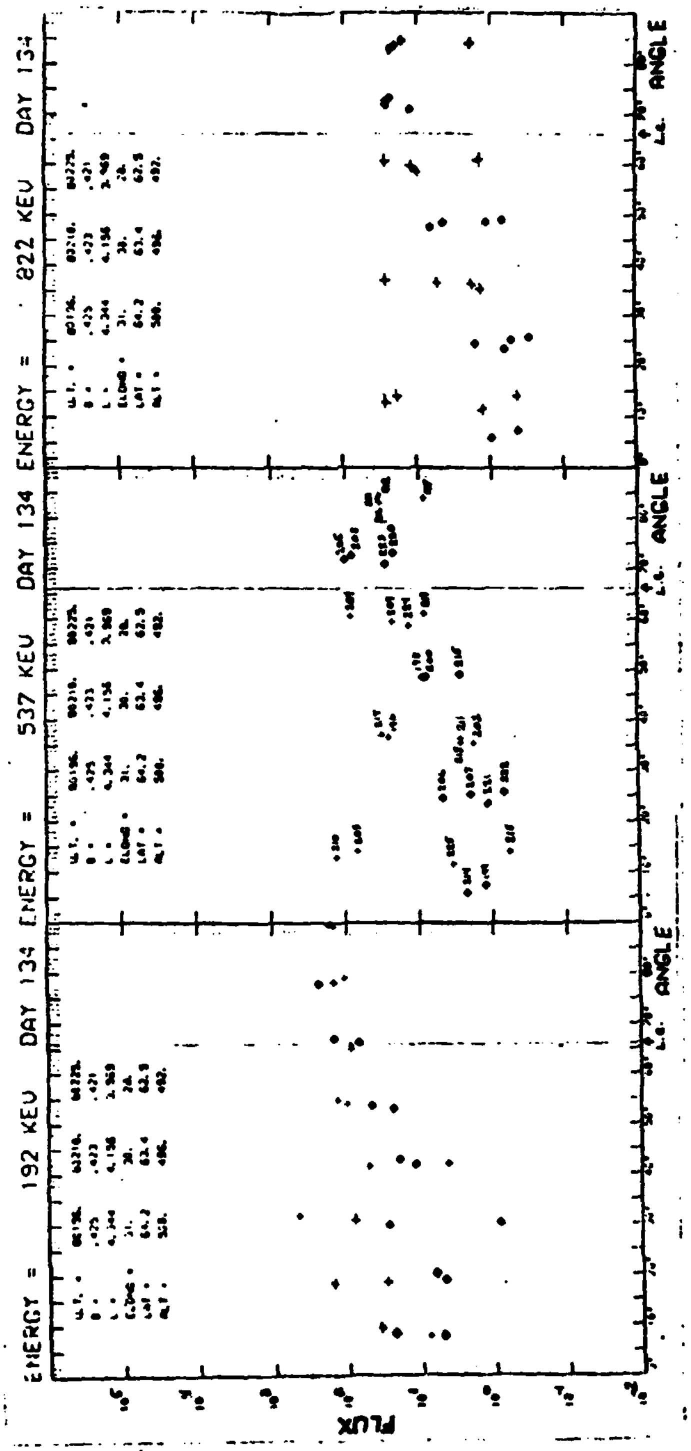
ENERGY = 192 KEV DAY 134
ENERGY = 537 KEV DAY 134
ENERGY = 822 KEV DAY 134
ANGLE
ANGLE
ANGLE
FLUX

A time sequence in pitch angle versus differential flux for the same local midnight outer zone pass (day 134) for channels 444, and 537 keV are shown in Figs. A-11 a and b respectively. Data samples are subjectively connected to display the most "normal" distribution. This is difficult because of the wide spread in pitch angles (~50^0) between samples and compounded by a few missing samples. The 444 keV channel is the highest energy measured by the LEMS whereas the 537 keV channel is the lowest for the HEMS. Thus, Fig. A-11 a is 165^0 out of phase with Figs. A-11b. Each sample is identified by the last three digits of the U.T. in seconds. "Normal" upward and downward loss cone distributions are evident at all energies after sample 213. The upper envelope (dashed line -U) connects the locally trapped flux (pitch angles ~90^0) and the lower (dashed line-L) connects the lowest flux into the loss cones (pitch angles ~0^0, 180^0). It is evident that the envelopes nearly close in at least a few places towards the outer edge of the outer zone though the instrument is viewing almost 2 1/2 orders of magnitude into the loss cone. Most notable is the isotropic (upward viewing loss cone) flux in Fig. A-11b at sample 188 (80188 U.T.).

The magnetic activity for this event as well as Alaska forward scatter absorption are illustrated in Fig. A-12. The Alaska forward scatter absorption on day 134 was greater than 10 db from 19:40 to 02:10 U.T. (09:40-16:10 Alaskan local time) with a peak absorption of 19 db at 20:12 U.T. The only other absorption recorded was early on days 132 and 137. Dst shows disturbed conditions

FIG A-11a. Time sequence of differential electron flux versus pitch angle for the 537 keV channel on DAY 134.

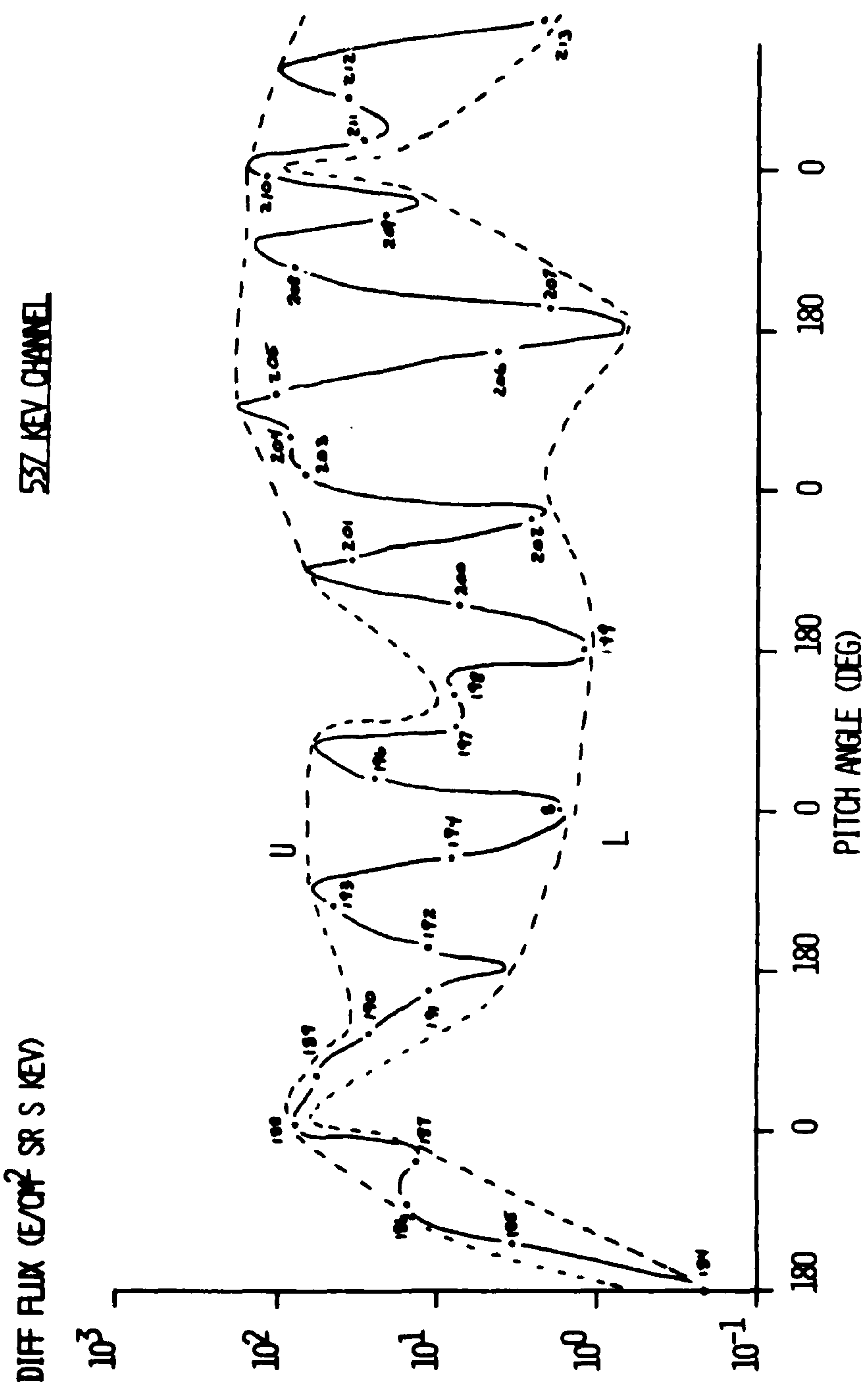
537 KEV CHANNEL
DIFF FLUX (E/CM2 SR S KEV)
10^3
10^2
10^1
10^0
10^-1
180
0
180
0
180
0
180
0
PITCH ANGLE (DEG)
U
L

FIG A-11b. Time sequence of differential electron flux versus pitch angle for the 444 keV channel on DAY 134.

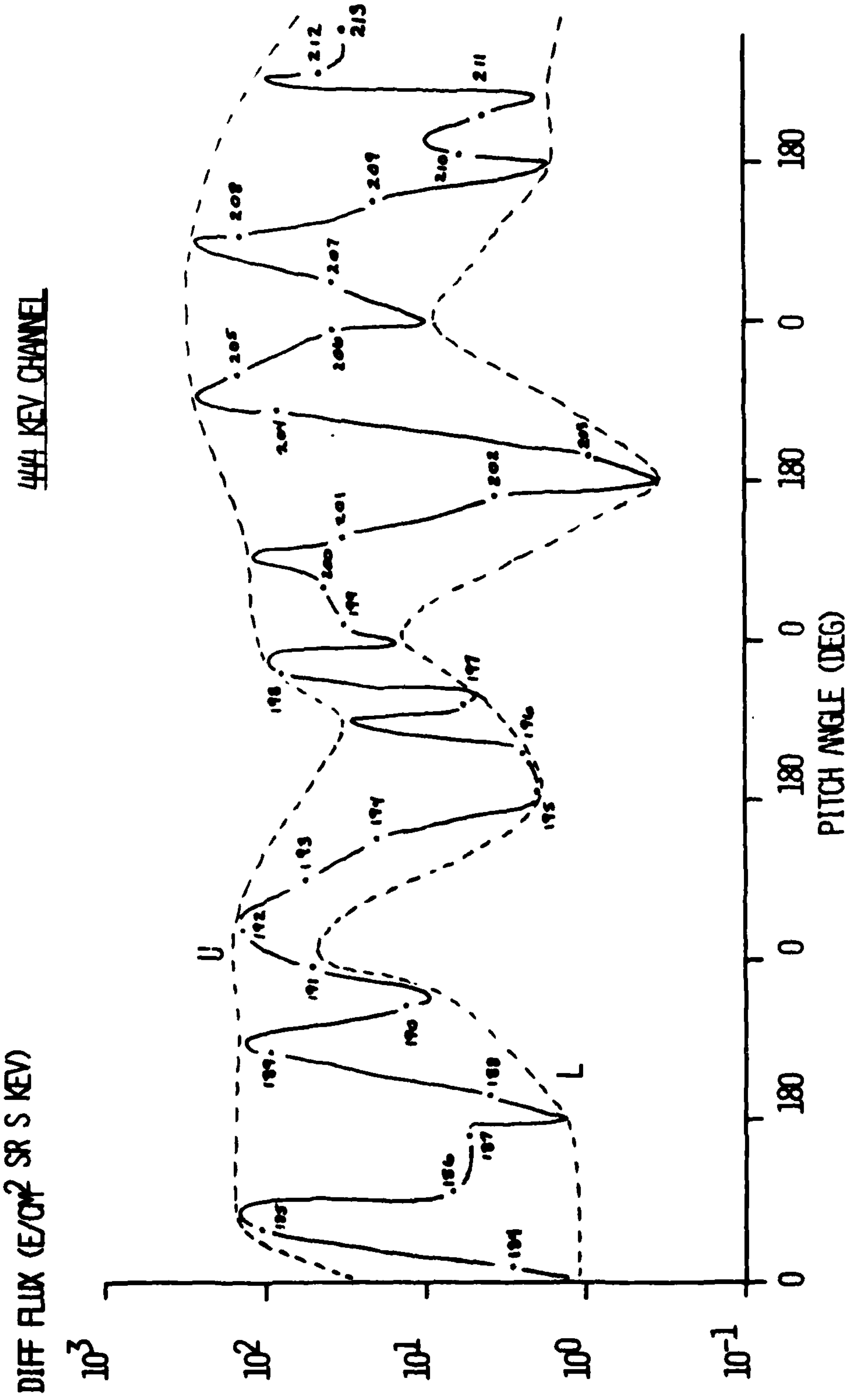
444 KEV CHANNEL
DIFF FLUX (E/CM2 SR S KEV)
10^3
10^2
10^1
10^0
10^-1
PITCH ANGLE (DEG)
0
180
0
180
0
180
0
180
U
L

FIG A-12. Dst for days 132 through 137; AE Index for parts of the UT day for days 134 and 135; Alaskan forward scatter absorption events are represented by the hatched boxes (Bailey, Personal Communication, 1973).

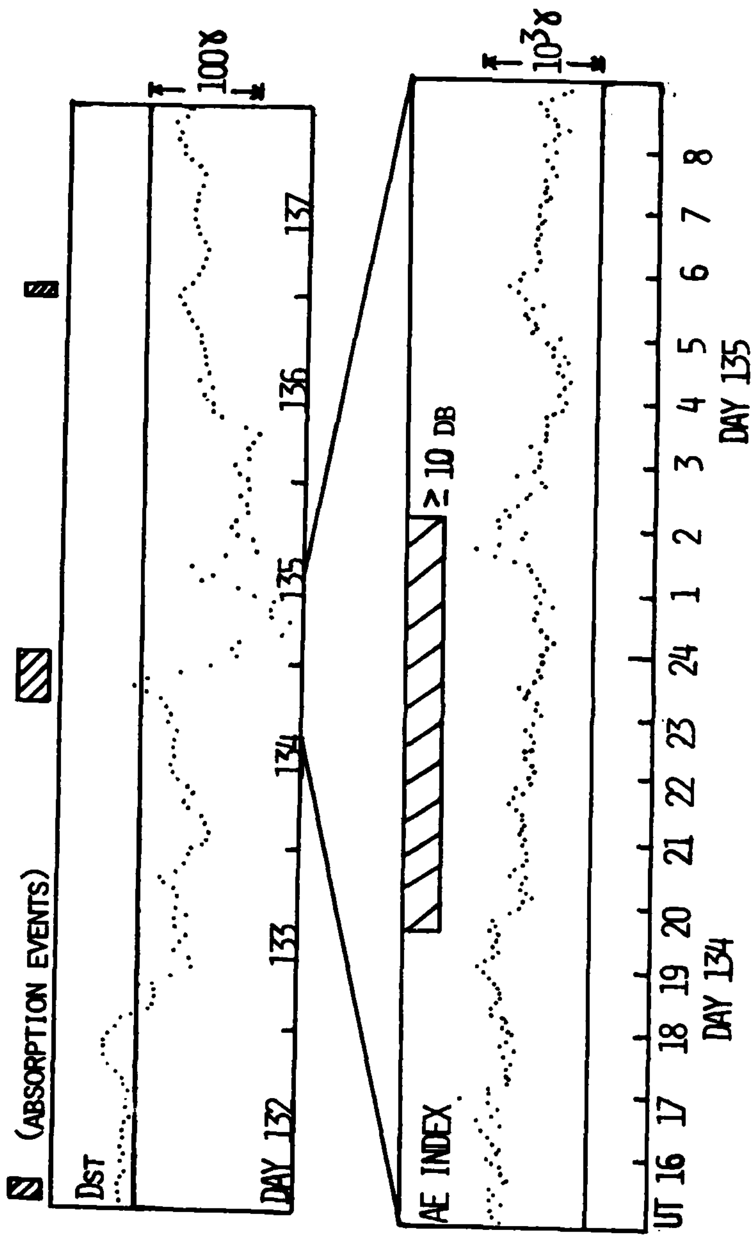
(ABSORPTION EVENTS)
DST
100γ
DAY 132
133
134
135
136
137
AE INDEX
≥ 10 DB
10^3γ
UT 16 17 18 19 20 21 22 23 24 1 2 3 4 5 6 7 8
DAY 134
DAY 135

from late on day 132 through recovery on day 137. A positive excursion is particularly noticeable near 22 U.T. on day 134 near the time of the satellite REP observation. This is followed by a >100γ depression early on day 135. AE shows a 1500γ increase at 20 U.T. on day 134 two hours before the satellite observation. It is interesting to note that although day 133 and 135 are strongly disturbed no forward scatter absorption occurred above Alaska (Thorne and Larsen, 1976). A local early morning and late evening pass by OV1-19 occurred on day 135. The local early morning pass did not sample the loss cone but even though the evening pass did, no REP was observed.

All three REPs observed occurred between local midnight and local dawn. The expected frequency of occurrence of REPs based on this study is 1-13% with a 90% confidence interval. The 50% confidence level indicates a fequency of 5% (see Fig. A-13). This is consistent with 5% frequency for moderate (>8 db absorption) REPs found by Bailey (1968).

The energy spectra for the three OV1-19 REPs are compared with the OV3-3 REP measured by Vampola (1971) in Fig. A-14. It is evident that they are comparable in hardness (approach to isoenergetic). So it is not surprising that the REPs will have a similarly predicted effect on the deposition of energy (represented by ion production) in the atmosphere as shown in Fig. A-15.

The conclusions of this study are that the OVI-19 was capable of observing strong diffusion events (REPs) from a few hundred keV to 1 keV energies. More REPs would probably have been observed if the loss cones were sampled more frequently. A similar data set with better statistics would yield more morphological information and possibly a clue to the type and relative importance of various mechanisms for causing REPs.

FIG A-13. REP frequency of occurrence for the OV1-19 Data Base.

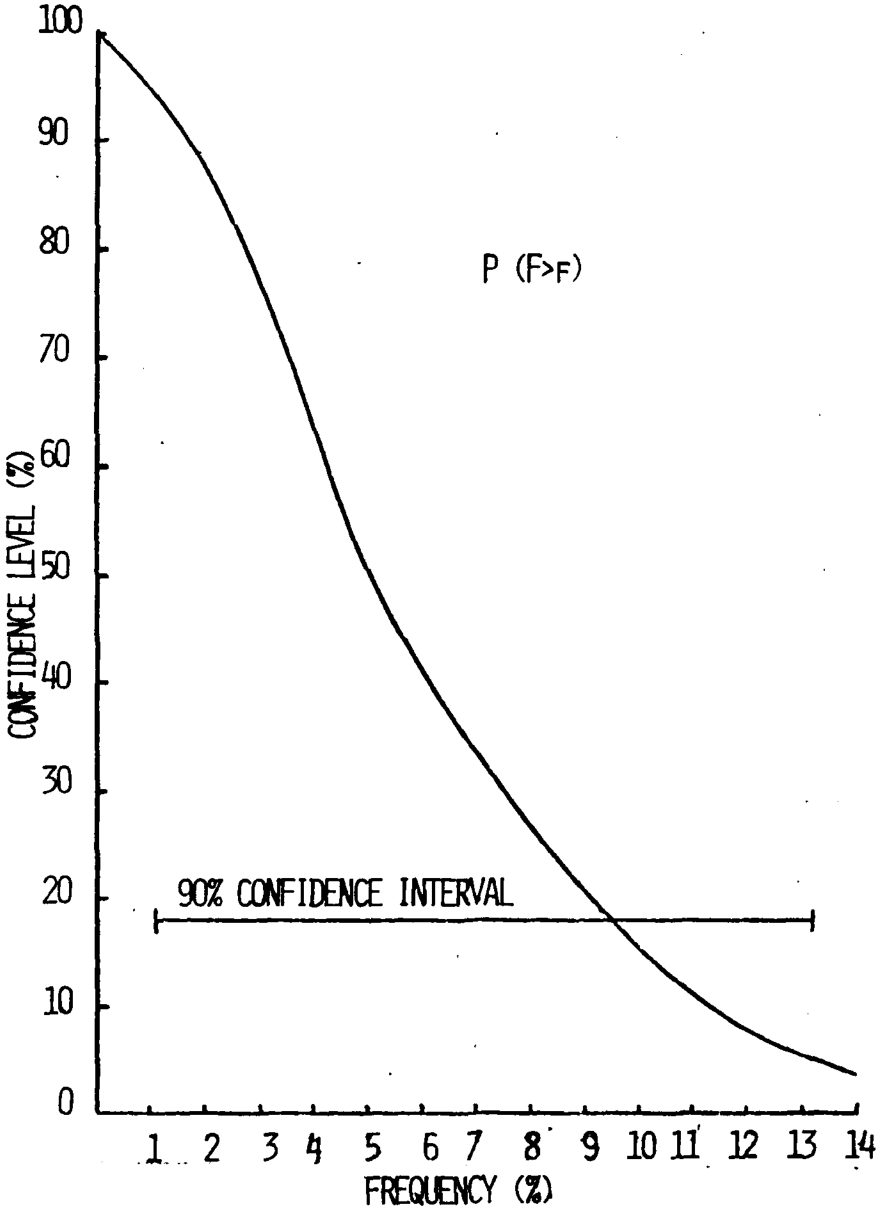
P (F>F)
90% CONFIDENCE INTERVAL
CONFIDENCE LEVEL (%)
100
90
80
70
60
50
40
30
20
10
0
1 2 3 4 5 6 7 8 9 10 11 12 13 14
FREQUENCY (%)

FIG A-14. REP energy spectra for the three OV1-19 events in 1969 compared with the Vampola OV3-3 spectrum of 1971.

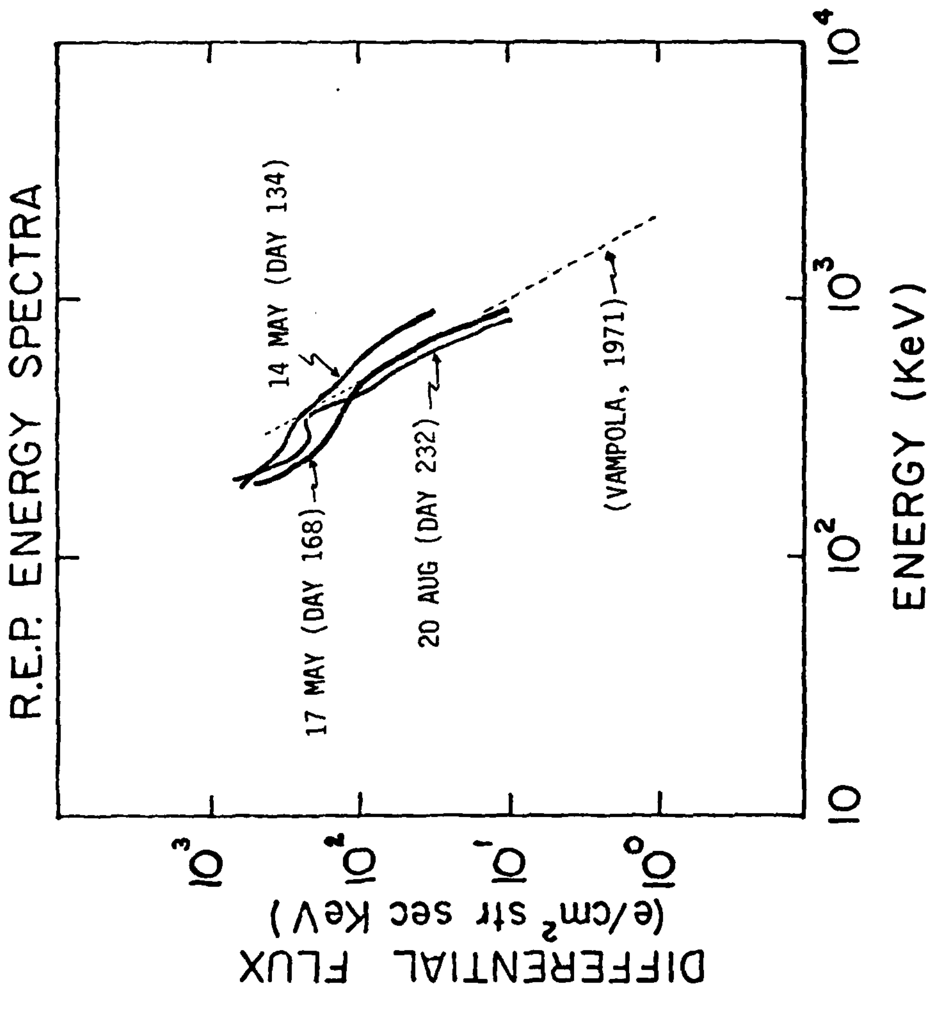

R.E.P. ENERGY SPECTRA
14 MAY (DAY 134)
17 MAY (DAY 168)
20 AUG (DAY 232)
(VAMPOLA, 1971)
DIFFERENTIAL FLUX
(e/cm² str sec KeV)
ENERGY (KeV)

FIG A-15. Ion production rate versus altitude for the OV1-19 REP, solar radiation, galactic cosmic rays and the solar proton event of 1972.

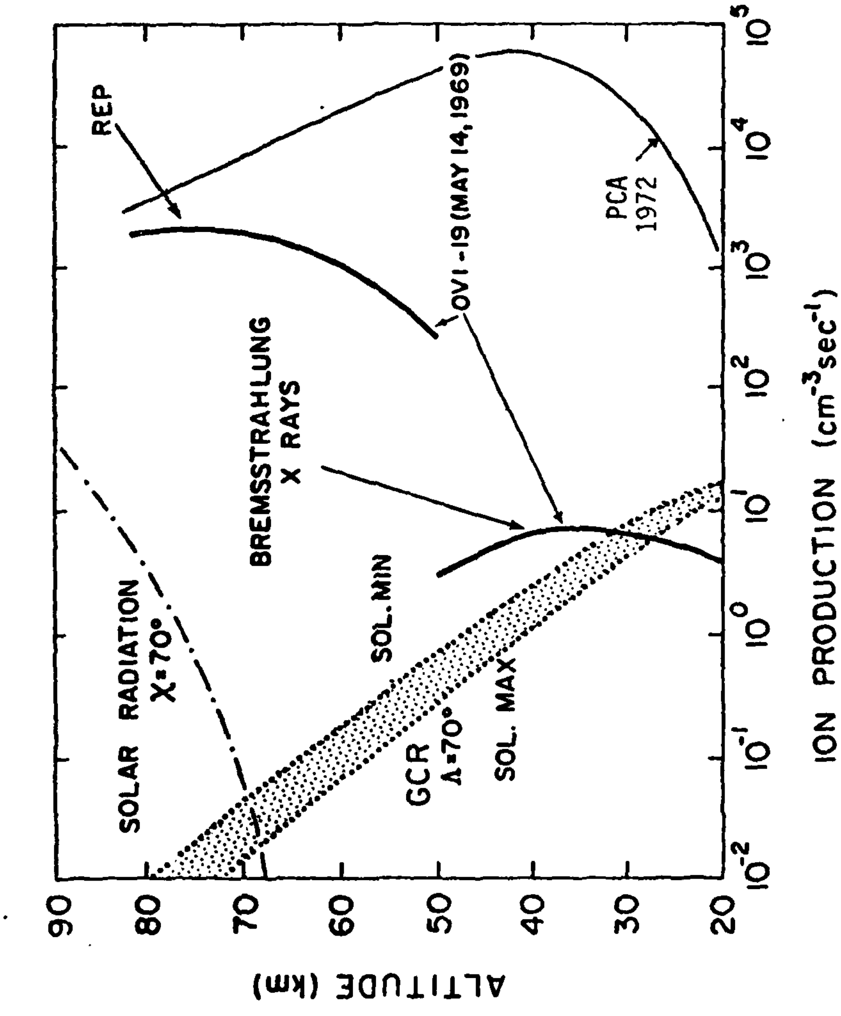
REP
OVI-19 (MAY 14, 1969)
PCA
1972
BREMSSTRAHLUNG
X RAYS
SOLAR RADIATION
χ=70°
SOL. MIN
GCR
Λ=70°
SOL. MAX
ION PRODUCTION (cm⁻³sec⁻¹)
ALTITUDE (km)

Appendix B - S3-3 Data Collection

The primary data set used in this dissertation was collected by a magnetic spectrometer aboard Air Force Space Test Program satellite STP 74-2 designated S3-3 launched in the summer of 1976. The S3-3 orbit is highly elliptical (schematically shown in Fig. B-1) with apogee/perigee nominally 8000/250 km. The maximum apogee of 8035 km was reached on 3 August 1976 and continues to decrease at a rate of 0.35 km/day. Orbit inclination is 97^{o} with a period of 180 minutes. The nodal drift rate is 0.27^{o}/day westward, i.e., the local time of orbit nodal crossing decreases 0.049 hr/day from launch values of 10:30 (ascending node) and 22:30 (descending node) as shown in Fig. B-2, panel a. The line of apsides (major axis of orbit) was initially placed less than 90^{o} from equator on the sun side (Fig. B-1) and slowly rotates toward the dark side at the rate of 0.94^{o}/day from a launch value of 63^{o} as shown in Fig. B-2, panel b. The satellite spin rate was maintained at approximately 3 rpm with the spin vector perpendicular to the orbit plane. In order to maintain the solar cells facing toward the sun (and the backside away for thermal control), the satellite was yawed 180^{o} on days 40-48 (around 14 February) 1977.

The S3-3 scientific payloads are listed with brief descriptions in Table B-1. Of prime interest is the CRLS-217 which will be described here in detail. Data from ONR-104 and CRLS-218 are referred to in Chapter 2 and only brief details will be provided.

FIG B-1. S3-3 Orbital parameters.

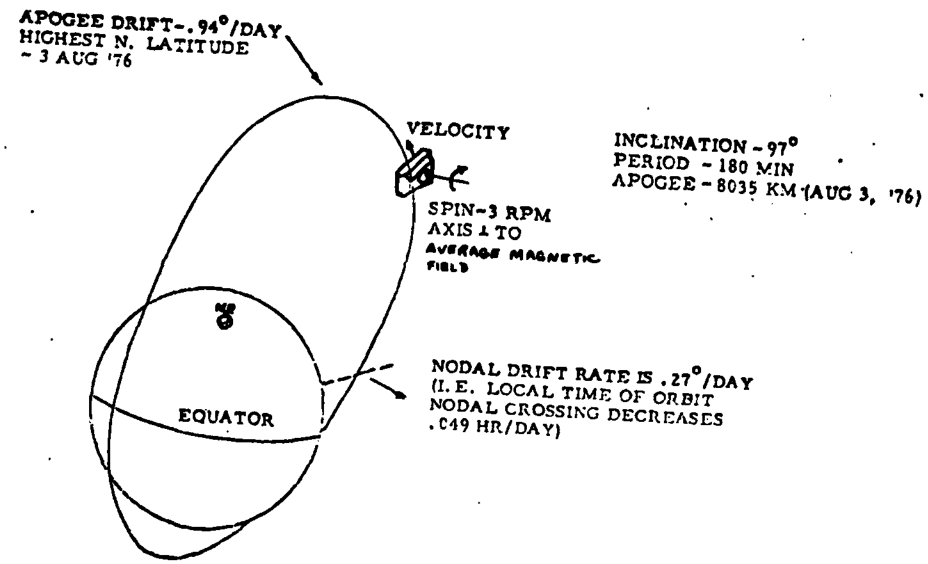
APOGEE DRIFT-.94°/DAY
HIGHEST N. LATITUDE
~ 3 AUG '76
VELOCITY
INCLINATION - 97°
PERIOD - 180 MIN
APOGEE - 8035 KM (AUG 3, '76)
SPIN-3 RPM
AXIS ⊥ TO
AVERAGE MAGNETIC
FIELD
EQUATOR
NODAL DRIFT RATE IS .27°/DAY
(I.E. LOCAL TIME OF ORBIT
NODAL CROSSING DECREASES
.C49 HR/DAY)

FIG B-2. Day of the year versus a) sun time of the orbit phase and b) latitude of apogee.

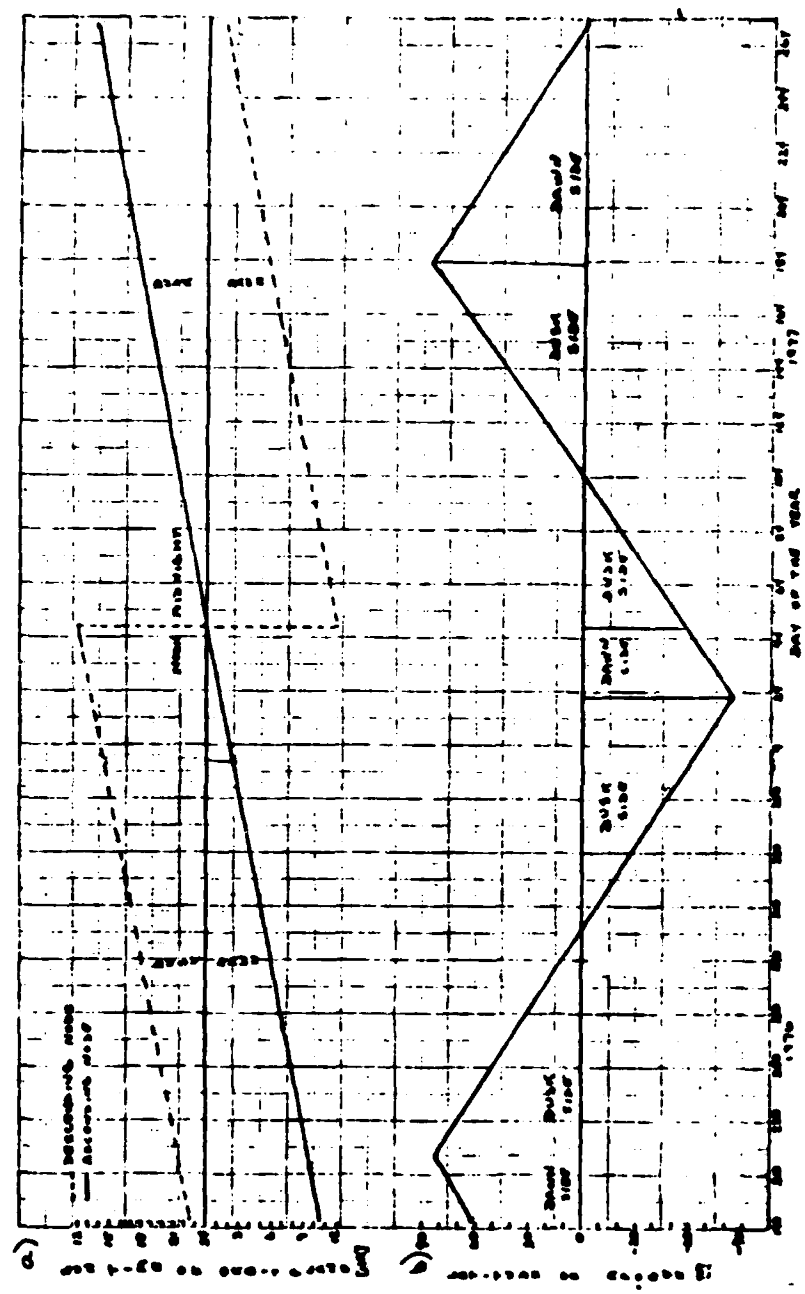

TABLE B-1. S3-3 Scientific payloads with prime investigators in parenthesis.

(

CRL-214 Trapped Proton Monitoring (Yates) AFGL

Solid state detectors are used to measure the spatial distributions, angular distribution and energy spectrum of protons with energy between .1 and 100 MeV.

ONR-118 Low Energy Particle Spectrometer (Sharp) Lockheed

Ions and electrons with energy between 0.5 to 16 KeV and 0.07 to 24 KeV, respectively, are detected using channel multipliers. Particle energy is determined using either magnetic deflection or penetration of particles through thin foils.

ONR-104 Electric Field Measurements (Mozer) UC Berkeley

3 dipoles are used to measure the three components of the DC & AC electrostatic electric field.

CRL-215 Electric Fields and Ion Drifts (Wildman) AFGL

Plasma probes are used to detect the bulk flow of plasma and hence to infer the electric field strength. Four electrostatic analyzers are sensitive to ions in the energy range of 0.1 to 30 eV.

CRLS-217 Energetic Electron Environment (Vampola) Aerospace

A magnetic spectrometer with solid state detectors is used to measure the differential electron flux between 0.012 and 1.6 MeV, protons from 0.08 to 3 MeV, and alphas above 4 MeV.

CRLS-218 Magnetospheric Hydrogen-Electron Abundance (Fennell) Aerospace

An electrostatic analyzer is used to measure the fluxes of low energy electrons and ions at several energies; electrons from 0.17 to 8.4 KeV, ions from 0.09 + 3.9 KeV/Q.

CRLS-225 ELF/VLF Fields (Koons) Aerospace

An air core magnetic loop and a dipole antenna are used to measure the intensity of magnetic and electric fields in the 0.1 to 20.0 KHz frequency range.

The satellite payload configuration is shown in Fig. B-3 with the spin vector perpendicular to the page. The CRLS-217 location is such that penetration thresholds are approximately 10 MeV for electrons and 100 MeV for protons.

CRLS-217 is a twelve differential energy channel magnetic electron spectrometer with an eight channel integral proton and alpha (1 channel) telescope. Permanent magnets (.53 and 1.64 kiloGauss) momentum analyze electrons entering the instrument aperture focusing them onto 12 silicon semiconductor detectors at the primary focus (180°). The instrument configuration is similar to the OV3-3 and OV1-19 instruments described in Appendix A except that the Low Energy Magnetic Spectrometer (LEMS) and High Energy Magnetic Spectrometer (HEMS) are built into one unit as shown in Fig. B-4. Pulseheight analysis of the energy deposits in the detectors is used to discriminate against bremsstrahlung, noise, and penetrating ion background. Also, an additional shiedled detector is used to monitor the background. The electron output of each detector channel corresponds to the uni-directional electron intensity of a given energy bin (typically ± 15 keV for LEMS, ± 100 keV for HEMS) and from these outputs an energy spectrum can be obtained.

The data format is presented in Table B-2. Included are the identification code, channel, sample rate, bits/sample, and geometric energy factor for 28 CRLS-217 and 2 (21, 22) CRLS-218 measurements. Measurements 1-5 are the 5 LEMS channels while 6-12 are the HEMS, with all channel accumulators read out every 1/16 second. Note that

FIG B-3. S3-3 Payload Configuration.

AEROSPACE

CRLS - 217
CRLS - 218
CRLS - 225

AF GEOPHYSICS LAB.

CRL - 214
CRL - 215

LOCKHEED RES. LAB.

ONR - 118

UC BERKELEY

ONR - 104

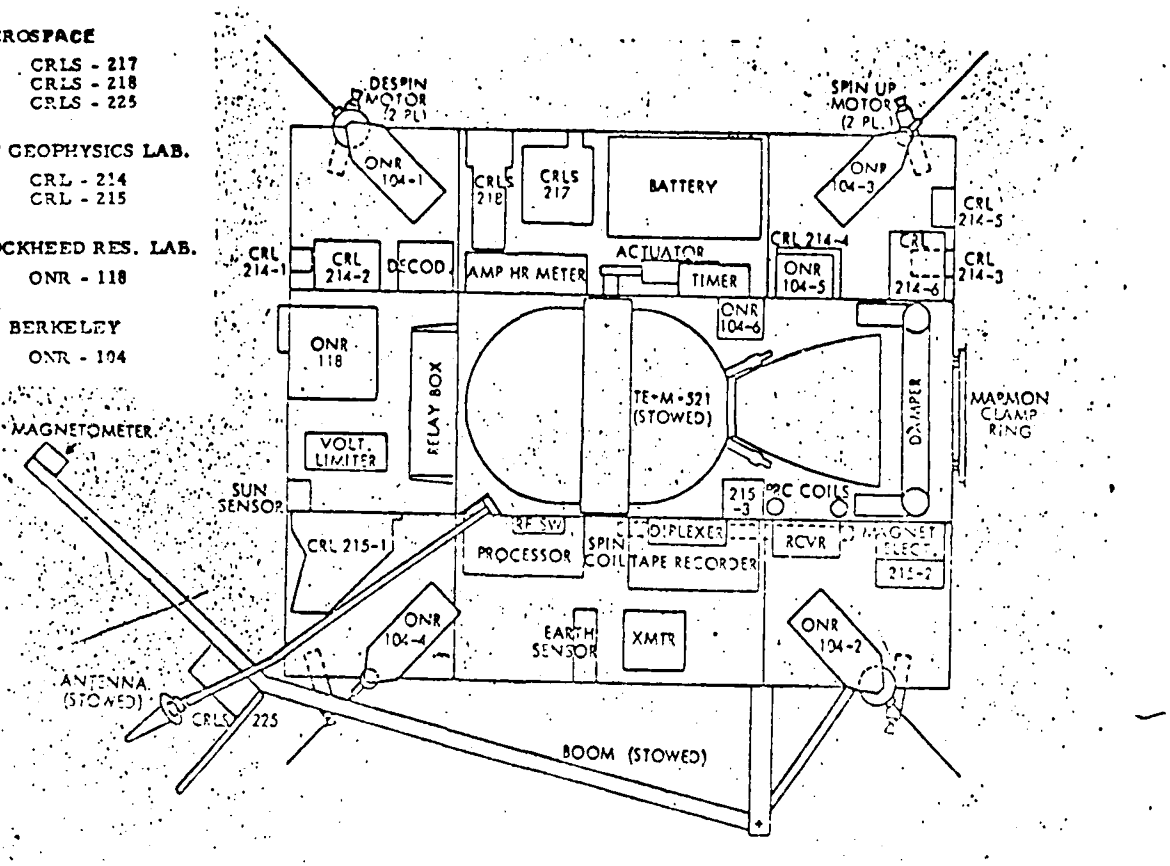

FIG B-4. S3-3 HEMS/LEMS Layout.

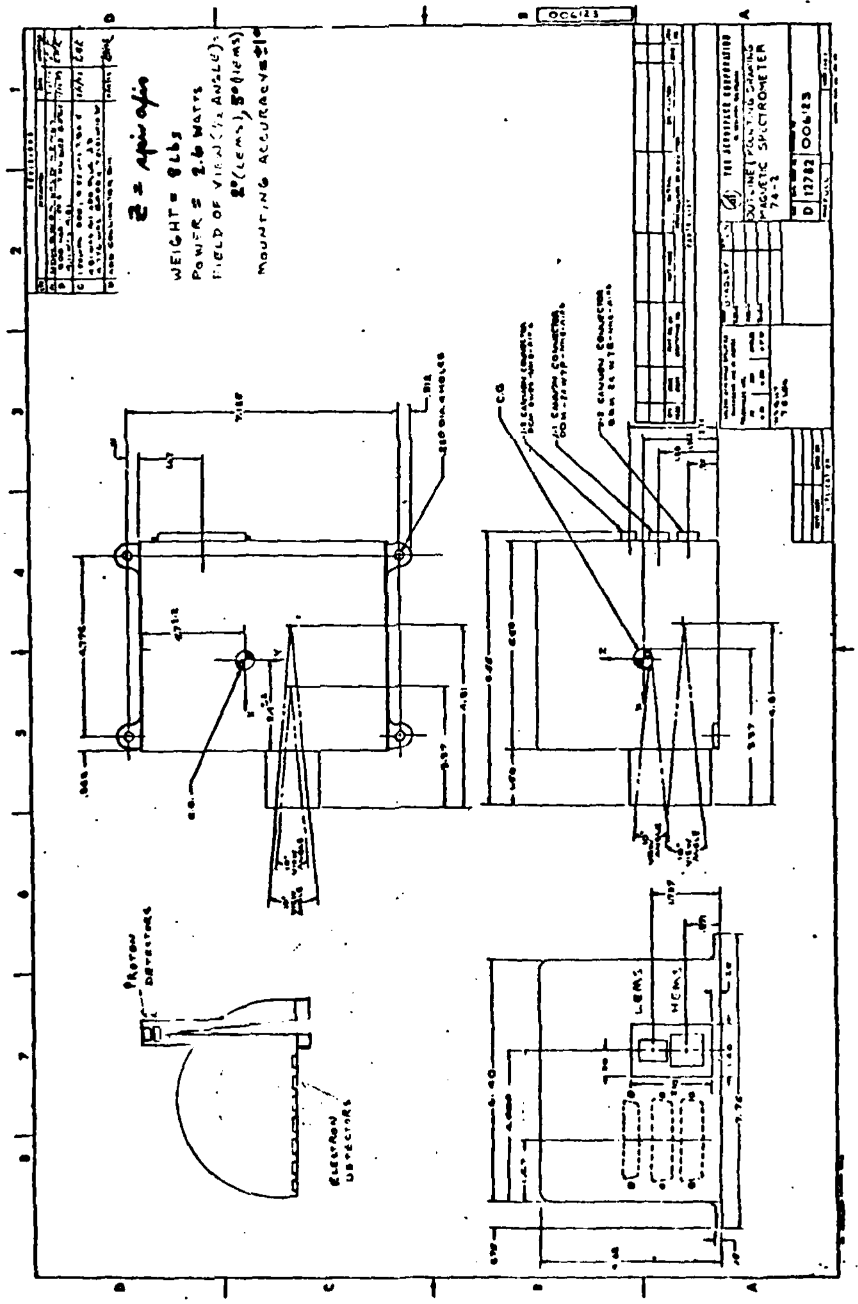
Z = spin axis
WEIGHT = 8 Lbs
POWER = 2.6 WATTS
FIELD OF VIEW (1/2 ANGLE): 2°(LEMS), 5°(HEMS)
MOUNTING ACCURACY ±1°
PROTON DETECTORS
ELECTRON DETECTORS
LEMS
HEMS
C.G.
THE AEROSPACE CORPORATION
OUTLINE / MOUNTING DRAWING
MAGNETIC SPECTROMETER 74-2
D 12782 006123

TABLE B-2. S3-3 HEMS/LEMS Data Format.

MEAS.	ID CODE	CHANNEL	SAMPLES/SEC	BITS/SAMPLE	GEOMETRIC - ENERGY FACTOR *	
1	ME1	$E_e \sim 12$ KeV	16	12**	0.0088	cm^2 ster KeV
2	ME2	$E_e \sim 33$ KeV			0.0029	
3	ME3	$E_e \sim 70$ KeV			0.0141	
4	ME4	$E_e \sim 110$ KeV			0.0036	
5	ME5	$E_e \sim 160$ KeV			0.0147	
6	ME6	$E_e \sim 235$ KeV			6.54	
7	ME7	$E_e \sim 435$ KeV			6.52	
8	ME8	$E_e \sim 655$ KeV			6.12	
9	ME9	$E_e \sim 880$ KeV			5.65	
10	ME 10	$E_e \sim 1.11$ MeV			5.17	
11	ME 11	$E_e \sim 1.35$ MeV			4.57	
12	ME 12	$E_e \sim 1.60$ MeV	16		4.04	cm^2 ster KeV
13	MP1 -S	$E_p > 50$ KeV	4		0.012	cm^2 ster
14	MP2 -S	$E_p > 100$ KeV				
15	MP3	3.2 MeV > $E_p > 80$ KeV				
16	MP4	" > $E_p > 150$ KeV				
17	MP5	" > $E_p > 350$ KeV				
18	MP6	" > $E_p > 770$ KeV				
19	MP7	" > $E_p > 1.55$ MeV				
20	MP8	$E_\alpha > 4.0$ MeV - 13.2 MeV			0.012	cm^2 ster
21	S	ESA STEP } GRLS-[illegible]			—	
22	L	ESA STEP	4		—	
23	EB1	E_e BKG 1	1		—	
24	EB2	E_e BKG 2			—	
25	ES1	$E_e \sim 12$ KeV			0.0088	cm^2 ster KeV
26	ES2	$E_e \sim 70$ KeV			0.0141	
27	ES3	$E_e \sim 235$ KeV			6.54	
28	ES4	$E_e \sim 880$ KeV			5.65	cm^2 ster KeV
29	EP1	$E_p > 80$ KeV			0.012	cm^2 ster
30	EP2	$E_\alpha > 4.0$ MeV	1		0.012	cm^2 ster

* Assumed spectrum is E^0 with 100% efficiency.

** 2^{21} bit accumulator formated into floating point 12 bit output with 0.2% resolution.

the geometric energy factor decreases with energy for the LEMS and HEMS, i.e., sensitivity decreases with increase in energy (given flux will produce less counts/sec for a reduced geometric energy factor). In addition, S3-3 HEMS channels are more than a factor of 2.5 higher in geometric energy factor than OV1-19 LEMS channels to ~450 keV (see Table A-1) but more than a factor of 5.8 lower than OV1-19 HEMS channels to ~1.1 MEV (see Table A-2). Measurements 13-19 and 20 show specs for the integral proton and alpha channels which were also sampled at a rate of 1/sec.

A functional block diagram of the instrument is shown in Fig. B-5a. The lower level discriminator is set at 50% of the minimum expected energy deposit to reject bremsstrahlung and noise and the upper level discriminator is set at an upper threshold of 110% of the maximum expected energy to reject penetrating particles (cosmic rays and energetic protons).

Each electron energy channel is calibrated to find the channel response curve from which the absolute peak (EAPEAK), minimum (EAMIN), and maximum (EAMAX) values are determined (see Fig. B-5 b). A triangle which best matches the slopes of the response curve then yields its peak (E), minimum (ERMIN), and maximum (ERMAX) values. Center values of the two triangle slopes determine EMIN and EMAX. Vertical lines are estended through EMIN and EMAX. The vertical extension of these two lines continues until the resulting rectangle area formed with line segment H equals the area under the actual response curve. This representative rectangle is then used as the

FIG B-5. a) Electron Channel component schematic; b) general response curve; c) channel values for E^{O} with 100% efficiency.

A)

B)

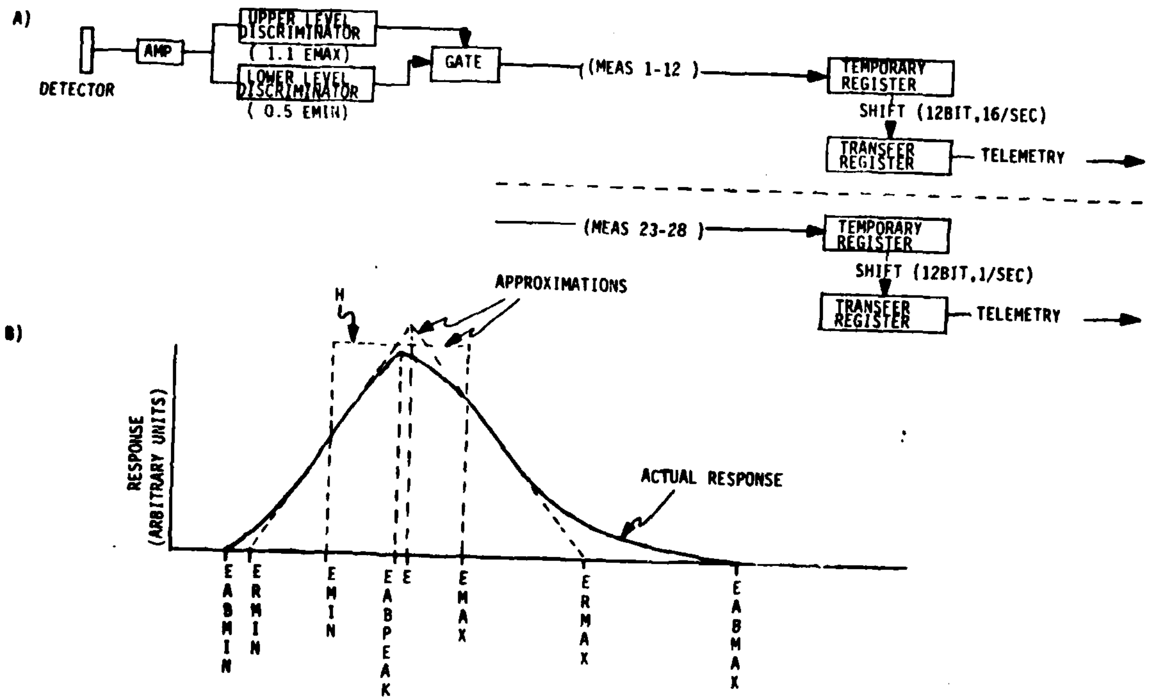

C)

	EABPEAK	EMAX	EMIH	ERMAX	ERMIN	EABMAX	EABMIN	E
LEMS	11.90	14.56	10.21	17.26	6.50	16.98	8.47	11.08
	33.42	39.62	31.86	46.12	30.19	41.14	30.20	33.57
	67.79	73.86	64.33	79.52	60.20	78.99	60.03	68.31
	108.12	118.00	108.47	127.99	106.65	130.16	102.61	108.31
	159.07	167.23	154.00	179.76	148.36	179.53	148.10	159.01
	238.77	328.07	260.18	417.10	192.78	456.97	95.91	288.00
	436.97	635.68	345.86	636.04	257.79	662.21	269.90	438.12
HEMS	665.78	761.76	551.26	864.76	457.01	894.53	481.11	649.34
	894.92	995.93	784.46	1101.32	680.97	1137.31	680.03	878.51
	1130.11	1232.96	1019.32	1339.60	914.91	1376.63	910.51	1126.62
	1369.00	1473.85	1256.45	1581.76	1148.14	1618.14	1148.00	1365.37
	1610.61	1717.02	1498.79	1827.49	1389.98	1861.36	1358.15	1608.08

channel response for data analysis. (This is identical to the description in Appendix A and depiction in Fig. A-2 for instruments OV3-3 or OV1-19.) Values for the above parameters for an assumed spectrum of E^0 with 100% efficiency are listed in Fig. B-5 c. A typical three dimensional response is shown in Fig. B-6 for the 435 KEV channel.

The instrument loss cone response for 655 keV channel is shown in Figs. B-7 a-c as the result of an input distribution isotropic everywhere outside the loss cone and falling off about an order of magnitude per 2^o in the loss cone for pitch angles of 8^o, 18^o, 28^o, respectively. Response to a sharp cutoff can be demonstrated by a zero input distribution at the loss cone but is not represented here. Except for pitch angles less than $\sim 10^o$, an order of magnitude drop in response is about 9^o into the loss cone. This response obviously affects the subjective selection of isotropic distributions in the loss cone and is further discussed in Appendix C.

The spin rate of ~3 RPM allows the instrument to complete a pitch angle plot ($0-180^o$) in approximately 10 seconds (compared to ~4 seconds for OV1-19). At 16 samples/sec, the instrument will collect ~150 samples for a pitch angle plot, nearly a factor of 40 better than the OV1-19. The S3-3 advantage is clear when the two data sets are compared for analysis.

The proton/alpha telescope consists of two silicon detectors in series as shown in Fig. B-8. Detector D1 (100 μm thick) has a

FIG B-6. Typical three dimensional response curve for HEMS 435 keV electron channel.

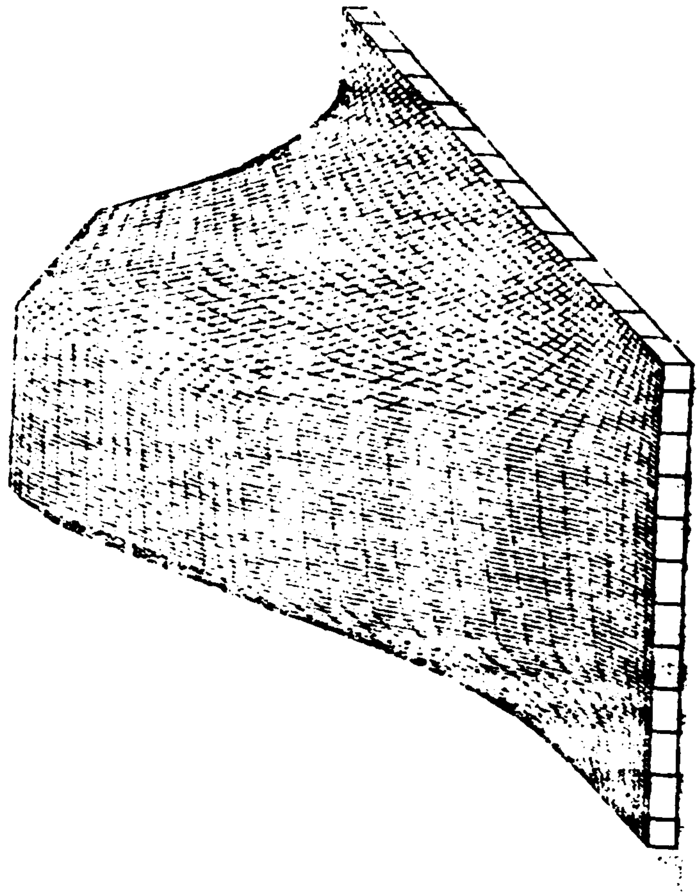

FIG B-7. Typical instrument loss cone response for the 655 keV electron channel for pitch angles 8^{o}, 18^{o}, and 28^{o}.

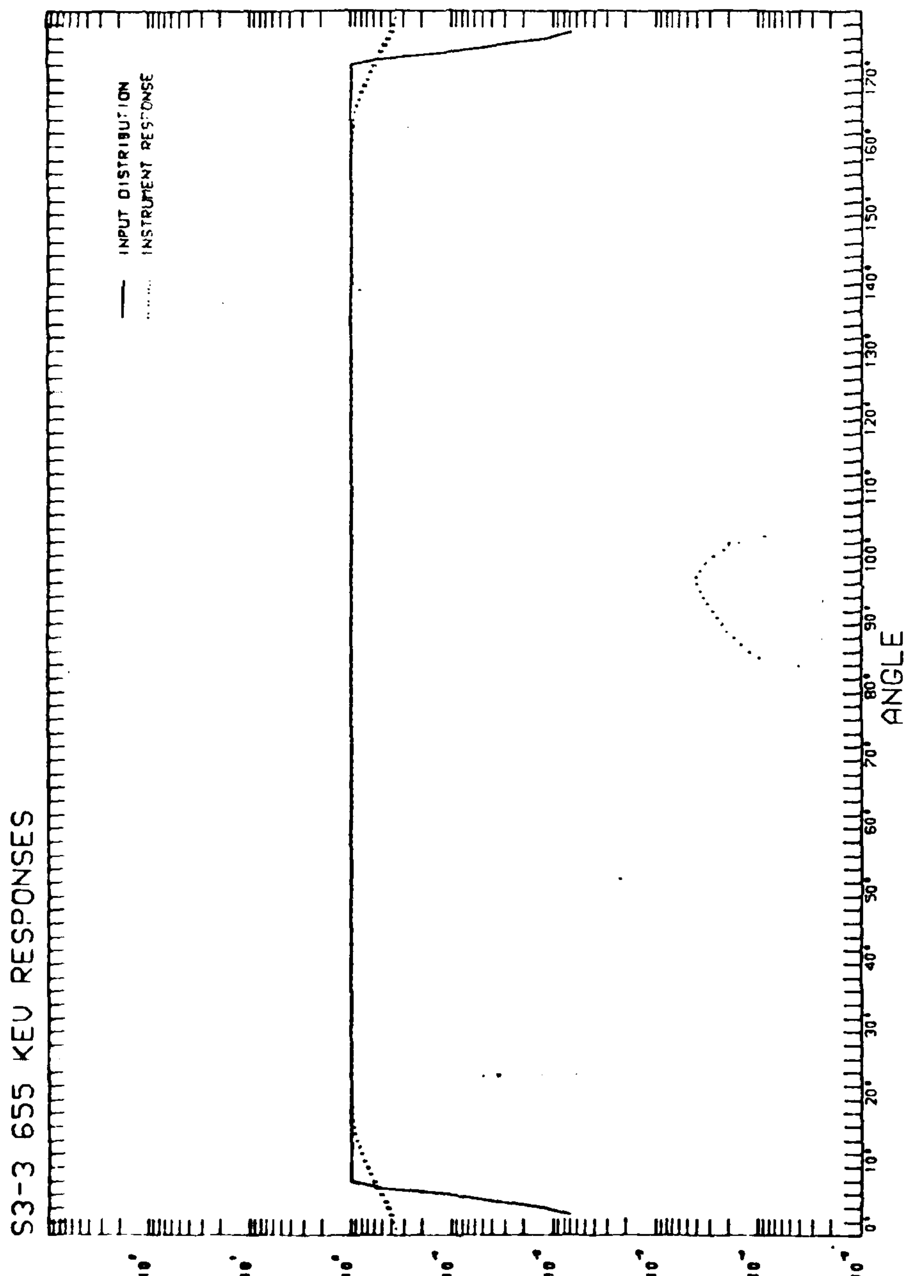
S3-3 655 KEV RESPONSES
INPUT DISTRIBUTION
INSTRUMENT RESPONSE
0°
10°
20°
30°
40°
50°
60°
70°
80°
90°
100°
110°
120°
130°
140°
150°
160°
170°
ANGLE
RESPONSE

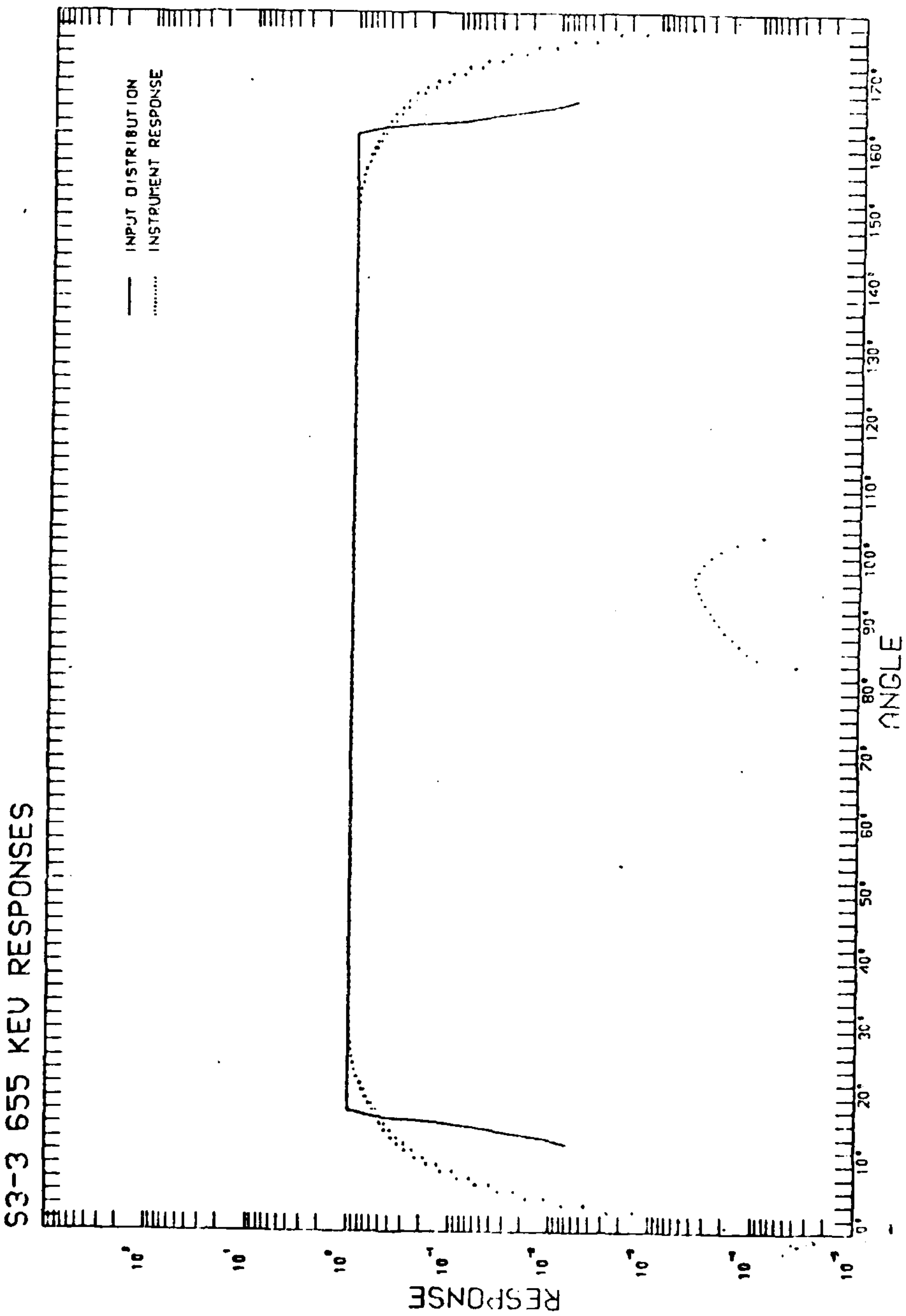

S3-3 655 KEV RESPONSES
INPUT DISTRIBUTION
INSTRUMENT RESPONSE
ANGLE
RESPONSE
0°
10°
20°
30°
40°
50°
60°
70°
80°
90°
100°
110°
120°
130°
140°
150°
160°
170°

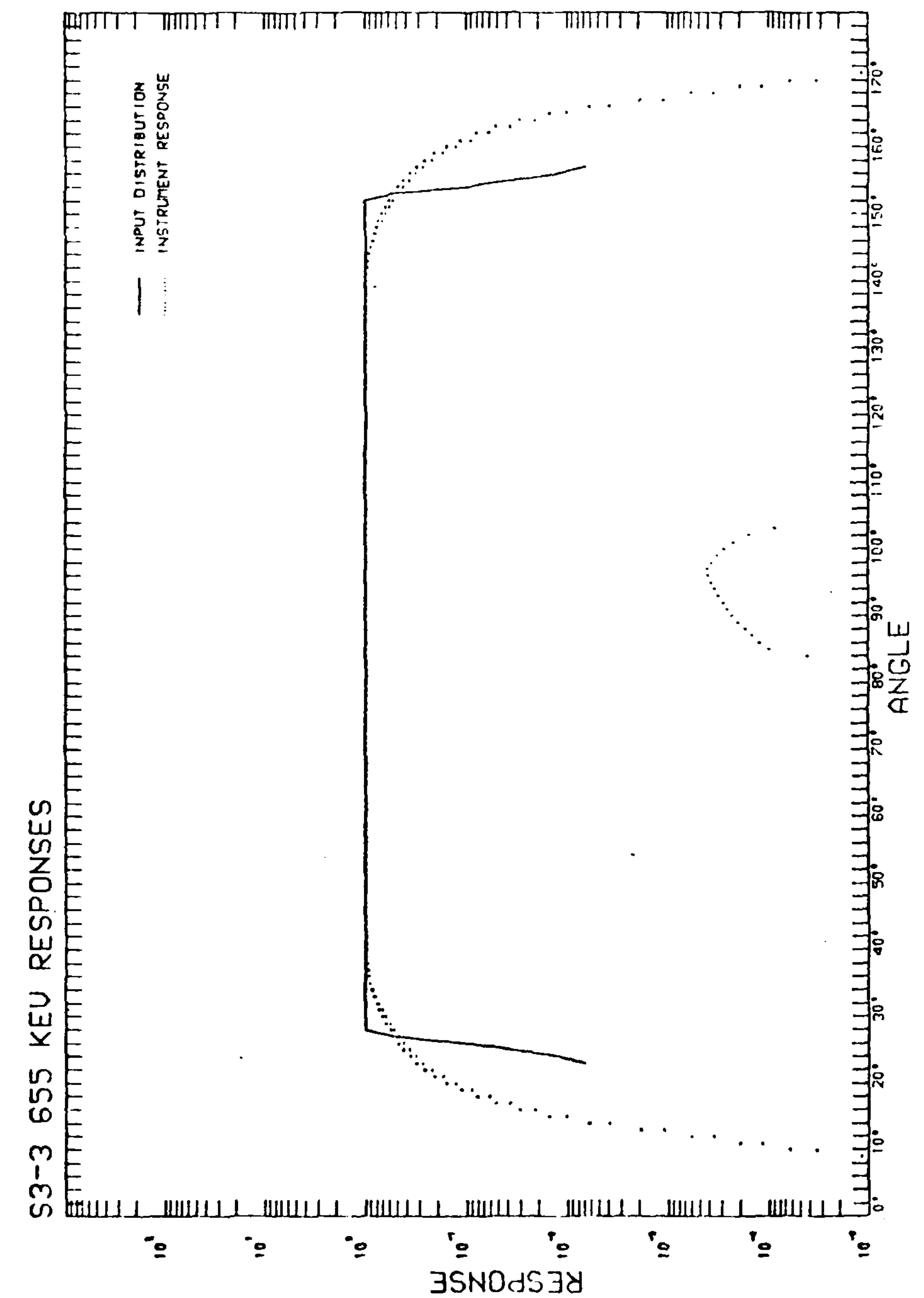

S3-3 655 KEV RESPONSES
INPUT DISTRIBUTION
INSTRUMENT RESPONSE
RESPONSE
ANGLE
0°
10°
20°
30°
40°
50°
60°
70°
80°
90°
100°
110°
120°
130°
140°
150°
160°
170°

lower threshold of 50 keV and detector D2 (200 um thick) has a lower threshold of 100 keV and is the anti to reject energetic protons and cosmic rays penetrating through D1. Particles depositing more than about 4 MeV are assumed to be alphas since p^+ >3.2 MeV would pass through D1 and be antied out by D2. All channels are sampled at 4 samples/sec and E_p> 80 keV and E_α> 4.0 MeV are also sampled at 1/sec.

The S3-3 wave experiment by the Berkeley group (Mozer et al., 1977) obtained the three orthogonal components of the static or fluctuating electric field by measuring the potential differences between three orthogonal pairs of separated spheres. Two pairs of spheres were separated by 37 m in the satellite spin plane and one pair by 6 m along the spin axis. One sphere on the long boom could be operated as a Langmuir probe to make relative density fluctuations. Broadband signals (.05 - 16 kHz) were transmitted in real time to ground stations for 15 min periods on about 25% of the orbits (Kintner et al., 1978). The percentage of concurrent real time wave data and stored plasma data (CRLS 217) is much less. Only filtered wave data in bands from .03-100 kHz are available for most of the stored plasma data presented here.

FIG B-8. S3-3 Proton/alpha telescope data schematic.

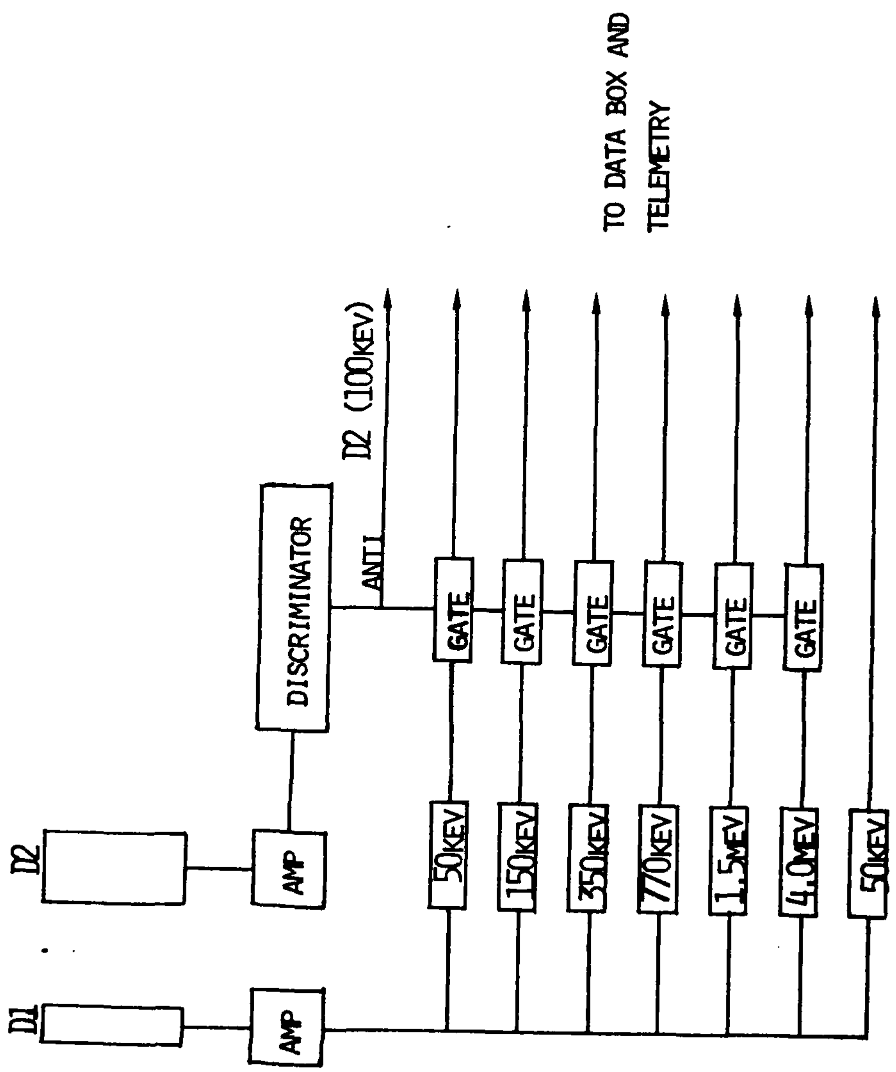
D1
D2
AMP
AMP
DISCRIMINATOR
ANTI
D2 (100KEV)
GATE
GATE
GATE
GATE
GATE
GATE
50KEV
150KEV
350KEV
770KEV
1.5MEV
4.0MEV
50KEV
TO DATA BOX AND
TELEMETRY

Appendix C - REP Event Identification and Catalog Use

In order to select REP events, it was necessary to be able to identify regions of isotropic fluxes on microfiche time plots of the electron and proton fluxes indicative of strong diffusion. Fig. C-1 shows such a plot for the 12, 235, 435, 655 and 850 keV electron and 80 keV proton channels for rev 1661 on a logarithmic scale; UT is measured in sec. The microfiche displays only every fourth data point. The variation in fluxes are due to pitch angle modulation. The key feature one must recognize is the missing upward viewing loss cone indicative of a full or isotropic loss cone. This feature is readily evident throughout the 12 keV electron channel from L = 4.0 - 8.0 and the 80 keV proton channel from L = 4.5 - 6.0. The 235, 435, 655, and 850 keV channels exhibit missing loss cones at L $\sim$ 4.5 with the rest of the outer zone mostly erroded. Effects such as data drops and low altitude diminished flux values similarly appear as missing loss cones so it is extremely important to follow up with examination of the actual pitch-angle plot. Fig. C-2 shows pitch-angle plots for the 235, 435, 655, and 850 keV channels of the example in Fig. C-1 for UT 61092 and 61109 secs. The magnetic field direction is zero in the southward direction at the equator so for this Southern Hemisphere example, 180° is the up-the-field-line direction. The pitch angle is approximately 20°. Also, every data point is displayed and differential flux values can be obtained by dividing by the geometric value per channel (Table B-2). The top panel shows normal loss cone distributions both up and down the field line indicative of expected radiation belt distributions. (However, the belts are disturbed since normally quiet times produce loss cones 3 1/2 orders of magnitude down from trapped flux). The bottom panel (data toward the outer edge of the outer zone) shows the pitch angle 17 secs later. Although normal distributions are evident down the field line, viewing up the field line shows isotropic distributions in all channels. Similar plots can be obtained for the proton channels.

Since the satellite spin axis is not always directly perpendicular to the local magnetic field line and the instrument has a field of view of approximately 5^0 (half angle), we chose only those cases with data at least 10^0 into the local loss cone. A few exceptions were made when the excursion into the loss cone was greater than 6^0 and isotropic fluxes were me-sured on previous and succeeding revs. Less than 3% of the 325 events selected for further pitch-angle analysis were rejected for the 'less than 10^0 in the loss cone' criteria.

Apogee/perigee bias in the flux data was investigated and found to be not important except in the actual appearance of the flux versus time distributions. At apogee the loss cones are small and the counting rates are high. Here we merely insisted on the '10^0 into the loss cone' criteria for validation. At perigee the loss cones are large, the extent (in time) of the entire outer zone is narrow, and the flux counting rates of both trapped and precipitated particles is small. The learning process to identify isotropic fluxes on the microfiche plots was accomplished by a series of trial and error analyses taking about 3 months of time and 150 samples. A high

Fig. C-1. Logarithmic flux (counts/sec) versus UT (sec) for the 12, 235, 435, 655, 850 keV electron and 80 keV proton channel for rev 1661.

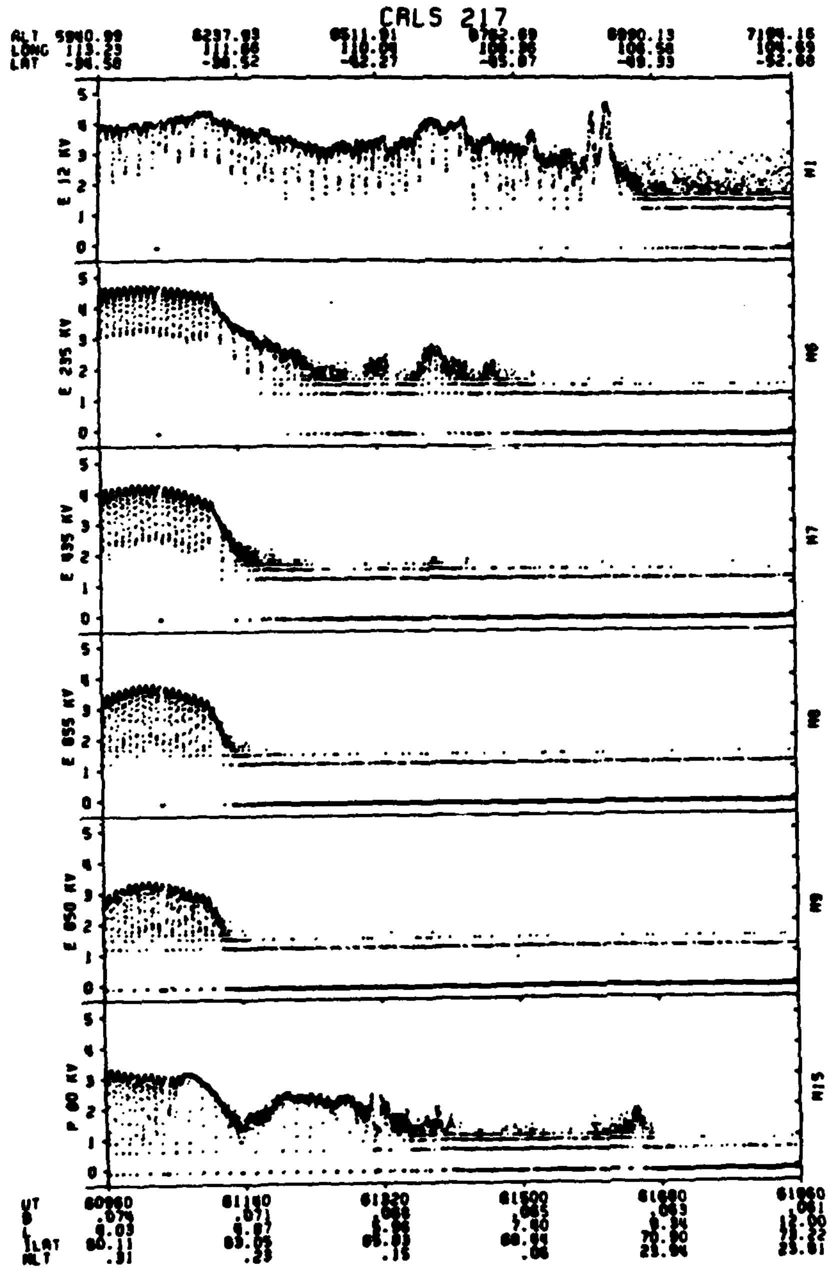

CALS 217
ALT
LONG
LAT
E 12 KV
E 235 KV
E 435 KV
E 855 KV
E 850 KV
P 80 KV
UT

Fig. C-2. Flux (counts/sec) versus pitch angle (degrees) for rev 1661 at 61092 UT (top) and 61109 UT (bottom) for the 235, 435, 655, 880 keV channels. Loss cone is ~20^{o} with the upward looking loss cone at 160^{o} indicated by a vertical line.

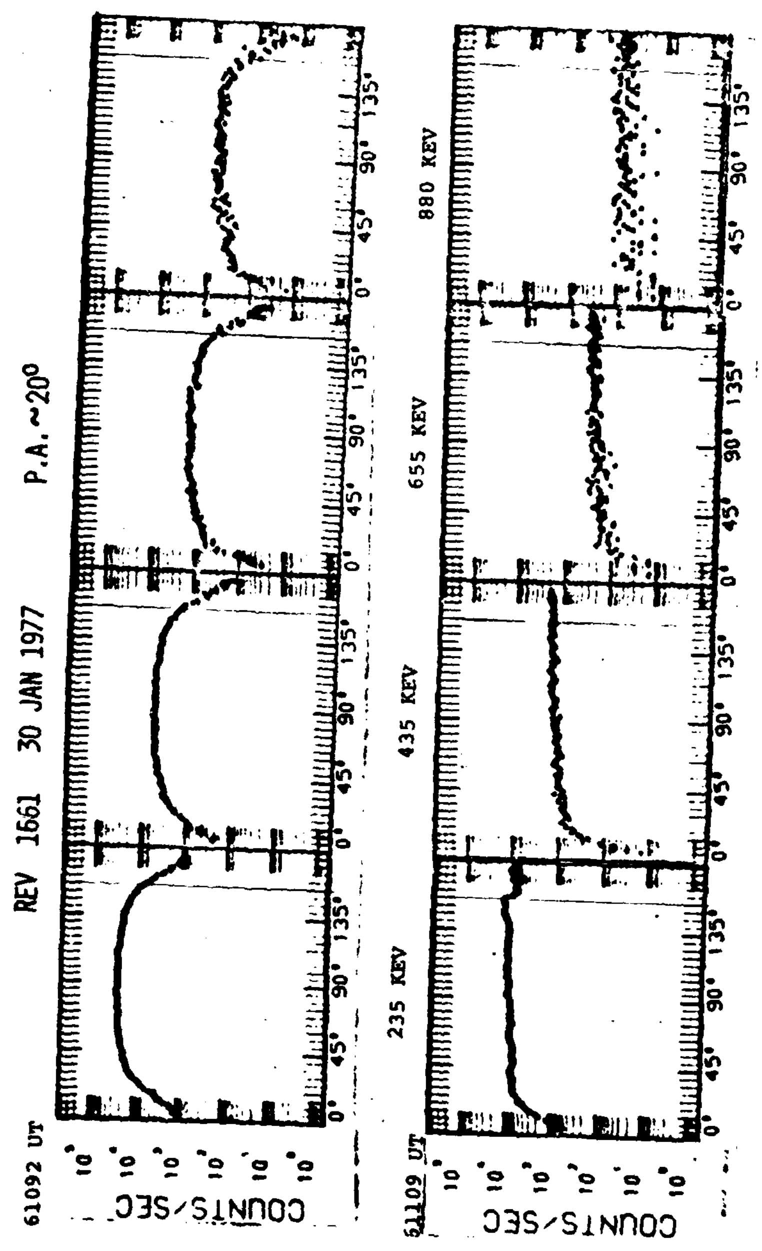
REV 1661 30 JAN 1977 P.A. ~20°
61092 UT
COUNTS/SEC
235 KEV
435 KEV
655 KEV
880 KEV
61109 UT
COUNTS/SEC

Fig. C-3. Microfiche layout with each logarithm of flux (counts/sec) as ordinate for each channel and abscissa the UT (sec) every 180 sec for 900 sec (16 samples/sec), ALT [km], LONG [deg-E], LAT [deg], B [Gauss], L [ ], ILAT [deg], MLT [hr]. E.G. Eight panels (15 min each) of 12, 33, 70 electrons, 8 panels 110, 160, 235 keV electrons, etc. P = Protons, A = Alphas, PD = Proton Detector, BG = Background.

16 SAMPLES/SEC								1 SAMPLE/S
12, 33, 70 KEV ◄15 MIN►	"	"	"	"	"	"	"	BG1, BG2 ◄1 HR►
"	110, 160, 235 KEV	"	"	"	"	"	"	"
"	"	435, 655, 850 KEV	"	"	"	"	"	12, 70, 235 KEV
"	"	"	1.11, 1.35, 1.60 MEV	"	"	"	"	"
"	"	"	"	PD1, PD2, P80 KEV	"	"	"	850, 80 KEV, A4.0 MEV
"	"	"	"	"	P150, P350, P770 KEV	"	"	"
"	"	"	"	"	"	A1.55, A4.00 MEV	"	

Table C-1. Listing of individual microfiche by Readout REV NO (Station and Number), DATE of REV (Last Digit of Yr, Month, Day), Beginning and Ending TIME OF REV IN HRS (Hours, Minutes, Seconds), Beginning and Ending TIME OF REV IN SECS (Seconds), Precip Category (1 $\leq$ 235 keV, 2 $\leq$ 435 keV, 3 $\leq$ 655 keV, 4 $\leq$ 850 keV), COMMENTS (12 = 12 keV electron channel, etc.; 80, 150 = 80, 150 keV Proton Channel, etc; L = L value).

1 - only 235
2 - 235, 435
3 - 235, 435, 655
4 - 235, 435, 655, 880 or more

REV NO.		DATE OF REV	TIME OF REV IN HRS		TIME OF REV IN SECS		COMMENTS
~~COO~~	~~0024~~	~~60711~~	~~[illegible]~~	~~[illegible]~~	~~[illegible]~~	~~[illegible]~~	
~~HUL~~	~~0027~~	~~60712~~	~~[illegible]~~	~~[illegible]~~	~~[illegible]~~	~~[illegible]~~	
~~IND~~	~~0026~~	~~60712~~	~~[illegible]~~	~~[illegible]~~	~~[illegible]~~	~~[illegible]~~	
~~COO~~	~~0032~~	~~60712~~	~~[illegible]~~	~~[illegible]~~	~~[illegible]~~	~~[illegible]~~	
~~COO~~	~~0033~~	~~60712~~	~~[illegible]~~	~~[illegible]~~	~~[illegible]~~	~~[illegible]~~	
~~HUL~~	~~0032~~	~~60712~~	~~[illegible]~~	~~[illegible]~~	~~[illegible]~~	~~[illegible]~~	
~~HUL~~	~~0032~~	~~60712~~	~~[illegible]~~	~~[illegible]~~	~~[illegible]~~	~~[illegible]~~	COMMENTS
COO	0037	60713	45855	65225	17935	24745	
COO	0036	60713	65242	83707	24762	31027	P* along pump L=5-7,
POG	0044	60714	2530	13651	1530	5011	P* along pump L=5.5-6
HUL	0043	60714	13700	32354	5820	12234	
BOS	0049	60714	152005	162251	55205	58971	235 e- pump L=6 80 P* L=5.6
HUL	0047	60714	162308	181844	58988	65924	
HUL	0055	60715	91415	101952	33255	37192	
BOS	0054	60715	102015	121233	37215	43953	P* along pump L=14 19 3
IND	0063	60716	83005	101744	30605	37064	P*sp L=5.5
COO	0062	60716	101807	120822	37087	43702	P*sp L>13
POG	0066	60716	210130	224000	75690	81600	P*sp L=5-8
COO	0065	60716	224017	10	81617	10	P*sp L>10
COO	0072	60717	145521	164644	53721	60404	12,35 e- L=8-14, P* 80 [illegible] L=6-8
POG	0071	60717	164700	175358	60420	64438	12 e- L=8-10 Drop-trapped 850 e- at L=5.5
HUL	0096	60720	53340	65845	20020	25125	12 e- L=15-20, 80 P* L=6-[illegible]
IND	0095	60720	65901	83219	25141	30739	12 e- L=8-9 L=6-7
HUL	0104	60721	22614	33746	8774	13066	12 e- L=6-9, 80,150 P* L=6-7
HUL	0103	60721	33802	52450	13082	19490	
COO	0111	60722	111426	123253	40468	45173	12 e- L=8-9, L=7-8, 80 P* L=6, 5-7
BOS	0110	60722	123319	141304	45199	51184	12 e- L=7-11, 850 e- Drop-trap flux L=5.3
~~IND~~	~~0115~~	~~60723~~	~~[illegible]~~	~~[illegible]~~	~~[illegible]~~	~~[illegible]~~	
IND	0115	60723	20914	32012	7754	12012	12 e- L=8-11, 80 P* L=6-7
~~HUL~~	~~0115~~	~~60723~~	~~[illegible]~~	~~[illegible]~~	~~[illegible]~~	~~[illegible]~~	
HUL	0115	60723	32034	50743	12034	18463	12, 33 e- L=7.5-14, L=6-8, L=6-7
BOS	0126	60723	230138	1353	82898	833.	12 e- L=7, 80 P* L=7-8
IND	0123	60724	1409	20014	849	7214	←——— 80 P* L=7
IND	0131	60724	195410	210537	71650	75937	12 e- (along [illegible]) L=8-12, 80+150 P* L=5-7
COO	0129	60724	210554	225247	75954	82367	12 e- L=7-10, 33 e- 7-10 ——— 80 P* L=14-16
COO	0145	60726	163816	175815	59896	64695	——— 80+150 P* L=5.9-6
POG	0144	60726	175830	193655	64710	70615	12 e- L=14-15
COO	0153	60727	163004	180819	59404	65299	12 e- L=6-8, 850 e- Trap flux drop L=2, 80,150 P* L=5.75
POG	0152	60727	180835	192827	65315	70107	12 e- L=12-20
IND	0160	60728	132226	144045	48146	52845	12 e- ~~[illegible]~~ L=9-10 L=6-13; 80,150 P* L=6-13
POG	0159	60728	144102	162103	52862	58863	12, 33 e- L=6-12, ——— 80 P* L=[illegible]
COO	0169	60729	101502	115339	36952	42819	12, 33 e- L=6-10, 8-9, 14-16, 80,150 P* L=5-9
HUL	0168	60729	115355	131339	42835	47619	12 e- L=12, 33 e- L=8-9, 80 P* L=12-15; 80,150 P* L=5
BOS	0178	60730	70739	80554	25659	29154	80,150 P* L=5-8
HUL	0176	60730	80611	100616	29171	36376	33 e- L>8, 80 P* >7
HUL	0184	60731	40021	51144	14421	18704	——— ←———
COO	0182	60731	51200	65849	18720	25129	33 e- L=7 ——— 7
HUL	0188	60801	5250	20926	3170	7764	80,150 P* L=[illegible]
~~HUL~~	~~0188~~	~~60801~~	~~5250~~	~~[illegible]~~	~~[illegible]~~	~~[illegible]~~	
IND	0187	60801	20943	35129	7783	13889	
~~IND~~	~~0187~~	~~60801~~	~~[illegible]~~	~~[illegible]~~	~~[illegible]~~	~~[illegible]~~	
HUL	0195	60801	214528	230007	78328	82807	80,150 P* L>5, L>5.
COO	0194	60801	230023	4404	82823	2644	33 e- L=8-12, ~~235, 435 [illegible]~~
COO	0202	60802	183812	200307	67092	72187	80 P* L=6-7
COO	0201	60802	200324	213641	72204	77801	
BOS	0215	60804	2747	15158	1667	6718	12,33 e- L=7, 80,150 P* L>7
HUL	0212	60804	15214	32607	6734	12367	33 e- L=8-12, ~~[illegible]~~
COO	0218	60804	182109	194612	66069	71172	
COO	0217	60804	194629	211943	71189	76783	
HUL	0225	60805	121434	133932	44074	49172	80 P* L=6-7
~~HUL~~	~~0225~~	~~60805~~	~~[illegible]~~	~~[illegible]~~	~~[illegible]~~	~~[illegible]~~	
COO	0223	60805	133949	151309	49189	54789	
~~HUL~~	~~0235~~	~~60806~~	~~[illegible]~~	~~[illegible]~~	~~[illegible]~~	~~[illegible]~~	
HUL	0235	60806	90654	103153	32814	37913	80 P* L=6-7
~~COO~~	~~0234~~	~~60806~~	~~[illegible]~~	~~[illegible]~~	~~[illegible]~~	~~[illegible]~~	
COO	0234	60806	103209	120530	37929	43530	
~~BOS~~	~~0239~~	~~60807~~	~~[illegible]~~	~~[illegible]~~	~~[illegible]~~	~~[illegible]~~	
BOS	0239	60807	55915	72215	21555	26535	
~~COO~~	~~0238~~	~~60807~~	~~[illegible]~~	~~[illegible]~~	~~[illegible]~~	~~[illegible]~~	
COO	0238	60807	72231	85750	26551	32270	
COO	0246	60808	25210	41007	10330	15007	80 P* L=6-7
~~COO~~	~~0246~~	~~60808~~	~~[illegible]~~	~~[illegible]~~	~~[illegible]~~	~~[illegible]~~	
GUA	0245	60808	41024	55011	15024	21011	
~~GUA~~	~~0245~~	~~60808~~	~~[illegible]~~	~~[illegible]~~	~~[illegible]~~	~~[illegible]~~	
IND	0251	60808	204502	220959	74702	79799	80 P* L=7
~~IND~~	~~0251~~	~~60808~~	~~[illegible]~~	~~[illegible]~~	~~[illegible]~~	~~[illegible]~~	
POG	0250	60808	221017	234336	79817	85416	
~~POG~~	~~0250~~	~~60808~~	~~[illegible]~~	~~[illegible]~~	~~[illegible]~~	~~[illegible]~~	
GUA	0258	60809	143829	160031	52709	57631	235 e- (strange) L=6-6.5; 80,150 P* L=5-7, 5-7
~~GUA~~	~~0258~~	~~60809~~	~~[illegible]~~	~~[illegible]~~	~~[illegible]~~	~~[illegible]~~	
POG	0257	60809	160047	173702	57647	63422	
~~POG~~	~~0257~~	~~60809~~	~~[illegible]~~	~~[illegible]~~	~~[illegible]~~	~~[illegible]~~	
~~GUA~~	~~0262~~	~~60810~~	~~[illegible]~~	~~[illegible]~~	~~[illegible]~~	~~[illegible]~~	
GUA	0262	60810	23408	35123	9248	13883	80,150 P* L=5-6 Trap flux drop ([illegible])
~~HUL~~	~~0261~~	~~60810~~	~~[illegible]~~	~~[illegible]~~	~~[illegible]~~	~~[illegible]~~	
HUL	0261	60810	35144	53242	13904	19962	33 e- L=7-10 80,150 P* L=11-12, 6-7
GUA	0266	60810	142944	155447	52184	57287	33 e- ([illegible]) L=8, 80 P* L=6-9
~~GUA~~	~~0266~~	~~60810~~	~~[illegible]~~	~~[illegible]~~	~~[illegible]~~	~~[illegible]~~	
POG	0265	60810	155503	172817	57303	62897	33 e- L=8-13
~~POG~~	~~0265~~	~~60810~~	~~[illegible]~~	~~[illegible]~~	~~[illegible]~~	~~[illegible]~~	
BOS	0270	60811	52423	64134	19463	24894	80 P* L=5.5-7
~~BOS~~	~~0270~~	~~60811~~	~~[illegible]~~	~~[illegible]~~	~~[illegible]~~	~~[illegible]~~	
~~BOS~~	~~0270~~	~~60811~~	~~[illegible]~~	~~[illegible]~~	~~[illegible]~~	~~[illegible]~~	
BOS	0269	60811	64151	82250	24111	30170	33 e- L=7-11
~~BOS~~	~~0269~~	~~60811~~	~~[illegible]~~	~~[illegible]~~	~~[illegible]~~	~~[illegible]~~	
~~BOS~~	~~0268~~	~~60811~~	~~[illegible]~~	~~[illegible]~~	~~[illegible]~~	~~[illegible]~~	
~~POG~~	~~0274~~	~~60811~~	~~[illegible]~~	~~[illegible]~~	~~[illegible]~~	~~[illegible]~~	
POG	0274	60811	171955	184314	62395	67394	
~~COO~~	~~0273~~	~~60811~~	~~[illegible]~~	~~[illegible]~~	~~[illegible]~~	~~73106~~	
COO	0273	60811	184341	201826	67421	73106	

REV NO.		DATE OF REV	TIME OF REV IN HRS		TIME OF REV IN SECS		
~~BOS~~	~~0278~~	~~60812~~	~~21636~~	~~34708~~	~~8196~~	~~13628~~	
~~BOS~~	~~0278~~	~~60812~~	~~21636~~	~~34708~~	~~8196~~	~~13628~~	
BOS	0278	60812	21636	34708	8196	13628	80 P⁺ L=8-9
~~HUL~~	~~0277~~	~~60812~~	~~34743~~	~~51500~~	~~13663~~	~~18900~~	
~~HUL~~	~~0277~~	~~60812~~	~~34725~~	~~51509~~	~~13645~~	~~18909~~	
HUL	0277	60812	34725	51509	13645	18909	33 e⁻ L=11, 21 (apogee)
POG	0282	60812	141212	153712	51132	56232	80 P⁺ L=6
GUA	0281	60812	153729	171046	56249	61846	
~~COO~~	~~0289~~	~~60813~~	~~110434~~	~~122935~~	~~39874~~	~~44975~~	
COO	0289	60813	110438	122935	39878	44975	
~~POG~~	~~0288~~	~~60813~~	~~122953~~	~~140307~~	~~44993~~	~~50587~~	
POG	0288	60813	122958	140307	44998	50587	
~~COO~~	~~0298~~	~~60814~~	~~75653~~	~~90830~~	~~28613~~	~~32910~~	
~~COO~~	~~0298~~	~~60814~~	~~75653~~	~~90830~~	~~28613~~	~~32910~~	
COO	0298	60814	75656	90831	28616	32911	
~~HUL~~	~~0295~~	~~60814~~	~~90846~~	~~105527~~	~~32926~~	~~39327~~	
~~HUL~~	~~0295~~	~~60814~~	~~90846~~	~~105527~~	~~32926~~	~~39327~~	
HUL	0295	60814	90848	105528	32928	39328	
HUL	0305	60815	44905	60721	17345	22041	
~~HUL~~	~~0305~~	~~60815~~	~~44905~~	~~60721~~	~~17345~~	~~22041~~	
COO	0304	60815	60738	74741	22058	28061	
~~COO~~	~~0304~~	~~60815~~	~~60738~~	~~74741~~	~~22058~~	~~28061~~	
COO	0311	60816	14116	30600	6076	11160	rapid onset zone dropoff at 235 keV vs. keV
~~COO~~	~~0311~~	~~60816~~	~~14116~~	~~30600~~	~~6076~~	~~11160~~	
~~COO~~	~~0311~~	~~60816~~	~~14116~~	~~30600~~	~~6076~~	~~11160~~	
COO	0309	60816	30616	43948	11176	16788	
COO	0318	60816	223340	235120	81220	85880	rapid onset zone dropoff 235 keV e⁻, 80 P⁺ L=6 (neutrals?)
COO	0317	60816	235136	13200	85896	5520	
BOS	0326	60817	192537	205044	69937	75044	
COO	0323	60817	205109	222408	75069	80648	
COO	0330	60818	161745	173559	58665	63359	
COO	0329	60818	173614	191617	63374	69377	
BOS	0346	60820	155952	172452	57592	62692	Bad compaction problem
HUL	0345	60820	172508	185824	62708	68304	
~~COO~~	~~0355~~	~~60821~~	~~125159~~	~~141235~~	~~46319~~	~~51155~~	
COO	0355	60821	125204	141236	46324	51156	80 P⁺ L=6-7
~~COO~~	~~0353~~	~~60821~~	~~141251~~	~~155033~~	~~51171~~	~~57033~~	
COO	0353	60821	141252	155034	51172	57034	33 e⁻ L=8-12, 80 P⁺ L=6-8
~~POG~~	~~0362~~	~~60822~~	~~94412~~	~~110852~~	~~35052~~	~~40132~~	
POG	0362	60822	94413	110852	35053	40132	bad dropouts
~~COO~~	~~0360~~	~~60822~~	~~110817~~	~~124243~~	~~40157~~	~~45763~~	
COO	0360	60822	110909	124243	40149	45763	33 e⁻ L=7-12, 80,150 P⁺ L=8-11
~~POG~~	~~0369~~	~~60823~~	~~63621~~	~~74753~~	~~23781~~	~~28073~~	
POG	0369	60823	63623	74754	23783	28074	80,150 P⁺ L=4-5
~~COO~~	~~0368~~	~~60823~~	~~74809~~	~~93453~~	~~28089~~	~~34493~~	
COO	0368	60823	74815	93454	28095	34494	33 e⁻ L=5-6 235 keV L=5-6, 80,150 P⁺ L=5.5-6
COO	0371	60823	194244	204038	70964	74438	80 P⁺ L=5.5
POG	0370	60823	204054	222044	74454	80444	80,150 P⁺ L>4 Bad compaction problem
HUL	0374	60824	32831	43329	12511	16409	80,150 P⁺ L 4-5
HUL	0373	60824	43346	62703	16426	23223	4 33 e⁻ L>6 235 L 7.5 80,150 P⁺ L>5, 6.9-10
~~HUL~~	~~0373~~	~~60824~~	~~43346~~	~~62703~~	~~16426~~	~~23223~~	
~~HUL~~	~~0373~~	~~60824~~	~~43346~~	~~62703~~	~~16426~~	~~23223~~	
~~HUL~~	~~0373~~	~~60824~~	~~43346~~	~~62703~~	~~16426~~	~~23223~~	
~~HUL~~	~~0373~~	~~60824~~	~~43346~~	~~62703~~	~~16426~~	~~23223~~	
~~COO~~	~~0377~~	~~60824~~	~~122500~~	~~133648~~	~~44700~~	~~49008~~	
COO	0377	60824	122513	133648	44713	49008	80,150 P⁺ L=5-6 Bad dropouts.
~~COO~~	~~0376~~	~~60824~~	~~133705~~	~~152343~~	~~49025~~	~~55423~~	
COO	0376	60824	133713	152343	49033	55423	33 e⁻ L=7-10, 80,150 P⁺ L=6-11
~~HUL~~	~~0381~~	~~60824~~	~~212147~~	~~224700~~	~~76907~~	~~82020~~	
HUL	0381	60824	212154	224701	76914	82021	1 33, 235 e⁻ L=7 80,150 P⁺ L=5-8, 5-8
~~COO~~	~~0379~~	~~60824~~	~~224710~~	~~2000~~	~~82030~~	~~1200~~	
COO	0379	60824	224722	2021	82042	1221	33 e⁻ L=7-9 80 P⁺ L=11, 16
~~HUL~~	~~0384~~	~~60825~~	~~91710~~	~~104224~~	~~33430~~	~~38544~~	
HUL	0384	60825	91722	104228	33442	38548	33 e⁻ L=6-8, 235 ... at L=6, 80,150 P⁺ L=6-12
~~POG~~	~~0383~~	~~60825~~	~~104244~~	~~121552~~	~~38564~~	~~44152~~	
POG	0383	60825	104251	121553	38571	44153	33 e⁻ L>8 80 P⁺ L>6
~~GUA~~	~~0390~~	~~60825~~	~~181357~~	~~192536~~	~~65637~~	~~69936~~	
~~GUA~~	~~0390~~	~~60825~~	~~181357~~	~~192536~~	~~65637~~	~~69936~~	
GUA	0390	60825	181403	192536	65643	69936	80,150 P⁺ L=6-7
~~COO~~	~~0386~~	~~60825~~	~~192553~~	~~211231~~	~~69953~~	~~76351~~	
~~COO~~	~~0386~~	~~60825~~	~~192553~~	~~211231~~	~~69953~~	~~76351~~	
COO	0386	60825	192555	211231	69955	76351	1 33 e⁻ L=6.5, 7-10, 235 e⁻ L=8 ... 80,150 P⁺ L=5-8 ... L=6
~~POG~~	~~0394~~	~~60826~~	~~132720~~	~~150037~~	~~48440~~	~~54037~~	
POG	0394	60826	132725	150038	48445	54038	12 e⁻ L>9 80,150 P⁺ L=6-8
~~POG~~	~~0393~~	~~60826~~	~~150055~~	~~165729~~	~~54055~~	~~61049~~	
POG	0393	60826	150101	165730	54061	61050	235 e⁻ L=7 (weak), 80,150 P⁺ L=6-9, 6-9
~~HUL~~	~~0398~~	~~60827~~	~~247~~	~~11343~~	~~167~~	~~4423~~	
HUL	0398	60827	247	11343	167	4423	1, 2 12, 33 e⁻ L=6-10, 235, 435 e⁻ L=6 (weak) 80,150 P⁺ ...
POG	0397	60827	11400	30119	4440	10879	
~~POG~~	~~0397~~	~~60827~~	~~11400~~	~~30119~~	~~4440~~	~~10879~~	
~~IND~~	~~0401~~	~~60827~~	~~115810~~	~~131643~~	~~43090~~	~~47803~~	
IND	0401	60827	115822	131643	43102	47803	80,150 P⁺ L=6-8
~~POG~~	~~0400~~	~~60827~~	~~131707~~	~~145650~~	~~47827~~	~~53810~~	
POG	0400	60827	131702	145651	47822	53811	80,150 P⁺ L=6-7
COO	0405	60827	205455	221842	75295	80322	2 235 e⁻, 455 e⁻ L=4.5 80,150 P⁺ L=4.5, 6
HUL	0403	60827	221901	235329	80341	86009	33 e⁻ L 7-8
~~BOS~~	~~0408~~	~~60828~~	~~85030~~	~~101528~~	~~31830~~	~~36928~~	
BOS	0408	60828	85027	101528	31827	36928	80 P⁺ L 6-7
~~COO~~	~~0407~~	~~60828~~	~~101603~~	~~114901~~	~~36963~~	~~42541~~	
COO	0407	60828	101545	114901	36945	42541	1 33 e⁻ L=8-11, 235 L=9 80,150 P⁺ L=6-7
~~COO~~	~~0413~~	~~60828~~	~~174706~~	~~191158~~	~~64026~~	~~69118~~	
~~COO~~	~~0413~~	~~60828~~	~~174706~~	~~191158~~	~~64026~~	~~69118~~	
COO	0413	60828	174713	191159	64033	69119	12, 33 e⁻ L>6 235 e⁻ weak ... L=8 ... 80 P⁺ L=5-7
~~POG~~	~~0410~~	~~60828~~	~~191215~~	~~204538~~	~~69135~~	~~74738~~	
~~POG~~	~~0410~~	~~60828~~	~~191215~~	~~204538~~	~~69135~~	~~74738~~	
POG	0410	60828	191217	204539	69137	74739	1 12, 33 e⁻ L=6-11 235 L=8 80 P⁺ L>8
~~HUL~~	~~0418~~	~~60829~~	~~143818~~	~~154934~~	~~52738~~	~~56974~~	
HUL	0418	60829	143906	154934	52746	56974	12, 33 e⁻ L 8 235 e⁻ weak ... L 8 80 P⁺ L=6-8
~~COO~~	~~0417~~	~~60829~~	~~154061~~	~~173734~~	~~56991~~	~~63484~~	
COO	0417	60829	154954	173734	56994	63484	12 e⁻ L=6-21 80 P⁺ L=5-7

REV NO.		DATE OF REV	TIME OF REV IN HRS		TIME OF REV IN SECS			
~~COO~~	~~0426~~	~~60830~~	~~83206~~	~~95704~~	~~30726~~	~~35824~~		
~~COO~~	~~0426~~	~~60830~~	~~83206~~	~~95704~~	~~30726~~	~~35824~~		
COO	0426	60830	83212	95732	30732	35852		29 e⁻ small spike L=7.6
~~BOS~~	~~0425~~	~~60830~~	~~95720~~	~~113036~~	~~35840~~	~~41436~~		
~~BOS~~	~~0425~~	~~60830~~	~~95720~~	~~113036~~	~~35840~~	~~41436~~		
BOS	0425	60830	95732	113037	35852	41437		
~~COO~~	~~0435~~	~~60831~~	~~52401~~	~~64215~~	~~19441~~	~~24135~~		
COO	0435	60831	52406	64215	19446	24135		80,150 P⁻ L=6
~~MUL~~	~~0430~~	~~60831~~	~~64231~~	~~82231~~	~~24151~~	~~30151~~		
MUL	0430	60831	64231	82230	24151	30159		33e⁻ L>8
~~MUL~~	~~0440~~	~~60901~~	~~21554~~	~~33417~~	~~8154~~	~~12857~~		
~~MUL~~	~~0440~~	~~60901~~	~~21554~~	~~33417~~	~~8154~~	~~12857~~		
MUL	0440	60901	21559	33420	8159	12860		80,150 P⁻ L=5.5
~~COO~~	~~0439~~	~~60901~~	~~33435~~	~~51424~~	~~12875~~	~~18864~~		
~~COO~~	~~0439~~	~~60901~~	~~33435~~	~~51424~~	~~12875~~	~~18864~~		
COO	0439	60901	33439	51425	12879	18865		33e⁻ L=7-10 80P⁻ L=8-9
~~POG~~	~~0443~~	~~60901~~	~~171006~~	~~183520~~	~~61806~~	~~66920~~		
~~POG~~	~~0443~~	~~60901~~	~~171008~~	~~183520~~	~~61808~~	~~66920~~		
POG	0443	60901	171008	183530	61808	66930		12e⁻ L=8-12 80,150 P⁻ L=5.5-6.2
~~POG~~	~~0442~~	~~60901~~	~~183544~~	~~200837~~	~~66944~~	~~72517~~		
~~POG~~	~~0442~~	~~60901~~	~~183554~~	~~200837~~	~~66954~~	~~72517~~		
POG	0442	60901	183552	200838	66952	72518		12,33e⁻ L=6.5 80P⁻ L=7-8
~~IND~~	~~0448~~	~~60902~~	~~91510~~	~~105614~~	~~33310~~	~~39374~~		
IND	0448	60902	91518	105615	33318	39375		12,33e⁻ L=6, 6-12 80,150P⁻ L=5-6
~~COO~~	~~0447~~	~~60902~~	~~105631~~	~~125357~~	~~39391~~	~~46437~~		
COO	0447	60902	105631	125357	39391	46437		12,33e⁻ L=6.9 235e⁻ [illegible] L=6, 80,150P⁻ L=6
~~COO~~	~~0452~~	~~60902~~	~~195943~~	~~211101~~	~~71983~~	~~76261~~		
COO	0452	60902	195946	211102	71986	76262		80,150P⁻ L=6-9
~~COO~~	~~0451~~	~~60902~~	~~211118~~	~~225812~~	~~76278~~	~~82692~~		
COO	0451	60902	211122	225813	76282	82693		12,33e⁻ L=7-4 80,150P⁻ L=6-7
COO	0455	60903	45615	62119	17775	22879		12,33e⁻ L=5.8 80P⁻ L=5-6
POG	0454	60903	62139	75444	22899	28484		
COO	0458	60903	135246	150419	49966	54259		12e⁻ L=12 bad dropout
IND	0457	60903	150434	165116	54274	60676		12e⁻ 33 L=8
POG	0462	60903	224917	29	82157	29		~~[illegible]~~ 80,150P⁻ L=4
BOS	0460	60904	112	14748	72	6468		~~[illegible]~~ 80P⁻ L=6.5
~~COO~~	~~0467~~	~~60904~~	~~104441~~	~~120953~~	~~38681~~	~~43793~~		
COO	0467	60904	104445	120954	38685	43794		12e⁻ L=6-8 80,150P⁻ L=8
~~MUL~~	~~0464~~	~~60904~~	~~121016~~	~~134310~~	~~43816~~	~~49390~~		
MUL	0464	60904	121013	134311	43813	49391		12e⁻ L>9
COO	0473	60905	73634	85628	27394	32188		80P⁻ L=6
IND	0472	60905	85644	103505	32204	38105		35e⁻ L>7 ~~[illegible]~~ L=6.5
~~BOS~~	~~0479~~	~~60906~~	~~12944~~	~~23945~~	~~5384~~	~~9585~~		
BOS	0479	60906	12943	23946	5383	9586	4	12e⁻ L=6-9 235e⁻ L=5 80,150P⁻ L=5
~~GUA~~	~~0478~~	~~60906~~	~~24000~~	~~42808~~	~~9600~~	~~16088~~		
GUA	0478	60906	24008	42809	9608	16089		12&33e⁻ L=7-13 80,150P⁻ L=6-8
~~POG~~	~~0490~~	~~60907~~	~~101650~~	~~114148~~	~~37010~~	~~42108~~		
POG	0490	60907	101658	114149	37018	42109		12e⁻ L=7 80P⁻ L=6.5
~~POG~~	~~0488~~	~~60907~~	~~114204~~	~~131530~~	~~42124~~	~~47730~~		
POG	0488	60907	114210	131520	42130	47720		12,33e⁻ L=7-12 80,150P⁻ L=7-5
MUL	0500	60908	190402	202842	68642	73722		12e⁻ L=[illegible]
COO	0499	60908	202919	220211	73759	79331		80P⁻ L=7-8
POG	0507	60909	125632	141451	46592	51291		12,33e⁻ L=6,9 80,150P⁻ L=5-10
COO	0506	60909	141509	155501	51309	57301		12e⁻ L=6-8 80P⁻ L=6
COO	0511	60910	5146	20313	3106	7393		80P⁻ L=7
COO	0510	60910	20330	35015	7410	13815		12,33e⁻ L=7-8
COO	0523	60911	34102	45141	13262	17501		80e⁻ [illegible] L=6-7 (noisy)
COO	0520	60911	45156	63930	17516	23970		12e⁻ L=9
BOS	0529	60912	3238	14901	1958	6541		12e⁻ L=12, 8 80P⁻ L=5.5-8
BOS	0527	60912	14918	33108	6558	12668		12e⁻ L=6-10
~~COO~~	~~0540~~	~~60913~~	~~181603~~	~~194055~~	~~65763~~	~~70855~~		
COO	0540	60913	181557	194056	65757	70856		
~~POG~~	~~0539~~	~~60913~~	~~194112~~	~~211424~~	~~70872~~	~~76464~~		
POG	0539	60913	194117	211425	70877	76465		
COO	0547	60914	61111	71559	22271	26159	2	12,33e⁻ L=5.8 235e⁻ L=6.5 80,150P⁻ L=5.5
~~COO~~	~~0547~~	~~60914~~	~~61111~~	~~71559~~	~~22271~~	~~26159~~		
COO	0546	60914	71615	90939	26175	32979		12e⁻ L>6
~~COO~~	~~0546~~	~~60914~~	~~71615~~	~~90939~~	~~26175~~	~~32979~~		
~~BOS~~	~~0555~~	~~60915~~	~~90084~~	~~101840~~	~~32484~~	~~37120~~		
BOS	0555	60915	90224	101848	32544	37128		12e⁻ L=7-6, 5-6 235e⁻ small spike L=7 80P⁻ L=[illegible]
~~BOS~~	~~0554~~	~~60915~~	~~101905~~	~~115853~~	~~37145~~	~~43133~~		
BOS	0554	60915	101905	115853	37145	43133		33e⁻ L=7-8 80,150P⁻ L=5-6
BOS	0561	60916	85051	100229	31851	36149		12e⁻ L=6
COO	0560	60916	100245	114920	36165	42560		12e⁻ L=7
~~BOS~~	~~0563~~	~~60916~~	~~163040~~	~~182039~~	~~59920~~	~~66039~~		
BOS	0563	60916	163040	182040	59920	66040		235e⁻ [illegible] L=8
~~MUL~~	~~0562~~	~~60916~~	~~182050~~	~~200451~~	~~66050~~	~~72291~~		
MUL	0562	60916	182057	200451	66057	72291		
~~IND~~	~~0568~~	~~60917~~	~~4315~~	~~20525~~	~~2595~~	~~7525~~		
IND	0568	60917	4314	20526	2594	7526		12e⁻ L≈7
~~MUL~~	~~0565~~	~~60917~~	~~20609~~	~~35510~~	~~7569~~	~~14110~~		
MUL	0565	60917	20546	35519	7546	14119		12,33e⁻ L=5.8 80P⁻ L=6
~~COO~~	~~0570~~	~~60917~~	~~130803~~	~~145309~~	~~47283~~	~~53589~~		
COO	0570	60917	130803	145309	47283	53589		235 small spike L=8, [illegible] L=8
~~COO~~	~~0570~~	~~60917~~	~~130805~~	~~145309~~	~~47285~~	~~53589~~		
BOS	0569	60917	145327	164642	53607	60402		
BOS	0569	60917	145326	164642	53606	60402		
~~BOS~~	~~0569~~	~~60917~~	~~145326~~	~~164642~~	~~53606~~	~~60402~~		
~~IND~~	~~0576~~	~~60918~~	~~70640~~	~~84531~~	~~25940~~	~~31531~~		
~~IND~~	~~0576~~	~~60918~~	~~70029~~	~~84535~~	~~25229~~	~~31535~~		
IND	0576	60918	70029	84535	25229	31535		12,33e⁻ L=5-8, 4-7 235e⁻ [illegible] 80P⁻
~~BOS~~	~~0575~~	~~60918~~	~~84550~~	~~103903~~	~~31550~~	~~38343~~		
~~BOS~~	~~0575~~	~~60918~~	~~84557~~	~~103904~~	~~31557~~	~~38344~~		
BOS	0575	60918	84557	103904	31557	38344	2	12,33e⁻ L=6-9 235,435e⁻ L=5 80,150P⁻ L=[illegible]
COO	0579	60918	142925	154047	52165	56447		12e⁻ L=7 235 [illegible] spike L=5 80,150P⁻ L=5-6
IND	0578	60918	154103	172740	56463	62860		12e⁻ L=7 80P⁻ L=5.6
POG	0582	60918	232550	3647	84330	2207		bad compression
BOS	0581	60919	3703	22356	2223	8636		235e⁻ L=6 → [illegible] compression 80,150P⁻ L=6
IND	0586	60919	82147	94003	30107	34803		12e⁻ L=6-7 80P⁻ L=5.5
~~IND~~	~~0586~~	~~60919~~	~~82160~~	~~94003~~	~~30110~~	~~34803~~		

REV NO.		DATE OF REV	TIME OF REV IN HRS		TIME OF REV IN SECS	
IND	0584	60919	94024	112011	34824	40811
~~BOS~~	~~0590~~	~~60919~~	~~231532~~	~~3323~~	~~83732~~	~~[illegible]~~
BOS	0590	60919	231536	3326	83736	2006
~~MUL~~	~~0589~~	~~60920~~	~~3342~~	~~21358~~	~~[illegible]~~	~~[illegible]~~
MUL	0589	60920	3344	21359	2024	8039
IND	0592	60920	73542	81131	27342	29491
~~BOS~~	~~0595~~	~~60920~~	~~140918~~	~~152053~~	~~[illegible]~~	~~[illegible]~~
BOS	0595	60920	140921	152056	50961	55256
~~IND~~	~~0594~~	~~60920~~	~~152110~~	~~170744~~	~~[illegible]~~	~~[illegible]~~
IND	0594	60920	152113	170745	55273	61665
~~COO~~	~~0596~~	~~60920~~	~~211830~~	~~230520~~	~~[illegible]~~	~~[illegible]~~
COO	0596	60920	211833	230520	76713	83120
~~BOS~~	~~0599~~	~~60921~~	~~20420~~	~~31817~~	~~7460~~	~~[illegible]~~
BOS	0599	60921	20426	31818	7466	11898
~~GUA~~	~~0598~~	~~60921~~	~~31835~~	~~50246~~	~~11915~~	~~[illegible]~~
GUA	0598	60921	31834	50246	11914	18166
~~BOS~~	~~0602~~	~~60921~~	~~110037~~	~~121509~~	~~39637~~	~~[illegible]~~
BOS	0602	60921	110042	121509	39642	44109
~~BOS~~	~~0601~~	~~60921~~	~~121526~~	~~135902~~	~~44126~~	~~50342~~
BOS	0601	60921	121530	135902	44130	50342
~~BOS~~	~~0609~~	~~60921~~	~~225530~~	~~1532~~	~~82530~~	~~932~~
BOS	0609	60921	225539	1532	82539	932
~~IND~~	~~0608~~	~~60922~~	~~1555~~	~~15410~~	~~955~~	~~6850~~
IND	0608	60922	1555	15410	955	6850
COO	0612	60922	164811	175944	60491	64784
BOS	0611	60922	180023	194636	64823	71196
BOS	0615	60923	14426	30618	6266	11178
GUA	0614	60923	30634	44252	11194	16972
COO	0619	60923	104041	115220	38441	42740
BOS	0617	60923	115237	133907	42757	49147
BOS	0623	60923	223545	234730	81345	85650
GUA	0622	60923	234746	13409	85666	5649
MUL	0629	60924	192700	203850	70020	74330
COO	0628	60924	203919	222527	74359	80727
COO	0641	60926	11434	22607	4474	8767
BOS	0639	60926	22624	41259	8784	15179
POG	0648	60927	10424	24921	3864	10161
POG	0646	60927	24936	40247	10176	14567
POG	0651	60927	115404	134120	42844	49280
MUL	0649	60927	134137	153240	49297	55960
GUA	0654	60927	215515	231321	78915	83601
COO	0653	60927	231338	5338	83618	3218
GUA	0659	60928	135401	153746	50041	56266
MUL	0658	60928	153801	173234	56281	63154
COO	0665	60929	64106	75156	24066	28316
COO	0664	60929	75213	93915	28333	34755
GUA	0671	60929	170951	185333	61791	68013
COO	0668	60929	185350	204347	68030	74627
COO	0676	60930	152643	164442	55603	60282
BOS	0675	60930	164511	182452	60311	66292
COO	0684	61001	114348	132843	42228	48523
BOS	0683	61001	132859	151544	48539	54944
BOS	0687	61002	1207	13656	727	5816
MUL	0686	61002	13728	31029	5848	11429
BOS	0690	61002	90813	102557	32893	37557
IND	0689	61002	102618	120635	37578	43595
MUL	0693	61002	180416	191539	65056	69339
COO	0692	61002	191556	210239	69356	75759
IND	0697	61003	30023	42232	10823	15752
POG	0695	61003	42249	55843	15769	21523
COO	0700	61003	145508	160636	53708	57996
BOS	0699	61003	160655	175329	58015	64409
BOS	0708	61004	114558	125718	42358	46638
MUL	0706	61004	125735	144421	46655	53061
MUL	0717	61005	83650	95506	31010	35706
IND	0713	61005	95522	113512	35722	41712
COO	0721	61006	52742	64544	19662	24344
BOS	0720	61006	64603	82603	24363	30363
MUL	0730	61007	21829	33335	8309	12815
BOS	0729	61007	33351	51635	12831	18995
GUA	0735	61007	230842	2006	83322	1206
MUL	0734	61008	2023	20659	1223	7619
IND	0745	61008	195905	211027	71945	76227
MUL	0741	61008	211042	225723	76242	82643
MUL	0754	61010	74239	85323	27759	32003
BOS	0753	61010	85339	104057	32019	38457
COO	0764	61011	132858	144656	48538	53216
IND	0763	61011	144713	162715	53233	59235
COO	0772	61012	101921	113724	37161	41844
MUL	0770	61012	113740	131740	41860	47860
BOS	0777	61013	11232	23035	4352	9035
GUA	0775	61013	23051	41048	9051	15048
GUA	0784	61014	10135	22617	3695	8777
POG	0783	61014	22635	35951	8795	14391
COO	0793	61015	5025	20826	3025	7706
COO	0791	61015	20842	34837	7722	13717
BOS	0796	61015	144343	161302	53023	58382
BOS	0795	61015	161319	175952	58399	64792
GUA	0799	61015	214017	225313	78017	82393
COO	0798	61015	225829	3831	82709	2311
IND	0803	61016	93429	111915	34469	40755
MUL	0802	61016	111932	123245	40772	45165
COO	0805	61016	171159	184158	61919	67318
BOS	0804	61016	184214	201545	67334	72945
GUA	0808	61017	2724	13831	1644	5911
MUL	0807	61017	13852	21652	5932	8212
GUA	0812	61017	122129	131502	44489	47702
IND	0811	61017	131532	151943	47732	55183
BOS	0816	61017	211710	222824	76630	80904
GUA	0815	61017	222841	1823	80921	983

REV NO.		DATE OF REV	TIME OF REV IN HRS		TIME OF REV IN SECS	
BOS	0819	61018	85513	102241	32113	37361
IND	0818	61018	102258	120936	37378	43776
BOS	0824	61019	408	12206	248	4926
GUA	0823	61019	12222	30224	4942	10944
POG	0828	61019	84615	101523	31575	36923
IND	0827	61019	101123	115803	36683	43083
BOS	0832	61019	235236	10213	85956	3733
COO	0831	61020	10230	25049	3750	10249
IND	0835	61020	83528	100620	30928	36380
COO	0834	61020	100637	114630	36397	42390
BOS	0840	61020	234102	5220	85262	3140
MUL	0839	61021	5236	23915	3156	9555
BOS	0846	61021	82407	94802	30247	35282
COO	0845	61021	94818	113455	35298	41695
BOS	0851	61022	80458	93617	29098	34577
COO	0850	61022	93632	112310	34592	40990
COO	0861	61023	75437	92405	28477	33845
BOS	0860	61023	92422	111101	33862	40261
BOS	0869	61024	104726	120706	38846	43626
IND	0867	61024	120722	135719	43642	50239
POG	0877	61025	100039	111709	36039	40629
BOS	0875	61025	111726	125039	40646	46239
BOS	0884	61026	101131	115248	36691	42768
BOS	0883	61026	115305	133300	42785	48780
COO	0893	61027	65824	84213	25104	31333
BOS	0891	61027	84230	102222	31350	37342
BOS	0897	61028	11504	22610	4504	8770
MUL	0896	61028	22627	41314	8787	15194
COO	0902	61028	100232	112831	36152	41311
COO	0901	61028	112848	130841	41328	47321
COO	0911	61029	92052	110255	33652	39775
COO	0910	61029	110312	125631	39792	46591
COO	0918	61030	91313	110029	33193	39629
COO	0917	61030	110133	124421	39693	45861
BOS	0924	61031	91443	105839	33283	39519
POG	0923	61031	105854	123157	39534	45117
GUA	0928	61031	175354	192731	64434	70051
MUL	0927	61031	192747	212710	70067	77230
~~BOS~~	~~0932~~	~~61101~~	~~90909~~	~~104853~~	~~32949~~	~~38933~~
BOS	0932	61101	90909	104853	32949	38933
IND	0931	61101	104909	121912	38949	44352
MUL	0936	61101	181622	193233	65782	70353
MUL	0934	61101	193249	211424	70369	76464
BOS	0940	61102	90820	102613	32900	37573
POG	0939	61102	102630	120625	37590	43585
IND	0946	61102	180335	192128	65015	69688
MUL	0943	61102	192144	210138	69704	75698
BOS	0949	61103	115359	131134	42839	47496
BOS	0948	61103	131153	145205	47513	53525
BOS	0957	61103	234738	10525	85658	3925
IND	0955	61104	10542	24542	3942	9942
IND	0962	61104	233451	4135	84891	2495
MUL	0960	61105	4152	23255	2512	9175
MUL	0969	61105	232211	3318	84131	1998
COO	0968	61106	3332	22011	2012	8411
COO	0974	61106	111541	122651	40541	44811
COO	0973	61106	122707	141347	44827	51227
IND	0979	61107	20745	32535	7665	12335
GUA	0978	61107	32551	50548	12351	18348
COO	0984	61107	140116	151235	50476	54755
COO	0982	61107	151251	165917	54771	61157
IND	0988	61108	75114	90907	28274	32947
POG	0987	61108	90923	104914	32963	38954
IND	0996	61109	43932	55720	16772	21440
IND	0994	61109	55936	73733	21576	27453
BOS	1005	61110	102311	114054	37391	42054
IND	1004	61110	114110	132113	42070	48073
IND	1011	61111	11452	23904	4492	9544
MUL	1009	61111	23921	41251	9561	15171
GUA	1018	61111	220309	231417	79389	83657
GUA	1017	61111	231432	10109	83672	3669
BOS	1021	61112	91008	103505	33008	38105
IND	1020	61112	103522	124847	38122	46127
MUL	1025	61112	214948	230052	78588	82852
GUA	1024	61112	230109	4748	82869	2868
COO	1030	61113	124127	140652	45687	50812
BOS	1029	61113	140708	154035	50828	56435
BOS	1034	61114	3447	14538	2087	6338
GUA	1033	61114	14553	33246	6353	12766
COO	1038	61114	122805	135022	44885	49822
BOS	1037	61114	135039	152205	49839	55325
BOS	1045	61115	91621	102729	33381	37649
IND	1044	61115	102751	121418	37671	44058
GUA	1050	61115	210926	222707	76166	80827
GUA	1049	61115	222724	722	80844	442
POG	1059	61116	235350	11133	86030	4293
GUA	1057	61117	11149	25146	4309	10306
COO	1063	61117	114654	131048	42414	47448
POG	1061	61117	131105	144452	47465	53092
COO	1072	61118	53629	70051	20189	25251
MUL	1071	61118	70107	83424	25267	30864
BOS	1078	61119	111912	125020	40752	46220
IND	1076	61119	125035	141707	46235	51427
GUA	1090	61120	170150	181247	61310	65567
MUL	1088	61120	181304	195947	65584	71987
COO	1095	61121	105127	120906	39087	43746
COO	1094	61121	120922	134917	43762	49757
COO	1103	61122	14221	30641	6141	11201
BOS	1101	61122	30657	44014	11217	16014
BOS	1111	61123	102230	114446	37350	42406

REV NO.		DATE OF REV	TIME OF REV IN HRS		TIME OF REV IN SECS	
BOS	1110	61123	114703	132020	42423	48020
BOS	1118	61124	70952	82733	25792	30453
BOS	1117	61124	82804	100746	30484	36466
BOS	1126	61125	35724	52840	14244	19720
POG	1123	61125	52856	65516	19736	24916
IND	1131	61126	4454	15916	2694	7156
GUA	1130	61126	15935	34240	7175	13360
IND	1139	61126	144816	163234	53296	59554
COO	1136	61126	163516	182652	59716	66412
BOS	1144	61127	122331	133422	44611	48862
BOS	1143	61127	133451	152124	48891	55284
BOS	1151	61128	91101	102202	33061	37322
BOS	1150	61128	102218	120856	37338	43736
GUA	1158	61129	206	10617	126	3977
HUL	1154	61129	10634	30000	3994	10800
POG	1162	61129	204911	220006	74951	79206
IND	1160	61129	220023	234701	79223	85621
IND	1172	61130	173609	184614	63369	67574
BOS	1168	61130	184631	203359	67591	74039
COO	1177	61201	142309	154701	51789	56821
BOS	1176	61201	154717	172104	56837	62464
POG	1183	61202	111009	125600	40209	46560
GUA	1182	61202	125617	140757	46577	50877
IND	1188	61202	230246	1348	82966	828
HUL	1186	61203	1404	20034	844	7234
BOS	1191	61203	125558	143305	46558	52385
BOS	1190	61203	143321	161040	52401	58240
IND	1196	61204	14611	30343	6371	11023
GUA	1195	61204	30400	44359	11040	17039
IND	1205	61204	223312	234408	81192	85448
GUA	1202	61204	234425	13104	85465	5464
IND	1212	61205	192020	203710	69620	74230
COO	1209	61205	203735	221809	74255	80289
POG	1219	61206	160722	172457	58042	62697
GUA	1218	61206	172513	190513	62713	68713
IND	1225	61207	175506	185811	64506	68291
BOS	1224	61207	185827	204533	68307	74733
BOS	1231	61208	64320	75403	24200	28443
IND	1229	61208	75420	94105	28460	34865
HUL	1234	61208	183545	194621	66945	71181
IND	1233	61208	194637	213331	71197	77611
BOS	1239	61209	62809	73838	23289	27518
IND	1237	61209	73854	92557	27534	33957
COO	1248	61210	31453	43230	11693	16350
IND	1244	61210	43247	61231	16367	22351
IND	1252	61211	140	12548	100	5148
HUL	1251	61211	12603	25924	5163	10764
GUA	1259	61211	204901	215913	74941	79153
IND	1257	61211	215929	234607	79169	85567
GUA	1267	61212	173504	184558	63304	67558
HUL	1266	61212	184615	203251	67575	73971
HUL	1275	61213	171953	183039	62393	66639
BOS	1273	61213	183056	201735	66656	73055
HUL	1283	61214	140616	151658	50776	55018
COO	1280	61214	151713	170350	55033	61430
COO	1289	61215	105236	120325	39156	43405
BOS	1287	61215	120340	135021	43420	49821
COO	1296	61216	73900	90312	27540	32592
POG	1295	61216	90329	103644	32609	38204
HUL	1306	61217	93857	112214	34737	40934
POG	1303	61217	112231	131730	40951	47880
BOS	1311	61218	65846	82805	25126	30485
HUL	1310	61218	82822	100536	30502	36336
HUL	1314	61218	154825	171250	56905	61970
COO	1313	61218	171306	185945	61986	68385
POG	1317	61219	3612	13620	3372	5780
HUL	1315	61219	13637	31824	5797	11904
HUL	1322	61219	94431	110118	35071	39678
COO	1321	61219	110134	124806	39694	46086
HUL	1331	61220	92358	105142	33838	39102
IND	1330	61220	105159	123231	39119	45151
BOS	1336	61221	82606	103225	30366	37945
POG	1335	61221	103241	120439	37961	43479
HUL	1338	61221	183727	193712	67047	70632
HUL	1338	61221	213634	223707	77794	81427
GUA	1340	61222	3825	13050	2305	5930
GUA	1340	61222	34029	44029	13229	16829
IND	1342	61222	64156	74219	24116	27739
IND	1342	61222	93046	103611	34726	38171
POG	1343	61222	123208	132944	45128	48584
COO	1345	61222	152539	162319	55539	58999
COO	1345	61222	182115	192048	66075	69648
GUA	1349	61222	212107	222058	76867	80458
GUA	1349	61223	2121	12059	1281	4859
IND	1350	61223	92157	101944	33717	37184
IND	1350	61223	121547	130942	44147	47382
IND	1354	61223	150947	160729	54587	58049
IND	1357	61224	514	14958	314	6598
GUA	1356	61224	15015	34344	6615	13424
GUA	1363	61224	172610	185015	62770	67815
COO	1362	61224	185031	202351	67831	73431
IND	1369	61225	141215	150709	51135	54429
BOS	1368	61225	150726	164110	54446	60070
HUL	1371	61225	203615	213443	74175	77683
HUL	1371	61225	233346	3243	84826	1963
GUA	1373	61226	23140	33051	9100	12651
GUA	1373	61226	54211	64931	20531	24571
COO	1374	61226	84141	93634	31301	34594
HUL	1375	61226	113319	123159	41599	45119
IND	1377	61226	142546	152430	51946	55470

REV NO.		DATE OF REV	TIME OF REV IN HRS		TIME OF REV IN SECS	
IND	1377	61226	172219	182103	62539	66063
HUL	1379	61226	202612	211751	73572	76671
HUL	1379	61226	231957	2046	83997	1246
GUA	1380	61227	22236	32313	8556	12193
IND	1382	61227	52604	62506	19564	23106
IND	1382	61227	82255	92034	30175	33634
COO	1387	61227	111654	121444	40614	44084
COO	1387	61227	141106	141936	51066	51576
HUL	1386	61227	141937	150850	51577	54530
HUL	1386	61227	170513	180249	61513	64969
GUA	1396	61228	132430	144154	48270	52914
COO	1395	61228	144211	162210	52931	58930
IND	1398	61229	45621	55421	17781	21261
IND	1398	61229	75055	84042	28255	31722
GUA	1400	61229	104518	114316	38718	42196
GUA	1400	61229	133952	143738	49192	52658
IND	1402	61229	163435	173351	59675	63231
IND	1402	61229	193258	203210	70378	73930
GUA	1404	61229	223936	233234	81576	84754
GUA	1404	61230	13526	23618	5726	9378
IND	1406	61230	43908	54013	16748	20413
IND	1406	61230	73835	83437	27515	30877
HUL	1407	61230	103051	112837	37851	41317
GUA	1408	61230	132451	142239	48291	51759
IND	1410	61230	162050	171954	58850	62394
IND	1410	61230	191839	201720	69519	73049
COO	1411	61230	221615	231512	80175	83712
GUA	1413	61231	14845	34211	6525	13331
GUA	1420	61231	83328	101952	30808	37192
COO	1419	61231	102008	121205	37208	43925
COO	1427	70101	92217	103934	33737	38374
IND	1423	70101	103951	121956	38391	44396
COO	1435	70102	60810	74529	22090	27929
COO	1430	70102	74546	90548	27946	32748
GUA	1440	70103	25359	41123	10439	15083
IND	1439	70103	41139	55139	15099	21099
GUA	1440	70103	233952	4858	85192	2938
IND	1447	70104	4915	22549	2955	8749
COO	1450	70104	150220	160102	54140	57662
IND	1455	70105	85959	101051	32399	36651
COO	1459	70105	145032	155432	53432	57272
BOS	1458	70105	155448	174138	57288	63698
GUA	1468	70106	140229	150723	50549	54443
IND	1467	70106	150747	165425	54467	60865
GUA	1477	70107	161300	172642	58380	62802
IND	1475	70107	172700	190702	62820	68822
GUA	1485	70108	185503	200754	68103	72474
HUL	1484	70108	200811	215954	72491	79194
BOS	1494	70109	213224	225301	77544	82381
GUA	1493	70109	225317	4013	82397	2413
IND	1507	70110	121443	134209	44083	49329
GUA	1505	70110	134225	150905	49345	54545
GUA	1501	70110	152557	164918	55557	60558
COO	1499	70110	164934	182254	60574	66174
COO	1511	70112	724	12933	444	5373
BOS	1510	70112	12950	30953	5390	11393
HUL	1516	70112	100328	111443	36208	40483
COO	1515	70112	111500	130112	40500	46872
BOS	1522	70113	933	12008	573	4808
BOS	1518	70113	12024	30708	4824	11228
GUA	1525	70113	175710	190741	64630	68861
COO	1524	70113	190758	205438	68878	75278
BOS	1530	70114	54107	65732	20467	25052
HUL	1528	70114	65748	83723	25068	31043
IND	1535	70115	23426	34247	9266	13367
COO	1535	70115	34304	53158	13384	19918
IND	1547	70116	21738	32815	8258	12495
BOS	1542	70116	32042	51507	12522	18907
BOS	1551	70116	230247	1317	82967	797
BOS	1550	70117	1334	20022	814	7222
HUL	1557	70117	165007	180008	60607	64808
COO	1556	70117	180025	194741	64825	71261
HUL	1560	70118	44205	55054	16925	21534
COO	1559	70118	55917	73917	21557	27557
COO	1568	70118	193117	204152	70277	74512
HUL	1565	70118	204208	222852	74528	80932
BOS	1571	70119	100905	131845	36545	47925
GUA	1570	70119	115605	142937	42965	52177
BOS	1574	70119	160502	191435	57902	69275
HUL	1573	70119	175154	202535	64314	73535
HUL	1580	70120	70640	81650	25600	29810
HUL	1577	70120	81712	100351	29832	36231
GUA	1585	70121	94709	110503	35229	39903
GUA	1585	70121	105810	124443	39490	45883
HUL	1589	70121	154258	165331	56578	60811
COO	1588	70121	165346	184026	60826	67226
COO	1596	70122	63219	75522	23539	28522
HUL	1593	70122	75539	92945	28539	34185
HUL	1601	70123	31725	42709	11845	16029
COO	1600	70123	42725	61449	16045	22489
HUL	1605	70123	151013	163231	54613	59551
COO	1604	70123	163253	180617	59573	65177
HUL	1613	70124	30014	41041	10814	15041
COO	1608	70124	41102	55605	15062	21365
HUL	1617	70124	234519	10212	85519	3732
COO	1616	70125	10247	24250	3767	9770
COO	1620	70125	143440	154511	52480	56711
GUA	1619	70125	154528	173209	56728	63129
COO	1624	70125	232017	4523	84497	2723
BOS	1623	70126	4545	22543	2745	8743

REV NO.		DATE OF REV	TIME OF REV IN HRS		TIME OF REV IN SECS	
MUL	1630	70126	171546	182552	62146	66352
IND	1628	70126	182618	201256	66378	72776
BOS	1632	70127	20914	32615	7754	12375
BOS	1631	70127	33506	50632	12906	18392
MUL	1638	70127	140027	151055	50427	54655
IND	1636	70127	151111	165759	54671	61079
MUL	1644	70128	104532	120914	38732	43754
COO	1645	70128	120932	134303	43772	49383
COO	1648	70129	24045	34433	9645	13473
COO	1648	70129	53909	63006	20349	23406
MUL	1650	70129	83006	93703	30606	34623
MUL	1650	70129	113550	122637	41750	44797
IND	1652	70129	141334	151302	51214	54782
IND	1652	70129	171302	181206	61982	65526
MUL	1654	70129	201230	211318	72750	76398
MUL	1654	70129	230550	1622	83150	982
COO	1656	70130	21855	31935	8335	11975
COO	1656	70130	51911	61642	19151	22602
MUL	1658	70130	81319	91103	29599	33063
MUL	1658	70130	110727	120449	40047	43489
BOS	1659	70130	140047	145822	50447	53902
COO	1661	70130	165600	175514	60960	64514
COO	1661	70130	195424	205330	71664	75210
MUL	1662	70130	225616	235819	82576	86299
COO	1664	70131	20712	31157	7632	11517
COO	1664	70131	51040	60537	18640	21937
IND	1665	70131	75834	85401	28714	32161
IND	1665	70131	105133	114850	39893	42530
IND	1668	70131	134241	144130	49361	52890
IND	1668	70131	164017	173853	60017	63533
MUL	1670	70131	193737	203626	70657	74186
MUL	1670	70131	223857	234120	81537	85280
IND	1672	70201	45058	55218	17458	21138
IND	1672	70201	74522	83658	27922	31018
MUL	1674	70201	103146	113022	37906	41422
IND	1676	70201	132730	142417	48450	51857
IND	1676	70201	162122	172018	58882	62418
MUL	1678	70201	191946	201911	69586	73151
MUL	1678	70201	222139	232316	80499	84196
IND	1681	70202	82838	92349	30518	33829
IND	1681	70202	101735	110901	37055	40141
IND	1684	70202	130349	140235	47029	50555
IND	1684	70202	160048	165923	57648	61163
MUL	1686	70202	185735	195619	68255	71779
BOS	1688	70203	10244	20533	3764	7533
MUL	1690	70203	74109	82730	27669	30450
IND	1692	70203	124801	134145	46081	49305
IND	1692	70203	162352	181138	59832	65498
MUL	1694	70203	185551	193931	68151	70771
MUL	1694	70203	214310	223740	78190	81460
BOS	1695	70204	4526	14745	2726	6465
COO	1697	70204	35328	45600	14008	17760
COO	1697	70204	65322	74820	24802	28100
GUA	1699	70204	94054	113612	34854	41772
GUA	1708	70205	121552	131406	44152	47646
GUA	1715	70206	34144	53942	13304	20382
IND	1721	70206	231634	12433	83794	5073
IND	1725	70207	141458	161312	51298	58392
MUL	1734	70208	162700	174404	59220	63844
IND	1733	70208	174419	192427	63859	69867
~~IND~~	~~1733~~	~~70208~~	~~174420~~	~~192427~~	~~63860~~	~~69867~~
IND	1741	70209	71557	82608	26157	30368
GUA	1739	70209	82623	101316	30383	36796
~~GUA~~	~~1739~~	~~70209~~	~~82637~~	~~101317~~	~~30397~~	~~36797~~
GUA	1747	70210	65006	80825	25086	29305
MUL	1746	70210	80842	95526	29322	35726
GUA	1748	70210	144227	162919	52947	59359
IND	1753	70210	213241	231712	77561	83832
POG	1752	70210	231729	4413	83849	2653
GUA	1755	70211	62507	80218	23107	28938
MUL	1754	70211	80234	93731	28954	34651
MUL	1762	70211	133858	151700	49138	55020
BOS	1760	70211	151717	171731	55037	62251
MUL	1767	70212	102043	120234	37243	43354
IND	1765	70212	120300	135913	43380	50353
BOS	1769	70212	235959	12539	86399	5139
BOS	1768	70213	12555	30602	5155	11162
GUA	1771	70213	63201	80812	23521	29292
POG	1770	70213	80829	90131	29309	32491
IND	1773	70213	145719	164319	53839	60199
IND	1773	70213	164219	175445	60139	64485
POG	1776	70213	203829	215441	74309	78881
MUL	1775	70213	215450	232852	78890	84532
COO	1778	70214	30415	41705	11055	15425
BOS	1777	70214	41936	60019	15576	21619
GUA	1780	70214	91116	103349	33076	38029
MUL	1779	70214	103412	120043	38052	43243
COO	1785	70214	173646	185329	63406	68009
BOS	1784	70214	185345	203408	68025	74048
IND	1790	70215	60103	71825	21663	26305
GUA	1788	70215	71840	85057	26320	32337
IND	1790	70216	113432	133230	41672	48750
MUL	1803	70217	81809	101619	29889	36979
BOS	1808	70217	210809	230619	76089	83179
COO	1811	70218	80650	100452	29210	36292
GUA	1812	70218	110426	130237	39866	46957
GUA	1813	70218	140207	160022	50527	57622
BOS	1817	70219	15313	35128	6793	13888
GUA	1819	70219	74043	94659	28123	35219
IND	1821	70219	134428	154228	49468	56548

REV	NO.	DATE OF REV	TIME OF REV IN HRS		TIME OF REV IN SECS	
IND	1829	70220	132624	152438	48384	55478
HUL	1836	70221	91130	110944	33090	40184
IND	1839	70221	170532	190346	61532	68626
GUA	1844	70222	91845	111655	33525	40615
BOS	1849	70222	201008	220819	72608	79699
POG	1865	70224	113059	133702	41939	49022
IND	1866	70225	42556	62344	15956	23024
IND	1870	70225	111740	131815	40660	47895
POG	1880	70226	105359	120413	39239	43453
GUA	1886	70227	104423	124227	38663	45747
COO	1871	70227	183801	203611	67081	74171
GUA	1893	70228	102520	122340	37520	44620
GUA	1901	70301	100649	120454	36409	43494
BOS	1907	70301	235554	15356	86154	6836
GUA	1909	70302	94803	114607	35283	42367
GUA	1917	70303	92916	112720	34156	41240
BOS	1922	70303	231813	11440	83893	4480
HUL	1933	70305	85143	104947	31903	38987
POG	1937	70305	194304	214111	70984	78071
HUL	1941	70306	83254	103100	30776	37860
IND	1944	70306	184417	204228	67457	74548
BOS	1947	70307	33721	53525	13041	20125
HUL	1948	70307	63458	83305	23698	30785
IND	1952	70307	182538	202341	66338	73421
HUL	1956	70308	31835	51639	11915	18999
HUL	1964	70309	51244	71045	18764	25845
HUL	1965	70309	82612	100822	30372	36502
GUA	1967	70309	113013	130556	41413	47156
POG	1968	70309	170301	181425	61381	65665
COO	1968	70309	181445	190104	65685	68464
POG	1970	70309	200053	215838	72053	79118
BOS	1972	70310	15606	35348	6966	14028
HUL	1973	70310	75054	94857	28254	35337
IND	1975	70310	140326	154408	50606	56648
IND	1977	70310	200103	213918	72063	77958
COO	1980	70311	13623	33425	5783	12865
BOS	1986	70311	211848	235437	76728	86077
BOS	1987	70312	11712	31506	4632	11706
POG	1988	70312	41440	61235	15280	22355
HUL	1990	70312	100929	120731	36569	43651
IND	1992	70312	160425	180226	57865	64946
BOS	1994	70312	220009	235817	79209	86297
HUL	1996	70313	35522	55326	14122	21206
POG	1998	70313	95034	114835	35434	42518
POG	2000	70313	154539	174346	56739	63826
BOS	2002	70313	214059	233855	78059	85135
IND	2006	70314	122844	142647	44924	52007
HUL	2014	70315	54749	74547	20869	27947
POG	2020	70316	22950	42747	8990	16067
HUL	2029	70316	211335	231129	76415	83489
512007	IND	1854	702251	115752		
512006	IND	926	703062			
IND	2031	70317	110128	125920	39688	46760
IND	2032	70317	151840	162448	55120	59088
IND	2033	70317	182321	202126	66281	73286
BOS	2035	70317	204329	221949	74609	80389
COO	2036	70318	21641	41448	8201	15288
COO	2038	70318	81145	100947	29505	36587
GUA	2040	70318	140643	160447	50803	57887
POG	2041	70318	170412	190218	61452	68538
BOS	2043	70318	200145	215949	72105	79189
COO	2044	70319	15651	35449	7011	14089
POG	2045	70319	45419	65221	17659	24741
POG	2047	70319	104915	124719	38955	46039
IND	2048	70319	134651	154449	49611	56689
BOS	2051	70319	194148	213950	70908	77990
COO	2052	70320	13652	33449	5812	12889
IND	2058	70320	185005	204802	67805	74882
HUL	2063	70321	92623	112424	33983	41064
BOS	2067	70321	193127	212925	70287	77365
POG	2071	70322	90504	110255	32704	39775
GUA	2072	70322	120744	132058	43664	48058
IND	2073	70322	155824	175510	57504	64510
BOS	2075	70322	185408	205100	68048	75060
COO	2076	70323	4545	24243	2745	9763
BOS	2077	70323	34553	54346	13553	20626
POG	2079	70323	64313	84104	24193	31264
IND	2080	70323	123745	143543	45465	52543
IND	2082	70323	153506	173301	56106	63181
BOS	2083	70323	212946	232739	77386	84459
COO	2084	70324	2706	22457	1626	8697
HUL	2085	70324	32426	52218	12266	19338
COO	2086	70324	62139	81936	22899	29976
POG	2087	70324	91859	111510	33539	40510
BOS	2099	70325	80156	95953	28916	35993
HUL	2103	70326	74044	93425	27644	34465
POG	2104	70326	112550	132351	41150	48231
IND	2105	70326	142318	162114	51798	58874
IND	2106	70326	173143	191839	63103	69519
BOS	2107	70326	201759	221600	73079	80160
BOS	2108	70326	231527	11140	83727	4300
HUL	2109	70327	21255	41047	7975	15047
POG	2112	70327	51544	60989	18944	22149
POG	2112	70327	80744	83959	29264	31199
COO	2111	70327	84552	102007	31552	37207
IND	2113	70327	140224	160022	50544	57622
POG	2115	70327	165944	185745	61184	68268
BOS	2116	70327	225433	5105	82473	3068
COO	2117	70328	15201	34954	6721	13794
POG	2119	70328	65801	85622	25081	32182
POG	2123	70328	194634	214424	71194	78264
COO	2126	70329	35955	53704	14395	20224

REV NO.		DATE OF REV	TIME OF REV IN HRS		TIME OF REV IN SECS	
GUA	2129	70329	92523	103324	33923	38004
HUL	2128	70329	103355	122129	38035	44489
IND	2131	70329	161812	181611	58692	65771
GUA	2137	70330	120949	140730	43789	50850
~~[illegible]~~	~~[illegible]~~	~~[illegible]~~	~~[illegible]~~	~~[illegible]~~	~~[illegible]~~	~~[illegible]~~
BOS	2140	70330	220030	235825	79230	86305
HUL	2144	70331	85031	104810	31831	38890
HUL	2152	70401	82841	102614	30521	37574
BOS	2156	70401	181217	201003	65537	72603
IND	2162	70402	115611	135359	42971	50039
COO	2165	70402	204756	224553	74876	81953
IND	2170	70403	143157	162947	52317	59387
FOG	2175	70404	41919	54148	15559	20508
FOG	2175	70404	54220	71026	20540	25826
FOG	2176	70404	81550	101341	29750	36821
FOG	2177	70404	111310	130514	40390	47114
IND	2178	70404	141022	160819	51022	58099
BOS	2180	70404	200503	215915	72303	79155
BOS	2181	70404	230223	10017	82943	3617
COO	2182	70405	20727	35734	7647	14254
IND	2185	70405	65512	80516	24912	29116
COO	2184	70405	80544	95213	29144	35533
IND	2186	70405	141048	154653	51048	56813
BOS	2188	70405	194337	214128	71017	78088
BOS	2189	70405	224057	3047	81657	2327
FOG	2190	70406	13809	33605	5889	12965
GUA	2194	70406	95114	112856	34274	41336
~~[illegible]~~	~~[illegible]~~	~~70406~~	~~[illegible]~~	~~[illegible]~~	~~[illegible]~~	~~[illegible]~~
BOS	2197	70406	221931	1720	80371	1040
FOG	2199	70407	13059	31439	5459	11679
COO	2200	70407	71118	90913	25878	32953
HUL	2201	70407	100852	120634	36532	43594
IND	2202	70407	130612	150353	47172	54233
IND	2204	70407	190052	205831	68452	75511
BOS	2205	70407	215756	235546	79076	86146
COO	2206	70408	5605	25257	3365	10377
FOG	2207	70408	41525	55011	15325	21011
FOG	2209	70408	94645	114435	35205	42275
IND	2211	70408	154110	173858	56470	63538
BOS	2213	70408	213534	233321	77734	84801
GUA	2216	70409	62714	82458	23234	30298
BOS	2218	70409	94039	112212	34839	40932
IND	2219	70409	151848	171635	55128	62195
COO	2222	70409	211312	231101	76392	83461
BOS	2224	70410	31546	50523	11746	18323
FOG	2226	70410	90201	105940	32521	39580
IND	2228	70410	142625	165412	51985	60892
BOS	2230	70410	212818	224840	76818	82120
COO	2232	70411	24514	44301	9914	16981
BOS	2237	70411	173015	192902	63015	70142
BOS	2261	70414	192120	211906	69680	76746
BOS	2267	70415	100721	120507	36441	43507
BOS	2270	70415	215610	235355	78970	86035
IND	2275	70416	94459	114244	35099	42164
BOS	2282	70417	62525	82310	23125	30190
IND	2285	70417	181405	201158	65645	72718
IND	2292	70418	111255	131044	40375	47444
COO	2297	70419	53744	73819	20264	27499
FOG	2298	70419	80024	93059	28824	34259
BOS	2299	70419	103016	122750	37816	44870
IND	2300	70419	132720	152500	48440	55500
IND	2301	70419	171032	182201	61832	66121
BOS	2302	70419	203440	221903	74080	76743
BOS	2303	70419	223008	1603	81008	963
BOS	2304	70420	12826	31305	5306	11585
HUL	2305	70420	42602	61006	15962	22206
FOG	2306	70420	75634	90708	28594	32828
IND	2307	70420	102002	120407	37202	43447
IND	2309	70420	160027	175800	57627	64680
BOS	2311	70420	215435	235209	78875	85929
HUL	2312	70421	10219	24913	3739	10153
BOS	2318	70421	163957	183738	59997	67058
BOS	2323	70422	13109	32853	5469	12533
BOS	2326	70422	161638	181422	58598	65662
COO	2333	70423	125616	145359	46576	53639
GUA	2338	70424	63049	83631	23929	30991
BOS	2343	70424	153002	172748	55802	62868
BOS	2347	70425	83715	100415	31035	36255
FOG	2348	70425	110331	130111	39811	46871
IND	2349	70425	140028	155812	50428	57492
BOS	2351	70425	175300	185511	64380	68111
COO	2352	70425	225548	4906	82548	2946
HUL	2353	70426	21636	34607	8196	13567
FOG	2354	70426	52229	64306	19349	24186
FOG	2355	70426	74209	94803	27729	34803
GUA	2356	70426	103919	123701	38359	45421
IND	2357	70426	142951	153403	52191	56043
IND	2358	70426	165919	183100	61159	66660
COO	2360	70426	222713	2456	80033	1496
BOS	2362	70427	14102	32150	6062	12110
BOS	2372	70428	62704	82441	23224	30281
BOS	2375	70428	151737	171516	55057	62116
COO	2381	70429	115547	135322	42947	50002
IND	2382	70429	150715	165017	54435	60617
BOS	2384	70429	204627	224404	74787	81844
FOG	2386	70430	24012	43733	9612	16673
FOG	2395	70501	51222	70959	18742	25799
COO	2398	70501	140302	160041	50582	57641
FOG	2402	70502	15039	34818	6639	13698
FOG	2403	70502	51143	64814	18703	24314

REV NO.		DATE OF REV	TIME OF REV IN HRS		TIME OF REV IN SECS		
GUA	2404	70502	80432	94208	29072	34928	12,33 L>4 235,435 L=4.5 80,150 L>4
BOS	2405	70502	112736	123634	41256	45394	
COO	2406	70502	134704	153556	49624	56156	12,33 L>4, 235 435 L=6 80,150,350 L>4
HUL	2407	70502	164816	183250	60496	66770	12,33 L>4, L=6-7 80,150,350 L=5-7
GUA	2408	70502	213009	222149	77409	80509	12,33 L=4-5, 235 L=6
HUL	2410	70503	12553	32331	5153	12211	12,33 L>4.6 80,150,350 L>4
FOG	2411	70503	51209	61439	18729	22479	12,33 L>4, 235 L=5-6 80,150 L>4
FOG	2412	70503	75033	91722	28233	33442	80,150 L>4
FOG	2413	70503	103634	121415	38194	44055	12,33 L>5 80,150,350 L=3.5 L>5
BOS	2414	70503	133658	151109	49018	54669	12 L>5 80,150 L>6
HUL	2415	70503	162730	180803	59250	65283	80,150 L>5
~~BOS~~	~~2416~~	~~70503~~	~~194110~~	~~210456~~	~~70070~~	~~75070~~	
BOS	2416	70503	194122	210456	70882	75896	80,150 L=6-8
COO	2427	70505	3604	23342	2164	9222	12,33 L>6 80,150 L>5
FOG	2429	70505	92637	112410	33997	41050	12,33 L=6-8 435 (Light) L=6-8 80,150 L=6-7
COO	2434	70506	1046	20818	646	7698	235,435 L=6 80,150 L=5-6
HUL	2443	70507	24214	43944	9734	16704	
COO	2450	70507	202313	222044	73393	80444	33 L76.5 235 (light) L=12
COO	2456	70508	195731	215505	71851	78905	80 L=6
FOG	2462	70509	104127	123901	38487	45541	12,33 L>5 235 light L=6 80,150 L>5
GUA	2465	70509	163501	183237	59701	66757	12,33 L=5-7.5, 235 light L=12 80 L>6
COO	2474	70509	224048	31	81648	31	
BOS	2471	70510	130902	151008	47342	54608	12,33 L=6-8 80,150 L=5-6
HUL	2472	70510	163004	180637	59404	65217	80,150 L>5
BOS	2473	70510	191214	210344	69134	75824	235 L=6 80 L=6
FOG	2476	70511	35631	55405	14191	21245	80 L=5-6
COO	2477	70511	72207	85055	26527	31855	235,435,655, 850 (Light) L=6.5 80,150,350 L>4.5
BOS	2479	70511	124312	144428	45792	53068	12,33 L=5-6 235 light L=5-6 80,150 L=4-6
HUL	2480	70511	160536	174116	57936	63676	12,33 L>4 235 L=4.5 80,150,350 L>4
BOS	2481	70511	184824	203802	67704	74282	33 L=4-6 L>5 235 L=7 light 80,150 L>5
BOS	2482	70511	225321	3347	82401	2027	80 L=5-6
HUL	2483	70512	10905	23130	4145	9098	12,33 L=6 235 L=6 80 L>5
BOS	2484	70512	42009	52826	15609	19706	235 L=5, 235-1.6 L=4.85 80,150,350 L>4
BOS	2485	70512	65001	82513	24601	30313	235,435 L=4.5-5 80,150,350 L>4
COO	2487	70512	121802	141046	44282	51526	12,33 L=6-10 235 L=5 80,150 L=4.5-5
HUL	2488	70512	150358	171535	54238	62135	235 L=6 80 L=5-6
GUA	2489	70512	182130	201221	66090	72741	80 L=5-6
BOS	2491	70513	627	20556	507	7556	80 (Light) L=5-6
COO	2493	70513	60155	75932	21715	28772	33 L=6-8,
HUL	2005	70513	63331	83137	23611	30697	
COO	2495	70513	115219	135306	42739	49986	
IND	2503	70514	142637	162411	51997	59051	12 L=6-7, 80 (Light) L=4-6
COO	2506	70514	172326	192059	62606	69659	
COO	2515	70515	165735	184129	61055	67289	
GUA	2514	70515	184151	185512	67311	68112	
GUA	2514	70515	195007	213051	71407	77451	12,33 L=5-8, 235,435 L=6 80 L=5-6
HUL	2523	70516	222441	532	80641	332	33 L>5 235,435,655 L=5.5 80,150 L=5-7
HUL	2526	70517	71458	91224	26098	33144	33 L77 235 light L=13 80,150 L=5-12
IND	2528	70517	130818	150550	47298	54350	12,33 L>5 235 (435 L=6 80,150 L=5-6
GUA	2530	70517	190142	205915	68502	75555	
BOS	2531	70517	220443	235559	79483	86159	12,33 L=6-8 80,150 L=6-7
BOS	2533	70518	35156	54926	13916	20966	12,33 L=8 235,435 light L=7,8 80,150 L=5-6
COO	2535	70518	94516	114249	35116	42169	12,33 L76 80,150 L=6
BOS	2537	70518	153043	173615	56323	63375	
COO	2539	70518	213213	232941	77533	84581	235 L=7.7 80 L=6-7
COO	2549	70519	151336	170953	54816	61793	
BOS	2546	70519	180918	194958	65358	71398	12,33 L=6-8 235 L=8 80 L=6-7
COO	2556	70520	174251	194012	63771	70812	
GUA	2555	70520	203936	222022	74376	80422	33 L77 (235 L=8) 235 L=6.5 80,150 L>
HUL	2564	70521	171633	191353	62193	69233	
BOS	2612	70521	193213	193232	70333	70352	
BOS	2563	70521	201346	215406	72826	78846	
BOS	2612	70521	203138	221226	73898	79946	
BOS	2573	70522	165018	184740	60618	67660	
BOS	2571	70522	194700	212749	71220	77269	80 L=6-7
HUL	2580	70523	162401	182120	59041	66080	80 L=5.5-6.5
COO	2579	70523	192053	210130	69653	75690	
COO	2589	70524	155742	175520	57462	64520	
BOS	2587	70524	185503	203515	68103	74115	12,33 L=6-12 235 L=7 80 L=6-7
COO	2596	70525	182809	200855	66489	72535	80 L=7-8
HUL	2609	70526	150451	170227	54291	61347	
HUL	2605	70526	180125	180125	64885	64885	
FOG	2604	70526	180154	194221	64914	70941	80 L=6-7
COO	2621	70528	170822	190211	61702	68531	
COO	2620	70528	190228	190556	68548	68756	
COO	2620	70528	200502	214552	72302	78352	12 L=6-7 80 L=5-6
FOG	2631	70529	164215	183256	60135	66776	
COO	2628	70529	183319	183921	66799	67161	
COO	2628	70529	193032	211915	70712	76755	80 (light) L=5-6
GUA	2637	70530	161510	181246	58520	65566	
GUA	2637	70530	191150	191154	69110	69114	
FOG	2636	70530	191217	205240	69137	75160	
HUL	2646	70531	154835	174611	56915	63971	
BOS	2645	70531	184535	202604	67535	73564	
GUA	2652	70601	181852	195928	65932	71968	
FOG	2664	70602	145523	165245	53723	60765	
FOG	2661	70602	175216	193257	64336	70377	
COO	2671	70603	172547	192306	62747	69786	
COO	2680	70605	44546	64314	17146	24194	12,33 L77 80,150 L=6-7
FOG	2683	70605	133547	153311	48947	55991	12,33 L=5-7 235 (light) 80,150 L=6
COO	2688	70606	41852	61622	15532	22582	80 L=6-7
GUA	2706	70608	5015	23440	3015	9280	
COO	2716	70609	2314	20814	1394	7694	
GUA	2714	70609	32009	50043	12009	18043	
FOG	2723	70609	235623	14110	86183	6070	
BOS	2722	70610	14130	15357	6090	6837	
BOS	2722	70610	25314	45351	10394	18431	235,435,655 L=5-6 80 L=5-6
FOG	2731	70611	22606	42325	8766	15805	
GUA	2729	70611	52252	70334	19372	25414	12,33 L76, 80 L=5-6
HUL	2736	70612	15910	35641	7150	14203	

92039 HUL 2697 70528 153605 1

REV NO.		DATE OF REV	TIME OF REV IN HRS		TIME OF REV IN SECS	
COO	2746	70613	13221	32939	5541	12579
POG	2745	70613	42911	60948	16151	22188
HUL	2756	70614	40217	55932	14537	21572
POG	2754	70614	65905	83944	25145	31184
GUA	2761	70615	3906	23633	2346	9393
BOS	2766	70615	152227	171957	55347	62397
COO	2770	70616	1229	20937	749	7777
HUL	2769	70616	30916	44955	11356	17395
COO	2778	70616	234551	14306	85551	6186
POG	2777	70617	24238	42319	9758	15799
COO	2784	70617	202247	222208	73367	80528
GUA	2795	70619	44601	64333	17161	24213
COO	2802	70620	41931	61657	15571	22617
POG	2812	70621	91525	111239	33325	40359
BOS	2815	70621	190349	210112	68629	75672
COO	2821	70622	114423	134144	42263	49304
GUA	2823	70622	173727	193451	63447	70491
BOS	2824	70622	204738	223127	74858	81087
POG	2825	70623	2930	22650	1770	8810
POG	2827	70623	52344	72107	19424	26467
HUL	2829	70623	111648	131415	40608	47655
HUL	2830	70623	143537	161054	52537	58254
GUA	2832	70623	200641	220404	72401	79444
COO	2833	70623	231545	10042	83745	3642
COO	2835	70624	45626	65354	17786	24834
IND	2837	70624	104938	124706	38978	46026
HUL	2839	70624	164250	184018	60170	67218
COO	2841	70624	194947	213655	71387	77815
HUL	2843	70625	42915	62641	16155	23201
COO	2845	70625	102228	121954	37348	44394
HUL	2846	70625	132916	151632	48556	54992
HUL	2847	70625	162052	181306	58852	65586
POG	2848	70625	191932	210942	69572	76182
HUL	2849	70626	10533	25222	3933	10342
HUL	2850	70626	40205	54822	14525	20902
COO	2852	70626	65837	85606	25117	32166
BOS	2853	70626	101501	115244	36901	42764
COO	2854	70626	130222	144921	46942	53361
HUL	2857	70627	3822	21536	2302	8136
HUL	2859	70627	33503	53219	12903	19939
IND	2861	70627	92807	112531	34087	41131
IND	2865	70627	152119	171844	55279	62324
IND	2869	70628	90057	105820	32457	39500
COO	2878	70629	83346	103110	30826	37870
GUA	2880	70629	182227	201949	66147	73189
COO	2887	70630	110028	130032	39628	46832
BOS	2894	70701	111902	124344	40742	45824
COO	2895	70701	134254	154015	49374	56415
HUL	2896	70701	164054	183649	60054	67009
GUA	2897	70701	193558	213323	70558	77603
BOS	2900	70702	42551	62305	15951	22985
COO	2901	70702	74039	91940	27639	33580
BOS	2902	70702	102327	121612	37407	44172
COO	2903	70702	131527	151246	47727	54766
HUL	2904	70702	161216	180920	58336	65360
GUA	2905	70702	190832	210554	68912	75954
IND	2906	70702	220512	228	79512	148
IND	2898	70702	223230	2956	81150	1796
COO	2907	70703	10144	25901	3704	10741
GUA	2909	70703	65449	84041	24889	31241
BOS	2913	70703	192826	212546	70106	77146
COO	2919	70704	91226	110943	33146	40183
COO	2925	70705	64708	84432	24428	31472
COO	2928	70705	143756	163523	52676	59723
COO	2936	70706	81726	101445	29846	36885
GUA	2941	70707	45319	65042	17599	24642
COO	2944	70707	144152	163915	52912	59955
GUA	2949	70708	44121	62306	16881	22986
BOS	2951	70708	103057	122820	37857	44900
IND	2951	70708	132545	150425	48345	54265
GUA	2954	70708	194338	211757	71018	76677
POG	2956	70709	11338	31058	4418	11458
COO	2957	70709	50050	60731	18050	22051
POG	2958	70709	72946	90404	26986	32644
COO	2959	70709	100827	120033	36507	43233
HUL	2961	70709	155619	175336	57379	64416
POG	2962	70709	185243	205007	67963	75007
HUL	2963	70710	4548	22107	2748	8467
HUL	2964	70710	34220	51733	13340	19053
POG	2966	70710	63852	83615	23932	30975
POG	2967	70710	95044	113250	35444	41570
COO	2968	70710	123925	142923	45565	52163
HUL	2969	70710	153005	172557	55805	62757
GUA	2970	70710	183029	202230	66629	73350
BOS	2972	70711	1813	21538	1093	8138
BOS	2973	70711	40142	51214	14502	18734
BOS	2974	70711	61358	80846	22438	29326
POG	2975	70711	91526	110522	33326	39922
COO	2976	70711	121510	140155	44110	50515
BOS	2977	70711	150422	165828	54262	61108
GUA	2978	70711	184519	195503	67519	71703
COO	2979	70711	203615	222955	74175	80995
HUL	2981	70712	24719	44116	10039	16876
HUL	2985	70712	142048	161809	51648	58689
POG	2991	70713	85033	101041	32313	36641
BOS	2993	70713	140626	160343	50786	57823
BOS	2995	70713	195922	215645	71962	79005
IND	2996	70713	233946	5319	85186	3199
BOS	2998	70714	44907	64620	17347	24380
POG	2999	70714	83655	94254	30955	34474

REV NO.		DATE OF REV	TIME OF REV IN HRS		TIME OF REV IN SECS	
COO	3000	70714	111059	123925	40259	45565
HUL	3002	70714	164540	183233	60340	66753
GUA	3003	70714	193140	212906	70300	77346
IND	3004	70714	222812	2538	80892	1538
POG	3005	70715	12445	32212	5085	12132
BOS	3007	70715	71757	91521	26277	33321
POG	3008	70715	101645	121154	37005	43914
HUL	3009	70715	133045	150830	48645	54510
HUL	3010	70715	160741	180505	58061	65105
IND	3012	70715	220054	235810	79254	86290
BOS	3014	70716	35350	55117	14030	21077
BOS	3015	70716	65110	84750	24670	31670
BOS	3016	70716	102103	114427	37263	42267
HUL	3017	70716	124335	144059	45815	52859
GUA	3018	70716	154607	173732	56767	63452
IND	3020	70716	213319	233040	77599	84640
POG	3021	70717	2952	22714	1792	8834
BOS	3023	70717	62256	82021	22976	30021
BOS	3024	70717	93504	111658	34504	40618
COO	3025	70717	124920	141332	46160	51212
HUL	3026	70717	155313	171005	57193	61805
BOS	3027	70717	180913	200637	65353	72397
BOS	3028	70717	215529	230313	78929	82993
BOS	3030	70718	25857	45619	10737	17779
COO	3031	70718	60538	75255	21938	28375
COO	3032	70718	93410	104928	34450	38968
COO	3033	70718	114842	134600	42522	49560
GUA	3034	70718	144516	164234	53116	60154
POG	3035	70718	174146	193909	63706	70749
BOS	3036	70718	211643	223544	76603	81344
BOS	3038	70719	23123	42849	9083	16129
BOS	3039	70719	54715	72525	20835	26725
POG	3040	70719	82436	102157	30276	37317
COO	3041	70719	112556	131831	41156	47911
POG	3042	70719	143540	161506	52540	58506
POG	3044	70719	201052	220813	72652	79693
POG	3046	70720	20405	40120	7445	14480
BOS	3047	70720	51621	65753	18981	25073
HUL	3048	70720	83853	95422	31133	35662
BOS	3049	70720	110605	125052	39965	46252
GUA	3050	70720	143918	154722	52758	56842
BOS	3052	70720	194254	214018	70974	78018
HUL	3053	70720	234830	13540	85710	5740
BOS	3055	70721	43231	62949	16351	23389
IND	3056	70721	73111	92620	27071	33980
HUL	3059	70721	133039	151923	48639	55163
HUL	3065	70722	94249	114012	34969	42012
BOS	3071	70723	12410	32128	5050	12088
COO	3074	70723	121122	140836	43882	50916
COO	3082	70724	114308	134032	42188	49232
HUL	3087	70725	22533	42257	8733	15777
COO	3093	70725	151022	170744	54622	61664
BOS	3096	70726	45359	65121	17639	24681
COO	3106	70727	72225	91945	26545	33585
BOS	3109	70727	161153	180912	58313	65352
GUA	3117	70728	154043	174107	56443	63667
HUL	3119	70729	31652	50521	11812	18321
COO	3121	70729	52836	72557	19716	26757
HUL	3122	70729	93028	112115	34228	40875
HUL	3123	70729	122204	141739	44524	51459
GUA	3124	70729	151644	171408	55004	62048
GUA	3125	70729	181317	201034	65597	72634
IND	3126	70729	211141	230116	76301	82876
BOS	3128	70730	30245	45956	10965	17996
BOS	3129	70730	61126	75624	22286	28584
COO	3130	70730	90926	105253	32966	39173
COO	3131	70730	115158	134916	42718	49756
GUA	3133	70730	175846	194213	64726	70933
IND	3134	70730	204119	223838	74479	81518
HUL	3135	70730	233751	13505	85071	5705
BOS	3137	70731	53039	72758	19839	26878
BOS	3138	70731	84608	102428	31568	37468
HUL	3139	70731	115832	132056	43112	48056
HUL	3140	70731	145648	161723	53808	58643
HUL	3144	70801	15233	34953	6753	13793
HUL	3155	70802	71707	91424	26227	33264
POG	3160	70802	215924	235622	79164	86182
BOS	3164	70803	123629	143854	45389	52734
POG	3169	70804	32350	52110	12230	19270
HUL	3175	70804	180607	200325	65167	72205
POG	3179	70805	84824	102621	31704	37581
HUL	3179	70805	102640	121021	37600	43821
BOS	3181	70805	153208	165221	55928	60741
POG	3183	70805	204721	224516	74841	81916
COO	3184	70806	2329	14142	1409	6102
POG	3186	70806	53713	73436	20233	27276
BOS	3187	70806	85058	103105	31858	37865
COO	3188	70806	113010	132729	41410	48449
BOS	3189	70806	143554	162358	52554	59038
COO	3191	70806	201930	221650	73170	80210
BOS	3193	70807	21235	40944	7955	14984
BOS	3194	70807	52035	70613	19235	25573
HUL	3195	70807	80523	100239	29123	36159
COO	3196	70807	111052	125907	40252	46747
GUA	3197	70807	142100	155534	51660	57334
BOS	3198	70807	165439	185159	60879	67919
HUL	3203	70808	72205	91926	26525	33566
HUL	3200	70808	220422	36	79462	36
POG	3210	70810	32816	52522	12496	19522
COO	3223	70810	181001	200716	65401	72436

	REV NO.	DATE OF REV	TIME OF REV IN HRS		TIME OF REV IN SECS	
COO	3228	70811	94858	110505	35338	39905
HUL	3229	70811	121618	140130	44178	50490
HUL	3230	70811	150035	165753	54035	61073
GUA	3238	70812	154736	175148	56856	64308
COO	3244	70813	53454	71928	20094	26368
BOS	3249	70813	184407	202913	67447	73753
HUL	3254	70814	102231	121944	37351	44384
GUA	3255	70814	170608	182819	61568	66499
BOS	3256	70814	194744	212443	71264	77083
COO	3257	70815	12016	23028	4816	9028
COO	3260	70815	65745	85416	25065	32056
COO	3265	70815	184234	203945	67354	74385
COO	3269	70816	62803	82515	23283	30315
HUL	3279	70817	124133	140522	45693	50722
IND	3280	70817	180053	194657	64853	71217
COO	3281	70817	205709	225427	75429	82467
POG	3283	70818	24958	44713	10198	17233
COO	3285	70818	74350	94110	27830	34870
COO	3286	70818	113902	133623	41942	48983
BOS	3287	70818	143527	163243	52527	59563
HUL	3289	70818	202823	222528	73703	80728
BOS	3291	70819	22056	41814	8456	15494
COO	3294	70819	71456	91213	26096	33133
COO	3297	70819	194153	213910	70913	77950
HUL	3303	70820	102338	122051	37418	44451
COO	3310	70821	65755	85513	25075	32113
COO	3314	70821	213940	233654	77980	85014
BOS	3320	70822	122125	141837	44485	51517
GUA	3324	70823	30302	50018	10982	18018
BOS	3331	70823	204104	223820	74464	81500
GUA	3332	70824	53008	70346	19808	25426
BOS	3333	70824	71608	82610	26168	30370
HUL	3334	70824	84009	112000	31209	40800
POG	3334	70824	114049	123525	42049	45325
GUA	3336	70824	141337	161622	51217	58582
BOS	3340	70825	20526	40140	7526	14500
COO	3346	70825	194211	213916	70931	77956
BOS	3353	70826	102324	122035	37404	44435
COO	3359	70827	65718	85426	25038	32066
BOS	3364	70827	213839	233548	77919	84948
HUL	3368	70828	121952	141704	44392	51424
HUL	3376	70829	85345	105054	32025	39054
HUL	3384	70830	82347	102101	30227	37261
POG	3388	70830	200852	220605	72532	79565
BOS	3391	70831	75357	95108	28437	35468
BOS	3402	70901	92126	111834	33686	40714
POG	3407	70902	65344	85053	24824	31853
COO	3413	70902	213457	233201	77697	84721
HUL	3416	70903	101619	121540	36979	44140
HUL	3425	70904	94652	114529	35212	42329
COO	3428	70904	203428	223139	74068	81099
BOS	3432	70905	91805	111520	33485	40520
BOS	3439	70905	230030	5741	82830	3461
BOS	3442	70906	134135	153846	49295	56326
HUL	3449	70907	42216	61920	15736	22760
POG	3453	70907	190250	205953	68570	75593
HUL	3458	70908	94322	114027	35002	42027
HUL	3465	70909	91212	110922	33132	40162
GUA	3466	70909	120821	140531	43701	50731
IND	3469	70909	205645	225349	75405	82429
COO	3472	70909	235341	14956	86021	6596
HUL	3473	70910	84358	103816	32438	38296
GUA	3475	70910	113718	133423	41838	48863
POG	3476	70910	202535	212828	73535	77308
BOS	3477	70910	213719	222249	77839	80569
BOS	3477	70910	232139	1621	84099	981
POG	3478	70911	2959	11853	1799	4733
BOS	3480	70911	51400	71104	18840	25864
BOS	3481	70911	83640	100713	31000	36433
COO	3482	70911	112800	130319	41280	46999
HUL	3483	70911	143808	155926	52688	57566
GUA	3484	70911	173121	185534	63081	68134
COO	3485	70911	195433	215138	71673	78698
COO	3488	70912	44257	63959	16977	23999
BOS	3494	70912	192331	212034	69811	76834
BOS	3500	70913	100404	120109	36244	43269
HUL	3506	70914	83413	103119	30853	37879
POG	3511	70914	211710	231412	76630	83652
BOS	3616	70915	70100	85756	25260	32276
HUL	3515	70915	90119	105822	32479	39502
COO	3521	70916	53336	73040	20016	27040
IND	3526	70916	171745	191448	62265	69288
COO	3529	70917	20554	40254	7554	14574
POG	3538	70918	43012	62715	16212	23235
BOS	3542	70918	191029	210727	69029	76047
COO	3546	70919	65430	85136	24870	31896
HUL	3548	70919	134030	151113	49230	54673
POG	3549	70919	161455	181156	58495	65516
IND	3550	70919	193447	210758	70487	76078
POG	3551	70919	221839	355	80319	235
POG	3553	70920	35855	55557	14335	21357
~~[illegible]~~	~~[illegible]~~	~~[illegible]~~	~~[illegible]~~	~~[illegible]~~	~~[illegible]~~	~~[illegible]~~
COO	3554	70920	71648	85158	26208	31918
HUL	3555	70920	101920	113717	37160	41837
GUA	3556	70920	123648	143353	45408	52433
GUA	3557	70920	153608	172953	56168	62993
IND	3558	70920	182857	202553	66537	73553
POG	3559	70920	213105	232154	77465	84114
IND	3559	70921	4529	21755	2729	8275
GUA	3561	70921	31657	51353	11817	18833

REV NO.		DATE OF REV	TIME OF REV IN HRS		TIME OF REV IN SECS	
COO	3562	70921	62306	80956	22986	29396
POG	3563	70921	93122	110555	34282	39955
GUA	3564	70921	123250	140155	45170	50515
POG	3565	70921	150058	165753	54058	61073
IND	3568	70921	234851	14554	85731	6354
POG	3569	70922	24451	44153	9891	16913
HUL	3570	70922	55515	73755	21315	27675
HUL	3572	70922	121852	132956	44332	48596
GUA	3573	70922	142852	162524	52132	59124
COO	3577	70923	21253	40954	7973	14994
HUL	3578	70923	52645	70556	19605	25556
HUL	3579	70923	81933	100156	29973	36116
COO	3580	70923	111230	125757	40350	46677
GUA	3581	70923	135654	155354	50214	57234
BOS	3583	70923	165254	184954	60774	67794
COO	3585	70924	14047	33738	6047	13058
BOS	3586	70924	50551	63328	18351	23608
COO	3587	70924	20855	92918	29335	34158
COO	3588	70924	105157	122504	39117	44704
HUL	3589	70924	132400	152054	48240	55254
BOS	3590	70924	161952	181642	58792	65802
COO	3593	70925	10713	30409	4033	11049
BOS	3595	70925	65857	85546	25137	32146
COO	3596	70925	104457	115134	38697	42694
HUL	3597	70925	132226	144726	48146	53246
GUA	3598	70925	155826	174315	57506	63795
BOS	3602	70926	34115	52629	13275	19589
BOS	3603	70926	62531	82217	23131	30137
COO	3611	70927	55355	75040	21235	28240
COO	3612	70927	92803	104910	34083	38950
HUL	3613	70927	121203	134700	43923	49620
BOS	3614	70927	145331	164413	53611	60253

aliability in identifying REPs was obtained.

Fig. C-3 shows how each microfiche is layed out and Table C-1 is a listing of the individual microfiche by Rev Number, Date, UT of Rev in hrs and secs, and notes on electron and proton precipitation events. Approximately 1212 microfiche were examined three times by one individual (the author) and once by another graduate student (T. Kelley) for comparison. A list of 358 outer zone transits were identified for further discrimination by pitch-angle. 313 outer zone REP revs were confirmed by the pitch-angle analysis and are listed in Table C-2. The remaining case was eliminated by the loss-cone criteria previously described, bad data drop outs, low flux values, and spike events. This table also subjectively groups the revs into 173 'events' by combining consecutive revs with strong precipitation. Since each revs last 3 hrs and there was no AE data set available to determine substorm duration this grouping maybe off as much as 25% in total event number.

Table C-2. Revs with strong precipitation $\geq$ 235 keV electrons by EVENT (one or more consecutive revs with strong precipitation), DATE (last digit of year, month, day), Readout REV (first letter of station, number), LAT (North, degrees), East LONG (degrees), L-VAL, MLT (hrs), j(e/cm^2 s str keV) = differential flux value of precipitating electrons from 235 keV to highest energy channel at which strong precipitation occurred, J(p/cm^{2}s str) = integral flux of strong diffusion precipitation of protons per energy channel if any, 80 p^+ L-VAL = L value of 80 keV proton precipitation if any, strong precip 12, 33, L-VAL = check if 12, 33 keV electron channels had strong precip and L value of 12 keV channel, UT (sec)= time at which 235 keV electron precip occurred.

EVENT	DATE	REV	LAT	(E) LONG	L-VAL	MLT	j [#/(cm² s sr keV)] 255	485	655	850	1.1	1.55	1.6	J [#/cm² s sr] 80	150	850	80P+ L-Val	STRONG PROP 1.2	33	L-VAL	(Hrs) UT
1	60714	B49 ✓	68.1	293.4	6.19	21.2	3.06+1							1.66+4	6.66+3		6.5-6	✓		6-12	16.2
2	60809	C258 ✓	62.0	59.8	6.4	20.4	7.65+1							3.33+4	8.33+3		5-6.5		✓	6.4	15.8
3	60824	A373 ✓	65.1	52.8	7.0	10.3	3.06+2							8.33+3			9-10	✓		6-8.5	5.6
4	60824	A381 ✓	47.6	314.2	7.1	20.1	1.53+1							2.5+4	8.33+3		6.9-6.6				22.5
5	60825	C386 ✓	56.8	354.8	7.8	20.2	3.06+1							2.5+5	8.33+4		5.5-7.5	✓	✓	6-7.5	19.5
6	60827	N398 ✓	-82.2	12.0	7.9	21.8	3.06+1							1.66+4	2.5+3		5-10	✓	✓	5-10	.2
	60827	N398 ✓	42.5	274.7	6.2	19.5	1.53+2	3.07+1						8.33+4	2.5+4		5-7				1.2
7	60827	C405 ✓	44.3	319.9	5.7	20.1	4.6+2	3.53+1						4.5+4	8.33+3		4-8	✓		6	22.1
8	60828	C407 ✓	55.9	321.9	9.5	9.7	6.12+1											✓	✓	8-11	11.2
9	60828	P410 ✓	63.1	192.5	7.5	7.7	4.6+2							6.66+3			8-10	✓	✓	6-12	20.1
10	60906	B479 ✓	-77.9	305.3	5.3	22.0	1.0+3	1.99+2	8.66+1	3.54+1	7.7+0	6.5+0	4.95+0	2.5+4	8.33+3		5-6,8-9	✓		5.7-9	1.7
11	60914	C547 ✓	65.4	206.5	6.4	22.5	1.53+2	9.2+0						7.5+3	1.3+3		5-6	✓	✓	5-7	6.4
12	60918	B575 ✓	45.0	157.3	4.3	20.3	7.65+1	1.8+1						1.1+5	7.5+4	8.3+3	4-7	✓	✓	4-7	8.9
13	60919	I584 ✓	50.4	308.1	5.4	8.3	9.2+2							8.3+3	6.7+2		7-9	✓	✓	5-6	10.9
14	60920	H589 ✓	67.5	95.9	7.0	8.5	1.1+3	2.8+1						8.3+3			9-12	✓	✓	6-10	1.7
	60920	I592 ✓	63.0	2.2	7.1	9.3	7.65+1							2.5+3			9-12	✓	✓	6-9	7.7
	60920	B595 ✓	-74.3	219.8	7.3	7.8	1.4+3	2.3+1						1.5+3			10-20	✓	✓	5-20	14.3
15	60921	B599 ✓	61.4	55.5	6.0	3.7	3.06+1	6.1+0						7.5+4	1.0+4		5-6	✓	✓	4.5-20	2.2
	60921	B599 ✓	-77.0	285.0	6.1	22.2	3.06+2	3.06+1						1.0+5	1.6+4		5-6	✓	✓	5-8	2.3
	60921	B598 ✓	65.0	50.5	6.0	9.1	1.2+3											✓	✓	6-11	4.5
	60921	B602 ✓	-47.5	118.6	6.0	19.4	4.6+1							9.3+4	3.3+4		5-6	✓		6-8	11.4
16	60922	I608 ✓	74.8	110.8	10.5	8.7	3.06+1											✓	✓	12-17	1.3

2

EVENT	DATE	REV	LAT	(°) LONG	L-VAL	MLT	j [e/cm² sec sr keV] 235	435	655	850	1.1	1.35	1.6	I [e/cm² sec] 80	150	350	10 … L-VAL	STRONG PRECIP 12	33	L-VAL	(HRS) UT
17	60923	C 619✓	-51.2	123.4	8.0	19.6	1.2E2							2.5+5	6.6+4	2.5+3	4.6-9	✓	✓	6-10	11.1
18	60926	C 641✓	-76.8	290.2	6.7	21.5	3.5+1							3.3+4	4.2+3		5-7	✓		5-6	1.5
19	60929	C 665✓	-57.0	182.0	6.9	21.1	1.5+2							8.3+2			6-8	✓		6-8	7.01
20	61002	I 639✓	53.4	288.0	7.2	7.4	7.6+2	3.0+1						8.3+3			8-10	✓	✓	5-12	11.8
21	61003	I 697✓	-75.8	14.1	7.2	2.0	4.6+1	1.5+1						7.5+3			6-7	✓		6-8	3.2
	61003	I 697✓	-73.5	250.1	6.0	21.8	1.5+2	2.0+1	7.0+0					4.2+4	6.7+3		6-7	✓		6-7	3.3
22	61016	I 803✓	-76.2	264.6	6.7	5.0	6.1+2							1.0+4	5.8+3		6-7	✓	✓	5-8	9.8
23	61017	B 808✓	-58.0	62.0	6.2	4.0	4.6+1	1.4+1						8.3+3	1.6+3		5-6	✓	✓	4-8	.6
	61017	B 808✓	-73.0	280.0	6.0	19.6	4.6+2	4.6+1						2.6+4	8.3+3		>5	✓	✓	>5	.9
24	61021	C 845✓	69.3	283.8	7.3	16.7	4.6+1							7.5+3			6-6.5				1.1
25	61028	C 901✓	56.0	253.7	6.5	5.2	1.1+2												✓	6.5	12.9
26	61031	B 924✓	-76.3	255.7	6.0	4.7	7.7+1							8.3+4	5.0+4		6-7	✓	✓	4-7	9.9
27	61110	I 1004✓	59.5	242.7	6.4	4.4	4.6+1							2.5+3			7	✓	✓	6-9	13.2
28	61111	I 1011✓	-65.3	25.5	6.4	1.6	9.1+1							1.6+4	7.5+3		6-7				1.6
	61111	I 1011✓	-69.4	238.0	7.3	19.6	4.6+1							2.5+3			6-7				1.9
29	61112	I 1025✓	-50.5	85.2	5.5	3.0	3.06+1							2.5+4	7.5+3		5	✓	✓	5	22.1
30	61114✓	B1034✓	-64.3	35.2	7.1	1.5	2.0+1							4.2+4	1.7+4		6-7	✓		6.5-6	.9
	61114✓	B1033✓	71.9	39.0	7.5	7.0	1.4+2											✓	✓	6-10	3.3
31	61201	C 1177✓	-58.9	178.0	7.2	4.5	1.8+1							2.5+3			6	✓	✓	4.5	14.8
32	61204	B 1202✓	70.5	188.5	8.7	12.4	5.0+1							8.3+3			>12		✓	7-12	1.3
33	61209	B 1239✓	-74.0	273.8	7.0	2.3	4.6+1	4.6+0						6.7+3	2.5+3		6	✓	✓	5-9	71

EVENT	DATE	REV	LAT	(E) LONG	L-VAL	MLT	j [e/cm² sec sr keV] 235	435	655	850	1.1	1.35	1.6	J [p/cm² s sr] 80	150	350	SOPA L-VAL	STRONG 12	PRECIP 33	L-VAL	3 (HRS) UT
34	61211	I1252	-63.2	22.9	7.0	0.5	6.1+1	7.7+0						1.25+4	3.3+3		5-6	✓	✓	5-9	.6
35	61212	H1266	52.3	272.5	8.8	14.0	1.5+2	4.6+1						6.7+3	8.3+2		6-8		✓	6-13	20.2
36	1219	P1317	-60.4	4.7	5.1-6	0.6	2.0+1							4.2+4	1.7+4		5-5.4	✓	✓	5-6	1.6
37	61221	H1338	-48.5	109.7	7.0	1.82	3.06+1							8.3+3	1.7+3		7	✓		7	18.7
38	61222	G1340	-67.9	322.5	5.6	0.6	6.1+1	1.2+1	1.6+1	7.5+0				2.5+4	5.8+3		5.6-6.5				3.9
39	61222	D342	-64.9	236.6	5.8	2.9	9.2+0							5.0+3			5.5	✓	✓	5-6	9.8
40	61222	C1345	-49.0	157.2	5.4	2.9	2.0+1							8.3+3			5.4	✓	✓	4-6	15.5
	61222	C1345	-44.8	114.5	5.4	2.0	8.0+1							1.1+4			5.5	✓	✓	5	18.5
41	61223	I1350	66.2	338.2	6.1	2.8	1.5+1							1.7+3			6		✓	6	9.5
42	61225	I1369	50.3	166.0	5.8-6.3	2.9	1.1+2							2.5+4	6.7+3		5.3-6	✓	✓	5.2-6.5	14.8
	61225	H1371	51.8	76.1	7.3	0.8	1.2+1							3.3+3	9.2+2		7	✓		5-8	20.7
	61225	H1371	58.3	27.8	6.4	0.1	3.1+1							8.3+3			6				23.4
43	61227	C1380	67.8	338.1	6.5	0.1	1.5+1							2.5+3			6				2.6
44	61227	H1386	49.5	128.1	7.3	2.0	1.5+1							8.3+3	1.7+3		6-7	✓	✓	6-7	17.2
45	61229	I1398	-59.8	307.0	3.8	1.2	3.01+1							1.7+5	7.5+4	8.3+3	3-5	✓	✓	4	5.0
	61229	I1398	-66.0	257.0	4.4-7.0	2.1	4.6+2							2.5+4	1.7+4	3.3+3	4-6	✓	✓	4-7	8.0
46	61229	C1404	-55.5	42.0	6.8	.01	1.5+2							7.5+4	1.7+4		5-7	✓	✓	7	22.7
47	61230	I1406	-71.5	297.6	7.3	0.6	1.5+1	6.1+0						9.2+3	2.5+3		6-7				4.9
	61230	I1406	-69.0	256.7	6.7	1.9	3.5+1	7.6+0						8.3+3	8.3+3		5.5-7	✓	✓	6	7.8
48	61231	C1413	73.0	130.0	6.0	12.1	2.0+2												✓	6-8	3.6
49	61231	G1420	58.8	262.0	7.0	2.5	1.4+1							3.3+3	8.3+2		6.0	✓		7	9.7
	61231	C1419	-63.0	221.0	6.5	2.6	1.4+1							2.5+3			6.5				10.4

EVENT	DATE	REV	LAT	(E) LONG	L-VAL	MLT	j [illegible] 285	435	655	850	1.1	1.35	1.6	J [illegible] 50	150	350	BOPT L-VAL	STR PREC. 12	33	L-VAL	HRS UT
50	70103	G1448	✓-58.8	12.0	5.8	23.8	1.5+2	1.5+1						1.7+4	3.3+3		6	✓		6	.4
51	70104	C1450	✓-44.0	156.0	5.2	2.2	1.5+2	1.2+2	6.5+1	2.3+1	7.7+0			4.2+4	8.3+3		5.2	✓	✓	>5	15.1
52	70105	I 1455	✓-64.5	236.2	6.5	2.1	1.5+1							1.7+4	2.5+3		6				9.5
53	70108	C1485	✓-49.2	77.7	6.6	0.3	1.5+2	3.1+1						8.3+3	1.7+3		6.5				20.0
54	70115	C1535	✓71.0	98.5	6.5	11.8	1.5+2							8.3+3			>6		✓	>5	5.5
55	70116	I1547	✓-71.0	308.0	7-8	23.2	3.01+1							6.7+3			6-7	✓	✓	8	9.4
56	70117	H1557	✓-44.0	107.1	6.0	0.6	1.4+1							4.2+3			6	✓	✓	6	17.6
	(70117	C1556	19.0)																		
57	70118	H1560	✓-62.3	210.5	5.0	0.5	3.01+1							2.5+4	8.3+3		5	✓	✓	5-5.5	5.7
58	70123	C1600	✓-69.2	289.8	7.1	23.7	4.6+1							2.5+3			7	✓		7	4.5
59	70124	C1608	✓-69.2	293.0	7.0	23.6	1.5+1							1.7+3			>6	✓		>6	4.2
60	70130	C1656	✓-63.0	275.5	5.0	0.04	4.6+2	7.7+1	1.5+1					2.5+4	6.7+3		>5	✓	✓	>5	5.5
	70130	H1658	✓-56.8	235.8	5.0	1.06	6.1+1	1.5+1	4.9+0					1.7+4	2.5+3		4.5-5.0	✓	✓	>4.5	8.4
	70130	H1658	✓-49.2	195.8	5.0	0.8	3.06+2	4.6+1	1.6+1					1.7+4	3.3+3		4.5-5	✓	✓	>5	11.2
	70130	B1659	✓-43.4	154.1	4.6	0.8	1.4+2	1.5+1						7.5+4	8.3+3		4.5-5.5	✓	✓	>4.5	14.1
	70130	C1661	✓-37.5	112.4	4.85	0.2	1.5+3	3.1+2	5.4+1	1.8+1	4.5+0			8.3+4	2.5+4	1.7+3	4.5-9	✓	✓	4-9	17.0
	70130	C1661	✓-39.9	66.5	4.5	23.6	6.1+2	7.7+1	1.6+1	4.1+0				4.2+4	1.7+4	6.7+3	4-9.3	✓	✓	4-6	20.0
	70130	H1662	✓-44.8	19.7	4.2	23.2	1.5+2	4.6+1	8.2+0	5.3+0				7.5+4	2.5+4	2.5+3	3.8-8	✓	✓	4-5	23.0
	70131	C1664	✓-63.2	323.2	5.9	22.9	4.6+1							7.5+4	1.7+4		4.4-8.6	✓	✓	5-6	2.3
	70131	C1664	✓-61.3	280.4	4.95	23.9	3.0+1							NO DATA				✓		4.8	5.2
	(70131	C1666	[illegible]	[illegible] 285	Pump)																
61	70131	I 1665	✓-49.7	199	5.1	1.0	1.7+1							3.3+4	7.5+3		5	✓	✓	5	10.9
	(70131	I1668	14.1)																		
62	70131	I 1668	✓-41.6	113.8	5.7	0.1	4.6+2	6.1+1						9.2+3	7.5+3		5.2-5.5	✓	✓	6	16.8
	70131	H 1670	✓-46.4	67.0	6.2	23.2	3.0+1							8.3+3	4.2+3		5.5-6.0	✓		6	19.8
63	70202	I 1681	✓-50.7	205.3	4.95	0.9	3.0+1							7.5+4	1.7+4		4.5	✓	✓	4.2-5	10.4
	70202	I 1684	✓-47.4	162.5	5.6	0.1	2.0+1							2.5+4	2.5+3		6				13.9

EVENT	DATE	REV	LAT	(e) LONG	L-VAL	MLT	j [°/cm² sec str keV] 235	435	655	850	1.1	1.35	1.6	j (°/cm² sec) 80	150	350	80P LVAL	12	33	L VAL	UT 5
	70202	I1684	40.5	121.2	4.9-7.5	8-.9	6.1+1	7.6+0						4.2+4	8.3+3		5-9	✓	✓	5-15	16.2
	(70202	H1686	19.2	235, 435 L=5.5		[illegible])															
	(70203	B1688	1.4	235, 435 L=6.5		")															
	(70203	H1690	7.9)																		
64	70203	I1692	-46.9	166.2	5.9	0.8	2.2+1							6.7+4			6	✓		6-7	13.0
65	70205	G1708	-48.3	172.5	6.2	0.8	1.5+2	2.0+1						1.7+4	6.7+3		6.5-6	✓	✓	6	12.5
66	70208	H1734	75.2	148.1	5.7-10	1.4	1.5+2	3.0+1						1.6+4	8.3+3		5-10	✓	✓	4-10	16.6
	70208	H1734	-41.0	97.5	5.7	23.4	1.5+2	2.0+1						8.3+4	1.7+4		4-10	✓	✓	4-10	17.5
67	70209	I1741	73.5	50.1	6-8	11.2	3.0+2							2.5+3			4-10		✓	4-10	7.3
68	70222	B1849	68.4	57.3	6	1.5	4.6+1							8.3+3			6	✓		4-8	21.8
69	70225	I1866	51.2	280.4	6.7	0.2	1.2+2	1.5+1						2.5+4	7.5+3		6-8	✓		>6	5.6
	70225	I1870	67.8	201.3	6.8	23.3	1.5+2	3.0+1						1.7+4	5.0+4		7	✓		7	11.5
	70225	I1870	-48.9	156.2	7.6	23.7	3.0+1							8.3+3	4.2+3		6-7	✓	✓	6-8	12.7
70	70302	G1909	64.9	219.1	7.8	22.8	1.5+1							6.7+3	8.3+2		6	✓	✓	5-10	9.9
71	70307	B1947	-66.9	270.8	6.2	22.4	1.4+1							1.7+3			5.7	✓		6.5	4.0
	70307	H1948	-59.0	232.0	6.0	23.1	1.5+1							3.3+3			5.5	✓		5-7	6.8
	70307	H1948	56.0	235.5	5.8	22.7	9.2+0							DATA	BAD						8.3
72	70309	H1964	-56.6	243.5	4.8-5	23.1	4.6+2	2.0+1						4.2+4	8.3+3		4.8-5	✓	✓	4.6-5.5	6.1
	(70309	H1965	71)																		
73	70309	G1967	-72.7	2.4	9-9.6	10.7	1.5+1							8.3+3			8	✓		7-8	12.7
	70309	P1968	-41.9	73.9	5.8	21.8	1.5+2	1.5+1						6.7+4	1.7+4		4.4-9	✓	✓	4.9-10	17.7
	70309	C1968	-73.0	273.8	6.0	13.3	1.5+3							8.3+3			7-14		✓	6-7	18.6
	70309	P1970	-51.3	244	5.7	21.3	6.6+2	7.7+1	6.5+0					5.0+4	2.5+3		4.8-7		✓	5.6	20.8
	(70310	B1972	3.0	Maybe 235 at L= 5.6, 21.3)																	
74	70310	H1975	-65.2	41.5	9.3	9.9	7.2+1							7.5+3			12		✓	7-10	9.8
	70310	I1975	-43.6	121.6	6-8	22.6	2.7+3	4.6+1						5.8+4	2.5+3		6-8	✓	✓	6-8	14.5
	70310	I1977	-56.6	251	7.0	20.1	1.5+1							2.5+4			5.5-6.5	✓	✓	6.6	20.6
75	70311	C1980	-68.1	285.5	6.2-6.6	21.8	4.6+2	3.5+1						8.3+3	6.7+3		5.5-7.0	✓		6-8	2.7
	70311	B1986	-62.0	340.0	5.3-5.6	21.0	7.6+2	1.6+2	8.2+1	3.5+1	7.7+0			8.3+4	2.5+4	2.5+3	4.9-10		✓	5.8	23.3

EVENT	DATE	REV	LAT	LONG (E)	L-VAL	MLT	j [/cm² s ster keV] 235	435	655	850	1.1	1.35	1.6	J (P/cm² s ster) 80	150	350	80° [illegible]	1.2	3.3	L-VAL	6 HRS UT
	(70312	B1987	2.4, 2.9 235 light)																		
76	70312	P1988 ✓	-67.0	246.9	6.6	22.8	3.5+1							8.3+4	1.6+4		5-6.5	✓	✓	5-6.5	5.3
	70312	H1990 ✓	-46.6	172.8	5.9	23.2	4.6+2	3.1+1						8.3+3	4.2+3		5.5-6.5	✓	✓	5.5-6.5	10.9
	70312	I1992 ✓	-41.4	86.5	5.8	21.9	4.6+1							8.3+4	2.5+4		5-6	✓		5-8	16.8
	70312	B1994 ✓	-55.5	349.6	4.7-5	21.3	1.5+3	2.8+2	2.1+2	8.8+1	1.9+1	1.1+1	7.4	1.1+5	5.0+4	4.2+3	4.4-6	✓	✓	>5	22.9
	70313	H1996 ✓	-65.2	252.9	6.4	22.6	1.4+1							5.8+4	8.5+3		5-6	✓		6-7	5.0
	(70313	P1998	10.7	11.3	235 light L~6 dayside night)																
77	70313	B2002 ✓	-58.2	352.0	5.5-6.2	20.7	3.0+2	2.0+1						1.7+4	7.5+3		5-6.3	✓	[illegible]	6-8	22.6
78	70314	I2008 ✓	-41.8	139.2	6.0	22.7	1.2+2	1.5+1						1.7+4	2.5+3		5-6		✓	6	13.2
79	70315	H2014 ✓	-60.4	221.2	6.2	23.1	3.5+1	9.2+0						8.3+3	1.7+3		6	✓		6	7.2
80	70316	P2020 ✓	-65.3	265.6	5.9	22.2	([illegible]) 3.0+1	1.4+1						1.7+4	1.7+3		6	?			4.0
81	70316	P2029 ✓	-53.9	7.7	5.3	21.0	3.3+2	2.5+2	6.5+1	2.1+1	3.9+0			5.8+4	1.7+4	1.7+3	4.8-6	✓		5.4-6	21.6
82	70317	B2035 ✓	-48.3	15.1	6-6.2	20.5	3.0+1							1.7+4	3.3+3		6	✓	✓	6	21.2
	70318	C2036 ✓	-67.5	269.1	6	21.6	3.0+1							1.7+4	2.5+3		5-6	✓		5.5-6.5	3.4
	70318	C2038 ✓	-51.5	195.5	5.4-5.9	23.0	4.6+1	9.2+1	2.1+1					1.7+4	2.5+3		5	✓		5.5-7	9.1
83	70319	B2051 ✓	-52.7	20.7	5.7	20.7	3.0+2							8.3+3	2.5+3		5.5				20.6
84	70320	C2052 ✓	-65.4	282.9	5.2-5.5	21.7	1.5+2	2.0+1						8.3+3	2.5+3		5.5	✓	✓	5.5	2.7
85	70320	C2058 ✓	-50.5	27.0	5.5	20.8	4.6+1							1.7+4	6.7+4		5-5.5	✓		5.5	20.2
	(70321	H2063	10.0)																		
86	70321	B2067 ✓	-47.0	32.4	5-6	20.9	1.4+2							1.7+5	7.5+3	1.7+3	4-7	✓	✓	5-7	19.8
87	70322	P2071 ✓	-60.1	222.9	6.4	22.1	4.6+1							2.5+3			6	✓	✓	6.4	9.2
88	70323	B2077 ✓	-66.3	230.8	6	22.3	9.2+1							2.5+3			6				4.6
	70323	P2079 ✓	-64.0	207.0	8.3-9.3	23	4.6+1							8.3+3	8.3+2		5-9	✓	✓	5-9	7.6
	(70323	P2079	8.1, 8.6 235 mod jump MLT: 9.5, 10.3)																		
89	70323	I2082 ✓	-42.7	88.9	6	21.6	1.5+2							4.3+3	4.2+3		5.5-6	✓	✓	6	16.1

EVENT	DATE	REV	LAT	(E) LONG	L-VAL	ALT	235	435	655	850	1.1	1.35	1.6	80	150	350	80 L-VAL	12	33	L-VAL	7 (NRD) UT
							j [illegible]							J [illegible]							
90	70324	C2084	✓ 61.2	304.3	4.5-4.7	21.2	7.6+2	1.5+2	3.3+1					6.7+4	1.7+4		4.5-6	✓	✓	4.5	1.3
	70324	H2085	✓ -64.3	257.1	5.5	21.9	1.5+2							8.3+3			5-5.5		✓	5.5	4.3
	70324	e2086	✓ -61.4	215.3	5.8-6.4	22.8	3.0+1							8.3+3	1.7+3		5-9	✓	✓	5-8	7.2
	70324	P2087	✓ -49.1	178.7	6.0	22.8	4.6+1							2.5+3			6		✓	6	10.0
91	70325	B2099	✓ -52.1	181.6	6.5	22.8	1.4+1							5.0+3			6				10.0
92	70326	P2104	✓ -42.3	146.7	5.7-6	22.3	6.1+1							2.5+4	1.7+3		5.5-6.5				12.1
	70326	P2105	✓ -47.4	99.8	6-10	21.5	4.6+1							8.3+4	8.3+3		5-12	✓	✓	6-12	15.1
	70326	P2106	✓ -45.8	56.1	5.7-6.1	20.8	1.5+2							8.3+3	2.5+3		5-5.7	✓	✓	6	18.1
93	70328	P2119	✓ 52.9	237.3	6	21.9	1.5+1							8.3+3	2.5+3		6				7.1
94	70329	e2126	✓ -67.7	232.2	7.2	22.9	1.5+2							8.3+3	7.5+4		6-7				5.5
95	70331	H2144	✓ 58.6	210.1	6.2	21.7	1.2+2							8.3+3	2.5+3		6				9.0
96	70401	H2152	✓ 59.2	215.3	6.5	21.7	1.5+1							2.5+3			6.5		✓	6.5	8.6
	70401	H2152	✓ -49.7	170.7	6.3	22.5	2.0+1							2.5+3			6				10.1
97	70404	P2177	✓ -44.1	143.2	5.9	21.9	6.1+1	3.01+1						5.0+4	8.3+3		6				12.0
98	70405	C2182	✓ -71.4	260.4	6.2	21.4	2.0+2	4.6+1	8.2+0					2.5+4	8.3+3		6		✓	6	3.0
	(All [illegible] light [illegible])																				
99	70406	C2189	✓ -68.7	313.4	5.6	20.0	7.6+1	4.6+0						8.3+4	2.5+4		5-6		✓	5.5	.2
	70406	P2190	✓ -71.6	265.1	6	21.2	6.1+2	4.6+1						4.2+4	1.1+4		5.5-6		✓	6	2.6
	70406	C2194	✓ 63.7	198.3	6.7	21.6	9.2+1							2.5+4	4.2+3		5.5-6				9.7
100	70406	B2197	✓ -61.2	325.5	4.4-4.9	20.2	2.0+2	2.0+1						5.0+5	1.7+5	1.0+4	4-9	✓	✓	4.5-5.5	23.2
	70407	P2199	✓ -63.9	278.9	4.3-4.5	21.2	1.2+2	6.1+1	3.3+1	1.8+1	5.8+0			1.7+5	8.3+4	8.3+3	4-12	✓	✓	4.5-8	2.2
	70407	e2200	✓																		
	70407	H2201	✓ -42.4	158.4	5.1	21.8	3.0+2	2.0+1	3.3+1	3.5+0				8.3+4	2.5+4	1.7+3	4.8-5.2		✓	5.1	10.8
	70407	I2201	✓ -39.7	115.2	5.1	21.3	NOT 130	4.6+1	8.2+0					8.3+4	2.5+4	1.7+3	4.8-9				13.7
	70407	I2202	✓ -87.0	4.0	12.5	11.5	4.6+1							2.5+3	8.3+2		9-16		✓	8-13	14.3
101	70408	C2206	✓ -70.8	276.0	6.0	20.9	2.0+2	1.5+1						2.5+5	2.5+4	6.7+3	5-6.5				1.9

EVENT	DATE	REV	LAT	(E) LONG	L-VAL	MLT	j [e/cm² s sr keV] 235	435	655	850	1.1	1.35	1.6	J (P/cm² s sr) 80	150	350	80° L-VAL	12	35	L-L-BL	8 UT
102	70408	B2211	-40.8	75.2	4.9	20.8	NOT 10 1.5+2	1.2+2	0.6+1	1.1+1	3.9+0			2.5+5	5.0+4	7.5+3	4.5-10	✓	✓	4.8-6	16.3
103	70409	B2218	-48.0	105.5	5.7-6	22.1	6.1+2	6.1+1						3.3+4	2.5+4	1.7+3	5.3-6	✓	✓	6	10.1
104	70410	P2226	-54.3	167.2	7.6	22.2	1.2+2	7.7+0						1.7+4	7.5+3		6.3-8				9.8
	70410	B2228	-45.5	82.9	6.0	20.5	1.5+2	4.6+1						5.8+4	1.7+4	1.7+3	5-6		✓	6	15.6
105	70411	C2232	-68.5	249.3	5.7	21.5	6.1+2	1.5+2	2.1+1					2.5+4	8.3+3		5-7	✓	✓	5-7	3.7
106	70419	C2297	-58.5	20.6	4.6-6.5	21.9	4.6+3							8.3+4	4.2+4	2.5+3	4.4-19	✓	✓	3.5-12	6.4
	70419	C2297	-67.6	10.8	6.7	9.8	1.5+2						★		MOVE				✓	6-7	7.3
	70419	C2298	-47.1	172.3	4.8	21.7	4.6+2	4.6+1						8.3+4	2.5+4	4.2+3	4.8	✓	✓	4.5	9.4
	70419	B2299	-54.8	169.3	4.4	21.4	3.0+2	4.6+1						2.5+5	8.3+4	8.3+3	4.55	✓	✓	4-4.5	10.7
	70419	I2300	-62.4	130.1	4.4-5.2	22.0	1.5+3	6.1+1	6.8+1					1.7+5	8.3+4	6.7+3	4.5-5.5		✓	5-5.5	13.6
	70419	I2301	-54.7	35.5	5.7	19.3	7.7+1							5.8+4	1.7+4	8.3+2	5-6				18.2
	(70419	B2302	data [illegible] not sampled)			MLT 20.8															
	70419	B2303	-53.9	351.3	5.7-6.2	22.9	1.5+2	1.5+1						2.5+4	8.3+3		5-6	✓	✓	6	22.5
	70420	A2304	42.1	301.1	5.4	22.1	7.6+2	7.7+1	1.1+1					1.7+5	6.7+4	7.5+4	4.8-5.5	✓	✓	5-6	1.6
	70420	H2305	45.9	258.6	5.9-6.4	21.2	1.1+3	1.2+2	1.5+1					2.5+4	8.3+3	8.3+2	5-6	✓		6-6.5	4.5
	70420	H2305	-63.3	212.4	6	21.9	6.1+1	7.7+0						2.5+4	2.5+3		5-9		✓	6	6.1
	70420	P2306	-57.7	174.8	5-6.6	21.7	9.2+2	6.1+1	9.8+0					8.3+4	2.5+4	8.3+2	5-6				8.9
	70420	I2307	-47.8	132.8	7.1	21.0	7.7+1							1.7+4	8.3+3		6-7		✓	7	11.8
	70420	I2309	64.0	92.2	5.5	22.6	1.5+2	4.6+1	1.6+1					8.3+4	1.1+4	2.5+3	5-5.5				16.1
	(70420	B2311	22.0)																		
107	70421	H2312	-70.7	254.1	5.95	20.6	2.0+2	3.5+1	1.6+1	8.9+0	4.5+0			5.0+4	1.7+4		5.5-6				2.8 2.4
108	70422	B2323	-72.7	256.3	5.9	20.8	3.0+1							8.3+3	2.5+3		6				↓
109	70423	C2333	-45.2	105.5	6.0	20.3	NOT 10 7.6+1 [illegible]	5.1+1	1.6+1					1.1+4	8.3+3		6				13.6
110	70425	B2347	-48.4	159.1	5.8	21.3	7.7+1	1.5+1						1.7+4	2.5+3		4.8-12	✓	✓	12	9.8
	70425	P2348	-61.3	160.9	5.6	21.3	6.1+2	9.2+1	1.1+1					8.3+3	2.5+3		5-8	✓	✓	5.7	11.2
111	70429	B2384	52.6	359.4	5.4	22.3	2.0+2	1.2+1						3.3+4	8.3+3		5-5.5		✓	55	21.5
112	70430	P2386	43.2	265.9	6.1	20.9	4.6+1							8.3+3	2.5+3		5.5-6				3.6

EVENT	DATE	REV	LAT	(E) LONG	L-VAL	MLT	235	435	j (e/cm² s sr keV) 655	850	1.1	1.35	1.6	J (P/cm² s sr) 80	150	350	80° L-VAL	12	33	L-VAL	9 UT
113	70502	P2404	✓36.3	273.5	4.6	21.0	1.5+3	1.5+2	6.5+1	1.8+1				1.1+5	5.0+4	6.7+3	4.5-12	✓	✓	4.5-5	2.9
	(70504	P2403	60)				[illegible]														
114	70502	P2404	✓51.7	192.4	4.6	20.6	6.1+1	1.5+1						4.2+4	7.5+3		4-16	✓		4-9	8.5
115	70502	H2407	✓62.7	66.8	6.6	22.4	7.7+3	1.4+2						2.5+5	5.0+4	7.5+3	5.5-6.6	✓	✓	4.5-6.6	17.2
	70502	C2408	✓65.9	324.9	4.1	19.1	[illegible] 4.6+3 P 3.1+2	1.5+2 7.6+1	6.5+2 6.5+1	2.9+2 5.3+1	2.0+1	2.8+1	9.9+0	1.7+5	8.3+4	8.3+3	4.0-5				21.9
	70502	Q2408	✓-56.6	169.4	6	11.3	1.5+3	4.6+1						7.5+2			6	✓	✓	6	22.1
	(70503	H2410	2.0)																		
116	70503	P2411	✓46.7	239.5	5.7-6	20.5	1.5+2							2.5+4	6.7+3		4.5-6.5	✓	✓	4.5-6.5	5.2
117	70506	C2434	✓41.8	297.8	6	21.4	4.6+2	1.5+1						8.3+3	1.7+3		5.5-6	✓		6-6.5	1.1
118	70510	B2473	✓57.2	R.4	6	21.9	6.1+1							2.5+4			5.3-6				19.9
	(70511	P2476	40)																		
119	70511	C2477	✓49.0	196.2	4.5	20.0	[illegible] 4.6+2 P 4.6+1	2.0+2 9.6+1	1.6+2 3.2+1	9.4+1 5.3+1	3.8+1 2.5+1	2.8+1	7.4+0	3.3+4	3.3+4	4.2+3	4.5-5				7.8
	70511	B2479	✓65.0	1190	6.3	21.0	1.5+1							8.3+3	1.3+2		4.6-6.3	✓	✓	5-5.5	13.5
	70511	H2480	✓55.1	66.9	4.6	21.4	2.0+1							3.3+4	7.5+3	L=4 1.5+3	3.9-9	✓	✓	4.5-8	16.6
120	70512	H2482	✓39.9	285.8	5.7	20.8	7.7+1	9.2+0						8.3+2	L=5 1.7+3		5-6	✓	✓	6	1.6
	70512	H2484	✓40.0	242.0	4.8-5	20.1	6.1+1	1.1+1						7.5+4	2.5+4	2.5+3	4.25-4.9		✓	4.5	4.5
	70512	H2484	✓38.8	240.9	4.2	20.2	[illegible] 3.4+3 [illegible] 7.7+2	7.7+2 3.5+2	2.0+2 9.8+1	8.9+1	5.8+1	4.4+1	1.7+1	"	"	"	"				4.6
	70512	H2485	✓49.0	201.8	4.3-4.7	20.1	1.1+2	3.1+1						8.3+3	2.5+3	L=4 2.5+3	4-5		✓	4.7	7.4
	70512	C2487	✓59.6	119.9	5.1	21.0	1.2+2							1.7+4	2.5+3		4.5-5	✓	✓	5-5.5	13.1
	70512	H2488	✓61.7	77.3	5.9	21.6	1.5+1							7.5+3			5-5.5	✓?			16.1
121	70515	C2514	✓53.8	360.0	6	22.1	1.5+2	1.5+1						7.5+3	1.7+3		5.2-6		✓	6	20.8
122	70516	A2523	✓41.1	314.5	5.3-5.6	21.1	1.1+3	1.5+2	2.1+1	8.9+0	3.9+0			5.8+4	9.2+3		5.4-6.5		✓	5-5.5	23.5
123	70517	S2528	✓64.4	108.0	6.4	21.1	1.5+2	1.5+1						5.8+3			5.6-6.2	✓	✓	6.5	13.9
124	70518	B2533	✓51.6	237.1	7.4-7.7	19.8	1.5+1							6.7+4	2.5+3		5.5-8	✓	✓	7.5-8	4.8
125	70518	C2539	✓62.5	332	7.7	21.6	6.1+1							6.7+3			6-7				22.5
126	70519	B2546	✓63.9	303	8.0	21.9	3.6+1							2.5+3			6.6				18.9

EVENT	DATE	REV	LAT	LONG (W)	L-VAL	MLT	j[e/cm² s sr keV] 235	435	655	850	1.1	1.35	1.6	J(p+/cm² s sr) 80	150	350	80 keV L-VAL	12	37	L-VAL	10 UT (HRS)
127	70520	G2555	✓50.5	342.2	6.5	21.5	1.5+1							2.5+4	6.7+3		5.5-6		✓	6.5	21.7
128	70524	B2587	✓55.9	8.6	6.8	21.5	4.6+1							8.3+3			6-6.5				19.9
129	70610	B2722	✓45.0	234.1	5.3	18.7	E 4.6+0 P 3.1+1	1.5+2 4.6+1	4.9+1 1.6+1	1.2+1	NO P			8.3+3	1.7+3		5.3-6				3.8
130	70702	G2905	✓53.1	333.6	7.0	19.5	7.7+0							8.3+3			5.5-7	✓	✓	9.5	00.4
131	70710	H2963	✓62.4	306.8	5.6-9.8	5.7	3.5+2	1.1+1						4.2+3	1.1+3		6-9	✓	✓	5-10	1.1
132	70710	C2968	✓63.9	74.4	7.0	19.0	1.5+1							8.3+1			5.8-7		✓	5.5	13.7
133	70710	G2970	✓53.2	338.3	6.7	19.2	2.0+2	7.7+0						8.3+3	2.5+3		5.5-7				19.7
134	70716	B3015	✓53.4	324.2	5.5	5.5	5.0+3							3.3+4	2.5+3		5-15	✓	✓	4.9-14	7.0
	(70716	B3010	41.0)																		
135	70716	H3017	✓47.6	239	5.8	3.9	3.5+1							8.3+4			5	✓	✓	4.7-6	12.8
	70716	H3017	✓65.9	69.4	6.3-22	18.8	1.7+4							6.7+4	8.3+3		5-13	✓	✓	6-12	13.8
136	70718	G3034	✓59.0	200.2	7.2	3.2	1.5+1							2.5+3			5.8-7.5	✓	✓	5.5-7.5	15.0
	70718	P3035	✓63.5	152.7	6.6	3.5	3.5+1							8.3+2			6.2	✓	✓	6.2-7.0	18.0
137	70720	H3053	✓-57.8	76.6	7.3	4.08	3.1+1							2.5+3			7	✓	✓	5.5-8	0.8
138	70722	H3061	✓-46.1	277.2	6.9	4.3	2.0+1							2.5+3			5.6-7	✓	✓	5-7	10.0
139	70723	B3074	✓-64.4	49.6	7.0	3.6	6.1+1							4.2+3			7.3	✓	✓	7	2.8
140	70729	C3121	✓-66.0	5.0	4.5	4.3	3.1+0							8.3+3	2.5+3	1.7+3 (770 → 8.3+2)	4.5	✓	✓	4.5	5.8
141	70805	H3179	✓78.5	306.1	5.4	7	1.2+3	1.5+1						1.7+3	8.3+2		7.5-10		✓	4-7	11.2
142	70806	C3184	✓63.0	44.5	7-8	4.5	1.2+2							2.5+3	8.3+2		7-8		✓	7-8	4.4
	70806	P3186	✓43.5	325.0	6.7-8	4.3	1.5+2	1.5+1						6.7+4	8.3+3	8.3+2	5.7-8	✓	✓	5-10	6.1
	70806	B3187	✓11.8	285.6	6	3.6	1.1+2							2.5+4	8.3+3	8.3+2	6-7		✓	6-7	8.9
	70806	C3188	✓46.5	238.7	6.7	2.6	4.6+2	3.1+1						5.8+4	1.7+4	2.5+3	5-6.6		✓	6-7.5	11.9
	70806	B3189	✓58.9	186.0	7	2.1	3.1+1	1.5+1						4.7+4	2.5+3		6-7	✓	✓	5.7-7	15.1

EVENT	DATE	REJ	LAT	(E) LONG	L-VAL	MLT	j [#/cm² sr sec] 235	435	655	850	1.1	1.35	1.6	J (P/cm² sec) 80	150	350	Post L-VAL	1a	3s	L-VAL	11 (HRS) UT
143	70807	B3194 ✓	53.0	327.0	7-10	4.4	1.5+1							2.5+3			6.5-7		✓	6-11	5.7
	70807	H3195 ✓	44.0	290.4	6.8-7	3.6	1.5+2							1.7+4	2.5+3		6-7	✓	✓	6-7	8.4
	70807	C3196 ✓	45.9	245.8	6-6.5	2.8	1.5+2							8.3+4	1.7+4		5.5-7				11.4
	70807	G3197 ✓	58.9	193.0	7	2.1	1.2+2							4.2+4	8.3+3		5.9-7				14.6
	70807	B3198 ✓	64.7	144.3	7.8	2.5	1.5+2							1.7+4	7.5+3		6-8		✓	6-8	17.6
144	70808	B3203 ✓	44.4	297.2	6.8	3.7	1.2+2							8.3+3	2.5+3		6-6.5	✓	✓	6-8	8.0
145	70810	P3211 ✓	49.5	351.0	6	4.5	1.5+2	2.0+1						4.2+3			5.5	✓	✓	5.5-7	4.2
146	70810	B3223 ✓	63.3	120.7	5.7-8	3.0	1.5+2	1.2+1						2.5+4	8.3+2		5.5-8	✓	✓	5.5-8	19.1
147	70814	H3254 ✓	45.0	241.9	6.9	2.7	1.4+2	1.5+1						1.7+4	4.2+3		5.3-6.0	✓	✓	5.5-6.0	11.0
	70814	G3255 ✓	63.9	146.1	7	2.2	8.1+1							2.5+4	7.5+3		6-7		✓	7	17.2
148	70815	C3260 ✓	43.0	298.0	6.9	[illegible]	3.1+2	9.2+0						8.3+3	6.7+3		5.5-6	✓	✓	6	7.6
149	70818	C3285 ✓	43.3	274.2	[illegible]	2.9	7.6+1							8.3+3	1.7+3		6-6.6	✓	✓	7	9.1
	70818	C3286 ✓	57.0	225.0	5.5-8	[illegible]	1.5+1	1.5+1						1.7+3	1.7+3		6-7	✓	✓	5.5-8	12.1
	70818	B3287 ✓	43.0	[illegible]	[illegible]	[illegible]	4.6+1							1.7+4	3.3+3		6-8		✓	6-8	15.0
	70818	H3289 ✓	64.3	83.6	6.5	3.4	1.5+1							8.3+3	2.5+3		6-6.7		✓	6.5	21.2
150	70819	C3294 ✓	-28.1	2.0	8	4.3	1.5+1							4.2+3			8	✓	✓	8	7.3
	70819	C3294 ✓	42.5	280.9	6.3	3.0	4.6+1							8.3+3	1.7+3		6-6.4		✓	6	8.6
	70819	C3297 ✓	66.6	87.7	6.5-8	1.2	3.1+1	4.6+0						8.3+3	2.5+3		5.5-6	✓	✓	6.5-8	20.7
151	70820	H3304 ✓	51.0	239.1	7.8	2.0	1.4+2	1.5+1						2.5+3			6.5		✓	7.5	11.2
152	70826	B3353 ✓	43.5	238.0	5.5	2.1	4.6+1	2.0+1	1.3+1					8.3+3			5-5.5	✓	✓	4.5-7	11.1
153	70828	H3368 ✓	56.2	201.0	6.3	1.4	3.1+1							8.3+3			6	✓		6.3	13.2
154	70829	H3370 ✓	47.2	237.5	7	2.1	1.5+1							1.7+3			5.5-7.5		✓	7	9.6
155	70830	H3384 ✓	44.0	265.1	6.8	2.4	9.2+0							1.7+3			6.4	✓	✓	6.8	9.1
156	70902	C3413 ✓	60.3	56	5.5	2.8	9.2+0							1.7+4	4.2+3		6				22.5

							j (e/cm² s sr keV)							J (p/cm² s sr)							12.0
EVENT	DATE	REV	LAT	(E) LONG	L-VAL	MLT	835	435	655	850	1.1	1.35	1.6	80	150	350	80° P L-VAL	12	33	L-VAL	HRS UT
157	70909	I 3469	✓64.3	57.8	6.6	2.4	1.5+1							3.3+3			6				21.9
	70909	C 3472	✓60.8	343.5	6.9	3.3	3.1+1							1.1+5			6.9	✓	✓	6-6.5	.8
158	70910	H 3473	✓45	253.5	5.8-6	1.8	4.6+1							1.7+3			5.7	✓	✓	5.5-6	9.4
	(70910	G 3475	(2.0)																		
159	70910	P 3476	✓63.2	65.9	5.9	2.3	1.5+2	4.6+0						7.5+3	2.5+3		6		✓	6	21.4
160	70911	B 3481	✓41.7	262.2	5.5	1.95	1.1+2	6.1+0						8.3+3	2.5+3		5-5.5				8.8
	70911	C 3482	✓54.6	211.4	5.6-6	1.1	1.4+2	1.2+1						8.3+3	2.5+3		5-6	✓		5.5	11.9
	70911	H 3483	✓59.7	163.9	5	1.4	1.4+2	3.1+1						8.3+3	6.7+3		4.5-5	✓		4.5-5	14.9
	70911	G 3484	✓69.5	110.5	5.1-12	1.7	4.6+1	6.1+0						8.3+3	2.5+3		4.5-18	✓	✓	5-18	18.0
161	70912	B 3494	✓64.3	79.3	6	2	1.5+1							8.3+2			6				20.4
162	70913	B 3500	✓46.9	229.9	5.0	1.3	9.2+2	3.1+2	1.6+2	7.1+1				2.5+4	1.1+4	2.5+3	4.8-5	✓	✓	4.7-5.4	10.8
	70913	B 3500	✓-67.8	21.7	4.6-7	12	9.2+2			inner edge of the zone				2.5+3			7				11.9
163	70915	H 3515	✓48.4	243.7	6.1	1.3	7.6+1	1.5+1						8.3+4	8.3+3		5.5-15	✓	✓	5-11	9.8
	70915	H 3515	✓-65.5	38.6	5.9-7	11.5	9.2+2							NONE					✓	6-10	10.9
164	70918	P 3538	✓48.2	309.8	6.9	2.6	3.1+1							7.5+3			6		✓	6.9	5.2
165	70919	C 3546	✓46.0	274.3	6.6	1.8	1.5+1							8.3+2			6.6		✓	6.6	7.6
166	70919	I 3550	✓74.6	92.0	10-10.6	1.2	7.7+0							8.3+3	8.3+3		6.2-10		✓	6.2-9	19.6
167	70920	P 3553	✓43.8	326.8	4.5-5	2.7	6.1+2	6.1+1	8.2+0					2.5+4	8.3+3		4.3-5		✓	4	4.1
	70920	P 3553	✓-66.3	330.2	4.5-5	2.8	3.1+2	3.1+1	4.9+0					1.7+4	2.5+3		4-6		✓	4-6	5.5
	70920	C 3554	✓69.9	290.5	5.1	4.2	2.0+2	1.4+1						1.7+4	3.3+3		5		✓	5	8.4
	70920	H 3555	✓-78.0	10.0	5-6	4.9	1.5+3							2.5+3			6		✓	4-10	11.8
	70920	G 3556	✓63.8	182.7	6.6-25	0.1	3.1+1							7.5+3			4-8.5		✓	7	13.1
	70920	G 3556	✓51.5	188.1	5.2	4.4	4.6+2							5.0+3	8.3+2		4.5-56		✓	4.5-5.5	14.4
	70920	C 3557	✓59.1	142.1	4.3-5.6	1.3	6.1+2	4.6+1	6.5+0					2.5+4	2.5+3		4.1-4.8	✓	✓	4.1-4.8	16.0
	70920	C 3557	✓45.3	141.1	5.5-6	3.4	1.2+3							8.3+3			5-6		✓	5.5-6	17.5
	70920	I 3558	✓-46.6	97.7	5.4	1.7	3.1+1							1.7+4	2.5+3		4.5-5.5	✓	✓	5-6	20.4
	70920	P 3559	✓72.5	31.9	9.4	1.9	1.5+1							8.3+2	7.5+3		6-9	✓	✓	5-12	22.0
	70920	P 3559	✓-52.7	56.6	6.9	1.9	1.5+1							7.5+4	8.3+3		5.5-11	✓		5-6	23.2

EVENT	DATE	REV	LAT	(E) LONG	L-VAL	MLT	j [#/cm² s sr keV] 235	435	655	850	1.1	1.35	1.6	J [#/cm² s sr] 80	150	350	80°P L VAL	12	33	L-VAL	13 HRS UT
168	70921	B3561 ✓	52.5	330.0	5.5-12	2.6	1.5+2	4.6+0						8.3+3	8.3+2		5-18		✓	5-16	3.7
	70921	B3561 ✓	62.9	323.1	5.4	2.6	6.1+1	3.1+1						6.7+4	8.3+3		5-8	✓	✓	5-7	3.8
	70921	C3562 ✓	44.5	289.8	6.2	.1	6.1+1							7.5+4	8.3+3		5.5-14		✓	5.1-6	6.5
	70921	C3562 ✓	-78.1	316.8	6.2-8.4	4.2	1.2+2							8.3+4	8.3+3		4.5-8	✓	✓	5-8	7.8
	70921	P3563 ✓	-81.2	293.0	5.9	5.5	7.7+3							6.7+4	2.5+4	2.5+3	5.5-10		✓	4.5-9.5	10.7
	70921	B3564 ✓	-82.4	283.6	9.7	9.4	1.5+2							2.5+3			10.5-9		✓	5.6-11	13.6
	70921	P3565 ✓	63.6	146.4	5.1	1.0	1.1+2	3.1+1						8.3+3	6.7+3	2.5+3	4.5-5		✓	5	15.5
	70921	I3568 ✓	69.1	8.6	6-20	3.0	2.0+2							6.7+4	1.7+4		5-46	✓	✓	5-40	.4
	70922	P3569 ✓	55.0	336.1	6.3	2.6	6.1+3	1.5+2	2.1+1	7.1+0				4.2+4	1.7+4		6.5-7.5	✓	✓	4.3-25	2.2
	70922	P3569 ✓	70.5	182.7	7.0	14.6	1.5+2							3.3+4	1.7+4		5-12				3.6
	70922	P3569 ✓	-51.9	143.5	4.8	14.5	1.5+3							8.3+3	4.2+3		9-16		✓	5	4.1
	70922	P3569 ✓	-78.3	9.2	14	2.4	1.5+1							2.5+4	7.5+3		7-8		✓	7-12	4.3
	70922	N3570 ✓	41.5	298.7	5.4	2.1	1.5+2	1.5+1						2.5+3			5.4-6		✓	5.4	5.9
	70922	N3570 ✓	-73.0	311.0	6.3	3.5	1.5+1							8.3+3	6.7+3		5-6		✓	5-6	7.3
	(70922	N3572	12.0)																		
169	70922	G3573 ✓	60.2	156.5	4.8	.97	3.5+2	6.1+1	1.6+1					7.5+4	8.3+3		5-9	✓	✓	5	14.9
	70922	G3573 ✓	78.5	285.0	6.8-7	11.8	1.4+2							8.3+4	7.5+4	1.7+4	5-8		✓	4-5	15.9
	70922	G3573 ✓	-65.0	168.0	15	5.6	2.0+1							2.5+3	1.7+3	7.5+2	6-16		✓	5-16	16.1
170	70923	C3580 ✓	61.7	207.1	5.7	.6	1.4+2	6.1+1	1.6+1					2.5+4	1.7+4		5-5.8		✓	5.6	11.4
	70923	C3580 ✓	75.1	234.6	8-9	6.8	2.0+1							2.5+3	8.3+2		6-9		✓	4.5-10	12.6
	70923	G3581 ✓	65.2	160.1	5.3-6.3	.6	3.1+2	4.6+1	1.8+0					1.7+4	5.8+3		5-6.5		✓	5-6.5	14.4
	70923	G3581 ✓	-45.9	164.1	5.1	3.7	1.1+4							8.3+3			5-9		✓	5.5-5	15.8
	70923	B3583 ✓	68.9	112.1	6.5	1.0	4.6+1							6.7+4	2.5+4		5.5-6		✓	5-8	17.4
	70923	B3583 ✓	-42.9	118.7	5.8	2.8	6.1+1	1.2+1						2.5+4	8.3+3		5-6		✓	5.5-7.5	18.8
	70924	C3585 ✓	-64.3	358.9	5.9	2.0	3.1+1							8.3+3	5.8+3		5-5.5		✓	5-5.5	3.3
[illegible]	70924	H3589 ✓	67.4	165.6	6.7-7	.2	2.0+1							2.5+3			6-7		✓	7	13.9
	70924	B3590 ✓	74.0	105	6-12	.5	6.1+1							4.2+3	1.7+3		6-12		✓	6-12	16.9
	70925	C3598 ✓	60.1	355.7	6.2	2.5	6.1+1	7.7+0						8.3+3	2.5+3		5-6		✓	6-9	1.6
	[illegible]	[illegible]	[illegible]	[illegible]	6.9	.6	4.6+1							1.7+3			6.7		✓	7	16.3
	[illegible]	[illegible]	[illegible]	[illegible]	7.7-8	3.4	4.6+1							1.7+3			6		✓	7	17.6

AD-A092 545 AIR FORCE INST OF TECH WRIGHT-PATTERSON AFB OH F/G 4/1
RELATIVISTIC ELECTRON PRECIPITATION: AN OBSERVATIONAL STUDY.(U)
1980 L J ANDREOLI
UNCLASSIFIED AFIT-CI-80-260 NL

4 OF 4
AD
A092545

END
DATE
FILMED
1-81
DTIC

Appendix D - Computation of Electron and X-ray Energy Deposition Profiles

The precipitation of energetic electrons into the atmosphere is simulated by a finite difference numerical solution to the multi-dimensional Fokker-Planck diffusion equation developed by Walt et al. (1968). The technique was slightly modified to handle other than isotropic pitch angle distributions by Spjeldvik (1974) but this modification was not used here since the distribution over the downward hemisphere at 300 km is isotropic for all cases considered. The conversion of the Walt et al. (1968) program to the UCLA computer by Spjeldvik (1974), however, was used. Spjeldvik (1974) contains the computer listing.

The Walt program solves the following final version of the Fokker-Planck equation as derived by Chappell (1968):

$$\cos\alpha \frac{\partial}{\partial s}\left(\frac{f}{r}\right) = -\frac{3}{2}\frac{\sin\alpha}{R_E L}\frac{\partial}{\partial\alpha}\left(\frac{f}{r}\right) + \frac{(E+1)^2 2\pi}{E^2(E+2)^2}\left(\frac{q^2}{m_e c^2}\right)^2 \sum_i n_i Z_i^2 \ln \eta_i^{-1} \frac{1}{\sin\alpha}\frac{\partial}{\partial\alpha}\left[\sin\alpha \frac{\partial}{\partial\alpha}\left(\frac{f}{r}\right)\right] + \frac{2(E+1)}{E^{1/2}(E+2)^{1/2}}\frac{\partial}{\partial E}\left[\frac{(E+1)2\pi}{E^{1/2}(E+2)^{1/2}}\left(\frac{q^2}{m_e c^2}\right)^2 \sum_i n_i Z_i \ln \sigma_i \left(\frac{f}{r}\right)\right],$$

where Table D-1 defines the symbolism. Notice that the stochastic averages $\langle (\Delta E)^2 \rangle$, $\langle (\Delta\alpha\Delta E) \rangle$, and $\langle (\Delta E \Delta r) \rangle$ (small) and higher order terms have been eliminated. Steady state ($\frac{\partial f}{\partial t} = 0$) is assumed since precipitation is steady on times scales much longer than atmospheric transit times for precipitating electrons. Also, radial

Table D-1 Nomenclature (Spjeldvik, 1974)

f = electron distribution function averaged over cyclotron phase

t = time

c = speed of light

R_E = radius of the Earth

L = L-value, field line equatorial distance in units of R_E

E = electron energy in rest mass units

α = local pitch angle

α_o = equatorial pitch angle

r = electron gyro radius

s = length along the field line

q = electron charge

m_e = electron mass

e = the natural logarithm base, 2.7182...

n_i = number density of atmospheric species i

Z_i = atom number of atmospheric species i

l_i = average excitation potential of atmospheric species i

η_i = minimum scattering angle corresponding to maximum impact parameter (for thermal plasma, the Debye-length; for the neutral atmosphere, the atomic radius)

σi = $(e\ (E+2)/l_i)^{1/2}$

$\langle\ \rangle$ denotes stochastic ensemble average.

diffusion is ignored ($\frac{f}{r}$ = constant).

The program outputs the amount of average energy deposited per unit volume at each altitude below the incident altitude. Also, assuming an average of 35 eV is required to produce each ion pair, the rate of ion pair production is output versus altitude.

The complete altitude profile of energy deposition by bremsstrahlung is computed from the Berger, Seltzer, Maeda (1974) Monte Carlo simulation method. This work is essentially an extension of the earlier (Berger, Seltzer, Maeda, 1970; Berger and Seltzer, 1972) Monte Carlo simulation methods by this same group. Basically, a computation is made of 10,000 electron trajectories for each incident electron energy from 2 keV to 2 MeV for electrons injected into the atmosphere at 300 km altitude. The trajectories are histories of individual primary and secondary electrons as they coulomb scatter (elastic by nuclei collisions, inelastic by orbital electron collisions) off neutral constituents and deposit energy at various altitudes. In addition, the production of bremsstrahlung quanta in these interactions and their Compton scattering and consequent photoelectron absorption of the bremsstrahlung quanta in the atmosphere is followed. The Berger, Seltzer, Maeda (1974) results of energy deposition as a function of atmospheric depth (mass thickness) by bremsstrahlung from monoenergetic incident electron beams for wide-area precipitation flux isotropic over the downward hemisphere is given in Table D-2 in the form of energy deposited per unit mass thickness (ev/g cm^{-2}) per incident electron energy. From this

TABLE D-2. Energy deposition function for Bremsstrahlung, for the case of uniform wide-area precipitation of an electron flux isotropic over the downward hemisphere. The quantity given is A_{BR} (Z_m/T_o), in units of cm^2gm^{-1}. Number in parenthesis indicates powers of ten. (Berger, Seltzer, Maeda, 1974)

z_m/T_e (g cm^{-2} keV^{-1})	2000	1000	500	200	100	50	20	10	5	2
					T_e (keV)					
					$A_{br}(z)/T_e$, cm^2/g					
2·0(−6)	6·3(−4)									
4·0	7·6	1·0(−3)								
8·0	8·4	1·1	2·2(−3)							
2·0(−5)	9·3	1·2	2·4	5·0(−3)						
4·0	9·9	1·3	2·5	5·3	1·1(−2)					
8·0	1·1(−3)	1·4	2·5	5·0	7·0(−3)	7·3(−3)				
2·0(−4)	1·1	1·2	1·6	1·8	1·7	2·2	3·4(−3)			
4·0	6·8(−4)	5·5(−4)	5·2(−4)	6·5(−4)	8·4(−4)	1·1	1·7	2·0(−3)		
8·0	4·5	3·2	2·8	3·3	4·4	5·7(−4)	8·0(−4)	8·8(−4)	7·2(−4)	
2·0(−3)	2·9	1·9	1·5	1·5	1·9	2·3	3·0	2·7	1·4	8·6(−6)
4·0	1·9	1·3	9·9(−5)	8·8(−5)	1·0	1·1	1·3	9·4(−5)	3·3(−5)	5·1(−7)
8·0	9·2(−5)	8·3(−5)	6·5	5·2	5·4(−5)	5·4(−5)	5·7(−5)	2·8	5·2(−6)	
2·0(−2)	1·7	2·8	2·8	2·4	2·3	2·0	1·6	3·0(−6)	1·1(−7)	
4·0	1·2(−6)	5·5(−6)	9·5(−6)	1·1	1·1	8·3(−6)	5·3(−6)	3·3(−7)		
8·0		2·4(−7)	1·5	3·8(−6)	3·0(−6)	2·6	5·7(−7)	3·0(−8)		
2·0(−1)			6·0(−9)	1·7(−7)	5·4(−7)	3·1(−7)	2·9(−8)			
4·0				5·0(−9)	2·4(−8)	2·8(−8)				

starting point, we proceeded to work towards the final product, a profile of ion pair production by bremsstrahlung from an incident electron energy spectrum.

The CIRA (1965) reference atmosphere, Fig. D-1, was used to scale atmospheric depth to a representative altitude. The same reference atmosphere was used to compute the atmospheric density (g/cm^3) versus altitude (km). At each altitude the density was multiplied by the energy deposition function A_{BR}[keV/g cm^{-2}], to yield the stopping ratio, BR[keV/cm, column], normalized to an incident electron of a given incident energy (To). The resulting column stopping ratios, Br (altitude), are listed in Table D-3 and graphically represented in Fig. D-2. Due to the irregularity of the curves and diminishing contribution compared to electron production above 50 km in Fig. D-2, only value below 50 km were considered. For every 5 km of altitude between 15 and 50 km (inclusive), a linear (log-log) interpolation of incident electron energy (To) versus column stopping ratio of Bremsstrahlung photons was constructed. For example, at 15 km altitude, $Br = 10^x$ where x = 1.018342561 log To (keV) - 11.85638142 for initial energies To between 200-500 keV.

A computer program using the linear (log-log) interpolation curves as described above was written to calculate the production of ion pairs versus altitude for an input electron differential energy spectrum isotropic over downward hemisphere at 300 km by solving the equation

$$\text{Prod}_{IP}(\text{alt}) = \frac{1}{EMI} \iint Br \cdot \text{Dif}(E) \cdot d\Omega d\, E$$

FIG D-1. CIRA Reference Atmosphere of depth versus altitude (1965).

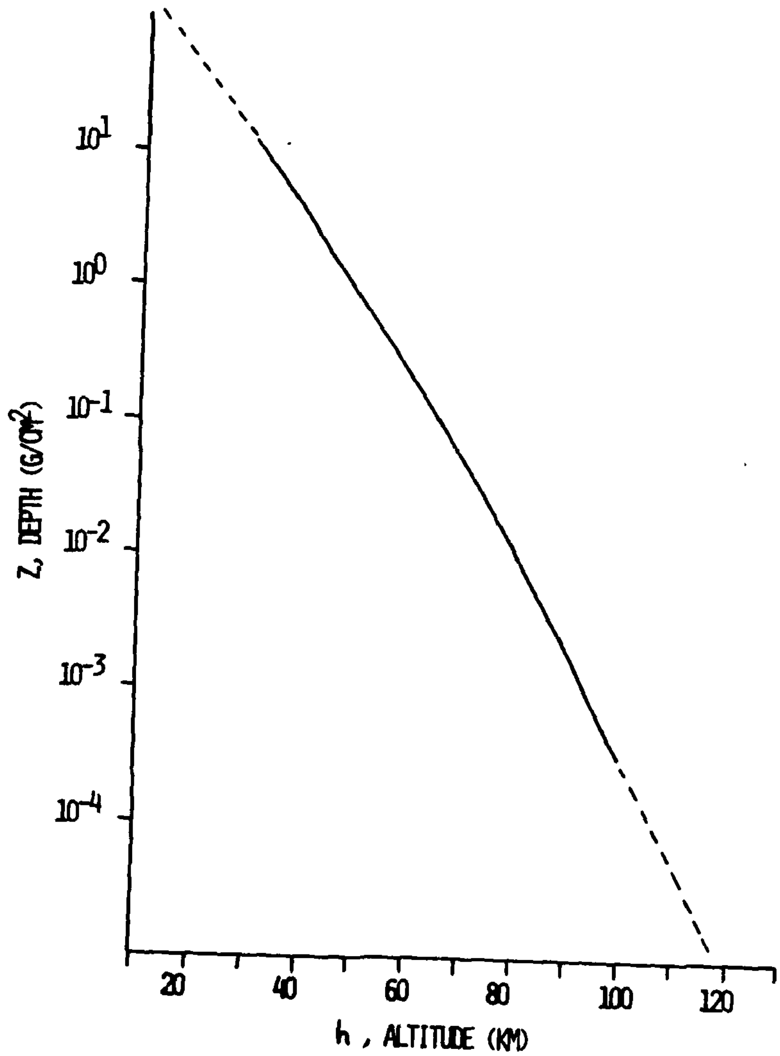

Z, DEPTH (G/CM^2)
10^1
10^0
10^{-1}
10^{-2}
10^{-3}
10^{-4}
20
40
60
80
100
120
h , ALTITUDE (KM)

TABLE D-3. B_r(keV/cm, column), stopping ratio, versus altitude for given incident electron energies.

h (KM)	T_0 (KEV) 2000	1000	500	200	100	50	20	10	5	2
86	8.9 (-9)	6.3 (-9)	6.9 (-9)	6.3 (-9)	6.9(-9)	2.3(-9)	4.8 (-10)	1.2 (-10)	2.3 (-11)	1.1 (-13)
82	1.9 (-8)	1.4 (-8)	1.5 (-8)	1.4 (-8)	1.0 (-8)	1.4 (-9)	4.3 (-10)	1.1 (-10)	8.9 (-12)	1.3 (-14)
77	4.2 (-8)	3.0 (-8)	3.1 (-8)	2.5 (-8)	4.3(-9)	1.4(-9)	4.0 (-10)	6.8(-11)	4.1 (-12)	
72	1.2(-7)	8.1 (-8)	7.8 (-8)	2.2 (-8)	5.2 (-9)	1.8 (-9)	3.7 (-10)	5.8 (-11)	1.6 (-12)	
67	2.5 (-7)	1.8 (-7)	1.0 (-7)	1.6 (-8)	5.5 (-9)	1.4 (-9)	3.3 (-10)	3.5 (-11)	6.9 (-14)	
62	5.4 (-7)	2.9 (-7)	6.3 (-8)	1.6 (-8)	4.6 (-9)	1.3 (-9)	2.8 (-10)	7.3 (-12)		
56	1.1 (-6)	2.8 (-7)	7.2 (-8)	1.6 (-8)	5.2 (-9)	1.4 (-9)	1.5 (-10)	2.0 (-12)		
50	1.4 (-6)	2.3 (-7)	7.8 (-8)	1.8(-8)	5.6 (-9)	1.0 (-9)	6.9 (-11)	4.1 (-13)		
45	1.8 (-6)	3.9 (-7)	1.0 (-7)	2.1 (-8)	4.7 (-9)	8.5 (-10)	2.3 (-11)			
38	3.2 (-6)	7.1 (-7)	1.8 (-7)	2.6 (-8)	6.0 (-9)	7.1 (-10)	3.2 (-12)			
33	4.4 (-6)	9.5 (-7)	1.6 (-7)	2.5 (-8)	4.5 (-9)	1.8 (-10)				
27	5.2 (-6)	7.9 (-7)	1.3 (-7)	2.1 (-8)	1.5 (-9)	4.0 (-11)				
20	3.2 (-6)	5.8 (-7)	7.1 (-8)	3.2 (-9)	2.3 (-10)					
14	6.2 (-7)	6.2 (-8)	7.7 (-10)	3.0 (-10)						

B_r (KEV/CM, COLUMN)

FIG D-2. $B_r(\mathfrak{z},E)$ versus altitude.

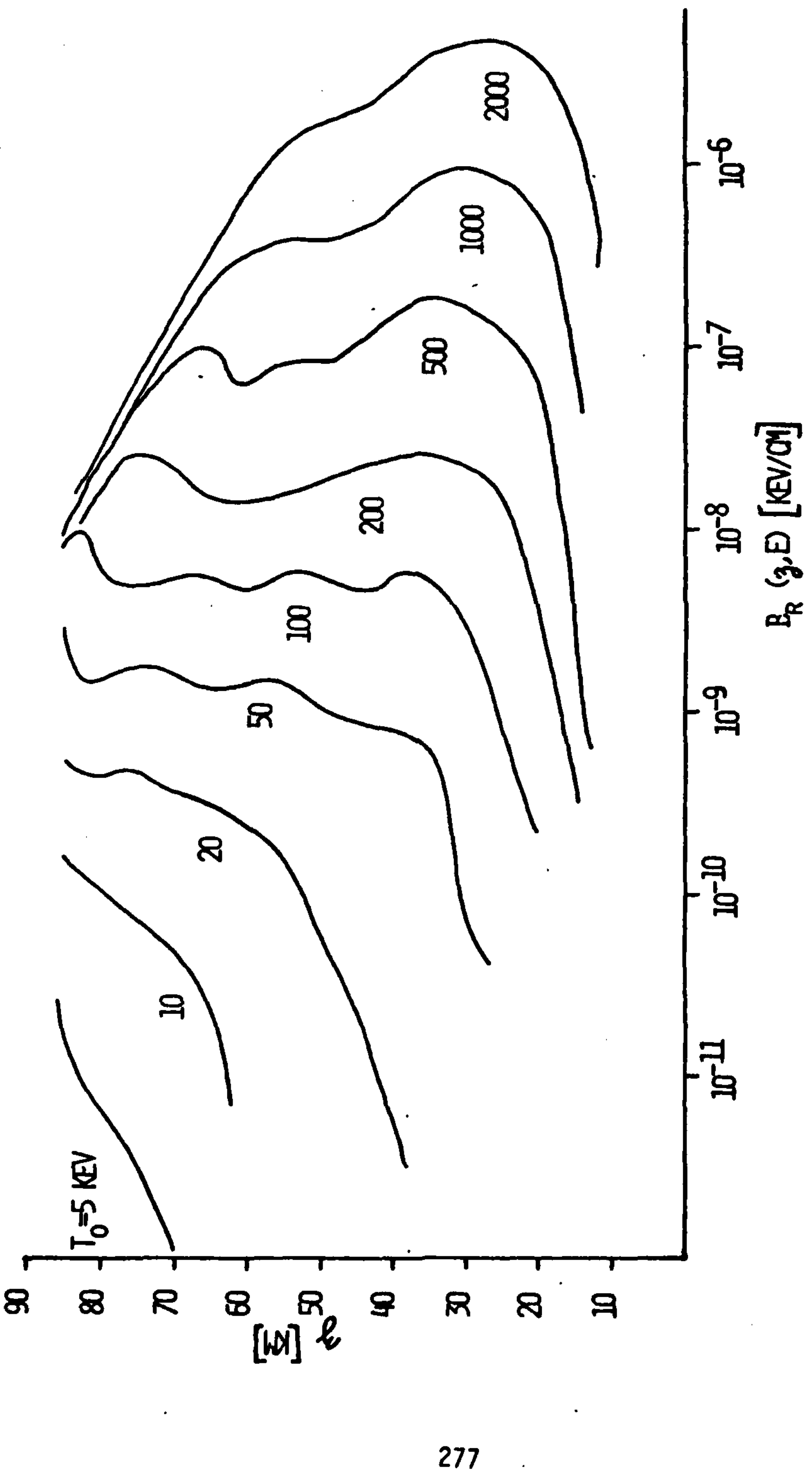

T_0=5 KEV
10
20
50
100
200
500
1000
2000
10^{-11}
10^{-10}
10^{-9}
10^{-8}
10^{-7}
10^{-6}
B_R (z,E) [KEV/CM]
90
80
70
60
50
40
30
20
10
z [KM]

where EMI = average minimum ionizing energy taken here to be 35 eV.

Dif (E) = differential electron flux at 300 km [$\#/cm^2$ sec str keV]

$d\Omega$ = solid angle $\simeq 2\pi$ here

dE = 1 keV intervals

Prod (alt) = ion pair production rate at each altitude [$\#/cm^3$ sec]

Also output is the total energy (keV) deposited at each altitude per (cm^3 str sec). The computer listing follows:

TABLE D-4. Bremsstrahlung deposition computer listing.

```
C*********************************************************************************
C                                                                               C
C   THIS PROGRAM CALCULATES THE ALTITUDE VS ENERGY DEPOSITION PROFILE FOR A     C
C   GIVEN PRECIPITATING ELECTRON SPECRUM.  THE ENERGY DEPOSITION FUNCTION,      C
C   BR, IS OBTAINED FROM THE BERGER, SELTZER, AND MAEDA (JATP, 1974, 36, 591)   C
C   FULL MONTE CARLO CALCULATIONS FOR UNIFORM WIDE AREA PRECIPITATION OF AN     C
C   ELECTRON FLUX ISOTROPIC OVER THE DOWNWARD HEMISPHERE.  ATMO DEPTH VS ALT    C
C   IS OBTAINED FROM CIRA, 1965 (MEAN STRUCTURE).                               C
C                                                                               C
C*********************************************************************************
      DIMENSION E(2000), DIF(2000)
C
C     INPUT - NUMBER OF DATA SETS  .
C
      READ (5,2) NDATA
    2 FORMAT (I2)
C
C     INPUT - DIFFERENTIAL ELECTRON FLUX (#/LL TSE) 10,20, 50, 100, 200, 500,
C             1000, 2000 KEV RESPECTIVELY.
C
    1 READ (5,10) DIF(1), DIF(11), DIF(41), DIF( 91), DIF(191), DIF(491)
     1, DIF(991), DIF(1991)
   10 FORMAT (8E10.5)
C
C     ENERGY, E, FROM 10 TO 2000 KEV
C
      DO 11 J=1,1991
   11 E(J)= 10.+ (J-1)
C
C     DIFFERENTIAL FLUX SPECTRUM IS GENERATED BY LINEAR FIT (ON LOG-LOG PLOT)
C     BETWEEN INPUT VALUES FROM ABOVE.
C
      DO 50 I=1,1991
      IF (I.GT.991.AND.I.LT.1991)  GO TO 61
      IF (I.GT.491.AND.I.LT. 991)  GO TO 59
      IF (I.GT.191.AND.I.LT. 491)  GO TO 57
      IF (I.GT. 91.AND.I.LT. 191)  GO TO 55
      IF (I.GT. 41.AND.I.LT.  91)  GO TO 53
      IF (I.GT. 11.AND.I.LT.  41)  GO TO 51
      IF (I.GT.  1.AND.I.LT.  11)  GO TO 47
      GO TO 50
   47 IF (DIF(1).NE.DIF(11)) GO TO 48
      DIF(I)=DIF(1)
      GO TO 50
   48 YARG=ALOG10((DIF(11))/DIF(1))
      XARG=ALOG10((E(11))/(E(1)))
      Y=ALOG10(DIF(1))
      X=ALOG10(E(1))
      GO TO 99
   51 IF (DIF(11).NE.DIF(41)) GO TO 52
      DIF(I)=DIF(11)
      GO TO 50
   52 YARG=ALOG10((DIF(41))/(DIF(11)))
      XARG=ALOG10((E(41))/(E(11)))
```

```
      Y=ALOG10(DIF(11))
      X=ALOG10(E(11))
      GO TO 99
   53 IF (DIF(41).NE.DIF(91)) GO TO 54
      DIF(I)=DIF(41)
      GO TO 50
   54 YARG=ALOG10((DIF(91))/(DIF(41)))
      XARG=ALOG10((E(91))/(E(41)))
      Y=ALOG10(DIF(41))
      X=ALOG10(E(41))
      GO TO 99
   55 IF (DIF(91).NE.DIF(191)) GO TO 56
      DIF(I)=DIF(91)
      GO TO 50
   56 YARG=ALOG10((DIF(191))/(DIF(91)))
      XARG=ALOG10((E(191))/(E(91)))
      Y=ALOG10(DIF(91))
      X=ALOG10(E(91))
      GO TO 99
   57 IF (DIF(191).NE.DIF(491)) GO TO 58
      DIF(I)=DIF(191)
      GO TO 50
   58 YARG=ALOG10((DIF(491))/(DIF(191)))
      XARG=ALOG10((E(491))/(E(191)))
      Y=ALOG10(DIF(191))
      X=ALOG10(E(191))
      GO TO 99
   59 IF (DIF(491).NE.DIF(991)) GO TO 60
      DIF(I)=DIF(491)
      GO TO 50
   60 YARG=ALOG10((DIF(991))/(DIF(491)))
      XARG=ALOG10((E(991))/(E(491)))
      Y=ALOG10(DIF(491))
      X=ALOG10(E(491))
      GO TO 99
   61 IF (DIF(1991).NE.DIF(991)) GO TO 62
      DIF(I)=DIF(991)
      GO TO 50
   62 YARG=ALOG10((DIF(1991))/(DIF(991)))
      XARG=ALOG10((E(1991))/(E(991)))
      Y=ALOG10(DIF(991))
      X=ALOG10(E(991))
   99 Z=ALOG10(E(I))
      DIF(I)=10**(((YARG/XARG)*(Z-X))+Y)
   50 CONTINUE
C
C     PERFORM INTEGRAL OF BR*DIF*DE AT EACH 5 KM ALTITUDE FROM 15 TO 50 KM.
C
      WRITE(6,13)
   13 FORMAT(1H1,10X,8HALTITUDE,6X,4HFLUX,13X,4HPROD / 13X,4H(KM),8X,8H
     1(E/LLLST),8X,9H(1/LLLT))
      Z=50.
  100 IF (Z.EQ.15.) GO TO 240
      IF (Z.EQ.20.) GO TO 230
```

```
      IF (Z.EQ.25.) GO TO 205
      IF (Z.EQ.30.) GO TO 185
      IF (Z.EQ.35.) GO TO 165
      IF (Z.EQ.40.) GO TO 145
      IF (Z.EQ.45.) GO TO 125
      TOTAL=0.0
      DO 70 I=1,1991
      IF (I.GT.91) GO TO 110
      X= 2.736669403*ALOG10(E(I))-13.72349432
      GO TO 120
  110 IF (I.GT.491) GO TO 115
      X= 1.534787611*ALOG10(E(I))-11.51973073
      GO TO 120
  115 X= 2.330286123*ALOG10(E(I))-12.74010386
  120 BR=10.**X
      XRAY=DIF(I)*BR
      TOTAL=TOTAL+XRAY
   70 CONTINUE
      GO TO 900
  125 TOTAL=0.0
      DO 71 I=11,1991
      IF (I.GT.41.) GO TO 130
      X= 3.923061797*ALOG10(E(I))-15.73833848
      GO TO 140
  130 IF (I.GT.191.) GO TO 135
      X= 2.323664191*ALOG10(E(I))-13.02100989
      GO TO 140
  135 X= 1.93720917*ALOG10(E(I))-12.1317653
  140 BR=10.**X
      XRAY=DIF(I)*BR
      TOTAL=TOTAL+XRAY
   71 CONTINUE
      GO TO 900
  145 TOTAL=0.0
      DO 72 I=11,1991
      IF(I.GT.41.) GO TO 150
      X= 5.331195138*ALOG10(E(I))-18.13209481
      GO TO 160
  150 IF (I.GT.91.) GO TO 155
      X= 2.907532307*ALOG10(E(I))-14.0653287
      GO TO 160
  155 X= 2.072102793*ALOG10(E(I))-12.38446027
  160 BR=10.**X
      XRAY=DIF(I)*BR
      TOTAL=TOTAL+XRAY
   72 CONTINUE
      GO TO 900
  165 TOTAL=0.0
      DO 73 I=41,1991
      IF (I.GT.91.) GO TO 170
      X= 3.886467478*ALOG10(E(I))-16.08185426
      GO TO 180
  170 IF (I.GT.191.) GO TO 175
      X= 2.174702312*ALOG10(E(I))-13.06232314
```

```
      GO TO 180
  175 X= 2.196634192*ALOG10(E(I))-12.64791196
  180 BR=10 **X
      XRAY=DIF(I)*BR
      TOTAL=TOTAL+XRAY
   73 CONTINUE
      GO TO 900
  185 TOTAL=0.0
      DO 74 I=41,1991
      IF (I.GT.91.) GO TO 187
      X= 4.787270676*ALOG10(E(I))-18.09799954
      GO TO 200
  187 IF (I.GT.191.) GO TO 190
      X= 2.96045826*ALOG10(E(I))-14.44437471
      GO TO 200
  190 IF (I.GT.491.) GO TO 195
      X= 2.[illegible]9319926*ALOG10(E(I))-12.25577687
      GO TO 200
  195 X= 2.510322759*ALOG10(E(I))-13.60796849
  200 BR=10 **X
      XRAY=DIF(I)*BR
      TOTAL=TOTAL+XRAY
   74 CONTINUE
      GO TO 900
  205 TOTAL=0.0
      DO 75 I=91,1991
      IF (I.GT.191.) GO TO 210
      X= 3.915288047*ALOG10(E(I))-16.57187825
      GO TO 220
  210 IF (I.GT.491.) GO TO 215
      X= 2.110124616*ALOG10(E(I))-12.64594502
      GO TO 220
  215 X= 2.683161107*ALOG10(E(I))-14.19255332
  220 BR=10 **X
      XRAY=DIF(I)*BR
      TOTAL=TOTAL+XRAY
   75 CONTINUE
      GO TO 900
  225 TOTAL=0.0
      DO 76 I=91,1991
      IF (I.GT.491.) GO TO 230
      X= 3.369323442*ALOG10(E(I))-16.78530779
      GO TO 235
  230 X= 2.75125017*ALOG10(E(I))-14.5773525
  235 BR=10**X
      XRAY=DIF(I)*BR
      TOTAL=TOTAL+XRAY
   76 CONTINUE
      GO TO 900
  240 TOTAL=0.0
      DO 77 I=191,1991
      IF (I.GT.491.) GO TO 245
      X= 1.018342561*ALOG10(E(I))-11.85638142
      GO TO 255
```

```
  245 IF (I.GT.991.) GO TO 250
      X= 6.321928C95*ALOG10(E(I))-26.17359969
      GO TO 255
  250 X= 3.321928095*ALOG10(E(I))-17.17059969
  255 BR=10.**X
      XRAY=DIE(I)*BR
      TOTAL=TOTAL+XRAY
   77 CONTINUE
      GO TO 900
C
C     ION PAIR PRODUCTION, PROD, CALCULATED BY MULTIPLYING TOTAL BY 2 PI, 1000
C     KEV, AND DIVIDING BY 35 EV.
C
  900 PROD=(TOTAL*2.*3.1415927*1000./35.
      WRITE (6,14) Z, TOTAL, PROD
   14 FORMAT (12X, F4.1, 7X, E11.6, 8X, F7.2)
      Z=Z-5.
      IF (Z.GE.15.) GO TO 100
      NDATA=NDATA - 1
      IF(NDATA.EQ.0) STOP
      GO TO 1
C*****************************************************************************
C*****************************************************************************
      END
```

OUT PUT EXAMPLE

ALTITUDE (KM)	FLUX (E/LLLST)	PROD (1/LLLT)
50.0	.628105E-01	11.28
~~45.0~~	~~.463892E-01~~	~~8.33~~
40.0	.412F86E-01	7.41
35.0	.179980E-01	3.23
30.0	.853777E-02	1.53
~~25.0~~	~~.912803E-03~~	~~0.16~~
20.0	.170287E-03	0.03
15.0	.443316E-06	0.00

Bibliography

Aikin, A. C. and S. J. Bauer, The Ionosphere, in Introduction to Space Science, edited by W. N. Hess, p. 161, Gordon and Breach, N. Y., 1965.

Anderson, R. R. and K. Maeda, Explorer 45 plasma measurements, J. Geophys. Res., 82, 135, 1977.

Ansari, Z. A., A peculiar type of daytime absorption in the auroral zone, J. Geophys. Res., 70, 3117, 1965.

Ashour-Abdalla, M. and R. M. Thorne, The importance of electrostatic ion-cyclotron instability for quiet-time proton auroral precipitation, Geophys. Res. Ltrs., 4, 1977.

Ashour-Abdalla, M. and C. F. Kennel, Nonconvective electron cyclotron harmonic instabilities, J. Geophys. Res., 83, 1531, 1978.

Ashour-Abdalla, M. and R. M. Thorne, Toward a unified view of diffuse auroral precipitation, 83, 4755, 1978.

Bailey, D. K. and M. A. Pomerantz, Relativistic electron precipitation into the mesosphere at subauroral latitudes, J. Geophys. Res., 70, 5823, 1965.

Bailey, D. K., M. A. Pomerantz, K. W. Sullivan and C. C. Taieb, Characteristics of precipitated electrons inferred from ionospheric forward scatter, J. Geophys. Res., 71, 5179, 1966.

Bailey, D. K., Some quantitative aspects of electron precipitation in and near the auroral zone, Rev. Geophys., 6, 289, 1968.

Bailey, D. K., R. R. Brown and M. H. Rees, Simultaneous forward-scatter, riometer, and Bremsstrahlung observations of a daytime electron precipitation event in the auroral zone, J. Atmos. Terr. Phys., 32, 149, 1970.

Barcus, J. R. and T. J. Rosenberg, Energy spectrum for auroral-zone X-rays, 1, Diurnal and type effects, J. Geophys. Res., 71, 803, 1966.

Berger, M. J., S. M. Seltzer and K. Maeda, Energy deposition by auroral electrons in the atmosphere, J. Atmos. Terr. Phys., 32, 1015, 1970.

Berger, M. J. and S. M. Seltzer, Bremsstrahlung in the atmosphere, J. Atmos. Terr. Phys., 34, 85, 1972.

Berger, M. J., S. M. Seltzer and K. Maeda, Some new results on electron transport in the atmosphere, J. Atmos. Terr. Phys., 36, 591, 1974.

Bewersdorff, A., G. Kremser, J. Stadsnes, H. Trefall and S. Ullaland, Simultaneous balloon measurements of auroral X-rays during slowly varying ionospheric absorption events, J. Atmos. Terr. Phys., 30, 591, 1968.

Blake, D. and R. S. Lindzen, Effect of photochemical models on calculated equilibria and cooling rates in the stratosphere, Mon. Wea. Rev., 10, 783, 1973.

Bossen, M., R. L. McPherron and C. T. Russell, A statistical study of PC 1 magnetic pulsations at synchronous orbit, J. Geophys. Res., 81, 6083, 1976.

Brown, R. R., A study of slowly varying and pulsating ionospheric absorption events in the auroral zone, J. Geophys. Res., 69, 2315, 1964.

Brown, J. W. and E. C. Stone, High energy electron spikes at high latitudes, J. Geophys. Res., 77, 3384, 1972.

Burton, R. K. and R. E. Holzer, The origin and propagation of chorus in the outer magnetosphere, J. Geophys. Res., 79, 1014, 1974.

Chapman, S. A., A theory of upper atmospheric ozone, Quart. J. Roy. Met. Soc., 3, 103,

Chappell, C. R., K. K. Harris and C. W. Sharp, The morphology of the bulge of the plasmasphere, J. Geophys. Res., 75, 3848, 1970.

Chappell, C. R., Detached plasma regions in the magnetosphere, J. Geophys. Res., 79, 1861, 1974.

Cornwall, J. M., Scattering of energetic trapped electrons by very low-frequency waves, J. Geophys. Res., 69, 1251, 1964.

Cornwall, J. M., Cyclotron instabilities and electromagnetic emission in the ultralow frequency and very low frequency ranges, J. Geophys. Res., 70, 61, 1965.

Cornwall, J. M., F. V. Coroniti and R. M. Thorne, Turbulent loss of ring current protons, J. Geophys. Res., 75, 4699, 1970.

Coroniti, F. V., R. W. Fredericks and R. White, Instability of ring current protons beyond the plasmapause during injection events, J. Geophys. Res., 77, 6243, 1972.

Crutzen, P. J. and C. J. Howard, The effect of the HO_2+NO reaction rate constant on one-dimensional model calculations of stratospheric ozone perturbations, Pure and Applied Geophys., 116, 497, 1978.

Crutzen, P. J., Private communication, 1980.

Davis, D. D., J. T. Herron and R. E. Huie, Absolute rate constants for reaction $O(^3P) + NO_2 \rightarrow NO + O_2$ over the temperature range 230^o-339^oK, J. Chem. Phys., 58, 530, 1973.

DeForest, S. E. and C. E. McIlwain, Plasma clouds in the magnetosphere, J. Geophys. Res., 76, 3587, 1971.

DeVore, J. G., Photochemical damping and mesospheric circulation, Master's Degree Thesis, Department of Atmospheric Sciences, UCLA 1977.

Dunckel, N. and R. A. Helliwell, Whistler-mode emissions on the OGO-1 satellite, J. Geophys. Res., 74, 6371, 1969.

Dungey, J. W., Loss of Van Allen electrons due to whistlers, Planet. Space Sci., 11, 591, 1963.

Frank, L. A., A survey of electrons E > 40 keV beyond 5 earth radii with Explorer 14, J. Geophys. Res., 70, 1593, 1965.

Fredericks, R. W. and F. L. Scarf, Recent studies of the magnetospheric electric field emissions about the electron gyrofrequency, J. Geophys. Res., 78, 310, 1973.

Gunton, R. C., R. E. Meyeroff and J. B. Reagan, Ion and neutral chemistry of the D-region during intense solar particle events of August 1972, Lockheed Report D556351, 1977.

Gurnett, D. A., G. W. Pfeiffer, R. A. Anderson, S. R. Mosier and D. P. Cauffman, Initial observations of VLF electric and magnetic fields with the Injun 5 satellite, J. Geophys. Res., 74, 4631, 1969.

Gurnett, D. A. and L. A. Frank, A region of intense plasma wave turbulence on auroral field lines, J. Geophys. Res., 82, 1031, 1977.

Heaps, M. G., The effect of a solar proton event on the minor neutral constituents of the summer polar mesosphere, U.S. Army Atmospheric Sci. Laboratory Report ASL-TR-0012, 1978.

Hones, E. W. Jr., S. Singer, L. J. Lanzerotti, J. D. Pierson and T. J. Rosenberg, Magnetospheric substorm of August 25-26, 1967, J. Geophys. Res., 76, 2977, -971.

Herron, J. T. and R. E. Huie, The reaction between NO and O, Chemical Kinetics Data Survey, N.B.S. Report 19828, National Bureau of Standards, U.S. Dept. of Commerce, Gaithersberg, Md., 108, 1972.

Imhoff, W. L., E. E. Gaines and J. B. Reagan, Dynamic variations in intensity and energy spectra of electrons in the inner radiation belt, J. Geophys. Res., 78, 4568, 1973.

Imhoff, W. L., G. H. Nakano, R. G. Johnson and J. B. Reagan, Satellite observations of Bremsstrahlung from widespread energetic electron precipitation events, J. Geophys. Res., 79, 565, 1974.

Imhoff, W. L., G. L. Nakano, E. E. Gaines and J. B. Reagan, A coordinated two-satellite study of energetic electron precipitation events, J. Geophys. Res., 80, 1975.

Imhoff, W. L., G. H. Nakano and J. B. Reagan, Satellite observations of impulsive Bremsstrahlung X-ray events associated with substorms, J. Geophys. Res., 83, 4237, 1978.

Jelly, D. and N. Brice, Changes in Van Allen radiation associated with polar substorms, J. Geophys. Res., 72, 5919, 1967.

Johannesen, A. and D. Krankowski, Positive-ion composition measurement in the upper mesosphere and lower thermosphere at high latitude during summer, J. Geophys. Res., 77, 2888, 1972.

Kaye, S. M., M. G. Kivelson and D. J. Southwood, Evolution of ion cyclotron instability in the plasma convection system of the magnetosphere, J. Geophys. Res., 84, 6397, 1979.

Kennel, C. F. and N. E. Petschek, Limit on stably trapped particle flux, J. Geophys. Res., 71, 1, 1966.

Kennel, C. F. and R. M. Thorne, Unstable growth of unducted whistlers propagating at an angle to the geomagnetic field, J. Geophys. Res., 72, 871, 1967.

Kennel, C. F., Consequences of a magnetospheric plasma, Rev. Geophys., 7, 379, 1969.

Kennel, C. F., F. L. Scarf, R. W. Fredericks, J. H. McGehee and F. V. Coroniti, VLF electric field observations in the magnetosphere, J. Geophys. Res., 75, 6136, 1970.

Kindel, J. M. and C. F. Kennel, Topside current instabilities, J. Geophys. Res., 76, 3055, 1971.

Kintner, P. M., M. C. Kelley and F. S. Mozer, Electrostatic hydrogen cyclotron waves near the one earth radius altitude in the polar magnetosphere, Geophys. Res. Ltrs., 5, 139, 1978.

Kintner, P. M., M. C. Kelley, R. D. Sharp, A. G. Ghielmeth, M. Temerin, C. Cattell, P. F. Mizera and J. F. Fennell, Simultaneous observations of energetic (keV) upstreaming and electrostatic hydrogen cyclotron waves, J. Geophys. Res., 84, 7201, 1979.

Kivelson, M. G., C. T. Russell, K. W. Chan and C. R. Chappell, An investigation of regions of high density cold plasma in the outer magnetosphere (Abstract), EOS Trans AGU, 53, 1103, 1972.

Koons, H. C., A. L. Vampola and D. A. McPherson, Strong pitch-angle scattering of energetic electrons in the presence of electrostatic waves above the ionospheric trough region, J. Geophys. Res., 77, 1771, 1972.

Kurth, W. W., M. M. Baumback and D. A. Gurnett, Direction-finding measurements of auroral kilometric radiation, J. Geophys. Res., 80, 2764, 1975.

Larsen, T. R., Disturbances in the high latitude lower ionosphere, REP 62, Norwegian Def. Res. Estab., Kjeller, Norway, 1973.

Larsen, T. R. and G. R. Thomas, Energy spectra measured during a relativistic electron precipitation event on 2 Feb 1969, J. Atmos. Terr. Phys., 36, 1613, 1974.

Larsen, T. R., J. B. Reagan, W. L. Imhoff, L. E. Montbriand and J. S. Belrose, A coordinated study of energetic electron precipitation and D-region electron concentrations over Ottawa during disturbed conditions, J. Geophys. Res., 81, 2200, 1976.

Lerfold, G. M. and C. G. Little, D-region electron density profiles during auroras, J. Geophys. Res., 69, 2857, 1964.

Lincoln, V. and I. Brophy, World Data Center A for solar-terrestrial physics, NOAA, Private communication, December 1978.

Lindalen, H. R., F. Søraas, K. Aarsnes and R. Amundsen, Variations in the high latitude proton trapping boundary associated with polar magnetic substorms, Planet. Space Sci., 19, 1041, 1971.

Lui, A. T. Y., D. Venkatesan, C. D. Anger, S.-I. Akasofu, W. J. Heikkila, J. D. Winningham and J. R. Burrows, Simultaneous observations of particle precipitation and auroral emissions by the ISIS 2 satellite in the 19-24 MLT sector, J. Geophys. Res., 82, 2210, 1977.

Lukkari, L., J. Kangas and R. R. Heacock, Simultaneous observations of evening magnetic pulsations and morning electron precipitation events in the auroral zone during the substorm, J. Atmos. Terr. Phys., 37, 1305, 1975.

Lukkari, L. and J. Kangas, Simultaneous ULF-wave and strong riometer absorption events at the plasmapause latitude in the afternoon sector, J. Atmos. Terr. Phys., 38, 1187, 1976.

Lukkari, L., J. Kangas and H. Ranta, Correlated electron precipitation and magnetic IPDP events near the plasmapause, J. Geophys. Res., 82, 4750, 1977.

Matthews, D. L. and D. J. Simons, Observation of relativistic electron precipitation at L = 6, J. Geophys. Res., 78, 7539, 1973.

Matthews, D. L., M. Pongratz and K. Papadopaulos, Nonlinear production of suprathermal tails in auroral electrons, J. Geophys. Res., 81, 123, 1976.

McPherron, R. L., G. K. Parks, F. V. Coroniti and S. H. Ward, Studies of the magnetosphere substorms, 2, correlated magnetic micropulsations and electron precipitation occurring during auroral substorms, J. Geophys. Res., 73, 1697, 1968.

McPherson, D. A. and H. C. Koons, Dependence of the occurrence of ELF emissions on the location of the plasmapause, J. Geophys. Res., 75, 5559, 1970.

Mizera, P. F., Observations of precipitating protons with ring current energies, J. Geophys. Res., 79, 581, 1974.

Morfill, G., M. Scholar and D. Hovestadt, Analysis of processes leading to localized electron enhancements in the outer radiation belt, Planet. Space Sci., 23, 1495, 1975.

Mozer, F. S., C. W. Carlson, M. K. Hudson, R. B. Torbert, B. Parody, J. Yatteau and M. C. Kelley, Observations of paired electrostatic shocks in the polar magnetosphere, Phys. Rev. Ltrs., 38, 292, 1977.

Parks, G. K., C. Gurgiolo and R. West, Relativistic electron precipitation, Geophys. Res. Ltrs., 6, 393, 1979.

Potemra, T. A. and A. J. Zmuda, Precipitating energetic electrons as an ionization source in the midlatitude nighttime D-region, J. Geophys. Res., 75, 7161, 1970.

Reagan, J. B., Ionization processes, Dynamical and Chemical Coupling, B. Grandal and J. A. Holtet (eds), Spatind, Norway, 1977.

Reagan, J. B., R. C. Gunton, J. E. Evans, R. W. Nightingale, R. G. Johnson, W. L. Imhoff and R. E. Meyerott, Effects of the August 1972 solar particle events on stratospheric ozone, Lockheed Report D 630455,

Rees, M. H., Auroral ionization and excitation by incident energetic electrons, Planet. Space Sci., 11, 1209, 1963.

Rosenberg, T. J., L. J. Lanzerotti, D. K. Bailey and J. D. Pierson, Energy spectra in relativistic electron precipitation events, J. Atmos. Terr. Phys., 34, 1977, 1972.

Rowe, J. N., A. P. Mitra, A. J. Ferraro and H. S. Lee, An experimental and theoretical study of the D-region-II. A semi-empirical model for mid latitude D-region, J. Atmos. Terr. Phys., 36, 755, 1974.

Scarf, F. L., R. W. Fredericks, C. F. Kennel and F. V. Coroniti, Satellite studies of magnetospheric substorms on August 5, 1968, OGO plasma wave observations, J. Geophys. Res., 78, 3119, 1973.

Shaw, R. R. and D. A. Gurnett, Electrostatic noise bands associated with the electron gyrofrequency and plasma frequency in the outer magnetosphere, J. Geophys. Res., 80, 4259, 1975.

Southwood, D. J., Plasma waves in the magnetosphere, Nature, 271, 309, 1978.

Spjeldvik, W. N., Application of the Fokker-Planck numerical method to describe anisotropic and energy dependent electron precipi-taion into the atmosphere, Plasma Physics Group Tech. Report, PPG-198, UCLA, 1974.

Spjeldvik, W. N. and R. M. Thorne, The cause of storm after effects in the middle latitude D-region, J. Atmos. Terr. Phys., 37, 777, 1975a.

Spjeldvik, W. N. and R. M. Thorne, A simplified D-region model and its application to magnetic storm after effects, J. Atmos. Terr. Phys., 37, 1313, 1975b.

Stix, T. H., The Theory of Plasma Waves, McGraw-Hill Book Co., New York, 1962.

Sullivan, K. W., Institute for Telecommunications Sciences and Aeronomy (Formerly), Boulder, Colorado, Private Communication, January 1979.

Thorne, R. M. and C. F. Kennel, Quasi-trapped VLF propagation in the outer magnetosphere, J. Geophys. Res., 72, 857, 1967.

Thorne, R. M. and C. F. Kennel, Relativistic electron precipitation during magnetic storm main phase, J. Geophys. Res., 76, 1971.

Thorne, R. M., A possible cause of dayside relativistic electron precipitation events, J. Atmos. Terr. Phys., 36, 635, 1974.

Thorne, R. M., Ionosphere-magnetosphere coupling, 3. A review of the role of wave-particle interactions, Rev. Geophys. Space Phys., 13, 878, 1975.

Thorne, R. M. and T. R. Larsen, An investigation of relativistic electron precipitation events and their association with magnetospheric substorm activity, J. Geophys. Res., 81, 5501, 1976.

Thorne, R. M., Energetic radiation belt electron precipitation: A natural depletion mechanism for stratospheric ozone, Science, 195, 287, 1977a.

Thorne, R. M., Influence of relativistic electron precipitation on the lower ionosphere and stratosphere, Dynamical and Chemical Coupling, B. Grandel and J. A. Holtet (eds.) Spatind, Norway, 1977b.

Thorne, R. M., The importance of energetic particle precipitation on the chemical composition of the middle atmosphere, Middle Atmosphere Symposium, Australia, 1979.

Tsurutani, B. J. and E. J. Smith, Postmidnight chorus: A substorm phenomenon, J. Geophys. Res., 79, 118, 1974.

Tsurutani, B. T. and E. J. Smith, Two types of magnetospheric ELF chorus and their substorm dependences, J. Geophys. Res., 82, 5112, 1977.

Vampola, A. L., Energetic electrons at latitudes above the outer-zone cutoff, J. Geophys. Res., 74, 1254, 1969.

Vampola, A. L., Access of solar electrons to closed field lines, J. Geophys. Res., 76, 36, 1971a.

Vampola, A. L., Electron pitch angle scattering in the outer zone during magnetically disturbed times, J. Geophys. Res., 76, 4685, 1971b.

Vampola, A. L., H. C. Koons and D. A. McPherson, Outer-zone electron precipitation, J. Geophys. Res., 76, 7609, 1971.

Vampola, A. L., The effect of strong pitch angle scattering on the location of the outer zone electron boundary as observed by low altitude satellites, J. Geophys. Res., 82, 2289, 1977.

Vij, K. K., D. Venkatesan, W. R. Sheldon, J. W. Kern, J. R. Benbrook and B. A. Whalen, Simultaneous investigations of parent electrons and Bremsstrahlung X-rays by rocket-borne detectors, J. Geophys. Res., 80, 2869, 1975.

Walt, M., W. M. MacDonald and W. E. Frances, Penetration of auroral electrons into the atmosphere, Physics of the Magnetosphere, McCormac, 534, 1968.

Webber, W., The production of free electrons in the ionospheric D-layer by solar and galactic cosmic rays and the resultant absorption of radio waves, J. Geophys. Res., 67, 5091, 1962.

Williams, D. J. and L. R. Lyons, The proton ring current and its interaction with the plasmapause: Storm recovery phase, J. Geophys. Res., 79, 1974.

World Data Center A, Upper Atmos. Geophys. Rep., 31, Boulder, Colorado, 1974.